Mon. Not. R. Astron. Soc. **000**, 1–59 (2010) Printed 15 January 2010 (MN LATEX style file v2.2)

A near IR imaging survey of intermediate and high-mass young stellar outflow candidates

Watson P. Varricatt[1⋆], Christopher J. Davis[1], Suzanne Ramsay[2] & Stephen P. Todd[3]
[1]*Joint Astronomy Centre, 660 N. Aohoku Place, Hilo, HI-96720, USA,* [2]*European Southern Observatory, Karl-Schwarzschild-Strasse 2, D-87548 Garching bei Muenchen, Germany,* [3]*UK Astronomy Technology Centre, ROE, Edinburgh, UK*

Accepted 2009 December 11. Received 2009 December 11; in original form 2008 November 17

ABSTRACT

We have carried out a near-infrared imaging survey of luminous young stellar outflow candidates using the United Kingdom Infrared Telescope. Observations were obtained in the broad band K (2.2 μm) and through narrow band filters at the wavelengths of H_2 v =1–0 S(1) (2.1218 μm) and Brγ (2.166 μm) lines. Fifty regions were imaged with a field of view of 2.2×2.2 arcmin^2. Several young embedded clusters are unveiled in our near-infrared images. 76% of the objects exhibit H_2 emission and 50% or more of the objects exhibit aligned H_2 emission features suggesting collimated outflows, many of which are new detections. These observations suggest that disk accretion is probably the leading mechanism in the formation of stars, at least up to late O spectral types. The young stellar objects responsible for many of these outflows are positively identified in our images based on their locations with respect to the outflow lobes, 2MASS colours and association with MSX, IRAS, millimetre and radio sources. The close association of molecular outflows detected in CO with the H_2 emission features produced by shock excitation by jets from the young stellar objects suggests that the outflows from these objects are jet-driven. Towards strong radio emitting sources, H_2 jets were either not detected or were weak when detected, implying that most of the accretion happens in the pre-UCHII phase; accretion and outflows are probably weak when the YSO has advanced to its UCHII stage.

Key words: Jets and Outflows – ISM: stars: formation – stars: – infrared: stars – stars: colours – circumstellar matter – ISM

1 INTRODUCTION

The formation of low and intermediate-mass stars ($M \leqslant 8\,M_\odot$) is explained through gravitational collapse and subsequent accretion of their parent molecular clouds (Palla & Stahler 1993). Observational evidence accumulated over the last two decades supports this hypothesis. During the process of accretion, they drive well collimated bipolar outflows, which point to the locations of the young stars and can be used as signposts of star formation. Do massive stars form through a mechanism similar to that of their lower mass counterparts?

While the scenario of low-mass star formation is reasonably well understood, not much is known about high-mass ($M > 8\,M_\odot$; O and early B spectral types) star formation. When compared to those from their lower mass counterparts, the outflows from High Mass Young Stellar Objects (HMYSOs) are much more energetic, massive, faster (100s of km s^{-1}; Churchwell 1999) and have shorter time scales of evolution. There are far fewer HMYSOs than low mass YSOs and most are at kpc distances. Additionally, since these objects are mostly confined to the galactic plane and are located in giant molecular clouds extending over several parsecs or tens of parsecs, they are subjected to large amounts of extinction and reddening. Thus, most of them appear fainter at optical and near-IR wavelengths, even though they are intrinsically much more luminous than their low-mass counterparts. It is known that massive stars form in clusters. Hence, to understand the formation of massive stars and their relation to their environments, we need to observe them at wavelengths at which we can see the emission from them, i.e. at IR and longer wavelengths, at high spatial resolution.

It has been proposed that the model of Palla & Stahler (1993) fails for stellar masses above ~10 $M_\odot$ (Stahler et al. 2000). These objects start core hydrogen burning before they finish accreting. For such stars, the radiation pressure on the dust in the infalling material may halt accretion and thus limit the growth of the YSO through accretion (e.g. Yorke & Krügel 1977; Wolfire & Cassinelli 1987; Bech & Mitalas 1994). Consequently, there are two different schools of thought on the formation of massive stars. Studies by Bonnell, Bate & Zinnecker (1998), Stahler et al. (2000), Bally (2002), etc. propose that the leading mechanism for the formation of massive stars is the merger of low and intermediate mass objects.

⋆ E-mail: w.varricatt@jach.hawaii.edu

An observational manifestation of this would be extremely poorly collimated outflows or no outflows. The other scenario is a direct extension of the mechanism for low-mass star formation, via accretion. This mechanism predicts that the outflows observed would be collimated, similar to those observed from low-mass YSOs, but at a larger scale. Studies by Jijina & Adams (1996) and Yorke & Sonnhalter (2002) conclude that massive stars up to ∼40 M⊙ could form through infall and accretion irrespective of the large radiation pressure. Numerical calculations of Krumholz, Klein & McKee (2005) show that the cavities carved by outflows from massive stars will provide an optically thin region through which radiation can escape and, thereby, reduce the radiation pressure on the accreted matter and aid the growth of the star through accretion. There is still difficulty in explaining the formation of extremely massive stars, however. Bally & Zinnecker (2005) gives a discussion on possible observational consequences of the different scenarios of massive star formation.

High mass star formation is usually clustered and is often associated with other high, intermediate and low mass star formation. Inadequate spatial resolution of the early studies, mostly with single dish telescopes at radio and millimetre wavelengths, gave an impression that the outflows from massive young stars are less collimated when compared to those from their lower mass counterparts (e.g. Richer et al. 2000; Ridge & Moore 2001).

However, more and more results are being obtained from recent observational studies which suggest that massive stars also form through accretion. Zhang et al. (2005) carried out a survey of several massive YSO outflows in CO (J=2-1). Nearly half of the outflows detected by them exhibited spatially resolved bipolar features. The dynamical time-scales estimated by them for the outflows (without correcting for the angle of inclination) were $\sim 10^4$–10^5 years and the energy of the outflows was $\sim 10^{46}$ ergs, similar to the turbulent energy in the core. Their large detection rate favoured an accretion process for the formation of HMYSOs. From the CO data, they estimated accretion rates of a few times 10^{-4} $M_\odot$ year^{-1} consistent with the value obtained by Beuther et al. (2002c). This is much higher than the average accretion rate derived from low-mass outflows (10^{-7}–10^{-5} $M_\odot$ year^{-1}; Bontemps et al. 1996). For HMYSOs, Kim & Kurtz (2006) estimate an accretion rate of 10^{-4} $M_\odot$ year^{-1}, which is large enough to overcome the radiation pressure from the central stars with $L_{bol} \leqslant 2{\times}10^4$ $L_\odot$. They conclude that the outflows from the HMYSOs are well collimated, similar to the low-mass outflows. Their comparison of the properties of the outflows from massive YSOs with those from low-mass YSOs shows that the collimation factors are similar (2.2±1.2) in the CO line, consistent with a similar formative mechanism for the low- and high-mass YSOs. From CO maps with better spatial resolution, Beuther et al. (2002c) derived a collimation factor of 2.1 for HMYSO outflows. From a large sample, Wu et al. (2004) derived average collimation factors of 2.8±2.2 and 2.1±1.0 for low- and high-mass outflows respectively. These observations show that the outflows from low- and high-mass YSOs have similar collimation within error limits.

There are several massive YSOs for which collimated bipolar outflows have been observed in CO and in the near-IR (e.g. Cesaroni et al. 1997; Beuther et al. 2002a,c; Beuther, Schilke & Stanke 2003; Davis et al. 1998, 2004; Kumar et al. 2002; Shepherd et al. 2000; Todd & Ramsay Howat 2006; Zhang et al. 2005). Studying the luminous YSO IRAS 19410+2336, Beuther et al. (2003) found that the field hosts multiple bipolar outflows, which are as collimated as the outflows from low-mass YSOs. They also derived an accretion rate of $\sim 10^{-4}$ $M_\odot$year^{-1}, which is necessary to overcome the radiation pressure from the massive star in a disc-dominated accretion (Stahler et al. 2000). Beuther et al. (2002a) resolved the outflow from IRAS 05358+3543 into three, with one of collimation factor ∼10, the highest observed among HMYSO outflows, similar to the largest collimation factor observed among outflows from low-mass YSOs. From a study of CO outflows of 26 massive YSOs, Beuther et al. (2002c) concludes that massive star formation is a scaled up version of low-mass star formation. From near-IR observations, Davis et al. (2004) and Caratti O Garatti et al. (2008) also conclude that the outflows from the luminous YSOs IRAS 18151-1208 and IRAS 20126+4104, both with L∼$2{\times}10^4$ $L_\odot$, are like scaled-up versions of outflows from low-mass YSOs.

From our understanding of the low-mass star formation nearby and through theoretical studies (Pudritz & Norman 1983; Shu et al. 1994), we expect that outflows require compact accretion discs. Such discs have been proposed before (Cesaroni et al. 1997, 1999a; Shepherd & Kurtz 1999). Evidence for rotating structures of radii of several 1000s of AU have been presented by several investigators (Cesaroni et al. 1997, 2005; Zhang, Hunter & Sridharan 1998; Beltrán et al. 2005, Zapata et al. 2009, etc). Direct imaging of the disc from HMYSOs is challenging because of the very high angular resolution required; recently Patel et al. (2005) reported the detection of a dusty accretion disc around a ∼15 $M_\odot$ protostar, using sub-millimetre interferometry.

Even with interferometric techniques, most of the millimetre and radio observations, which usually form the basis for the identification of HMYSOs, lack the spatial resolution required to probe these objects and their environments in sufficient detail. Due to their location in dense molecular clouds confined mostly to the galactic plane and the resulting high extinction towards shorter wavelengths, most of these objects are not observable at optical wavelengths. However, the near-IR regime offers a balance between the high extinction in the optical and the poor spatial resolution at millimetre and radio wavelengths. The availability of highly sensitive infrared arrays on large telescopes, which offer sub-arcsec resolution at IR wavelengths, and the presence of very good outflow tracers like the lines of molecular hydrogen, make the near-IR a very useful regime for studying embedded YSOs and their outflows. The purpose of our study presented in this paper is to understand the formation of massive stars through near-IR imaging. We have obtained near-IR images of 50 high- and intermediate-mass YSO candidates with good spatial resolution as outlined in Table 1. *K*-band and continuum-subtracted H_2 images are presented for all of the objects observed. We also present the images obtained using the Brγ filter for those objects which exhibited extended emission in Brγ.

1.1 Target Selection

Emission lines of NH_3 and CO are good indicators of sites of high-mass star formation and the associated outflow activity. The (1,1) and (2,2) lines of NH_3 are very good tracers of dense gas (Molinari et al. 1996). CO lines have been traditionally used to detect emission from cold gas in entrained molecular outflows from YSOs (Cabrit & Bertout 1986; Wouterloot & Brand 1989; Shepherd & Churchwell 1996a).

Maser emission from H_2O & CH_3OH have also been considered as sign posts of massive star formation. Some of the observations conclude that H_2O masers are formed in circumstellar discs (Torrelles et al. 1996, 1998; Goddi et al. 2004). However, many studies (e.g. Felli, Palagi & Tofani 1992; Torrelles et al. 1998) and recent multi-epoch very high angular resolution VLBI observations (Patel et al. 2000; Moscadelli, Cesaroni & Rioja 2000, 2005; Goddi

et al. 2005) of the locations and proper motions of H_2O maser spots confirm that the H_2O masers associated with massive YSOs originate in the shocked regions of jets.

Observations of CH_3OH masers provide valuable information about the formation of massive stars. Class I methanol masers are observed in high-mass star forming regions and are believed to be produced in the regions of interaction between the bipolar outflows from these YSOs and the dense ambient material or in cloud-cloud collision regions (Menten 1996). Observation of the 44 GHz methanol maser emission by Kurtz, Hofner & Álvarez (2004) support the idea that Class I methanol masers are mainly produced by molecular outflows. However, they posit that accretion shocks very near the central objects might also produce conditions conducive to the formation of Class I methanol masers. Class II methanol masers are found closer to the YSOs than Class I masers and are seen to be radiatively excited in the dense warm molecular material surrounding the compact HII regions excited by YSOs (Menten 1991, 1996) or in circumstellar discs (e.g. Nielbock et al. 2007), although there are examples where they appear to trace the directions of jets and outflows as well (De Buizer 2003; De Buizer et al. 2009).

We have selected targets which exhibit both H_2O maser and NH_3 line emission from Molinari et al. (1996), objects from Sridharan et al. (2002) which exhibit both H_2O & CH_3OH emission, and HMYSOs with molecular outflows evident in high-velocity CO line wing emission from the list of Shepherd & Churchwell (1996b) and Churchwell (1999). Fourteen of the sources that we have selected from Sridharan et al. (2002) are also shown to have molecular outflows, mapped in CO by Beuther et al. (2002c).

1.2 Organization of the paper

The details of observations and data reduction are presented in section 2. Table 1 summarizes the observations carried out. A compilation of the previous observations and our own detection of outflows in H_2 is presented in Table 2. The properties of the outflows deduced from our observations and the ZAMS spectral types corresponding to the luminosities of the sources are presented in Table 3. The results and discussion on the 50 fields studied in this paper are given in sub-sections A1–A50 of Appendix A. The figure numbers of the sources agree with the corresponding sub-section numbers. Each sub-section is self-contained so that those who are interested in any particular source can read that sub-section independently. The outflows detected in this work are assigned identification numbers in the Catalogue of Molecular Hydrogen Emission-Line Objects (MHOs) in Outflows from Young Stars[1] (Davis et al. 2009b), hosted by the Joint Astronomy Centre, Hilo, Hawaii. Table B1 of Appendix B gives a compilation of the 'MHO' numbers. Since the long-wavelength observations that are used along with our observations to draw conclusions on the 50 sources were obtained by different people using different telescopes, we have given a compilation of the sources from which these are taken, the frequencies of observations, telescopes used, the pointing accuracies and the spatial resolutions in Table C1 of Appendix C. Section 3 gives a discussion of the paper. The near-IR colours of the YSO candidates identified in the 50 fields are discussed in sub-section 3.1; their MSX and IRAS colours are discussed in sub-section 3.2. Our inferences from the H_2 detections and near-IR colours are discussed in sub-sections 3.3 and 3.4. The summary and conclusions are given in section 4.

[1] http://www.jach.hawaii.edu/UKIRT/MHCat/

2 OBSERVATIONS

Observations were carried out with the 3.8-m United Kingdom Infrared Telescope (UKIRT), Mauna Kea, Hawaii, using the facility near-IR camera UFTI (Roche et al. 2003). UFTI is a 1–2.5μm camera with a 1024×1024 HgCdTe array giving a plate scale of 0.091 arcsec pixel^{-1} and a field of view of 1.5×1.5 arcmin^2 at the f/36 Cassegrain focal plane of the UKIRT.

Fifty sources were observed using narrow band filters centred at the wavelengths of H_2 v=1–0 S(1) (2.1218 μm) and Brγ (2.166 μm) lines and a broad-band K (central wavelength=2.2 μm; FWHM = 0.34 μm) Mauna Kea Observatory (MKO) consortium filter. Two different filters were used for the H_2 observations - all observations before 2003 July were performed using a narrow-band filter named "2.122" with FWHM=0.02 μm. After this date, this filter was replaced with a filter "2.122MK" with an FWHM of 0.031 μm micron, designed for the MKO consortium. The central wavelength of both filters is 2.119 μm. All Brγ observations were done using an MKO consortium filter with a central wavelength of 2.166 μm and FWHM=0.022 μm. H_2 S(1) and Brγ were selected to yield complementary information on the warm, entrained, molecular outflow and the collimated, high-velocity, high-excitation jet respectively. The K-band images were used to continuum-subtract the line data, and to identify the likely outflow sources.

The observations were obtained by offsetting the telescope to nine positions on the sky around the object, separated by 20 arcsec from the base position resulting in a field of view of 2.2×2.2 arcmin^2 for the mosaics. Dark frames were obtained before each set of observations. The data were flat fielded using sky flats generated by median combining the observed object frames. The dithered frames were combined, matching the centroids of stars after applying the dark and the flat field corrections. For very crowded fields or regions with extended nebulosity, flat fielding was accomplished using the flat frames generated by observing less crowded regions nearby or using the flats from the object observation prior to or after the observation of the specific object of concern. Typically, a total integration time of 180 sec was used in K and 594 sec was used in H_2 and Brγ filters. At these integrations, we reached an average sensitivity of 5σ at 19 mag on point sources in K and a per pixel sensitivity of 5σ at 1.3×10^{-18} W m^{-2} arcsec^2 in the narrow-band filters.

H_2 S(1) and Brγ images, having their central wavelengths within the K band, were continuum-subtracted using scaled K-band images observed before or after the narrow-band images, employing the methods adopted by Varricatt, Davis & Adamson (2005). For continuum subtraction, in each field, the integrated, sky-subtracted counts on many isolated point sources (without any IR excess) were measured in the narrow-band filters and in the K filter using a circular aperture, typically ~4 times the FWHM. The ratios of the counts K/H_2 and K/Brγ were evaluated for these stars and the average values were taken. The constant sky background was subtracted from the K-band images. This image was then divided by the above ratios and and the resulting images were subtracted from the sky subtracted narrow-band filter images. The diffuse continuum was generally subtracted out well. However, stars often showed residuals due to changes in PSF between the broad- and the narrow-band observations. Sometimes, continuum-subtracted images exhibit large negative residuals on some objects because of reddening, caused by large extinction or IR excess or both. Table 1 gives a log of the observations and the average

Table 1. Log of observations

No.	Object Name (IRAS)	Mol[1]	UTDate (yyyymmdd)	Filters used	Sky Condition[2]	FWHM(K)[3] (arcsec)
1	00420+5530	3	20030915	K, 2.122MK, Brγ	Thin cirrus	0.56
2	04579+4703	7	20030417	K, 2.122, Brγ	Clear	0.96
3	05137+3919	8	20031012	K, 2.122MK, Brγ	Thin Cirrus	0.42
4	05168+3634	9	20031012	K, 2.122MK, Brγ	Thin Cirrus	0.48
5	05274+3345	10	20031012	K, 2.122MK, Brγ	Thin Cirrus	0.61
6	05345+3157	11	20030317	K, 2.122, Brγ	Clear	0.67
7	05358+3543		20030317	K, 2.122, Brγ	Clear	0.62
8	05373+2349	12	20030317	K, 2.122	Clear	0.63
9	05490+2658		20030315	K, 2.122, Brγ	Clear	0.59
10	05553+1631	14	20030315	K, 2.122, Brγ	Clear	0.65
11	06061+2151	16	20030315	K, 2.122, Brγ	Clear	0.47
12	06584-0852	28	20030315	K, 2.122, Brγ	Clear	0.59
13	18144-1723	45	20030528	K, 2.122	Clear	0.55
14	18151-1208	46	20030528	K, 2.122, Brγ	Clear	0.57
15	18159-1648	49	20031012	K, 2.122MK, Brγ	Thin Cirrus	0.66
16	18174-1612		20030616	K, 2.122, Brγ	Clear	0.52
17	18182-1433		20031012	K, 2.122MK, Brγ	Thin Cirrus	0.84
18	18264-1152		20031023	K, 2.122MK, Brγ	Clear	0.49
19	18316-0602	62	20030616	K, 2.122, Brγ	Clear	0.52
20	18345-0641		20031009	K, 2.122MK, Brγ	Thin cirrus	0.87
21	18360-0537	65	20031009	K, 2.122MK	Thin cirrus	0.90
22	18385-0512		20030823	K, 2.122MK	Clear	0.7
23	18507+0121	74	20030527	K, 2.122, Brγ	Clear	0.5
24	18517+0437	76	20030823	K, 2.122MK, Brγ	Clear	0.63
25	19088+0982	97	20031006	K, 2.122MK, Brγ	Clear	0.75
26	19092+0841	98	20031006	K, 2.122MK	Clear	0.68
27	19110+1045		20030926	K, 2.122MK, Brγ	Clear	1.12
28	19213+1723	103	20030926	K, 2.122MK, Brγ	Clear	0.64
29	19217+1651		20030512	K, 2.122	Thin cirrus?	0.43
30	19374+2352	109	20030512	K, 2.122, Brγ	Thin cirrus?	0.61
31	19388+2357	110	20030926	K, 2.122MK, Brγ	Clear	0.72
32	19410+2336		20030512	K, 2.122, Brγ	Thin cirrus?	0.57
33	20050+2720	114	20030518	K, 2.122, Brγ	Thin cirrus	0.50
34	20056+3350	115	20030518	K, 2.122, Brγ	Thin cirrus	0.46
35	20062+3550	116	20030518	K, 2.122, Brγ	Thin cirrus	0.42
36	20126+4104	119	20030330	K, 2.122, Brγ	Thin cirrus	0.83
37	20188+3928	121	20030330	K, 2.122, Brγ	Thin cirrus	0.74
38	20198+3716		20030518	K, 2.122, Brγ	Thin cirrus	0.39
39	20227+4154	124	20030517	K, 2.122, Brγ	Thin cirrus?	0.62
40	20286+4105	126	20030517	K, 2.122, Brγ	Thin cirrus?	0.50
41	20293+3952		20030516	K, 2.122, Brγ	Thin cirrus?	0.49
42	20444+4629	131	20031215	K, 2.122MK, Brγ	Clear	1.16
43	21078+5211	133	20030516	K, 2.122	Thin cirrus?	0.46
44	21307+5049	136	20030516	K, 2.122, Brγ	Thin cirrus?	0.73
45	21391+5802	138	20030808	K, 2.122MK, Brγ	Clear	0.62
46	21519+5613	139	20031215	K, 2.122MK, Brγ	Clear	0.99
47	22172+5549	143	20031215	K, 2.122MK, Brγ	Clear	0.99
48	22305+5803	148	20030808	K, 2.122MK, Brγ	Clear	0.64
49	22570+5912	153	20030915	K, 2.122MK, Brγ	Thin cirrus	0.62
50	23139+5939		20030915	K, 2.122MK, Brγ	Thin cirrus	0.68

[1]From Molinari et al. (1996), [2]A question mark is given when the presence of thin cirrus during the observations is suspected, [3]FWHM of the average PSF measured from each reduced K-band mosaic (the H_2, Brγ and K-band data were obtained consecutively).

FWHM measured on point sources from the K-band mosaics. Figs. A1–A50 show the observed images [2].

Astrometric corrections were applied to the coordinates of our images employing the starlink package GAIA, adopting the 2MASS positions as reference. Coordinates of typically six isolated unresolved bright point sources spread throughout the 2.2×2.2 arcmin^2 field of each image were compared with those of 2MASS, and the required coordinate corrections were applied to our images to match the positions with those of 2MASS. After applying the corrections, the coordinates of the unresolved objects in

[2] **The reduced images are available for download (as fits files) at http://cdsarc.u-strasbg.fr/ftp/cats/J/MNRAS/vol/page**

Table 2. Detections at different wavelengths. Column1 gives the reference numbers (same as in Table 1, the subsections in Appendix A and in the accompanying figures), columns 2–6 list the detections in ammonia, water maser, methanol maser, CO and radio with references, and columns 7–8 give the kinematic distances and the estimated luminosities with references. "—" implies that no published observation is available. "+" implies that not all references are listed in the table. Column 9 lists our detection in H_2. "Y" implies confirmed detection; "N" implies null detection; a "?" against "Y" shows that the detection is only tentative.

No	NH_3	H_2O	CH_3OH	CO line wings/outflow	radio (cm) emission[1]	d(kpc)	Luminosity ($10^3 L_\odot$)	H_2[2]
1	Y(m8)	Y(bb,m6,p1)	N(sh)	Y(bc,j1,w9)	Y(3.6-mb)	5.0(mb);7.72(m8)	12.4(mb);51.5(m8)	**Y(c)**
2	Y(m8)	Y(bb,m6,w7,w8)	Y(w8)	Y(w8);N(z3)	N(6-m9)	2.47(m8)	3.91(m8)	**Y(c)**
3	Y(m8)	Y(p1,m6)	N(sh)	Y(z3)	Y(3.6-mb)	11.5(mc)	225(mc)	**Y(c)**
4	Y(m8)	Y(p1,m6)	N(sa,sh)	Y?(z3)[3]	N(6-m9)	6.08(m8)	24.0(m8)	N
5	Y(m8,z2)	Y(p1,g2,t1)	Y(sa,sh)	Y(h5)	Y(3.6-t1)	1.55(m8)	4.35(m8)	Y(c)
6	Y(m8,v2)	Y(p1,t2,v2,w8)	—	Y(sc,w7,r1,z3)	Y(3.6-mb,t2)	1.8(m8)	1.38(m8)	Y(c)+(f)
7	Y(se)	Y(se,b6)	Y(sh,se,g1,m5)	Y(b4)	N(3.6-se)	1.8(se)	3.8(se)	Y(c)+(f)
8	Y(m8)	Y(p1)	N(sh)	Y(z3)	Y(3.6-mb)	1.17(m9)	0.47(ma)	**Y(c?)**
9	—	N(se)	N(se)	Y(sd)	N(3.6-se)	2.1(sd)	3.16(se);4.2(sd)	Y
10	Y(m8)	Y(bb,m1,p1)	N(se,m1)	Y(w7,sd,	Y(1.3-s8;3.6-se,s6;	2.5(sd);	6.5(sd);6.31(se);	Y(c)
10	—	Y(s6,w8+)		se,s5)	6-h3)	3.04(m8)	11.7(m8)	
11	Y(m8)	Y(bb,p1)	Y(g1,sh)	Y(w7,s2)	Y(3.6-k2)	0.1(m8);2.0(c1)	0.0278(m8);4.0(c1)	Y(c)
12	Y(m8)	Y(bb,p1)	—	Y(w7,z3)	N(2,6-m9)	4.48(m8)	5.67(ma)	N
13	Y(m8)	Y(p1)	Y(sh,k3)	N(z3)	N(6-m9)	4.33(ma)	21.2(ma)	Y(c?)
14	Y(m8)	N(b6,p1)	Y(b6)	Y(b5,se)	N(3.6-se)	3.0(se)	19.95(se)	Y(c)
15	Y(m8)	Y(p1)	Y(w1)	—	—	2.5(m8)	29.5(m8)	Y(c?)
16	Y(m3)	N(m3,j2)	Y(m5,ba,w2)	N(s3)	Y(2,6,21-f1)	2.1(w6)	433(w6)	Y(f)
17	Y(se)	Y(se,b6)	Y(se,w2)	Y(se,b5,b9)	Y(3.6,1.3-z1)	4.5,11.8(se)	20,125.9(se);50.1(w5)	N
18	Y(se)	Y(b6,se)	Y(b6,se)	Y(b5,se)	Y(3.6,1.3-z1)	3.5,12.5(se)	10,125.9(se)	Y(c)
19	Y(m8)	Y(bb,k4)	Y(w1,sa,sh)	Y(s2)	Y(3.6-k2,w2)	3.17(m8)	44.1(m8)	Y(c)
20	Y(se)	Y(b6,se,v1,sh)	Y(b6,sh,v1)	Y(b5,se)	Y(3.6-se)	9.5(se)	39.8(se)	Y
21	Y(m8)	Y(bb,p1)	N(v1)	—	—	6.28(m8)	116(m8)	N
22	—	Y(bb,b6,se)	N(b6,se,w2)	Y(se)	Y(3.6-se)	2,l3.1(se)	5,199.5(se);4.0(w5)	N
23	Y(m8)	Y(bb,m7)	Y(sh,s1)	—	Y(2,6-m7;6-m9,s9)	3.87(m8)	48.4(m8)	N
24	Y(m8)	Y(bb,c5,se)	Y(sh)	Y(se)	N(3.6-se)	2.9(se)	12.6(se)	Y(f)
25	Y(m8)	Y(bb,p1,m1)	N(m1,sh,v1)	Y(o1)	Y(6-m9)	4.71(m8)	29.9(m8)	N
26	Y(m8)	Y(bb,p1)	Y(m2,sh)	N(z3)	N(6-m9)	4.48(m8,ma)	9.2(ma)	N
27	—	Y(h1)	Y(c2,m5,sh)	Y(h6)	Y(2,6-w6;23.4-v3)	6(v3);8.3(h6);9.7(w6)	330(v3);588.8(h6)	N
28	Y(m8)	Y(bb,p1)	N(sh,sb,v1)	Y(z3)	Y(6-m9)[4]	4.12(m8)	28.2(m8)	Y(f)
29	Y(se)	Y(se,b6)	Y(se,b6)	Y(se,b6,b8)	Y(3.6-se)	10.5(se)	79.4(se)	N
30	Y(m8)	Y(bb,p1)	N(s1)	Y(z3)	Y(6-m9)	4.3(m8)	26.7(m8)	**Y(c?)**
31	Y(m8)	Y(bb,p1)	Y(s1,sa)	Y(z3)	Y(6-m9,h4)	4.27(m8)	14.8(m8)	Y(c)
32	Y(se)	Y(b6,se)	Y(b6,se,sh)	Y(se,b7)	Y(3.6-se)	2.1,6.4(se)	10,100(se)	Y(c)
33	Y(m8)	Y(p1)	—	Y(b1,z3)	Y(6-w3)[4]	0.73(m8)	0.388(m8)	**Y(c)**
34	Y(m8)	Y(bb,j1,p1)	—	Y(z3)	Y(3.6-j1)	1.67(m8)	4.0 (m8)	N
35	Y(m8)	Y(bb,p1)	Y(sb,sh,g1)	Y(z3)	N(6-m9)	4.9(mb)	3.2(mb)	**Y(c)**
36	Y(m8+)	Y(e1,md,p1,t1+)	Y(e1,g1,k3,+)	Y(l1,s7+)	Y(3.6-h2)	1.7(c4)	10(c4)	Y(c)
37	Y(m8,a1,+)	Y(a1,bb,j1,p1)	N(s1)	Y(l2,z3)	Y(3.6,1.95-j1;6-m9)	0.31(m8);3.91(p1)	0.343(m8);52.8(p1)	**Y(c)**
38	Y(d1)	Y(f4,h1)	Y(sh)	Y(m4,s4)	Y(6-w6)	0.9,5.5(d1)	20,605(d1)	Y(c)
39	Y(m8)	Y(p1,bb)	N(s1)	Y(k1)	N(2,6-w3)	0.1(m8);3.39(p1)	0.00914(m8);9.59(p1)	Y(c)
40	Y(m8)	Y(p1,bb)	—	Y(z3)	N(6-m9)	3.72(m8)	39(m8)	**Y(c)+(f)**
41	Y(se)	Y(se)	N(se)	Y(b5,b8)	Y(3.6-se)	1.3,2(se)	2.5,6.3(se)	Y(c)+(f)
42	Y(m8)	N(p1,w8)	N(m2)	Y(d2,w7)	Y(6-m9)	2.42(m8)	3.34(m8)	Y(f)
43	Y(m7,m8)	Y(p1,bb,c5,j1,+)	N(sh,sa)	Y(w7,b3)	Y(2,6-m7;6-m9)	1.49(m8)	13.4(m8)	N
44	Y(m8)	Y(p1)	Y(k3)	Y(f3,z3)	N(3.6-mb)[4,5]	3.6(mb)	4(mb)	**Y(c?)**
45	Y(m8)	Y(f2,t1,p2)	Y(k3)	Y(sg,w4,c6,b2)	Y(3.6-b2)	0.75(m8)	0.0939(m8);0.15(b2)	Y(c)
46	Y(m8)	Y(c3,w8)	N(m2)	Y(sf,w7,w8,z3)	N(6-m9)	7.3(m8)	19.1(m8)	**Y(c)**
47	Y(m8)	Y(c3,w8)	—	Y(w7,z3)	N(2,6-m9,6-mb)	2.4(mb)	1.8(mb)	Y(c)
48	Y(m8)	Y(p1)	—	Y(w7,z3)	Y(3.6-mb)	5.4(m8)	14.1(m8)	Y(c?)
49	N(m8)	N(p1,se)	N(sa,se,m2)	Y(se,b5)	Y(3.6-se)	2.92(m8);5.1(se)	20.1(m8);50.1(se)	**Y(c)+(f)**
50	—	Y(g3,t1,b6)	Y(sh)	Y(b5)	Y(3.6-se,t1)	4.8(se)	25(se)	Y?

[1]column is formatted as Y/N(cm-reference); [2]results from our H_2 line observations. "(c)" is given if the emission is collimated or is seen as a set of aligned knots; a question mark against "c" implies that collimated emission in H_2 is suspected and "f" is given when a fluorescent component to the H2 emission is suspected. Bold faces show new H_2 detections in this study; [3]CO outflow detected is away from the IRAS position; [4]extended; [5]emission is from a Supernova remnant.

References: a1-Anglada et al. (1997); b1-Bachiller et al. (1995); b2-Beltran et al. (2002); b3-Bernard et al. (1999); b4-Beuther et al. (2002a); b5-Beuther et al. (2002c); b6-Beuther et al. (2002d); b7-Beuther et al. (2003); b8-Beuther et al. (2004a); b9-Beuther et al. (2006); ba-Błaszkiewicz & Kus (2004); bb-Brand et al. (1994); bc-Brand et al. (2001); c1-Carpenter et al. (1995); c2-Caswell et al. (1995); c3-Cesaroni et al. (1988); c4-Cesaroni et al. (1997); c5-Codella et al. (1996); c6-Codella et al. (2001); d1-Dent et al. (1988); d2-Dobashi et al. (1995); e1-Edris et al. (2005); f1-Felli et al. (1984); f2-Felli et al. (1992); f3-Fontani et al. (2004); f4-Forster et al. (1978); g1-Galt (2004); g2-Goddi et al. (2004); g3-Goddi et al. (2005); h1-Hofner & Churchwell (1996); h2-Hofner et al. (1999); h3-Hughes & MacLeod (1993); h4-Hughes & MacLeod (1994); h5-Hunter et al. (1995); h6-Hunter et al. (1997); j1-Jenness et al. (1995); j2-Johnson et al. (1998); k1-Kim & Kurtz (2006); k2-Kurtz (1994); k3-Kurtz et al. (2004); k4-Kurtz & Hoffner (2005); l1-Lebrón et al. (2006); l2-Little et al. (1988); m1-MacLeod et al. (1998a); m2-MacLeod et al. (1998b); m3-Massi et al. (1988); m4-Matthews et al. (1986); m5-Menten et al. (1991); m6-Migenes et al. (1999); m7-Miralles et al. (1994); m8-Molinari et al. (1996); m9-Molinari et al. (1998); ma-Molinari et al. (2000); mb-Molinari et al. (2002); mc-Molinari et al. (2008); md-Moscadelli et al. (2000); o1-Osterloh et al. (1997); p1-Palla et al. (1991); p2-Patel et al. (2000); r1-Ridge & Moore (2001); s1-Schutte et al. (1993); s2-Shepherd & Churchwell (1996a); s3-Shepherd & Churchwell (1996b); s4-Shepherd et al. (1997); s5-Shepherd et al. (1998); s6-Shepherd & Kurtz (1999); s7-Shepherd et al. (2000); s8-Shepherd et al. (2004a); s9-Shepherd et al. (2004b); sa-Slysh et al (1990); sb-Slysh et al. (1999); sc-Snell et al. (1988); sd-Snell et al. (1990); se-Sridharan et al. (2002); sf-Su et al. (2004); sg-Sugitani et al. (1989); sh-Szymczak et al. (2000); t1-Tofani et al. (1995); t2-Torrelles et al. (1992b); v1-van derWalt et al. (1995); v2-Verdes-Montenegro et al. (1989); v3-Vig et al. (2006); w1-Walsh et al. (1997); w2-Walsh et al. (1998); w3-Wilking et al. (1989); w4-Wilking et al. (1990); w5-Williams et al. (2005); w6-Wood & Churchwell (1989b); w7-Wouterloot & Brand (1989); w8-Wouterloot et al. (1993); w9-Wu et al. (2001); z1- Zapata et al. (2006); z2-Zhang et al. (2002); z3-Zhang et al. (2005)

our images agreed well with those of 2MASS. For objects which were not resolved by 2MASS, but were resolved by us due to the higher spatial resolution of our data, the 2MASS positions would only be close to the centroids of the resolved components from our images. Positional accuracy of our data after the astrometric corrections is ~0.5 arcsec, which is the positional accuracy of 2MASS.

The spatial resolution of our images are limited by the seeing. The average FWHM measured in the K-band images of the fields observed are listed in Table 1. These are much better than the spatial resolution of IRAS (~1-2 arcmin), MSX (~18 arcsec) and 2MASS (~4 arcsec).

3 DISCUSSION

3.1 The near-IR colours

Unless otherwise stated, 2MASS JHK_s magnitudes are used to derive the colours of the YSO candidates indentified by us in the 50 fields studied here. Fig. 1 shows the $(J-H)$ - $(H-K_s)$ colour-colour diagram. The continuous line shows the locii of the intrinsic colours of main sequence stars from Koornneef (1983). The dashed line shows the location of Classical T Tauri stars (CTTS) from Meyer, Calvet & Hillenbrand (1997). The dotted lines show the reddening vectors up to A_V=30 for main sequence stars and CTTS. We adopted a reddening law with R=A_V/(E(B-V))=5, which is typical of dense clouds (Cardelli, Clayton & Mathis 1989). The objects in between the reddening vectors for the main sequence stars are expected to be reddened main sequence stars. The region below the lower reddening line for the main sequence stars is occupied by YSOs where CTTS, Herbig Ae/Be (HAeBe) stars and Luminous YSOs occupy different regimes (Lada & Adams 1992).

The 2MASS colours of the near-IR sources of interest described throughout the text are plotted in Fig. 1. Plot symbol adopted is the source number "1–50" (as in column 1 of Tables 1 and 2, and in the subsections A1–A50 for the 50 fields in Appendix A) subscripted by "A", "B", etc. for the near-IR objects identified in each field. The sources which we consider as the IR counterparts of the YSOs driving the outflows detected in H_2 are circled.

Most of the objects in the diagram are located in the region of the near-IR colour-colour diagram occupied by YSOs. The association of these objects with the MSX/IRAS, millimetre and radio continuum emissions and their location central to the detected outflows suggest that we are detecting the driving sources of the outflows in the near-IR. Even for several objects which are convincingly in the active outflow phase, we detect near-IR counterparts (e.g. IRAS 19410, 18151, 18316 [henceforth, IRAS names of our sources are often truncated to the first five digits]). The near-IR spectra available on some of these objects (e.g. IRAS 18151 - Davis et al. 2004; IRAS 06061, 19110 - Hanson et al. 2002; IRAS 04579, 05137 - Ishii et al. 2001) exhibit steeply rising SEDs on which emission lines of molecular hydrogen, and often of CO and Brγ, are superposed. This implies that in the near-IR we are mostly witnessing re-processed thermal emission from circumstellar gas+dust shells or spatially unresolved discs and therefore, not directly detecting the stellar photospheres.

Among UCHIIs and pre-UCHIIs, we do not find a large difference between their appearance in the near-IR, although we would expect more of the UCHIIs to be visible at JHK wavelengths. Even though many of the pre-UCHIIs are detected in JHK, several UCHIIs in our sample are not detected at NIR wavelengths (e.g. IRAS 18385, 19374, 21078); see also IRAS 18449-0115 of Bik (2004). The detection in the near-IR of both these classes is highly influenced by the foreground extinction. The near-IR counterparts identified for sources that are confirmed to be UCHIIs (based on their radio fluxes) are enclosed in green squares in Fig. 1. Three of the seven objects, IRAS 18174 (16_B), 19088 (25_A) and 19110 (27_{AB}), show large excess. However, 25_A and 27_{AB} are detected only in K_s by 2MASS, so their colours are highly uncertain. For 27_{AB}, two sources contribute to the 2MASS K_s magnitude, one of which is likely to be in a pre-UCHII stage. 16_B was detected only in H and K_s and has a large foreground extinction of A_V=40 (Nielbock et al. 2007). The large extinction may imply a $J-H$ colour which is redder than the limiting colour; hence, 16_B may be actually located further up in Fig. 1, closer to the reddening band. The four remaining UCHIIs are located either in the reddening band or very close to it. This is indicative of an evolutionary trend which suggests that when the object moves to a UCHII stage, more of the circumstellar matter which causes the excess and reddening is cleared and that the accretion and outflow will be at a lower rate when compared to pre-UCHII objects.

3.2 The MSX and IRAS colours

The MSX and IRAS colours are derived by taking the logarithms of the ratios of fluxes at different wavelengths. The MSX ([21.3 - 14.6]) vs. ([14.6 - 8.3]) colour-colour diagram is shown in the left panel of Fig. 2. The plot symbols adopted for the fifty sources are again "1–50", consistent with their labels in the tables, subsections A1–A50 of Appendix A where they are discussed, and in the 2MASS colour-colour diagram (Fig 1). The objects reliably detected in K, from which we detected outflows at 2.122 μm, are circled (when we have doubts about the identification of an outflow driving source in K, a dotted circle is used). These objects have colours implying rising SEDs. The driving sources of the outflows have a rough tendency to occupy intermediate [14.6-8.3] colours throughout the [21.3 - 14.6] colour regime. MSX counterparts of H_2 outflow driving sources not detected in K are enclosed in pentagons. When a YSO candidate is detected in the near-IR at the expected position, with an MSX counterpart identified, but for which no outflow was seen in H_2, it is enclosed in a triangle. When the near-IR detection was only suggestive of a YSO association, we have used a dotted triangle. Some of these objects with negative colours are likely to be evolved objects. MSX counterparts of the positively identified UCHIIs are enclosed in squares. Most of the UCHIIs, especially the luminous ones, occupy the upper region of the [14.6 - 8.3] colour in Fig. 2, showing a steeper SED in this regime when compared to an average outflow driving source, agreeing with their location close to the reddening band in Fig. 1.

The right panel of Fig. 2 shows the objects in a colour-colour diagram derived from the IRAS fluxes at 12, 25 and 60-μm. The plot symbols used are the same as in Fig. 2 - left. The IRAS colours of the H_2 outflow driving sources detected in K are enclosed in solid circles and those which have only tentative detection in K are shown with dotted circles. The IRAS colours of the outflow sources which do not have a K-band detection are enclosed in pentagons. The objects for which YSO counterparts were detected close to the IRAS position in K, but for which no outflows are detected in H_2 are enclosed in triangles. Confirmed UCHIIs are shown enclosed in squares.

The dotted lines in Fig. 2 (right) mark the IRAS colour criteria defined by Wood & Churchwell (1989a) ($\log_{10}$(F60 μm/F12 μm)$\geqslant$1.3 and $\log_{10}$(F25 μm/F12 μm)$\geqslant$0.57), where UCHIIs are expected to be located above and towards the

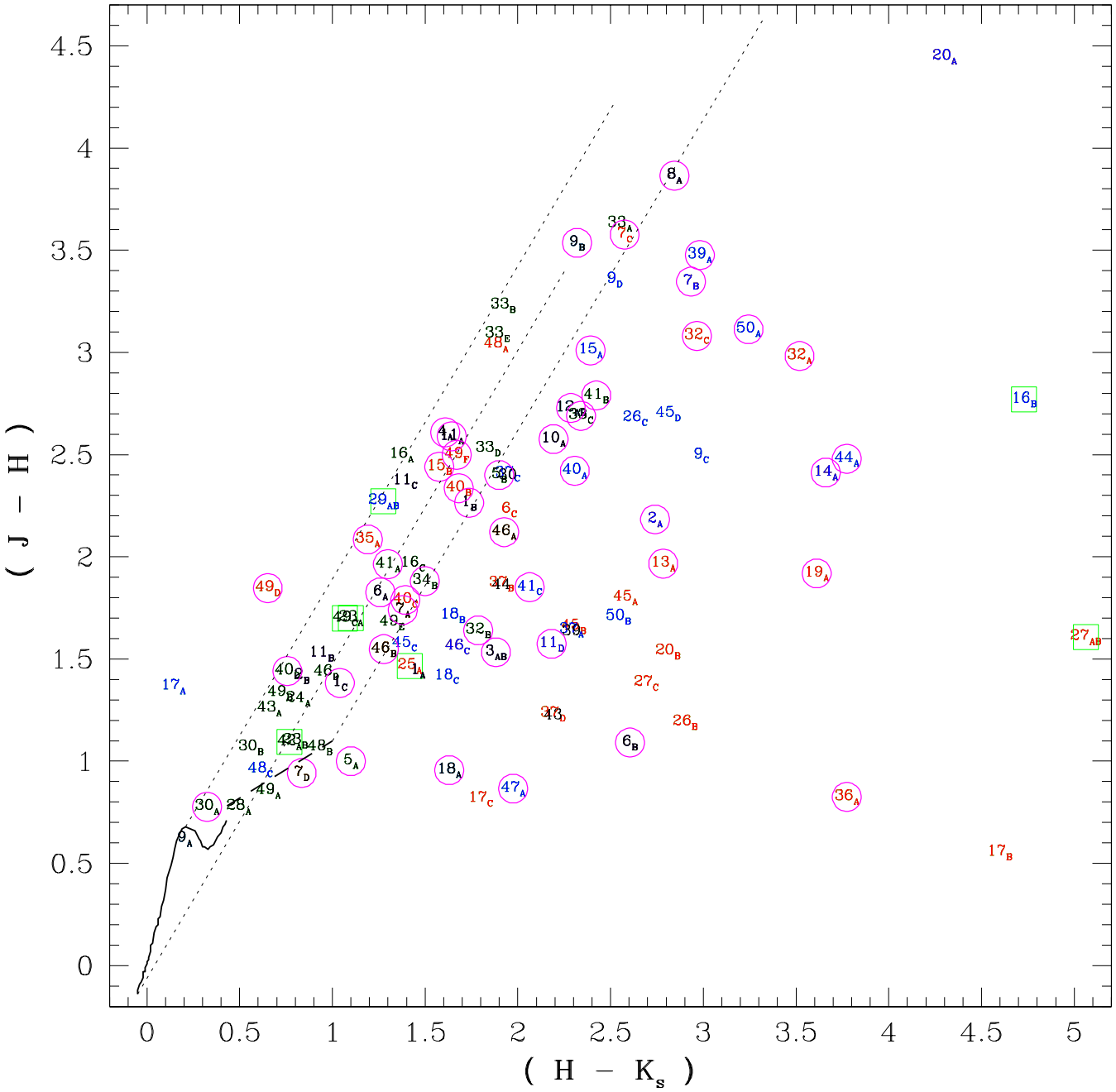

Figure 1. Near-IR colour-colour diagram produced using the 2MASS JHK_s magnitudes. The continuous line denotes the locii of the main sequence stars, the dashed line shows the locii of CTTS and the three dotted lines show the reddening vectors up to A_V=30. The sources which we think are the IR counterparts of the YSOs driving the outflows detected in this work are circled. Sources which are detected by 2MASS in all three bands are shown black in colour. Limiting colours of those which are detected in only two bands are shown in blue; limiting colours of those detected in only one band are shown in red. Objects which are not detected in *J* due to extinction may be located further up. Those which are not detected in *J* and *H* due to extinction may be located further up and right. Squares mark the near-IR counterparts of confirmed UCHII regions.

right, respectively, of the two dotted lines. A major fraction of our objects are located in this region. Our results and the available observations on these objects show that our sample is a mixture of UCHII and pre-UCHII objects. The radio detections, most of which are from VLA observations with good angular resolution and positional accuracy, are compared with the locations of the MSX sources and the IR counterparts of the YSOs identified in this work (based on their near-IR colours and location at the centroids of outflows). The MSX flux ratios in Fig. 2 show that the outflow sources have rising SEDs in the MSX bands and the MSX detections are the counterparts of the IRAS sources in a major fraction of these regions. Many of these are multiple sources embedded in clusters. As described above, the radio detections are not always from the YSOs driving the outflows; instead they are often from more evolved YSOs in the neighbourhoods of the driving sources of the outflows. The confirmed UCHIIs are all located in the region defined by the Wood & Churchwell colour criteria for UCHIIs, but they are mixed with pre-UCHIIs. The

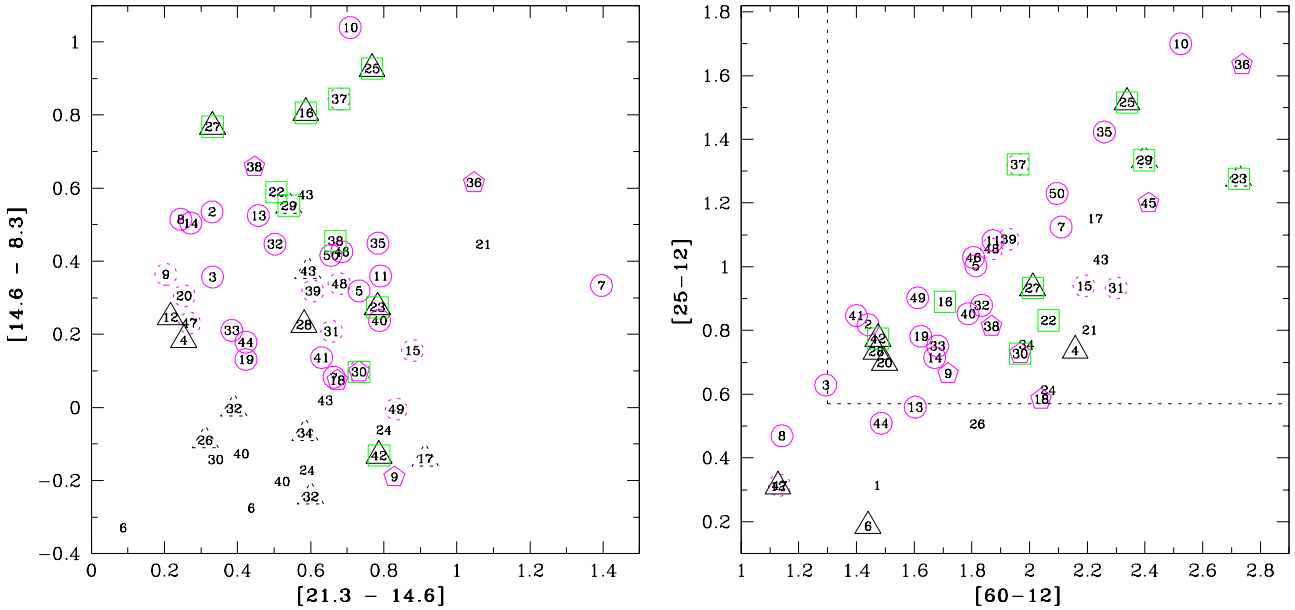

Figure 2. The colour-colour diagrams produced from the MSX fluxes (left) and the IRAS fluxes (right). The sources are labelled according to their numbers 1–50 given in Table. 1. Objects detected in *K* and appearing to be associated with H_2 outflows are circled; dotted circles show tentative identifications of the *K*-band conterparts. When an H_2 outflow is detected, but its driving source is not visible in *K*, its MSX or IRAS counterpart is enclosed in a pentagon. If no outflows are detected in H_2, but a YSO is identified in *K* to be associated with the MSX or IRAS source, a solid triangle is shown; a dotted triangle is given when the *K*-band detection is only tentative. Infrared counterparts of confirmed UCHII are enclosed in squares. The dotted lines on the IRAS plot show the colour criteria of Wood & Churchwell (1989a) for identifying UCHII.

colour criteria of Wood & Churchwell (1989a) are, thus, more representative of intermediate and luminous YSOs (UCHII and pre-UCHII) and the embedded clusters that contain these rather than just UCHII. Some of the previous studies have also noticed this (e.g. Bik 2004).

3.3 Detection of outflows

76 % (38 out of 50) of our objects display H_2 emission. 50 % (25 out of 50) of the objects exhibit collimated outflows as inferred from the aligned H_2 emission knots; including the objects with suspected collimated emission (objects with "?" in the last column of Table. 2), this fraction would be 62% (31 out of 50). Many of these are new detections. These numbers should be treated as lower limits only. Even at 2.122 μm, the extinction will hamper the the detection of several outflows. Fig. 3 shows the distribution of the survey objects in Galactic coordinates, where the objects are labelled by their distances from the Sun. The 12 objects from which outflows are not detected in H_2 (shown in red and enclosed in hexagons) are located symmetrically above and below the galactic plane. Most of these are located close to the galactic plane and are at large distances, indicating that the non-detections of outflows in many cases may be mainly due to extinction.

In most of the objects with outflows, we find good agreement between the centroids and directions of the outflows obtained from the aligned H_2 emission knots in our images and those deduced from published CO maps. The aligned knots that we see in H_2 emission are most certainly due to shocked emission from jets. These observations show that the outflows are mainly jet-driven as in low-mass stars and not wind-driven. (Some examples of spectroscopic verifications of shocked emission from HMYSO jets are: IRAS 20126 - Caratti O Garatti et al. 2008, IRAS 18151 - Davis et al. 2004, IRAS 11101-5928 - Gredel 2006, IRAS 18316 - Todd & Ramsay Howat 2006).

3.3.1 *Do massive stars form through disk accretion?*

Collimation factors derived from our H_2 line observations are listed in Table 3. (Collimation factors are derived by dividing the observed maximum lengths of the outflows from the driving sources by the widths, both measured from our H_2 images. We caution that collimation factors derived from H_2 will be affected by the large extinction at 2.122 μm and should not be compared directly with those derived from CO maps). Within the range of luminosities covered in our sample, the outflows are seen to be well collimated irrespective of the luminosities of the driving sources. The highest collimation ratio observed is ∼19 (for IRAS 05358+3543). The sample of H_2 jets presented in this paper seem to be as collimated as those from low-mass YSOs (a compilation of the lengths and opening angles of outflows in Orion, derived from H_2 images, can be seen in Davis et al. 2009a). The main sequence spectral types of single stars corresponding to the luminosities of the YSOs driving the outflows (Vacca, Garmany & Shull 1996; Morton & Adams 1968) are also listed in Table 3. From these observations, we infer that objects up to early B and late O-types produce collimated outflows, implying that disk accretion forms the main mechanism leading to their formation. However, accretion rates may be highly variable, as parcels of matter (like clumps of gas and dust) fall from the disc on to the central source (e.g: source #90 in IRAS 05361+3539, from photometric variability of the central source and the twisted outflow observed in H_2 - Varricatt et al. 2005; IRAS 20126+4104, from the apparently large precession angle - Shepherd et al. 2000). These large clumps may be capable of self-shielding against the large radiation pressure to a significant level, thereby aiding accre-

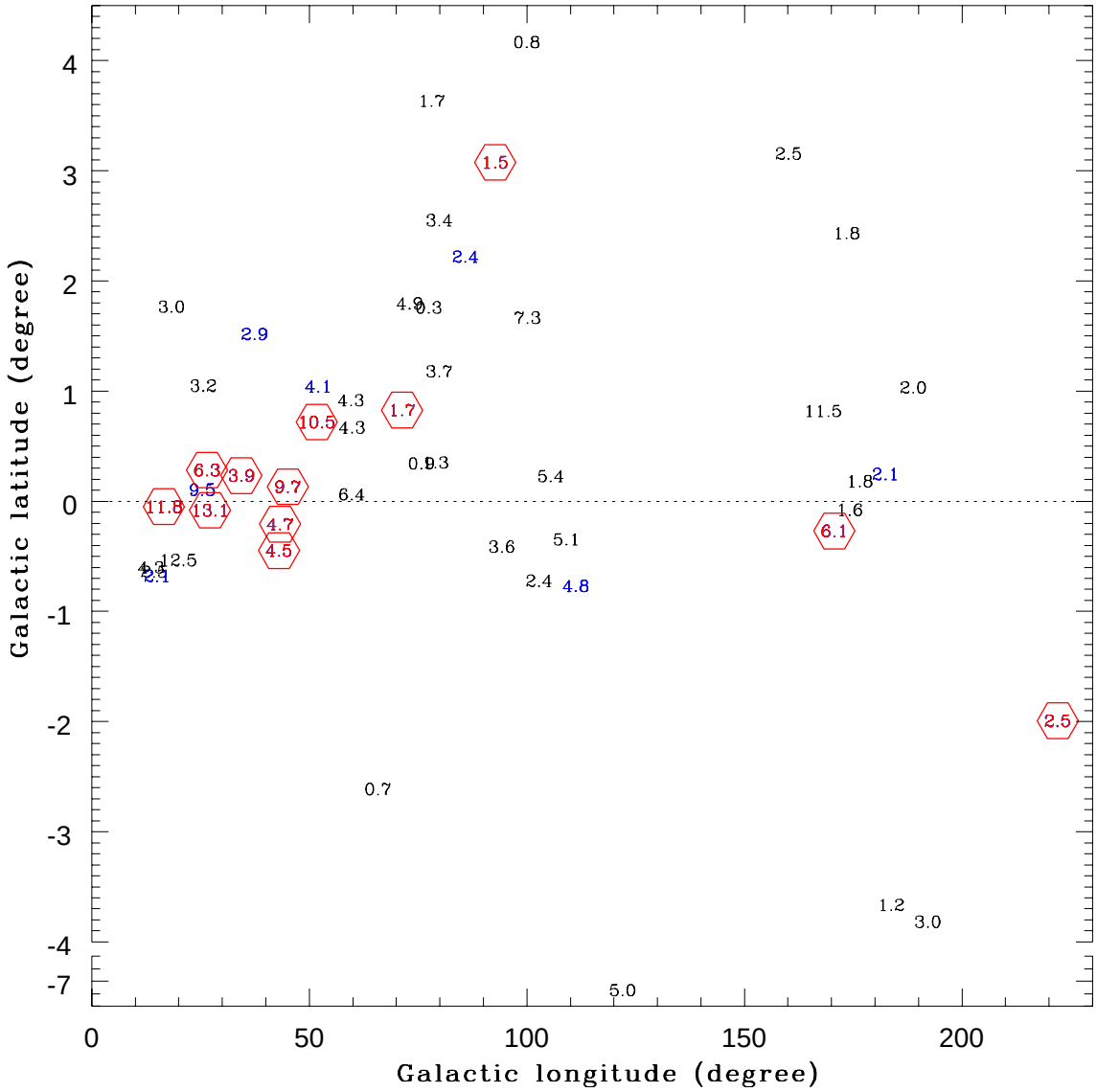

Figure 3. The location of the survey objects in the galactic coordinates. The fifty objects are labelled with their distances from the sun. Those from which outflows are positively detected in H_2 are shown black in colour and those with only a tentative detection of outflows in H_2 are shown in blue. The objects from which no H_2 outflows are seen in our images are shown in red and are enclosed in hexagons.

tion. This also points to the possibility of highly clumpy nature of the accretion discs.

It is noteworthy that with the present calculations (e.g. Yorke & Sonnhalter 2002) the scenario of radiation pressure halting the formation of massive stars by accretion is a problem only for very massive stars. The outflows from HMYSOs will also contribute to the reduction of radiation pressure on the accreted matter and thereby aid accretion (Krumholz et al. 2005). Our sample does not include any extremely massive object. The most luminous objects in our sample with outflows observed in H_2 are IRAS 18264 and 19410, which have L$\sim 10^5$ $L_\odot$. They may have single star ZAMS masses of $\sim$38 $M_\odot$ (M_{evol} from Vacca, Garmany & Shull 1996). However, IRAS 19410 is confirmed to host multiple YSOs and more than one are suspected to be present in IRAS 18264, which will further reduce their masses. Even within a dynamical time of $\sim 10^5$ years, with an accretion rate of $\sim 10^{-4}$ $M_\odot$year^{-1} (Zhang et al. 2005), these objects will accumulate only a maximum of a few 10's of $M_\odot$ more of matter. This will not take any of the 50 objects surveyed to the most massive limits, unless the accretion rate is significantly higher, frequent captures of dense clumps of gas and dust occur which will increase the effective accretion rate on the long run, or we are underestimating the present luminosity and mass. Indeed, some of the recent studies estimate accretion rates of $\sim 10^{-3}$ $M_\odot$year^{-1} (eg: Zapata et al. 2008 in W51-North; Sandell, Goss & Wright 2005 in NGC7538-IRS9).

3.3.2 *Objects that exhibit H_2 line emission*

Thirty eight objects in our sample exhibit H_2 line emission (Table 2). Twenty five of these (31 if we include the fields in which the detection of the jet in H_2 is only tentative) exhibit collimated emission. (For two objects, IRAS 18517 and 20444, the H_2 emission is very faint and doesn't appear to be from outflows). The HMYSOs are subject to very high interstellar extinction. If we integrate deeper, it is possible that we may detect H_2 emission from more. Except for a few cases, near-IR counterparts were detected

in our images for the YSOs driving the outflows. Their association with the H_2 line emission features, association with other tracers of star formation like millimetre or radio emission and masers, large reddening and excess and the location in the region of the near-IR colour-colour diagram (Fig. 1) occupied by YSOs suggest that we are detecting the driving sources of the outflows. Fig. 2 shows that these objects occupy specific regions in the MSX and IRAS colour-colour diagrams, which is indicative of the temperatures involved. Co-ordinates of YSOs identified and suspected YSOs are given throughout the text to enable future spectroscopic and high angular resolution investigations of these objects and their close environments.

3.3.3 Objects that do not exhibit any H_2 line emission

Twelve objects do not exhibit any H_2 emission at our level of sensitivity. These are: IRAS 05168, 06584, 18182, 18360, 18385, 18507, 19088, 19092, 19110, 19217, 20056 and 21078. For two other objects, IRAS 18517 and 20444, the H_2 emission is very faint and appears to be due to fluorescence. These 14 objects could be broadly classified into two different populations - the young and the old - based on whether they exhibit significant radio continuum emission or not. IRAS 05168, 06584, 18182, 18517, 19092, 20444 and 20056 did not exhibit any appreciable emission at radio frequencies, or the radio emission, when detected, was very weak. Among these, except for IRAS 05168, 06584 and 20444, near-IR counterparts of the YSOs are not positively identified in our images. These could represent very young objects. For IRAS 18517, it is possible that the YSO responsible for the CO outflow is not detected in our *K*-band image since it is highly embedded; for IRAS 18360, no radio observations have been reported; faint radio emission was detected from IRAS 20444 and it is probably a YSO of mid-B spectral type, in or approaching UCHII stage. The rest of the objects - IRAS 18385, 18507, 19088, 19110, 19217 and 21078 - do exhibit radio emission. Among these six objects, only two (IRAS 18385 and 21078) do not have convincing IR counterparts. For IRAS 19217, it is not clear if any of the NIR sources labelled on our image is the IR counterpart. Hence, the objects which exhibit radio emission and have NIR counterparts may be more evolved YSOs that are in the UCHII stage. The objects without any detected outflow in H_2 and without any significant radio emission are likely to be pre-UCHIIs that are in the early stages of their formation.

3.4 Do YSOs in the UCHII phase drive outflows?

Thirteen objects are seen with strong radio emission (more than a few mJy). Six of the strongest radio sources do not have any detection of jets in H_2 (IRAS 18385, 18507, 19088, 19110, 19217 and 21078). IRAS 18345 probably hosts an H_2 jet. The location of the radio source in this field is not available. However, our *K*-band image shows that there are possibly two YSOs in this field. For IRAS 19213 and 19374 the location of the radio sources do not agree with the possible locations of the YSOs identified from the IR colours. The remaining four objects (IRAS 20188, 20198, 20293 and 22570) have jets detected in H_2. However, the locations of the radio sources are offset from the driving sources of jets identified here or from the expected positions of the driving sources (the locations of the radio sources and the YSOs identified are labelled on the Figs. A1–A50). Thus, none of the strong radio emitters are convincingly associated with H_2 jets.

Among the 25 objects that are confirmed to be associated with H_2 jets, nine objects did not exhibit radio continuum emission. Out of the remaining 16, four objects have bright radio emission. For three of these bright radio emitters, IRAS 20198, 20293 and 22570, the radio sources are convincingly not the driving sources of the H_2 outflows (Fig. A38a, A41, A49) and for the fourth one (IRAS 20188, Fig. A37), the radio source appears to be different from the driving source of the H_2 jet, though it remains to be established. The remaining 12 objects are faint in radio. For some of these faint radio emitters, the radio sources detected are centred on the driving sources of the H_2 jets (eg. IRAS 05137, 05373, 05553, 18316, 20126); some of these are interpreted as emission from ionized jets (eg. IRAS 20126 - Hofner et al. 1999; IRAS 05553 - Shepherd & Kurtz 1999). Assuming that the strong radio sources are UCHIIs, we conclude that by the time the massive YSOs reach their UCHII phase, they would have already accumulated a major fraction of their main sequence mass, and thus, their accretion and outflow rates will be much lower when compared to those in the pre-UCHII stage. The location of the near-IR counterparts of UCHIIs close to the reddening band in the colour-colour diagram (Fig. 1) also suggests the same.

A massive YSO may still be accumulating mass after it has developed an HII region. Bulk rotation of molecular gas surrounding five massive UCHII objects have been detected recently by Klaassen et al. (2009). Ionized accretion have been proposed as a significant contributor to the growth of massive YSOs which have formed HII regions around them (eg. Keto 2002, 2003; Keto & Wood 2006); accretion and outflows are detected in some HCHII objects (eg. Keto & Klaassen 2008). However, it remains to be seen if this can add a large fraction of the existing mass after the star has appeared as a UCHII object.

4 SUMMARY AND CONCLUSIONS

(i) 76 % of our objects display H_2 emission. 50 % exhibit collimated outflows; including the objects with suspected collimated emission, this fraction would be 62%. These numbers should be considered as lower limits only. Even at 2.122 μm, the extinction will hamper the the detection of several outflows.

(ii) From the good agreement that we find between the centroids and directions of the outflows obtained from the aligned H_2 emission knots in our images and those deduced from the published CO maps, and from the available spectroscopic results suggesting shock excitation of the H_2 emission in jets, we conclude that the outflows are mainly jet-driven as in low-mass stars and not wind-driven.

(iii) Within the range of luminosities covered in our sample, the outflows are seen to be well collimated irrespective of the luminosities of their driving sources and are nearly as collimated as those from low-mass stars. Considering the main sequence spectral types of single stars corresponding to the luminosities of the outflow driving sources (Table 3), we infer that objects up to early B and late O-types produce collimated outflows, implying that disk accretion forms the main mechanism leading to their formation. However, accretion rates may be highly variable and non-uniform with the discs highly clumpy in nature and the individual clumps in the discs capable of self-shielding against the large radiation pressure to a significant level, thereby aiding accretion. Accretion rates larger than 10^{-4} $M_{\odot}$year^{-1} can produce even earlier spectral types. Accurate estimates of accretion rates are requiered to understand

Table 3. Outflow properties from our H_2 observations

No.	Object Name[1] (IRAS)	Outflow direction[2] (E of N)	Outflow length[3] (arcsec)	(parsec)[4]	Collimation factor	Log($L/L_\odot$)[4]	ZAMS sp. type[4,5]
2	04579+4703	125.5	>29.5	>0.35	7.3	3.59	B1.5
3	05137+3919(1)	19.1, 187	38	2.12	8.5	5.41	O8
	05137+3919(2)	166.5	14.5	0.81	6.6		
5	05274+3345(2)	313			??	3.64	B1.5
	05274+3345(1)	49	⩾33	⩾0.25			
6	05345+3157(I)	132	35.5	0.31	4.3	3.14	B3
	05345+3157(II)	36, 229	73	0.64			
7	05358+3543(I)	130.4	43.5	0.38	7.2	3.58	B1.5
	05358+3543(II)	170	83	0.72	18.8		
	05358+3543(III)	332.5	⩾48	⩾0.42	6.8		
8	05373+2349	45.5	20.5	0.12	2.55	2.67	B5
10	05553+1631	84, 287	66	0.97	1.9	4.07	B0.5
11	06061+2151	128	34	0.33	4.3	3.60	B1.5
13	18144-1723	274	18	0.38	10	4.33	B0.3
14	18151-1208(1)	131	⩾29	⩾0.42	⩾6.3	4.30	B0.3
	18151-1208(2)	35.5	10	0.15	5.7		
18	18264-1152	69.2, 286	⩾43.5	⩾0.74, ⩾2.64	7	4, 5.1	B0.5, O7
19	18316-0602	125, 315	50	0.77	4.5	4.64	B0.5
31	19388+2357					4.17	B0.5
32	19410+2336(II)	65	18	0.18, 0.56	4.1	4, 5	B0.5, O7
	19410+2336(I)	99.5	31.5	0.32, 0.98	3.8		
33	20050+2720	101	⩾28.3	⩾0.1	4	2.59	B5
35	20062+3550	43, 212	16	0.38	5.4	3.51	B2
37	20188+3928	0 and/or 50				2.54	B5
36	20126+4104(I)	122	⩾11.5	⩾0.09	5	4.00	B0.5
38	20198+3716	76.5 (and 61)			??	3.74	B1
39	20227+4154(II)	128	⩾20	⩾0.33	8.3	3.98	B0.7
	20227+4154(I)	239.5	24	⩽0.39	4.5		
40	20286+4105(1)	274			??	4.59	O9.5
	20286+4105(2)	329	7.5	0.14	??		
41	20293+3952	57				3.8, 3.4	B1, B2
44	21307+5049	141				3.6	B1.5
45	21391+5802	50	38	0.14	6.5	2.17	B7
	21391+5802	65	>27	>0.1	>9		
	21391+5802	128	9.9	0.04	4.6		
46	21519+5613(1)	48	8.1	0.29	3.3	4.28	B0.3
	21519+5913(2)	126.5	7.8	0.28	5.5		
47	22172+5549	189				3.26	B2.7
49	22570+5912(1)	149	15	0.37	11.5	4.7	O9
	22570+5912(2)	50.7	7	0.17	4.5		

[1]When multiple outflows are detected, outflow numbers (labelled on Figs. A1–A50) are given in brackets; [2]two values are given when the two lobes of the bipolar outflow deviate from a straight line containing the central source identified; [3]lower limits only since these are not corrected for the (unknown) angle of inclination (this will also affect the collimation factors derived); a "⩾" is shown against some sources since additional H_2 emission features could be a part of the outflows which will inrease the outflow length. These will in turn increase the collimation factors too; [4]two values separated by a comma are given when there is distance ambiguity; [5]ZAMS spectral types corresponding to the luminosites from Panagia (1973) (for B3 and early spectral types) and from Morton & Adams (1968) (for spectral types later than B3)

the formation of massive stars at the very high end of the ZAMS mass limit.

(iv) For the objects that exhibited H_2 line emission in our survey, except for a few cases, near-IR counterparts were detected in our images for the YSOs driving the outflows. These objects occupy specific regions in the MSX colour-colour diagram, which is indicative of the temperatures involved. Co-ordinates of YSO candidates identified are given throughout the text to enable future spectroscopic and high angular resolution investigations of these objects and their close environments.

(v) Fourteen objects from which H_2 emission was either not detected or, when detected, was suspected to be due to fluorescence could be broadly classified into two different populations - the young and the old - based on whether they exhibit significant radio continuum emission or not. The objects which exhibit radio emission and have NIR counterparts may be more evolved YSOs that are in the UCHII stage. The objects without any detected outflow in H_2 and without any significant radio emission are likely to be pre-UCHIIs that are in the early stages of their formation.

(vi) From the non-detection of strong H_2 jets from confirmed UCHIIs, we conclude that by the time the massive YSOs reach their UCHII phase, they would have already accumulated a major fraction of their main sequence mass, and thus, their accretion and outflow rates will be much lower when compared to pre-UCHIIs. The lack of high infrared excess implied by the location of the near-IR counterparts of UCHIIs close to the reddening band in the colour-

colour diagram (Fig. 1) also suggests that they have less circumstellar material than for pre-UCHIIs objects. Recent studies show that ionized accretion may significantly increase the mass of YSOs, which have already developed HII regions; it is to be understood how efficient it will be to add a significant amout of mass after they appear as UCHIIs.

(vii) As can be seen in Fig. 2 (right panel), most of our objects, which are a mixture of UCHIIs and pre-UCHIIs, are located within the region for UCHIIs defined by Wood & Churchwell (1989a). This shows that the objects identified by the colour criteria of Wood & Churchwell (1989a) are not always UCHIIs. Instead, they represent luminous YSOs which are UCHIIs and pre-UCHIIs located in clusters (see also Bik 2004).

(viii) The close spatial locations of the objects resolved in our *K*-band images is suggestive of a very large fraction of binarity or multiplicity (confirmation of which may need long term spectroscopic monitoring and multi-colour high angular resolution photometry). Several new clusters are revealed; multiple outflows are also observed in many of these clusters. Our study shows that poor collimation factors derived in many (if not all) of the outflow maps in CO are due to unresolved multiple outflows (e.g. IRAS 05137, 05345, 05358, 18151, 18316, 19410, 20227, etc., where we resolve multiple jets in H_2). Some of these have recently been resolved in CO itself with high angular resolution interferometric mapping (e.g. 05358 - Beuther et al. 2002a).

(ix) As previously observed by many other investigators, intermediate and high-mass stars form mostly in clusters and are associated with lower mass star formation.

(x) There are several candidate clusters in our sample which display a ring, arc, or flattened morphology (e.g. IRAS 05274, 06061, 20050, 20056, 20188, 21519, 22172, 22570). Another example outside this work is the ring cluster imaged by Kumar, Ojha & Davis (2003). The possible reasons for their morphologies need to be investigated.

(xi) Brγ emission is not detected in any of the outflows; as is the case with jets from low-mass YSOs, it remains a poor tracer of outflows from young stars. It is instead a better tracer of accretion process and has been used to measure accretion rates in both low and high-mass YSOs (e.g. Blum et al. 2004; Folha & Emerson 2001; Muzerolle, Hartmann & Calvet 1998). Brγ emission is detected from some the outflow driving sources identified by us (e.g. IRAS 04579 - Ishii et al. 2001 and our Fig. A2; IRAS 05137 - Ishii et al. 2001; IRAS 18151 - Davis et al. 2004).

ACKNOWLEDGMENTS

The United Kingdom Infrared Telescope is operated by the Joint Astronomy Centre on behalf of the Science and Technology Facilities Council (STFC) of the U.K. We have made use of 2MASS data obtained as a part of Two Micron All Sky Survey, a joint project of University of Massachusetts and the Infrared Processing and Analysis Centre/California Institute of Technology. This research has also made use of IRAS and MSX data products, and SIMBAD database operated by CDS, Strasbourg, France. We thank the referee Thomas Stanke for carefully going through the text and giving valuable inputs which have improved the quality of the paper.

REFERENCES

Ayala S., Curiel, S., Raga A. C., Noriega-Crespo A., Salas L., 1998, A&A, 332, 1055
Anandarao B. G., Chakraborty A., Ojha D. K., Testi L., 2004, A&A, 421, 1045
Anglada G., Sepulveda I., Gomez J. F., 1997, A&A, 325, 25
Araya E., Hofner P., Churchwell E., Kurtz S., 2002, ApJS, 138, 63
Bachiller R., Fuente A., Tafalla M., 1995, ApJ, 445, L51
Bally J., 2002, ASPC, 267, 219
Bally J., Zinnecker H., 2005, AJ, 129, 2281
Baudry A., Desmurs J. F., Wilson T. L., Cohen R. J., 1997, A&A, 325, 255
Beech M., Mitalas R., 1994, ApJS, 95, 517
Behrend R., Maeder A., 2001, A&A, 373, 190
Beltrán M. T., Girart J. M., Estalella R., Ho P. T. P., Palau A., 2002, ApJ, 573, 246
Beltrán M. T., Girart J. M., Estalella R., Ho P. T. P., 2004, A&A, 426, 941
Beltrán M. T., Cesaroni R., Neri R., Codella C., Furuya R. S., Testi L., Olmi L., 2005, A&A, 435, 901
Blum R. D., Barbosa C. L., Damineli A., Conti P. S., Ridgway S., 2004, ApJ, 617, 1167
Bernard J. P., Dobashi K., Momose M., 1999, A&A, 350, 197
Beuther H., Schilke P., Geuth F., McCaughrean M. J., Andersen M., Sridharan T. K., Menten K. M., 2002a, A&A, 387, 931
Beuther H., Schilke P., Menten K. M., Motte F., Sridharan T. K., Wyrowski F., 2002b, ApJ, 566, 945
Beuther H., Schilke P., Sridharan T. K., Menten K. M., Walmsley C. M., Wyrowski F., 2002c, A&A, 383, 892
Beuther H., Walsh A., Schilke P., Sridharan T. K., Menten K. M., Wyrowski F., 2002d, A&A, 390, 289
Beuther H., Schilke P., Stanke T., 2003, A&A, 408, 601
Beuther H., Schilke P., Gueth F., 2004a, ApJ, 608, 330
Beuther H., Schilke P., Wyrowski F., 2004b, ApJ, 615, 832
Beuther H., Zhang Q., Sridharan T. K., Lee C.-F., Zapata L. A., 2006, A&A, 454, 221
Bik A., 2004, Ph.D. thesis, University of Amsterdam
Błaszkiewicz L., Kus A. J., 2004, A&A, 413, 233
Bonnell I. A., Bate M. R., Zinnecker H., 1998, MNRAS, 298, 93
Bontemps S., Andre P., Tereby S., Cabrit S., 1996, A&A, 311, 858
Brand J., Blitz L., 1993 A&A, 275, 67
Brand J. et al., 1994, A&AS, 103, 541
Brand J., Cesaroni R., Palla F., Molinari S., 2001, A&A, 370, 230
Bronfman L., Nyman L. A., May J., 1996, A&AS, 115, 81
Cabrit S., Bertout C., 1986, ApJ, 307, 303
Campbell B., Persson S. E., Matthews K., 1989, AJ, 98, 643
Carral P., Kurtz S. E., Rodriguez L. F., de Pree C., Hofner P., 1997, ApJ, 486, L103
Caratti O Garatti A., Froebrich D., Eislöffel J., Giannini T., Nisini B., 2008, A&A, 485, 137
Cardelli J. A., Clayton G. C. & Mathis J. S., 1989, ApJ, 345, 245
Carpenter J. M., Snell R. L., Schloerb F. P., Skrutskie M. F., 1993, ApJ, 407, 657
Carpenter J. M., Snell R. L., Schloerb F. P., 1995, ApJ, 450, 201
Casoli F., Combes F., Dupraz C., Gerin M., Boulanger F., 1986, A&A, 169, 281
Caswell J. L., Vaile R. A., Ellingsen S. P., Whiteoak J. B., Norris R. P., 1995, MNRAS, 272, 96
Caswell J. L., 1997, MNRAS, 289, 203
Cesaroni R., Palagi F., Felli M., Catarzi M., Comoretto G., Di

Franco S., Giovanardi C., Palla F., 1988, A&AS, 76, 445
Cesaroni R., Felli M., Testi L., Walmsky C. M., Olmi L., 1997, A&A, 325, 725
Cesaroni R., Felli M., Jenness T., Neri R., Olmi L., Robberto M., Testi L., Walmsley C. M.,1999a, A&A, 345, 949
Cesaroni R., Felli M., Walmsley C. M., 1999b, A&AS, 136, 333
Cesaroni R., Neri R., Olmi R., Testi L., Walmsley C. M., Hofner P., 2005, A&A, 434, 1039
Chen H., Tafalla M., Greene T. P., Myers P. C., Wilner D. J., 1997, ApJ, 475, 163
Chen Y., Yao Y., Yang J., Hirao T., Ishii M., Nagata T., Sato S., 1999, AJ, 117, 446
Chen Y. F., Yao Y. Q., Yang J., Zeng Q., Sato S., 2003, A&A, 405, 655
Chini R., Elsäesser H., Neckel T., 1980, A&A, 91, 186
Chini R., Kreysa E., Mezger P. G., Gemünd H.-P, 1986, A&A, 154, L8
Chini R., Ward-Thompson D., Kirk J. M., Nielbock M., Reipurth B., Sievers A., 2001, A&A, 369, 155
Chini R., Hoffmeister V., Kimeswenger S., Nielbock M., Nürnberger D., Schmidtobreick L., Sterzik M., 2004, Nature, 429, 155
Churchwell E., 1999, in NATO science series, Vol. 540, ed. Lada C. J. and Kylafis D., p. 515
Codella C., Bachiller R., Nisini B., Saraceno P., Testi L., 2001, A&A, 376, 271
Codella C., Felli M., Natale V., 1996, A&A, 311, 971
Comoretto G. et al., 1990, A&AS, 84, 179
Comerón F., Torra J., 2001, A&A, 375, 539
Carnkner L., Kozak J. A., Feigelson E. D., 1998, AJ, 116, 1933
Davis C. J. et al., 2009, A&A, 496, 153
Davis C. J., Gell R., Khanzadyan T., Smith M. D., Jenness T., 2009, A&A (arXiv, 0910.5274)
Davis C. J., Moriarty-Schieven G. H., Eislöffel J., Hoare M. G., Ray T. P., 1998, AJ, 115, 1118
Davis C. J., Varricatt W. P., Todd S. P., Ramsay Howat S. K., 2004, A&A, 425, 981
De Buizer J. M., 2003, MNRAS, 341, 277
De Buizer J. M., 2007, ApJ, 654, L147
De Buizer J. M., Radomski J. T., Telesco C. M., Piña R. K., 2005, ApJS, 156, 179
De Buizer J. M., Redman R. O., Longmore S. N., Caswell J., Feldman P. A., 2009, A&A, 493, 127
Dent W. R. F., MacDonald G. H., Andersson M., 1988, MNRAS, 235,1397
Devine D., Bally J., Reipurth B., Shepherd D., Watson A., 1999, AJ, 117, 2919
Dobashi K. et al., 1995, PASJ, 47, 837
Edris K. A., Fuller G. A., Cohen R. J., Etoka S., 2005, A&A, 434, 213
Estalella R., Mauersberger R., Torrelles J. M., Anglada G., Gómez J. F., López R., Muders D., 1993, ApJ, 419, 698
Faúndez S., Bronfman L., Garay G., Chini R., Nyman L.-Å., May J., 2004, A&A, 426, 97
Felli M., Churchwell E., Massi M., 1984, A&A, 136, 53
Felli M., Johnston K. J., Churchwell E., 1980, ApJ, 242, L157
Felli M., Palagi F., Tofani G., 1992, A&A, 255, 293
Fich M., Dahl G. P., Treffers R. R., 1990, AJ, 99, 622
Folha D. F. M., Emerson J. P, 2001, A&A, 365, 90
Fontani F., Cesaroni R., Testi L., Molinari S., Zhang Q., Brand J., Walmsley C. M., 2004, A&A, 424, 179
Forster J. R., Welch W. J., Wright M. C. H., Baudry A., 1978, ApJ, 221, 137
Forster J. R., Caswell J. L., 1999, A&AS, 137, 43
Galt J., 2004, AJ, 127, 3479
Goddi C., Moscadelli L., Alef W., Brand J., 2004, A&A, 420, 929
Goddi C., Moscadelli L., Alef W., Tarchi A., Brand J., Pani M., 2005, A&A, 432, 161
Gredel R., 2006, A&A, 457, 157
Gyulbudaghian A. L., Rodriguez L. F., Curiel S., 1990, RMxAA, 20, 51
Hanson M. M., Luhman K. L., Rieke G. H., 2002, ApJS, 138, 35
Hardebeck E. G., Wilson W. J., 1971, ApJ, 169, L123
Harju J., Lehtinen K., Booth R. S., Zinchenko I., 1998, A&AS, 132, 211
Hodapp K.-W., 1994, ApJS, 94, 615
Hofner P., Churchwell E., 1996, A&AS, 120, 283
Hofner P., Cesaroni R., Rodríguez L. F., Martí J., 1999, A&A, 345, L43-46
Hughes V. A., MacLeod G. C., 1993, ApJ, 105, 1495
Hughes V. A., MacLeod G. C., 1994, ApJ, 427, 857
Hunter T. R., Testi L., Taylor G. B., Tofani G., Felli M., Phillips T. G., 1995, A&A, 302, 249
Hunter T. R., Phillips T. G., Menten K. M., 1997, ApJ, 478, 283
Hunter T. R., Testi L., Zhang Q., Sridharan T. K., 1999, AJ, 118, 477
Hunter T. R., Churchwell E., Watson C., Cox P., Benford D. J., Roelfsema P. R., 2000, AJ, 119, 2711
Indebetouw R., Watson C., Johnson K. E., Whitney B., Churchwell E., 2003, ApJ, 596, L83
Ishii M., Nagata T., Sato S., Yao Y., Jiang Z., Nakaya H., 2001, AJ, 121, 3191
Ishii M., Hirao T., Nagashima C., Nagata T., Sato S., Yao Y., 2002, AJ, 124, 430
Jijina J., Adams F., 1996, 462, 874
Jijina J., Myers P. C., Adams F. C., 1999, ApJS, 125, 161
Jenness T., Scott P. F., Padman R., 1995, MNRAS, 276, 1024
Johnson C. O., Depree C. G., Goss W. M., 1998, ApJ, 500, 302
Jourdain De Muizon M., D′Hendecourt L. B., Geballe T. R. 1990, A&A, 227, 526
Keto E., 2002, ApJ, 568, 754
Keto E., 2003, ApJ, 599, 1196
Keto E., Klaassen P., 2008. ApJ, 678, L109
Keto E., Wood K., 2006, ApJ, 637, 850
Khanzadyan T., Smith M. D., Davis C. J., Stanke T., 2004, A&A, 418, 163
Kim K-T., Kurtz S. E, 2006, ApJ., 643, 978
Klaassen P. D., Wilson C. D., Keto E. R., Zhang Q., ApJ, 703, 1308
Koornneef J., 1983, A&A, 128, 84
Kraemer K. E. et al., 2003, ApJ, 588, 918
Krumholz M. R., McKee C. F., Klein R. I., 2005, ApJ, 618, L33
Kumar M. S. N., Bachiller R., Davis C. J., 2002, ApJ, 576, 313
Kumar M. S. N., Ojha D. K., Davis C. J., 2003, ApJ, 598, 1107
Kurtz S., 2005, IAUS, 227, 111
Kurtz S., Hofner P., 2005, AJ, 130, 711
Kurtz S., Churchwell E., Wood D. O. S., 1994, ApJS, 91, 659
Kurtz S., Hofner P., Álvarez C. V., 2004, ApJS, 155, 149
Lada C. J. & Adams F. C., 1992, ApJ, 393, 278
Lebrón M., Beuther H., Schilke P., Stanke T., 2006, A&A, 448, 1037
Little L. T., Bergman P., Cunningham C. T., Heaton B. D., Knee L. B. G., MacDonald G. H., Richards P. J., Toriseva M., 1988, A&A, 205, 129

Matthews N., Anderson M., MacDonald G. H., 1986, A&A, 155, 99
MacLeod G. C., Scalise E. Jr., Saedt S., Galt J. A., Gaylard M. J., 1998a, AJ, 116, 1897
MacLeod G. C., Van Der Walt D. J., North A., Gaylard M. J., Galt J. A., Moriarty-Schieven G. H., 1998b, AJ, 116, 2936
Massi M., Felli M., Churchwell E., 1988, A&A, 194, 116
McCutcheon W. H., Sato T., Purton C. R., Matthews H. E., Dewdney P. E., 1995, AJ, 110, 1762
Menten K. M., 1991, ApJ, 380, L75
Menten K. M., 1996, 1996, IAUS, 178, 163
Meyer M. R., Calvet N., Hillenbrand L. A., 1997, AJ, 114, 288
Migenes V. et al., 1999, ApJS, 123, 487
Minier V., Conway J. E., Booth R. S., 2001, A&A, 369, 278
Minier V., Burton M. G., Hill T., Pestalozzi M. R., Purcell C. R., Garay G., Walsh A. J., Longmore S., 2005, A&A, 429, 945
Miralles, M. P,, Rodriguez L. F., Scalise E., 1994, ApJS, 92, 173
Molinari S., Brand J., Cesaroni R., Palla F., 1996, A&A, 308, 573
Molinari S., Brand J., Cesaroni R., Palla F., Palumbo G. G. C., 1998, A&A, 336, 339
Molinari S., Brand J., Cesaroni R., Palla F., 2000, A&A, 355, 617
Molinari S., Testi L., Rodríguez L. F., Zhang Q. 2002, ApJ, 570, 758
Molinari S., Pezzuto S., Cesaroni R., Brand J., Faustini F., Testi L., 2008, A&A, 481, 345
Morton D. C., Adams T. F, 1968, ApJ, 151, 611
Moscadelli L., Cesaroni R., Rioja M. J., 2000, A&A, 360, 663
Moscadelli L., Cesaroni R., Rioja M. J., 2005, A&A, 438, 889
Muzerolle J., Hartmann L., Calvet N., 1998, AJ, 116, 2965
Nakano T., Hasegawa T., Norman C., ApJ, 450, 183
Nielbock M., Chini R., Hoffmeister V. H., Scheyda C. M., Steinacker J., Nuernberger D., Siebenmorgen R., 2007, ApJ, 656, L81
Nisini B., Massi F., Vitali F., Giannini T., Lorenzetti D., Di Paola A., Codella C., D'Alessio F., Speziali R., 2001, A&A, 376, 553
Odenwald S. F., Schwartz P. R., 1989, ApJ, 345, L47
Osterloh M., Henning T., Launhardt R., 1997, ApJS, 110, 71
Palagi F., Cesaroni R., Comoretto G., Felli M., Natale V., 1993, A&AS, 101, 153
Palla F., Stahler S. W., 1993, ApJ, 418, 414
Palla F., Brand J., Cesaroni R., Comoretto G., Felli M., 1991, A&A, 246, 249
Palla F., Cesaroni R., Brand J., Caselli P., Comoretto G., Felli M., 1993, A&A, 280, 599
Panagia N., 1973, AJ, 78, 929
Patel N. A., Greenhill L. J., Herrnstein J., Zhang Q., Moran J. M., Ho P. T. P., Goldsmith P. F., 2000, ApJ, 538, 268
Patel N. A. et al., 2005, Natur., 437, 109
Porras A., Cruz-González I., Salas L., 2000, A&A, 361, 660
Pudritz R. E., Norman C. A., 1983, ApJ, 274, 677
Ramesh B., Bronfman L., Deguchi S., 1997, PASJ, 49, 307
Reipurth B., Armond T., Raga A., Bally J., 2003, ApJ, 593, L47
Richer J. S., Shepherd D. S., Cabrit S., Bachiller R., Churchwell E., 2000, in Protostars and Planets IV, ed. V. Mannings, A. P. Boss, S. S. Russell, Univ. Arizona Press, Tucson, p. 867
Ridge N. A., Moore T. J. T., 2001, A&A, 378, 495
Ridge N. A., Wilson T. L., Megeath S. T., Allen L. E., Myers P. C., 2003, AJ, 126, 286
Roche P. F. et al., 2003, in Iye M., Moorwood A. F., eds, Proc. SPIE, Vol.4841, Instrument Design and Performance for Optical/IR Ground-based Telescopes., SPIE, Bellingham, p. 901
Sandell G., Goss W. M., Wright M., 2005, ApJ, 621, 839
Saraceno P. et al., 1996, A&A, 315, L293
Schutte A. J., van der Walt D. J., Gaylard M. J., MacLeord G. C., 1993, MNRAS, 261, 783
Sewilo M., Churchwell E., Kurtz S., Goss W. M., Hofner P., 2004, ApJ, 605, 285
Shepherd D. S., Churchwell E., 1996a, ApJ, 457, 267
Shepherd D. S., Churchwell E., 1996b, ApJ, 472, 225
Shepherd D. S., Kurtz S. E., 1999, ApJ, 523, 690
Shepherd D. S., Churchwell E., Wilner D. J., 1997, ApJ, 482, 355
Shepherd D. S., Watson A. M., Sargent A. I., Churchwell E., 1998, ApJ, 507, 861
Shepherd D. S., Yu K. C, Bally J., Testi L., 2000, 535, 833
Shepherd D. S., Claussen M. J., Kurtz S. E., 2001, Sci, 292, 1513
Shepherd D. S., Borders T., Claussen M., Shirley Y., Kurtz S., 2004a, ApJ, 614, 211
Shepherd D. S., Nürnberger D. E. A., Bronfman L., 2004b, ApJ, 602, 850
Shu F., Najita J., Ostriker E., Wilkin F., Ruden S., Lizano S., 1994, ApJ, 429, 781
Slysh V. I., Dzura A. M., Val'tts I. E., Gerard E., 1994, A&AS, 106, 87
Slysh V. I., Val'tts I. E., Kalenskii S. V., Voronkov M. A., Palagi F., Tofani G., Catarzi M., 1999, A&AS, 134, 115
Snell R. L., Dickman R. L., Huang Y. -L., 1990, ApJ, 352, 139
Snell R. L., Huang Y. -L., Dickman R. L., Claussen M. J., 1988, ApJ, 325, 853
Sridharan T. K., Beuther H., Schilke P., Menten K. M., Wyrowski F., 2002, ApJ, 566, 931
Sridharan T. K., Williams S. J., Fuller G. A., 2005, ApJ, 631, L73-L76
Stahler S. W, Palla F., Ho P. T. P., 2000, in Protostars and Planets IV, ed. V. Mannings, A. P. Boss, S. S. Russell, Univ. Arizona Press, Tucson, p. 327
Sugitani K., Fukui Y., Mizuni A., Ohashi N., 1989, ApJ, 342, L87
Su Y-N, Zhang Q., Lim J., 2004, ApJ, 604, 258
Szymczak M., Hrynek G., Kus A. J., 2000, A&AS, 143, 269
Testi L., Felli M., Persi P., Roth M., 1994, A&A, 288, 646
Thompson M. A., Hatchell J., Walsh A. J., MacDonald G. H.; Millar T. J., 2006, A&A, 453, 1003
Todd S. P., Ramsay Howat S. K., 2006, 367, 238
Tofani G., Felli M., Taylor G. B., Hunter T. R., 1995, A&AS, 112, 299
Torrelles J. M., Eiroa C., Miranda L. F., Mauersberger R., Estalella R., Anglada G., 1992a, ApJ, 384, 528
Torrelles J. M., Gómez J. F., Anglada G., Estalella R., Mauersberger R., Eiroa C., 1992b, 392, 616
Torrelles J. M., Gómez J. F., Rodriguez L. F., Curiel S., Ho P. T. P., Garay G., 1996, ApJ, 457. L107
Torrelles J. M.. Gómez J. F., Rodrguez L. F., Curiel S., Anglada G., Ho P. T. P., 1998, ApJ, 505, 756
Vacca W. D., Garmany C. D., Shull M. J., 1996, ApJ, 460, 914
Van Der Walt D. J., Gaylard M. J., Macleod G. C., 1995, A&AS, 110, 81
Varricatt W. P., Davis C. J., Adamson A. J., 2005, MNRAS, 359, 2
Verdes-Montenegro L., Torrelles J. M., Rodriguez L. F., Anglada G., Lopez R., Estalella R., Canto J., Ho P. T. P., 1989, ApJ, 346, 193
Vig S., Ghosh S. K., Kulkarni V. K., Ojha D. K., Verma R. P., 2006, ApJ, 637, 400
Walsh A. J., Hyland A. R., Robinson G., Burton M. G., 1997, MNRAS, 291, 261

Walsh A. J., Burton M. G., Hyland A. R., Robinson G., 1998, MNRAS, 301, 640
Walsh A. J., Macdonald G. H., Alvey N. D. S., Burton M. G., Lee J.-K., 2003, A&A, 410, 597
Watson C., Araya E., Sewilo M., Churchwell E., Hofner P., Kurtz S., 2003, ApJ, 587, 714
Wilking B. A., Mundy L. G., Blackwell J. H., Howe J. E., 1989, ApJ, 345, 257
Wilking B. A., Blackwell J. H., Mundy L. G., 1990, AJ, 100, 758
Wilking B., Mundy L., McMullin J., Hezel T., Keene J., 1993, AJ, 106, 250
Williams S. J, Fuller G. A., Sridharan T. K., 2004, A&A, 417, 115
Williams S. J, Fuller G. A., Sridharan T. K., 2005, A&A, 434, 257
Wolfire M. G., Cassinelli J. P., 1987, ApJ, 319, 850
Wood D. O. S., Churchwell E., 1989a, ApJ, 340, 265
Wood D. O. S., Churchwell E., 1989b, ApJS, 69, 831
Wouterloot J. G. A., Brand J., 1989, A&AS, 80, 149
Wouterloot J. G. A., Brand J., Fiegle K., 1993, A&AS, 98, 589
Wu Y., Wei Y., Zhao M., Shi Y., Yu W., Qin S., Huang M., 2004, A&A, 426, 503
Wu Y., Wu J., Wang J., 2001, A&A, 380, 665
Yao Y., Ishii M., Nagata T., Nakaya H., Sato S., 2000, ApJ, 542, 392
Yorke H. W., Krügel E., 1977, A&A, 54, 183
Yorke H., Sonnhalter C., 2002, ApJ, 569, 846
Zavagno A., Cox P., Baluteau J.-P., 1992, A&A, 259, 241
Zavagno A., Deharveng L., Nadeau D., Caplan J., 2002, A&A, 394, 225
Zhang Q., Hunter T. R., Sridharan T. K., 1998, ApJ, 505, L151
Zhang Q., Hunter T. R., Sridharan T. K., Cesaroni R., 1999, ApJ, 527, L117
Zhang Q., Hunter T. R., Brand J., Sridharan T. K., Molinari S., Kramer M., Cesaroni R., 2001, ApJ, 552, L167
Zhang Q., Hunter T. R., Sridharan T. K., Ho P. T. P., 2002, ApJ, 566, 982
Zhang Q., Hunter T. R., Brand J., Sridharan T. K., Cesaroni R., Molinari S., Wang J., Kramer M., 2005, ApJ, 625, 864
Zapata L. A., Rodríguez L. F., Ho P. T. P., Beuther H., Zhang Q., 2006, AJ, 131, 939
Zapata L. A., Ho, P. T. P., Schilke P., Rodríguez L. F., Menten K., Palau A., Garrod R. T., 2009, ApJ, 698, 1422
Zapata L. A., Palau A., Ho P. T. P., Schilke P., Garrod R. T., Rodríguez, L. F., Menten, K., 2008, A&A, 479, L25
Zinchenko I., Henkel C., Mao R. Q., 2000, A&A, 361, 1079
Zoonematkermani S., Helfand D. J., Becker R. H., White R. L., Perley R. A., 1990, ApJS, 74, 181

APPENDIX A: RESULTS AND DISCUSSION ON INDIVIDUAL SOURCES

All of the YSO fields observed in the survey are discussed individually below in fifty subsections (A1–A50). Table 2 summarizes the details on each source, including previous observations and our H_2 detections. The order of presentation of the sources in the discussion below is the same as in Tables 1 & 2; the subsection numbers of the sources agree with their reference numbers in column 1 of the tables. The figures are also named accordingly. Conclusions from our images are discussed in context with existing observations. The *K*-band images are presented in all cases; H_2 and Brγ images are shown only when line emissions are detected at these wavelengths. H_2 emission line features are marked with circles, or dotted or dashed arrows and are numbered. We use letters for labelling point sources. The coordinates of several sources of interest detected in our images are listed throughout the paper. The coordinates given are in the J2000 epoch. The convention adopted is - the source label ("A, B" etc.; RA(α)=hours:minute:seconds, Dec(δ)=deg:arcmin:arcsec). The IRAS positions are marked on each figure using a "$\triangle$" sign. The positions of the objects detected by MSX (except for source 1, which does not have MSX observations available) are shown with a "+" sign. These are not specifically mentioned anywhere else in the text except for Figs. 1 and 2. Millimetre or sub-mm continuum peaks are marked on some of the images with a "*" sign; radio continuum positions are marked with "x". When a millimetre or radio position from an additional source of data is plotted on a figure, we use "#". Since the wavelengths and the literature from which the mm and radio observations were taken are different for each source, these are listed in the figure captions and in the text. A compilation of the spatial resolutions and pointing accuracies of the previous observations of these sources is given in Appendix B (Table C1) to help the readers understand the possible association of the YSO candidates identified by us in the near-IR with the YSOs identified in the long wavelength studies before. Since north-east, south-west, etc. are used frequently in the text, we have abbreviated these with NE, SW, etc.

A1 IRAS 00420+5530 – *Mol 3*

(*d = 5.0; 7.72 kpc, L = (12.4; 51.8)*$\times 10^3\ L_\odot$)

IRAS 00420+5530 was identified as a candidate high mass protostar based on its IRAS colours (Palla et al. 1991; Molinari et al. 1996). A series of survey papers show that the source is associated with NH_3 emission (Molinari et al. 1996) and with H_2O maser emission (Migenes et al. 1999; Palla et al. 1991; Brand et al. 1994). No 6.7-GHz CH_3OH maser was seen by Szymczak, Hrynek, Kus (2000). The lack of detected radio continuum (Molinari et al. 1998) combined with the other observed properties suggests that this source is young. Jenness, Scott & Padman (1995) detected an 850-μm source at a flux level of 5.7 Jy with a positional offset of 4.5 arcsec east and 23 arcsec south from the IRAS position. They detected ^{12}CO and C^{18}O emission from this region at -52 and -51.8 km s^{-1} respectively and weak H_2O maser emission at -45 km s^{-1} close to the 850-μm peak. They did not detect any radio continuum emission at 3.6 cm above a flux density of 0.3 mJy. Attribution of the line shapes to one or other of the properties of protostars (outflow, infall, different velocity components within the beam) was not possible with the sub-mm data. ^{13}CO (J=1-0) was detected by Wu, Wu & Wang (2001), who report no evidence of any velocity structure in their 55-arcsec beam. Brand et al. (2001) detected extended clumps of emission from ^{13}CO (2-1), C^{18}O (2-1), CS(3-2), C^{34}S(3-2) and HCO$^+$(1-0) peaking 24 arcsec south of the IRAS position. With the exception of the CS emission, which is more of a tracer of dense gas from the core, all lines show red and blue shifted components. Brand et al. (2001) estimated a lower limit for the total mass of the molecular material (from the ^{13}CO emission) to be 2.8×10^3 M$_\odot$.

Our near-IR images (Fig. A1) reveal a cluster of objects within the 2.2×2.2-arcmin^2 field. The 2MASS colours of the brightest of the near-IR sources located close to the IRAS position do not exhibit any IR excess. However, we see a set of IR-bright objects located close to the peak of the sub-mm continuum and the line emissions. Three objects are labelled here - "A"(α=00:44:58.30, δ=+55:46:49.7), "B"(α=00:44:58.03,

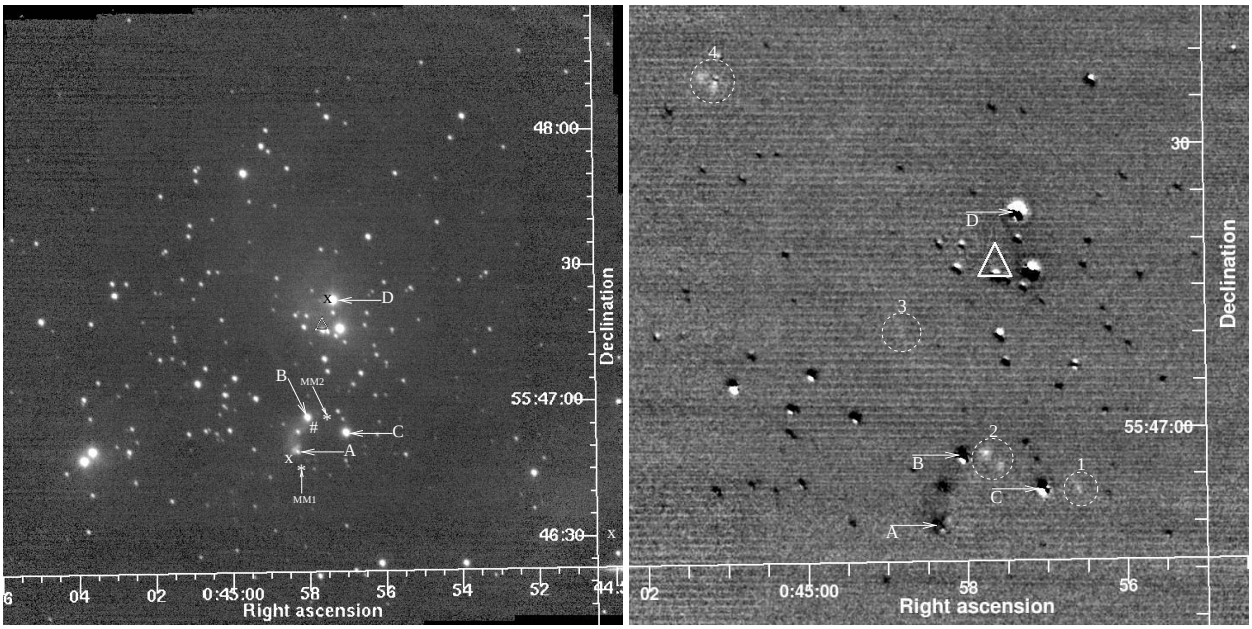

Figure A1. The left panel shows the *K*-band image of IRAS 00420+5530. The right panel shows the central part of the continuum-subtracted H_2 image. "△" shows the location of the IRAS source. The 850 μm position of Jenness et al. (1995) is shown by "#". "*" shows the two unresolved 3.4-mm continuum sources (MM1 and MM2) and "x" shows the 3.6-cm emission peaks of Molinari et al. (2002).

δ=+55:46:57.2) and "C"(α=00:44:57.03, δ=+55:46:53.8). All three objects show IR excess in Fig. 1, with "C" having the lowest excess of the three. "A" and "B" are apparently connected by nebulosity and there is a fainter object embedded in it, which was not detected by 2MASS. There is also a 'cap-like' nebulosity seen in the east and north directions of "A" at a separation of ∼1 arcsec from the star. The nebulosity disappears in the continuum-subtracted H_2 image. However, the H_2 image shows some faint line emission features which are circled on Fig. A1 and labelled "1–4". These are likely to be produced by an outflow in the field. At the present depth of integration, we cannot say for sure if more than one outflow is involved in producing the observed H_2 emission features. The two unresolved 3.4-mm sources detected by Molinari et al. (2002), the sub-mm source of Jenness et al. (1995) and the water masers are all located in the vicinity of the sources "A–C". The molecular line emissions mapped by Brand et al. (2001) are also peaked in this region, ∼2.1 arcsec NE of "A". This shows that this is a cluster where there is on-going star formation. Molinari et al. (2002) detected two faint point sources in this region at 3.6 cm (in addition to a brighter extended source near the lower right region of our field); the brighter one (0.32±0.03 mJy) almost coincides with one of the bright *K*-band sources near the IRAS position labelled "D" (α=00:44:57.33, δ=+55:47:23.1). The 2MASS colours of "D" do not exhibit any IR excess. The fainter radio source (0.17±0.03 mJy) is located very close to "A".

The emission detected by IRAS could be from multiple sources. The sub-mm, millimetre and CO emission could be from "A" or "B" or some other embedded source in their vicinity. It is not clear if any of these objects is the near-IR counterpart of the millimetre and sub-millimetre peaks and the driving source of a possible outflow implied by the H_2 emission features "1–4". From its location, "B" is a strong candidate. Observations in CO rotational transitions and mid-IR continuum with better spatial resolution and deeper H_2 imaging will be useful.

A2 IRAS 04579+4703 – *Mol 7*
(*d = 2.47 kpc, L = 3.91×10^3 L$_\odot$*)

The *JHKLM* photometric survey by Campbell, Persson & Matthews (1989) identified IRAS 04579+4703 as a possible luminous YSO. Multi-component H_2O maser emission was detected from this source by several investigators (Wouterloot & Brand 1989; Wouterloot, Brand & Fiegle 1993; Brand et al. 1994; Migenes et al. 1999). Wouterloot et al. (1993) also observed 12.2 GHz methanol maser and CO emission. However, the CO observations of Zhang et al. (2005) did not reveal any molecular outflow from IRAS 04579+4703. A dense core was observed towards this region in NH_3 emission by Molinari et al. (1996). The search by Molinari et al. (1998) did not detect any 6-cm radio emission from this region.

Our *K*, H_2 and Brγ images (Fig. A2) reveal a compact cluster with a bright central source ("A"; α=05:01:39.91, δ=47:07:21.6) located 2.35 arcsec SE of the IRAS position. "A" is associated with a cometary nebula seen in *K*, most of which disappears in the continuum-subtracted narrow-band images. Weak H_2 emission with a bipolar nature in the NW–east direction is observed very close to "A". The 2MASS position of "A" appears to be centred off the source due to the presence of strong nebulosity in its vicinity and its colours exhibit a large amount of reddening and excess (Fig. 1). Therefore, "A" is most probably the near-IR counterpart of the IRAS source. It should be noted that the MSX detection is merely 1.6 arcsec south of "A". There is a source 24.6 arcsec to the SW of "A", labelled "B" (α=05:01:41.91, δ=+47:07:7.7), which displays a bipolar outflow-like H_2 emission features. Both lobe-like features are circled and labelled "3" and "4" respectively. However, there are faint H_2 features in the diametrically opposite direction of "3" and "4" from "A", labelled "1" and "2". Another very faint H_2 emission is detected between "4" and "A". It is also important to note that the 2MASS colours of "B" do not exhibit any excess and place it well within the reddening band (Fig. 1). Thus, even though morphologically "3" and "4" appear to be the two lobes of a bipolar

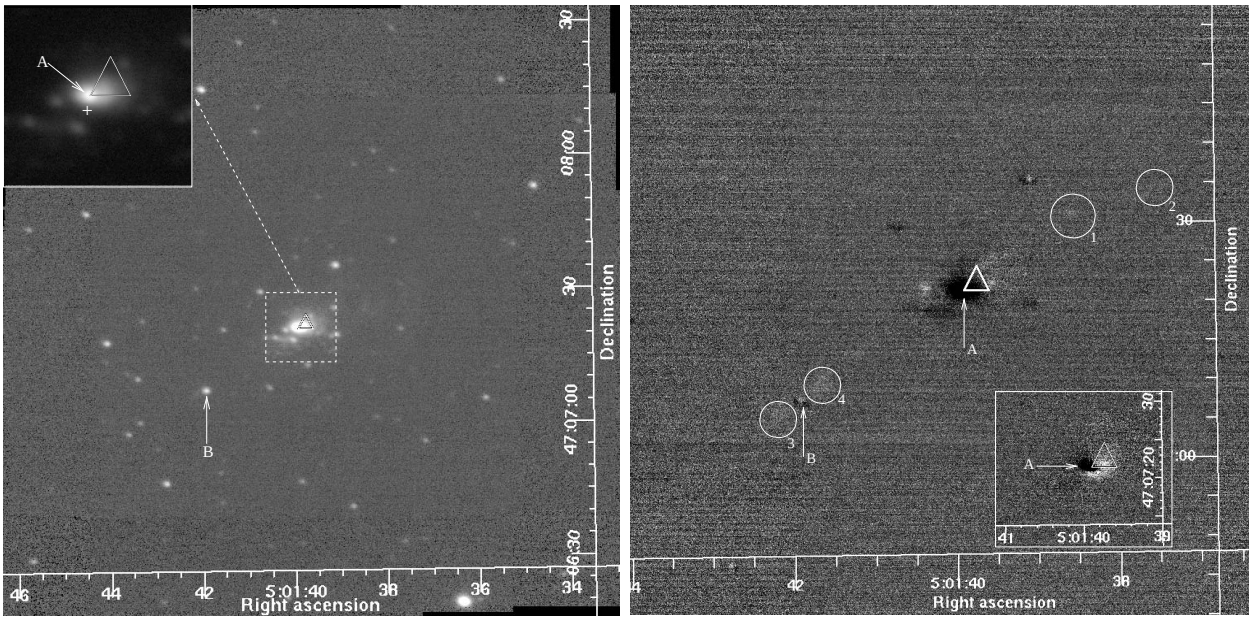

Figure A2. Left: *K*-band image of IRAS 04579+4703. An expanded view of the central source and its vicinity with better contrast is shown in the inset. Right: central region of the continuum-subtracted H_2 image on which the continuum-subtracted Brγ image of the central source is shown in the inset. "△" shows the location of the IRAS source and "+" shows the MSX source.

outflow emanating from "B", it is possible that these are parts of a major outflow from "A" in the NW-SE direction at an angle of ∼125°.5 in the sky plane. The outflow has a collimation factor of ∼7.3 if we include features "3" and "4".

As can be seen in the inset on the right half of Fig. A2, there is Brγ emission very close to "A", extending towards the west. Our detection of H_2 and Brγ emission in the vicinity of "A" is consistent with the spectrum observed by Ishii et al. (2001). The H_2 emission seen in their slit must be coming from the bipolar emission that we see close to the central source. The Brγ is from a region closer to the source than the location of the H_2 knots. Together, these observations show that this is a convincing case of an intermediate-mass/high mass YSO driving a collimated outflow.

A3 IRAS 05137+3919 – *Mol 8*

(*d = 11.5 kpc, L = 225×10^3 L$_\odot$*)

IRAS 05137+3919 was first identified as luminous YSO based on its IRAS colours. Modelling the SED, Molinari et al. (2008) derived a luminosity of $2.55\times10^5 L_\odot$ at a distance of 11.5 kpc. The dense core was detected in ammonia emission by Molinari et al. (1996). Water maser emission has been observed towards this source (Palla et al. 1991; Migenes et al. 1999), but no 6.7-GHz methanol maser emission was detected in the survey by Szymczak et al. (2000) and no SiO emission was detected by Harju et al. (1998). The VLA survey by Molinari et al. (1998) did not reveal any radio emission at 2 cm and 6 cm from IRAS 05137+3919.

Fig. A3 shows our *K* and H_2 images. An expanded view of the central region is shown in the inset on the *K*-band image. Through H_2 imaging, we discovered two spectacular well-collimated outflows. The brighter one is in the NE-SW direction and the fainter one in the NW–SE direction. There are two IR-bright sources embedded in nebulosity in the centre of our images. These sources are labelled "A" (α=05:17:13.73, δ=39:22:19.9) and "B" (α=05:17:13.68, δ=39:22:19.3). They are separated by 0.91 arcsec at a position angle of 50°. The "A,B" pair is well detected by 2MASS, but not resolved. The 2MASS near-IR colours of "A" and "B" combined place the pair in the region of large excess emission, typical of luminous YSOs, in the *JHK* colour-colour diagram (Fig. 1). The pair is located 7.25 arcsec NE of the IRAS position. MSX detected a source with a steep SED within one arcsecond of "A". We conclude that the two outflows discovered in our H_2 images are produced by the sources "A" and "B". On the H_2 image, we have shown the directions of the two outflows by the dotted and dashed arrows, labelled "1" and "2", at angles 19.5° and 167.5° respectively. The bow-shocks of outflow "1" are encircled and labelled "1a" and "1b" respectively. Both "1a" and "1b" are composed of multiple bow-shocks suggesting a possible precession of the jet. In H_2, the collimation factors could be ∼8.5 and ∼6.6 respectively for outflows "1" and "2".

Molinari et al. (2002) detected HCO^+ (1-0) emission from the central source, and from locations close to the NE and SW lobes of the H_2 jet "1" described above, using the OVRO millimeter wave array. They derived a position angle of ∼25° for the outflow, which is comparable to a value of 19.5° we measure for jet "1" from the H_2 emission knots. They detected 3.4-mm continuum emission from the central object. They also detected faint radio continuum emission from the central source at 3.6 cm (at a flux density of 0.33±0.03 mJy) using the VLA. From the HCO^+(1-0) spectrum of the central source, they suspect two distinct components nearly along the line of sight which is supported by the binary stars embedded in nebulosity as seen in our *K*-band image. Wu et al. (2001) observed a dense core towards this region in ^{13}CO (J=1-0). Brand et al. (2001) detected two velocity components in their ^{13}CO (J=1-0), HCO^+ and CS maps (at -25.5 km s^{-1} and -26.5 km s^{-1}) with the redshifted component centred on the IRAS position and on the 3.4-mm and 3.6-cm continuum maps from Molinari et al. (2002).

Previous infrared imaging by Ishii et al. (2002) did not resolve "A" and "B". *K*-band spectroscopy by Ishii et al. (2001) detected emission from H_2 v=1-0 S(1), Brγ and from the v=2-0 overtone band of CO. The H_2 emission they observed close to the central

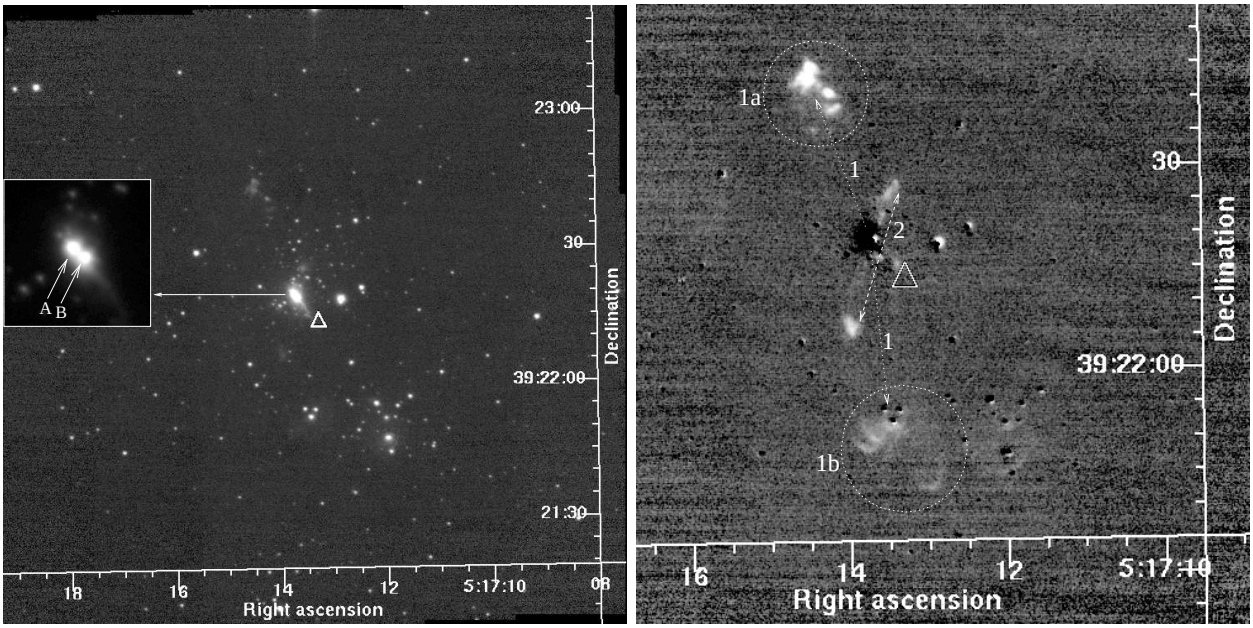

Figure A3. Left: *K*-band image of IRAS 05137+3919. The inset displays a magnified view of the central region to show the "A,B" pair resolved. "*" shows the 3.4-mm continuum peak (MM1) and "X" shows the 3.6-cm radio continuum peak of Molinari et al. (2002). Right: the central part of the continuum-subtracted H_2 image.

source must be due to the emission from the H_2 jet in the NW-SE direction that we see in our image, the base of which will be in their 2.4 arcsec wide slit. Zhang et al. (2005) also detected a very powerful outflow from this source in CO, with the blue- and red-shifted lobes roughly in the direction of our flow "1". These observations, along with the detection of two jets in our H_2 image, confirm that there are two outflows in this region and the jets that we see in H_2 emission are powering the large scale outflows in IRAS 05137+3919.

A4 IRAS 05168+3634 – *Mol 9*
(*d = 6.08 kpc, L = 24×10³ L⊙*)

IRAS 05168+3634 has water maser emission associated with it (Palla et al. 1991; Migenes et al. 1999), but there was no detection of any 6.7-GHz methanol maser emission by either Szymczak et al. (2000) or Slysh et al. (1999). Molinari et al. (1998) detected 6-cm radio emission from this region using the VLA. However, the location of their radio source is 102 arcsec away from the IRAS source. Hence, the radio detection is not from the IRAS source. In addition, Harju et al. (1998) detected the SiO (J=2-1) line at v_{peak}=-18.1 km s^{-1} and Zinchenko, Henkel & Mao (2000) observed $C^{18}O$ from this source. Zhang et al. (2005) discovered a bipolar molecular outflow in CO. The centroid of this outflow appears to be offset from the IRAS position by a few arcminutes and therefore, may be outside our field of view. The dense core was mapped by Bronfman, Nyman & May (1996) in CS emission and by Molinari et al. (1996) in NH_3.

Fig. A4 shows our *K*-band image of IRAS 05168+3634. The *K*-band image exhibits nebulosity extending northward from a bright infrared source labelled "A" (α=05:20:16.44, δ=+36:37:18.7), located near the centre of the field. This nebulosity disappears upon continuum subtraction; the subtracted H_2 and Brγ images do not reveal any line emission. Hence these images are not presented here. The 2MASS colours of "A" do not exhibit any IR excess (Fig. 1). However, it should be noticed that "A" is only poorly detected in *J*. The IRAS source is 3.4 arcsec NW of "A" and the MSX source is just 1.5 arcsec NW of "A", which implies that "A" is probably the luminous YSO. The lack of any observed H_2 emission and the absence of any significant near-IR colour excess for "A" imply that the source has probably passed the very early stages of its formation. More accurate photometry is required to derive the IR colours of "A" and its neighbours.

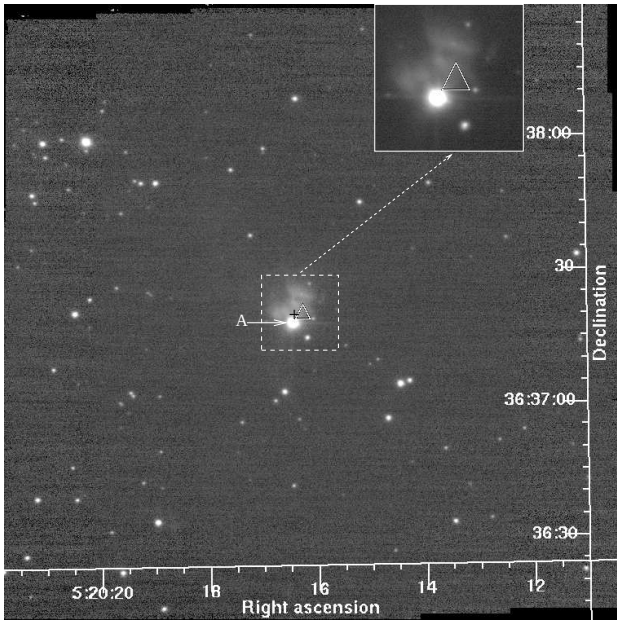

Figure A4. *K*-band image of IRAS 05168+3634. The inset shows an expanded view of the central region.

A5 IRAS 05274+3345 – *Mol 10*
(*d = 1.55 kpc, L = 4.35×10³ L⊙*)

Towards IRAS 05274+3345 (also referred to as AFGL 5142), there are two distinct sites of star forming activity. The high density core towards this source was detected in NH_3 emission by Molinari et al. (1996). A radio continuum source detected in this region (integrated flux of 0.83±0.12 mJy at 3.6 cm; Tofani et al. 1995) is offset ∼30 arcsec east of the IRAS position, and is coincident with the peak millimetre emission from dust (Hunter et al. 1999), an ammonia core and a possible compact disc (Zhang et al. 2002). The brightest infrared source in the previous *K*-band image from Hunter et al. (1995) is located near the centre of the error ellipse of the IRAS source position. However, the density distribution for the infrared sources in the field peaks close to the radio continuum peak. There is evidence for outflows centred on the radio position, observed in ^{12}CO and H_2 by Hunter et al. (1995) and in SiO and NH_3 by Zhang et al. (2002), who deduce the presence of a disc associated with this source. A sub-mm continuum peak was also detected by Jenness et al. (1995) at 850 μm within the IR cluster towards the east of the IRAS source. The H_2O maser emission from this source has been studied by many authors (Palla et al. 1991; Tofani et al. 1995; Goddi et al. 2004). The masers are located in the close vicinity of the radio continuum source and on either sides of it (Tofani et al. 1995). Most recently, Goddi et al. (2004) determined the proper motions of 7 of the 12 maser sources. The proper motions of a subset of these masers is consistent with Keplerian rotation in the disc posited by Zhang et al. (2002); the remainder are associated with the outflow. Detection of 6.7-GHz maser emission has been made by Szymczak et al. (2000) and Slysh et al. (1999). An extensive survey for molecular line emission associated with the H_2O maser activity in high mass YSOs by Cesaroni, Felli & Walmsley (1999b) detected ^{13}CO (2-1), HCO^+, HCN (1-0), CH_3CN, $C^{34}S$ and CS (3-2) peaking at the position of the water masers, with a second, quiescent clump located 12 arcsec south. The southern clump is detected only in $C^{34}S$ and CS. They propose that the northern clump associated with the water masers is at a later stage of star formation than the southern clump.

Fig. A5 shows the *K* and H_2 images of IRAS 05274+3345. The *K*-band image shows a cluster of IR sources with a bright object embedded in nebulosity (labelled "A"; α=05:30:46.07, δ=+33:47:54.1) located near the centre of the field. The nebulosity shows a mild cometary nature extending NW. There are many fainter objects close to "A", the closest being 1.7 arcsec NW of "A" and embedded in the nebulosity. Most of the other IR sources deteced in our image are located towards the east of "A". *JHK* photometry of Hunter et al. (1995) shows that "A" (their "IRS2") has reddening and excess. The 2MASS K_s magnitude of "A" has large uncertainty. It is possible that the 2MASS magnitudes of "A" are contaminated by the nebulosity and the presence of nearby stars. So we have used the *JHK* photometry of Hunter et al. (1995) to plot it in the colour-colour diagram (Fig. 1). "A" is located 6.1 arcsec NE of the IRAS position. MSX detected a source with a steep SED within 1.1 arcsec of "A", which suggests that "A" is probably a young source.

The continuum-subtracted H_2 image shows several emission features and generally agrees with the image presented by Hunter et al. (1995). Prominent emission features are labelled in Fig. A5 (right panel). This image is smoothed with a 2-pixel FWHM Gaussian to enhance the faint emission. Features circled and labelled "2–5" are located in an arc-like pattern extending from "A". More conspicuous is the set of aligned features in the direction of the arrow labelled "1" on Fig. A5, which appears to be a jet. This jet is inclined at an angle of 51°.5 and appears to be originating from one of the objects in the eastern cluster; the mm, sub-mm and radio emissions seen are from this cluster. The 3.6-cm radio continuum source detected by Tofani et al. (1995) is 24 arcsec east of "A". Many of the cluster members show reddening and excess. Being located in a cluster with several sources exhibiting reddening and excess, it is not sure if the radio source, the mm source and the source driving jet "1" are all the same. It is noteworthy that the IR source labelled "B" (α=05:27:29.94, δ=33:45:40.5; "IRS1" of Hunter et al. 1995) shows large reddening and excess (Fig. 1; colours are from Hunter et al. 1995 since it is detected only in K_s by 2MASS) and is located very close to the radio source and the associated H_2O masers detected by Tofani et al. (1995). From the positional accuracies of the maser and radio sources (Table C1) and their locations, they appear to be associated with "B". "B" is therefore a strong candidate for the driving source for an outflow in the direction of "1". "A" (IRS2) is likely to be the driving source of the large scale outflow mapped in CO(2-1) by Hunter et al. (1995). The location of the H_2 knot "2" is in the same direction from "A" as the blue shifted lobe of their CO outflow. The compact outflow perpendicular to the large scale outflow, mapped by Hunter et al., is roughly in the direction of "1" and is centred near "B", the radio source and the water masers. They propose that the radio emission could be from an ionized wind. There is an emission feature labelled "7", which is probably part of another outflow. Overall, it looks like this region hosts more than one YSO, with at least one well collimated outflow confirmed in H_2. The multiple H_2 knots in different directions imply multiple outflows.

A6 IRAS 05345+3157 – *Mol 11*
(*d = 1.8 kpc, L = 1.38×10³ L⊙*)

Towards IRAS 05345+3157, better known as AFGL 5157, Snell et al. (1988) and Ridge & Moore (2001) mapped an EW CO outflow at low spatial resolution, centred on a dense molecular core extending roughly in the NS direction that was mapped in NH_3 emission (Torrelles et al. 1992a; Molinari et al. 1996; Verdes-Montenegro et al. 1989). The CO outflow was also detected by Wouterloot & Brand (1989). Multiple H_2O masers were detected from the region close to the centre of the NH_3 core and CO outflow by several investigators (Verdes-Montenegro et al. 1989; Palla et al. 1991; Wouterloot et al. 1993; Brand et al. 1994; Torrelles et al. 1992b). Torrelles et al. (1992b) and Molinari et al. (2002) detected an HII region at 3.6 cm. The location of the radio emission is close to the centre of the NH_3, CO and H_2O maser emission. Chen et al. (1999, 2003) found an infrared cluster ∼1 arcmin SW of the core - coincident with the IRAS position - that is enveloped by diffuse, fluorescent H_2 filaments (associated with a PDR). They also observed a number of compact H_2 knots, implying the presence of multiple outflows in the region. Chen et al. (2003) show a schematic diagram summarising the many observations of AFGL 5157. The brightest 3.6-cm radio continuum position of Molinari et al. (2002) agrees with the 6-cm position given by Molinari et al. (1998), which is towards the NW of our images and is outside our field of view. The second brightest radio source of Molinari et al. (2002) (0.80±0.05 mJy) is located very close to an IR-bright source near the IRAS position and is extended. A fainter radio source (0.19±0.03 mJy) was detected by them, located close to the object labelled "C" in our image (Fig. A6). This radio source appears to be the same as the faint radio source detected by Torrelles et al. (1992b) at 3.6 cm and the locations of both agree within their beam sizes (Table C1). The

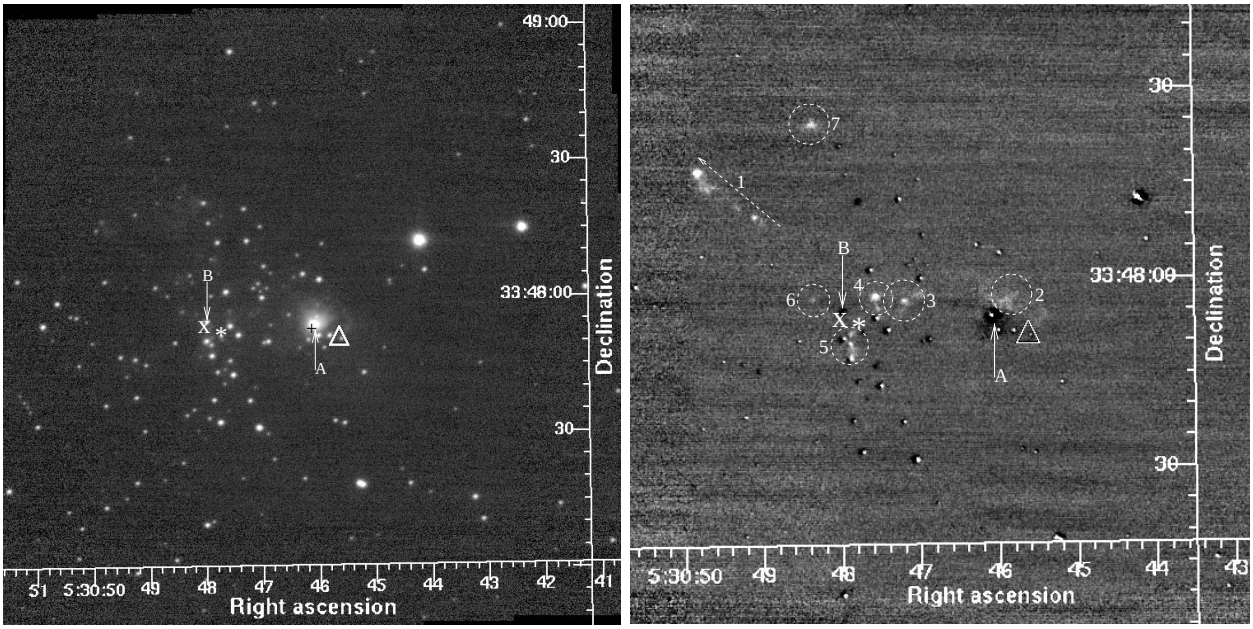

Figure A5. Left: the *K*-band image of IRAS 05274+3345. Right: the central part of the continuum-subtracted H_2 image. The prominent H_2 emission features are labelled on the figure. "*" shows the 850-μm position of Jenness et al. (1995). "x" shows the 3.6-cm position of Tofani et al. (1995).

positions of some of the H_2O maser spots detected by Torrelles et al. (1992b) agree well with that of "C". However, there are other H_2O maser spots observed by Torrelles et al. (1992b) further SE of the ones near "C", close to the location of the H_2O maser observed by Verdes-Montenegro et al. (1989). The location of the NH_3 emission peak detected by Verdes-Montenegro et al. (1989) is near "C", located between "B" and "C" and further north on Fig. A6. However, both "B" and "C" fall within the 1.4 arcmin beam of Verdes-Montenegro et al. (1989).

Fig. A6 displays our *K*-band and continuum-subtracted H_2 images. The *K*-band image reveals a cluster of IR-bright sources towards the centre of the field. The IRAS position is within this cluster. The image also shows emission in ridges around this cluster and towards the NE. The H_2 image reveals a well defined bipolar jet oriented SE-NW at an angle of 131°.6, in the direction of the dashed arrow labelled "I". Emission features circled and labelled "1–4" appear to be part of this jet. Close inspection of the H_2 image shows that there is more than one jet in this direction, or that the jet is precessing. The collimation factor of the jet would be ~4.3 if it is a single jet.

Three objects are labelled on the figures - "A" (α=05:37:49.83, δ=+31:59:47.9), "B" (α=05:37:50.07, δ=+31:59:52.5) and "C" (α=05:37:51.97, δ=+32:00:04.2). "A" appears to be a point source close to the centroid of the observed jet/s represented by "I". It exhibits reddening and excess. "B" shows copious amount of H_2 emision. The central region of "B" does not appear as a single point source in our image and has multiple nebulous extensions. The 2MASS JHK_s colours of "B" place it in the region occupied by YSOs in the colour-colour diagram (Fig. 1). The H_2 image shows several other emission features, the prominent ones are circled on our H_2 image. The featues "5–9" are located in a direction nearly perpendicular to the direction of the jet "I". These appear to be part of another jet. A dotted arrow is drawn in this direction and labelled "II". Two other knots ("10" and "11") are labelled on the H_2 image, with faint filementary features extendening towards them from "B", the directions of which are shown by dotted arrows labelled "?". "5–11" could be from multiple sources located in "B" or from a single wide angle outflow from "B".

Also prominent in the figure are filementary ridges of H_2 emission around the IR cluster surrounding the IRAS position. Dotted lines are drawn on the figure close to these features to guide the eyes. Labelled "12–14", these are the fluorescent filaments of H_2 emission detected by Chen et al. (2003). They are likely to be due to the UV emission from the more evolved hot stars in the infrared cluster.

The MSX mission detected three sources in this field, the positions of which are denoted by a "+" in our images. The brightest one is 13.5 arcsec SE of the IRAS position and is probably associated with the IR cluster near the IRAS position. The faintest of the three is 20 arcsec NW of the IRAS position. The third one is located NE in our field and is very close to "C". Source "C" has a nebulous patch of emission which is seen in *K*, with faint point sources in the vicinity; the nebula disappears upon continuum subtraction. It is detected only in K_s by 2MASS and the magnitude limits in the *J* and *H* bands imply strong excess. The proximity of the MSX source suggests that there is a deeply embedded YSO located here.

Our H_2 image reveals bow shocks produced by outflows from the deeply embedded core located NE of the IR-bright cluster. The locations of the radio continuum source, H_2O masers, NH_3 emission and the CO outflow all are near this core from which the H_2 emission knots appear to be emanating. The position of the IRAS source is centred off this region and is towards the IR cluster. However, an MSX source is detected near this region (only at 21 μm), the location of which is close to the centre of the NH_3 core. All these observations imply that there is multiple star formation occuring within this embedded core and that the HH-type features seen in the H_2 image are from a region which is much younger than the IR cluster at the centre of our field. With the positional accuracy of the radio detection given by Torrelles et al. (1992b) (Table C1) and our near-IR images, it appears that the radio emission near "C" is caused by a source which is different from those driving the outflows in the direction of "I" and "II" and is probably more evolved.

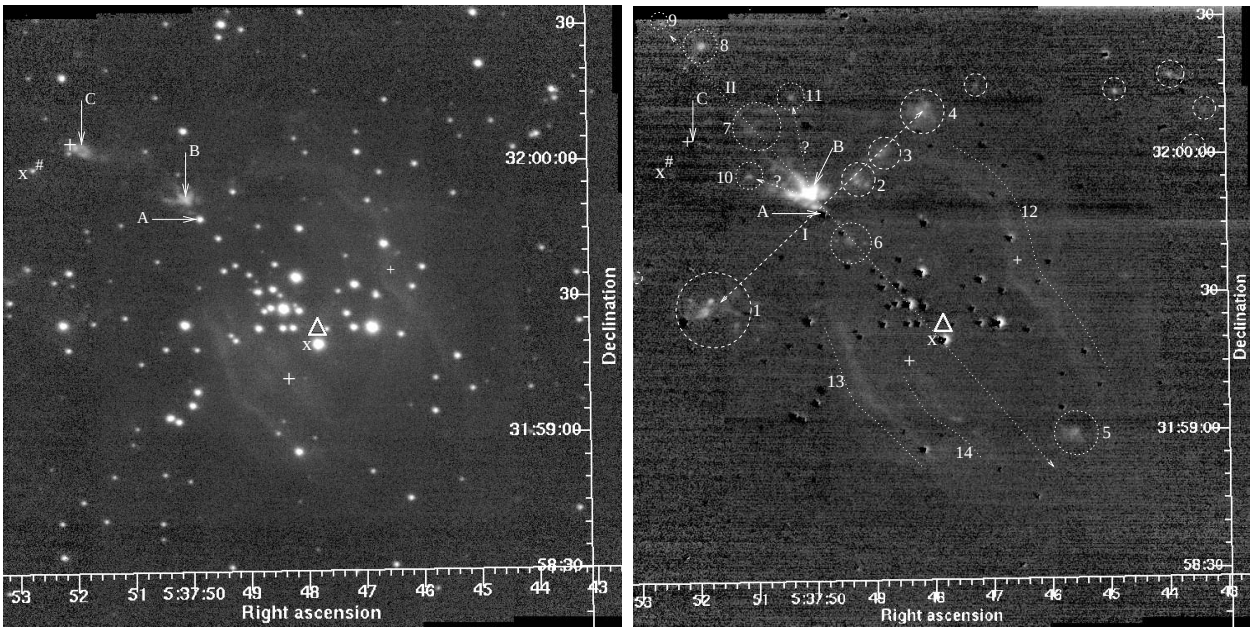

Figure A6. Left: the *K*-band image of IRAS 05345+3157. Right: the continuum-subtracted H_2 image smoothed with a Gaussian of FWHM=2 pixels. "x" shows the locations of the faint radio sources detected by Molinari et al. (2002). "#" shows the location of the 3.6-cm radio sources detected by Torrelles et al. (1992b).

Also, "C" does not appear to be the near-IR counterpart of the radio source. From the positional uncertainty of the MSX, it is not clear if the MSX detection is from "C", "B", the radio source, or a combination of all.

Overall, our observations support the results of Chen et al. (2003). It should be noted here that Zhang et al. (2005) also mapped a bipolar outflow in this region, the centroid of which is offset from the IRAS position by 43 arcsec each in RA and dec and is close to the YSOs that we detect in the NE region of the field.

A7 IRAS 05358+3543

(*d = 1.8 kpc, L = 3.8×10^3 L$_\odot$*)

IRAS 05358+3543 (S233IR) has been studied in the near-IR by a number of groups (Porras, Cruz-González & Salas 2000; Kumar, Bachiller & Davis 2002; Khanzadyan et al. 2004). S233 is associated with two embedded stellar clusters, the IRAS 12-μm position being coincident with the central cluster (referred to as the south-western cluster by Porras et al.). Methanol maser emission has been detected by a number of investigators (Menten 1991; Szymczak et al. 2000; Sridharan et al. 2002; Galt 2004). Single dish observations of Menten (1991) place the methanol maser in the NE cluster. Water maser emission observed in this region is from the NE cluster (Sridharan et al. 2002; Beuther et al. 2002d). In the CO maps of Beuther et al. (2002a), multiple molecular outflows have been resolved, which are traced by the H_2 images shown by Porras et al. (2000), Kumar et al. (2002) and Beuther et al. (2002a). The most prominent flow is oriented roughly NS and appears to be associated with the NE cluster, the IRAS 100-μm position and a density peak in the 1.2 mm continuum maps (Beuther et al. 2002a,b). The lobes of this outflow are capped by two prominent H_2 bow shocks, N1 and N6 (Porras et al. 2000; Kumar et al. 2002). The northern lobe is blue-shifted and the southern red-shifted. Additional outflows are traced in both CO and H_2 (Beuther et al. 2002a; Khanzadyan et al. 2004). Notably, Sridharan et al. (2002) did not detect 3.6-cm emission, down to 1 mJy, from the NE cluster and the density peak, which suggests that the driver of the north-south molecular flow (Beuther et al. 2002a) is in a pre-UCHII phase.

Fig. A7 shows our *K* and H_2 images. Both the central and the NE cluster are recorded in our images. Prominent H_2 emission features are circled in the diagram. Source "A" (α=05:39:09.93, δ=+35:45:17.2) is the IR-bright object close to the IRAS 12-μm position and is most probably the near-IR counterpart of the IRAS 12-μm source. There is a ring-like H_2 emission feature around it, which is probably due to fluorescence in a shell (Porras et al. 2000; Kumar et al. 2002) projected on to the sky plane. "A" is the brightest member of the central cluster and it exhibits IR excess in the colour-colour diagram (Fig. 1). A jet-like feature is emanating from this region; the two knots labelled "7" and "8" are probably shock-excited H_2 emission along this jet in the direction of the dotted arrow labelled "III" on Fig. A7. "A" appears to be the driving candidate for this jet. MSX detected two bright sources in this region; the bluer of the two is within 1.5 arcsec of "A".

We label two objects in the NE cluster: "B" (α=05:39:13.29, δ=+35:45:53.5) and "C" (α=05:39:12.66, δ=+35:45:52.2). As can be seen in the inset in Fig. A7, these objects are not point sources in our images and are resolved into multiple components. Both these objects, which are at similar reddening and are much more reddened compared to "A", exhibit IR excess in our *JHK* colour-colour plot (Fig. 1). Porras et al. (2000) presented *JHK* colour-colour and colour-magnitude diagrams and concluded that the NE cluster is much more reddened and is much younger than the central cluster. This is very much consistent with the difference in the reddening that we see between "A", and "B" and "C". The redder of the two bright MSX sources is located between "B" and "C".

Several H_2 emission features are seen associated with the NE cluster which provide evidence for multiple collimated outflows from this region. The feature labelled "6" is the southern bow shock of the main outflow (in the direction of the dotted arrow labelled "II") oriented NS in the figures of Beuther et al. (2002a) and Ku-

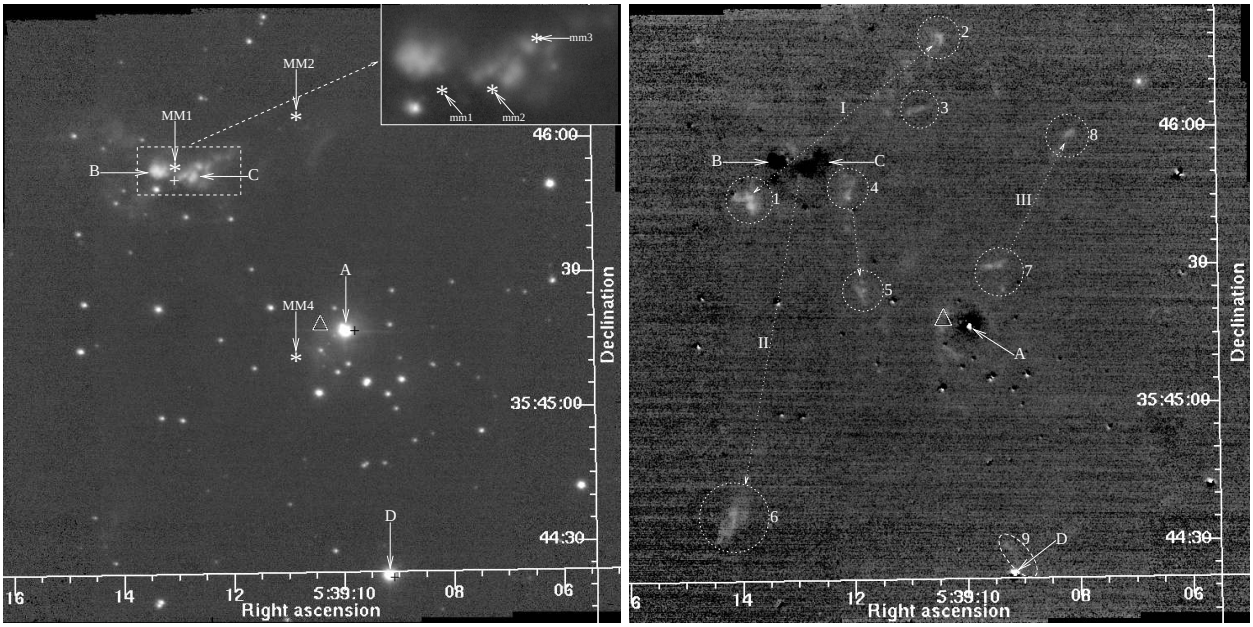

Figure A7. The left panel shows our *K*-band image of IRAS 05358+3543. "*" on the main figure shows the location of the three 1.2-mm peaks ("MM1, MM2, MM4") within our field listed by Minier et al. (2005). Labelled by "*" on the inset and named "mm1–mm3" are the three massive sub-cores resolved in this region by Beuther et al. (2002a) at 2.6 mm. The right panel shows the continuum-subtracted H_2 image smoothed with a 2-pixel FWHM Gaussian.

mar et al. (2002). The northern bow shock is outside our field. "1" and "2" are probably the bow shocks from a bipolar outflow in the direction "I". "1" appears double lobed and could be produced by more than one outflow, which has to be verified through velocity studies. "3" also appears to be part of a different outflow. There are two other features labelled "4" and "5", which could be produced by a different outflow from an obscured source.

Beuther et al. (2002b) detected four 1.2 mm sources in this region. All four are detected at 850 μm and three of these are detected at 450 μm by Minier et al. (2005); they label the 1.2 mm sources as "MM1–MM4". The location of the brightest mm peak, "MM1", is between our sources "B" and "C" and is probably the combined emission from both of these. (High-angular-resolution observations of Beuther et al. (2002a) at 2.6 mm in fact resolve "MM1" into three components, labelled "mm1–mm3" on Fig. A7). Modeling by Minier et al. (2005) shows that "MM1" is the most massive of the four clumps detected here in the mm. "MM2" is NW of "B" and "C" and is not detected in *K*. "MM3" is outside our field. "MM4" is close to "A", but is offset from it by 11.9 arcsec towards the SE. This offset is comparable to a beamsize of 11 arcsec of the the 1.2 mm observations of Beuther et al. (2002b) (Table C1). It has to be noted that the 21-μm MSX emission plotted by Minier et al. (2005) appears to be peaking at the locations of "B" and "A". From our observations, it appears that "A" drives an outflow in the direction of "III", which is detected in H_2. It is possibly the near IR counterpart of the MSX and IRAS sources. It needs to be verified through millimetre observations at high angular resolution and positional accuracy if "MM4" is the mm counter part of the detections here at lower wavelengths or is a younger and more embedded source. The near-IR source "D" (α=05:39:09.19, δ=+35:44:22.6) also appears to be associated with an outflow. An H_2 knot ("9") is detected close to it. "D" has a weak MSX detection. It is well detected by 2MASS and exhibits mild extinction and excess.

A8 IRAS 05373+2349 - *Mol 12*
(*d = 1.17 kpc, L = 0.47×10^3 L$_\odot$*)

IRAS 05373+2349 is one of the luminous YSOs selected by Molinari et al. (1996) and has been extensively studied by that group. This source is associated with ammonia emission from gas with a kinetic temperature of 21.2 K (Molinari et al. 1996) and there is no detection of radio emission at 2 cm or 6 cm (Molinari et al. 1998), from which it is concluded that no HII region has developed and that the source is in the younger population of their sources selected using IRAS colours. More recent, more sensitive, radio and millimetre observations (Molinari et al. 2002) detected IRAS 05373+2349 at 3.6 cm and 3.4 mm respectively. The emission derives from the vicinity of one of the two cores resolved in their HCO^+ observations. The radio emission is faint (0.70±0.04 mJy at 3.6 cm) and is thought to arise from an ionized wind. Searches for 6.7 GHz methanol maser emission by Szymczak et al. (2000) found none, even though water maser emission was detected by Palla et al. (1991). Sub-mm and mm observations at 0.35 mm, 0.45 mm, 0.8 mm, 1.1 mm, 1.3 mm and 2.0 mm were carried out by Molinari et al. (2000). From a fit to the SED, a mass of 8.8 M$_\odot$ is derived for IRAS 05373+2349 and an H_2 column density of 5.9×10^{22}cm^{-2}. This source has also been detected in many molecular species: $C^{34}S$, HCN (1-0), ^{13}CO (2-1) and CH_3CN (8-7) (Cesaroni et al. 1999b) and SiO (Harju et al. 1998). Zhang et al. (2005) mapped a bipolar outflow from this object, oriented roughly in the NE–SW direction.

Fig. A8 shows our *K*-band image of IRAS 05373+2349. The central region of the continuum-subtracted H_2 image is shown in the inset. The field was not observed in the Brγ filter. A bright source, labelled "A" (α=5:40:24.33, δ=23:50:54.6), is seen 2.8 arcsec NW of the IRAS position. The MSX mission detected an object 2.4 arcsec SW of "A". The 2MASS colours of "A" exhibit IR excess and very high reddening (Fig. 1), which is typical of HMYSOs. It is only weakly detected by 2MASS in *J*. The continuum-subtracted H_2 image shows several faint emission fea-

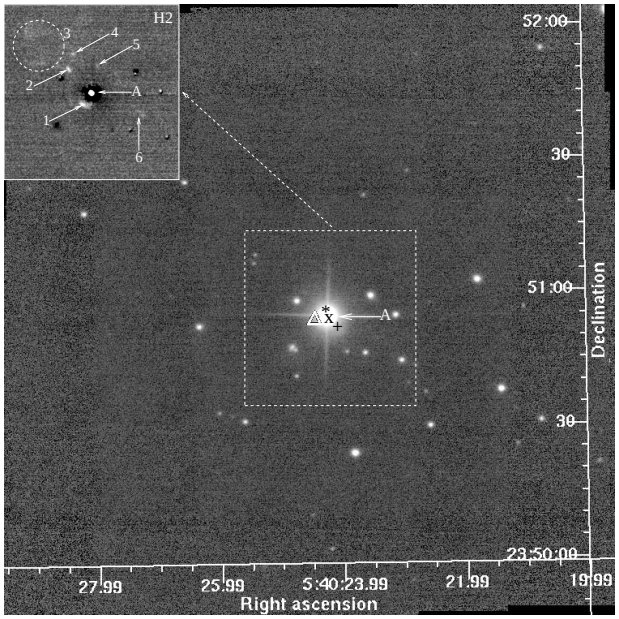

Figure A8. *K*-band image of IRAS 05373+2349. "*" shows the location of the 3.4-mm continuum peak and "x" shows the location of the 3.6-cm continuum peak detected by Molinari et al. (2002). The inset shows the central region of the continuum-subtracted H_2 image revealing the faint line emission.

tures around "A", the prominent ones of which are labelled "1–6". At the sensitivity of our imaging, these faint features do not make a conclusive case for a well collimated bipolar outflow. However, the NE-SW alignment of the line emission features centred on "A" is suggestive of a bipolar outflow in that direction with a collimation factor of ∼2.55. Deeper integration is required for a better understanding of the H_2 emission in this region. It is noteworthy that the H_2 knots are roughly aligned in the direction of the outflow mapped in CO by Zhang et al. (2005).

The observations show that "A" is likely to be the luminous YSO in this region. The 2.4 mm peak of Molinari et al. (2002) is within 1.6 arcsec of "A". Their faint 3.6-cm radio continuum source nearly coincides with "A". The presence of the weak radio emission and the weakness of the outflow suggest that it has probably evolved out of the very early stages and is approaching the UCHII stage.

A9 IRAS 05490+2658

(*d = 2.1 kpc, L = 3.16; 4.2×10^3 L$_\odot$*)

IRAS 05490+2658 is located ∼5 arcmin east of the HII region S242. Snell et al. (1990) detected an outflow in CO. In their low-resolution map, the blue- and red-shifted lobes of the outflow were found pronounced towards the NW of the IRAS position with the peak located ∼1 arcmin NW and nearly overlapping. This high-velocity emission seems to be coincident with an embedded cluster seen only at near-IR wavelengths (Carpenter et al. 1993), which is separate from a less-embedded cluster coincident with the IRAS position. In the 1.2-mm maps of Beuther et al. (2002b), knotty cloud cores are observed towards these two clusters, which are embedded in a more diffuse envelope that spreads over a 2×3 arcmin^2 field. Sridharan et al. (2002) did not detect H_2O and CH_3OH masers from this source. From the IRAS HiRes, MSX and 1.2-mm photometry they estimate a total luminosity for the region of ∼10$^{3.5}$ L$_\odot$ at a distance of 2.1 kpc.

Fig. A9 shows our *K* and H_2 images. The 2MASS colours of the bright star, "A" (α=05:52:13.83, δ=+26:59:40.8), place it within the reddening band and it does not exhibit any IR excess (Fig. 1). The IRAS position is ∼15 arcsec SW of "A". MSX detected an object within five arcsec of the IRAS position and one of the two 1.2-mm continuum peaks observed by Beuther et al. (2002b) is 7.8 arcsec west and 4.4 arcsec north of the IRAS position. The positional offsets of the IRAS, MSX and mm detections are in a similar direction from "A", confirming that the YSO is a deeply embedded object and that "A" is just a foreground star. There are two faint IR sources close to the mm position. Accurate photometry of the field is required to investigate if any of them could be the near-IR counterpart of the YSO detected at longer wavelengths.

Most of the nebulosity in the field disappears upon continuum subtraction. The continuum-subtracted H_2 image shows some emission features which are circled and labelled "1" and "2" in Fig. A9. "1" could be produced by an outflow from one or more sources near the centre of the image. Our Brγ image does not show any significant emission from the outflow.

There is a set of reddened sources (shown in the inset) in the region, located nearly one arcmin NW of the IRAS position. This is presumably a second cluster, NW of the cluster associated with the IRAS position, where the CO outflow discovered by Snell et al. (1990) is centred. Three sources are labelled in this cluster; all are plotted in our colour-colour diagram (Fig. 1). The locations of "A–D" on the colour-colour diagram show that the cluster containing "B–D" is at a much larger extinction when compared to "A". "B" (α=05:52:11.34, δ=+27:00:31.5) is located at the early-spectral-type limit of the reddening band. Hence it shows excess unless it is of very early spectral type. It is surrounded by nebulosity in our *K*-band image and is highly reddened. "B" has a fainter neighbour at a separation of ∼1.6 arcsec. "C" (α=05:52:11.59, δ=+27:00:25.7) is also reddened and shows IR excess. "D" (α=05:52:11.79, δ=+27:00:18.4) is embedded in nebulosity in *K*. It is resolved into a set of four objects with two equally bright components at a separation of ∼1 arcsec and two fainter components located on either sides of the pair. The 2MASS colours of "D" (aggregate of the four objects) show IR excess and its reddening is similar to that of "B". The NW outflow seen in the CO maps of Snell et al. (1990) is most likely to be produced by one or all of "B, C, D". The brighter of the two 1.2-mm sources imaged by Beuther et al. (2002b) is located 17.3 arcsec west and 58.8 arcsec north of the IRAS position and is only ∼2.9 arcsec east of the brighter component of "B". MSX observations reveal a second far-IR source four arcseconds SW of "B" which appears only at longer wavelengths. The location of the MSX source agrees with that of the mm source within the positional accuracy of MSX. Hence, it is likely that "B" or the fainter star near it is the YSO detected at longer wavelengths and is driving the CO outflow. The lack of any 3.6-cm emission above the 1-mJy detection limit of Sridharan et al. (2002) also suggests that the YSOs here are very young.

A10 IRAS 05553+1631 - G192.16-3.82 - *Mol 14*

(*d = 2.5; 3.04 kpc, L = 6.31; 11.7×10^3 L$_\odot$*)

A massive core was mapped in this region in CS by Beuther et al. (2002b), Bronfman et al. (1996) and Carpenter et al. (1995). Carpenter et al. observed the region in the near-IR *JHK* bands also. The core was detected in NH_3 emission by Molinari et al. (1996)

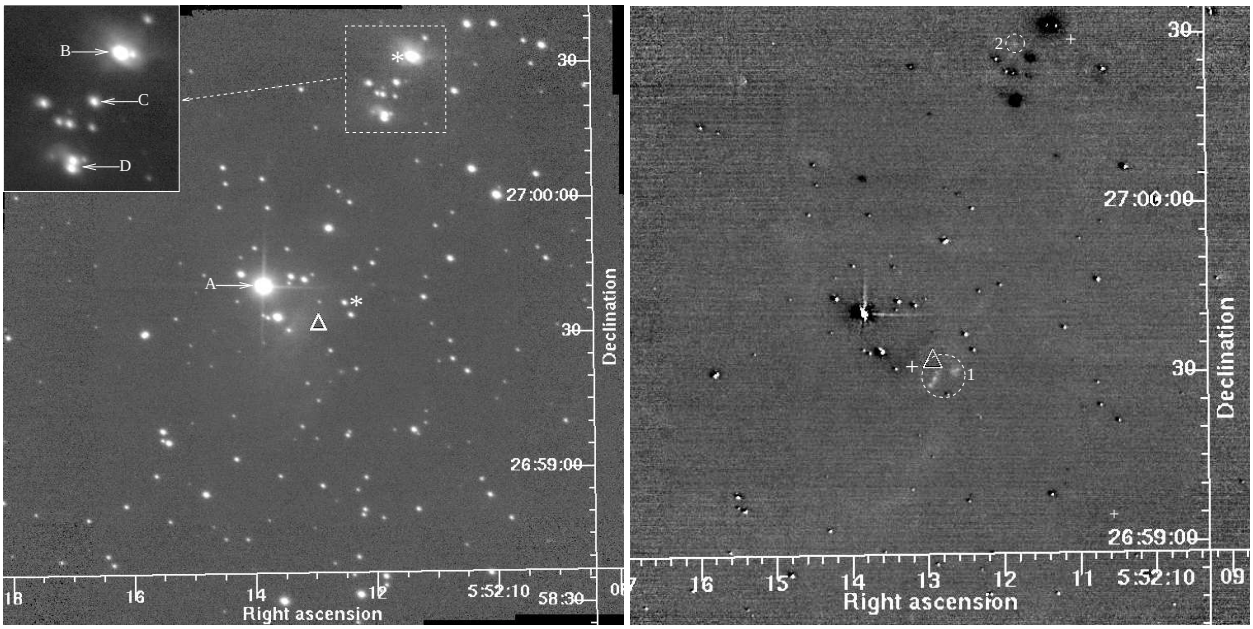

Figure A9. The left panel shows the *K*-band image of IRAS 05490+2658. The two 1.2-mm peaks detected by Beuther et al. (2002b) are shown by "*". The right panel shows the continuum-subtracted H_2 image.

and in 1.2-mm continuum emission by Beuther et al. (2002b). Observations by MacLeod et al. (1998a) and Sridharan et al. (2002) did not reveal any CH_3OH maser emission. Multi-component H_2O maser emission was detected at a range of velocities by several investigators (Palla et al. 1991; Brand et al. 1994; Wouterloot et al. 1993; MacLeod et al. 1998a; Shepherd & Kurtz 1999; Shepherd et al. 2004a).

CO line wing emission is detected towards this region by a number of investigators (Wouterloot & Brand 1989; Sridharan et al. 2002). The distance estimated by Wouterloot & Brand (1989) (1.17 kpc), and therefore the luminosity, are somewhat lower than that derived by Molinari et al. (1996) from the NH_3 observations. Snell et al. (1990) detected a bipolar outflow in CO with a spatial extent of 3 pc (4 arcmin). OVRO observations by Shepherd et al. (1998) at the wavelength of CO (J=1-0) line also revealed a well defined bipolar outflow in this field, roughly in the EW direction, originating from a B2-B3 star. They also detected shocked emission in the H_2 2.122-μm line.

The position of the MSX, mm and cm sources all agree to within 3.5 arcsec of each other. The 6-cm observations of Hughes & MacLeod (1993) showed emission with multiple structure (with an integrated flux density of 1.55 mJy), which was interpreted by them as due to a number of B3 stars. MacLeod et al. (1998a) proposed a spectral type of B2.7 for the exciting source. 3.6-cm observations by Shepherd & Kurtz (1999) revealed a total integrated flux density of 1.51 mJy with a central source of integrated flux density of 1.1 mJy. The source has also been detected at 3.6 cm by Sridharan et al. (2002) at 1.3 mJy; they do not detect any H_2O or CH_3OH maser from this region. Sridharan et al. detected emission in a number of molecular lines - SiO, CH_3OH and CH_3CN - from this region. From the spectral index derived from their 3.6-cm radio emission along with the 6-cm emission measured by Hughes & MacLeod (1993), Shepherd & Kurtz (1999) proposed an ionized jet. They suggested that the outflow from this source is driven by the thermal jet and a wide angle wind, contributing ~25% and ~75% respectively to the momentum. From the observed radio fluxes, Shepherd & Kurtz (1999) and Shepherd et al. (2004a) derive a B2 spectral type for the underlying protostar. Williams, Fuller & Sridharan (2005) also estimated an early-B spectral type for the exciting source.

The locations and velocities of the 22-GHz H_2O masers trace a 1000 AU Keplerian disc detected at mm wavelengths and an ionized jet detected at four wavelengths from 1.3 to 6 cm (Shepherd & Kurtz 1999; Shepherd et al. 2004a). Nevertheless, the high angular resolution observations of Shepherd et al. (2004a) did not strongly support or deny the disc origin of the masers. The 7-mm continuum observations of Shepherd, Claussen & Kurtz (2001), at an angular resolution of 40 mas, detected an inner 130-AU accretion disc. The orientation of the discs is roughly perpendicular to the large scale molecular outflow mapped by Shepherd et al. (1998).

Fig. A10 shows our *K*-band and continuum-subtracted H_2 images. The H_2 image has been smoothed with a 2-pixel FWHM Gaussian to enhance the appearance of the faint emission features. The outflow source itself appears to be highly obscured. In *K* we see an extended nebulosity in the NW-SE direction, most of which disappears in our continuum-subtracted H_2 image except for a few emission features. The *K*-band image shows a faint point source ("A"; α=5:38:13.59; δ=+16:31:58.05), from which a jet appears to emanate. The position of "A" agrees well with the mm and the cm positions given by Shepherd et al. (2004a). The 1.2-mm continuum peak imaged by Beuther et al. (2002b) is 1.24 arcsec SE from "A" and the 1.3-cm continuum source detected by Shepherd et al. (2004a) is only 0.85 arcsec from "A". The 2.7-mm continum peak of Shepherd et al. (1998) is only 1 arcsec away from "A" and it nearly coincides with the 1.3-cm source. The IRAS position is ~4.3 arcsec NE and the MSX position is ~3.2 arcsec NW of "A". Probably we are detecting the heated dust surrounding the YSO, rather than the source itself in the near-IR. The large negative residuals on the continuum-subtracted H_2 and Brγ images indicate the presence of a large amount of dust in the vicinity. Our continuum-subtracted H_2 image shows a collimated set of knots ("1") within 9.5 arcsec, mostly located eastward, of the central source "A" (Fig. A10 right: inset). In addition to these aligned emission knots close

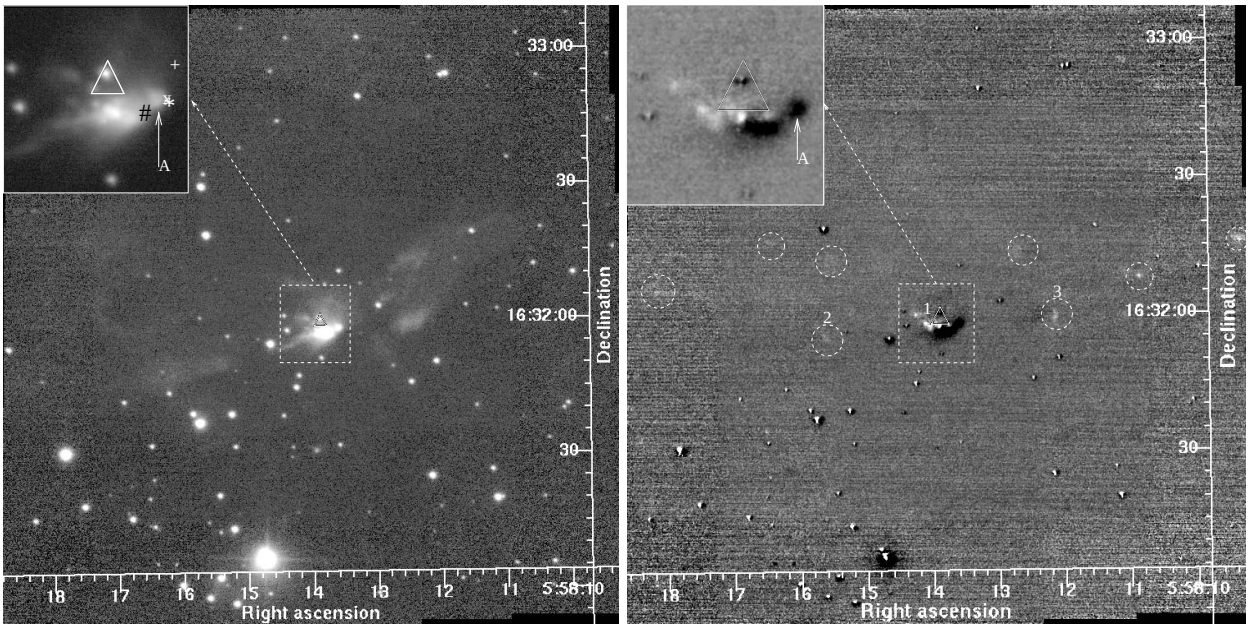

Figure A10. The left panel shows our *K*-band image of IRAS 05553+1631. The 2.7-mm continuum peak of Shepherd et al. (1998) is shown by "*" and the 1.2-mm continuum peak of Beuther et al. (2002b) is shown by "#". "x" shows the 1.3-cm radio continuum position of Shepherd et al. (2004a). The right panel shows the continuum-subtracted H_2 image. An expanded view of the region enclosed in the box is shown in the inset.

to the source, there are many other very faint emission features circled on the figure. These features are observed to be aligned roughly in the EW direction. The H_2 knots ("1") located close to "A", and two of the other knots at ∼29.6 arc SE ("2") and 21 arcsec NW ("3") from "A" were also detected by Indebetouw et al. (2003) (their Fig. 2). Considering all the H_2 emission features circled on Fig. A10, the outflow has a collimation factor of ∼1.9 and has a position angle of ∼84° in the east and ∼287° in the west.

The 2MASS images do not appear to resolve the point source "A" well from the nebulosity to the east. The 2MASS source is offset 2.7 arcsec SE of "A", is centred on the nebulosity, and shows excess (Fig. 1). Source "A" is well detected in the *K*-band images of Devine et al. (1999) and Indebetouw et al. (2003) and its coordinates derived by them agree well with ours. As is obvious from Fig. A10, this position is very close to the IRAS position and we identify "A" as the embedded YSO.

The direction of the outflow derived from CO maps (Shepherd et al. 1998; Snell et al. 1990) is consistent with the roughly EW alignment of the H_2 emission features detected in our image (Fig. A10 - right panel). The position angle of 84° for the outflow derived from our H_2 observations is similar to 80° derived by Shepherd et al. (1998) from their CO map. The bright H_2 line emission knots detected by us close to "A" in the east are in the direction of the blushifted lobe of the CO outflow.

Overall, IRAS 05553+1631 appears to be a luminous YSO driving outflow. From the wide opening angle defined for the CO outflow, the H_2 line emission knots and the ionized radio jet, Shepherd et al. (1998) and Shepherd & Kurtz (1999) proposed that the outflow is powered by a wide-angled wind and a jet. Eventhough the large scale distribution of the H_2 knots in Fig. A10 implies a wide angle, the arrangement of the H_2 knots in the vicinity of "A" is suggestive of a well-collimated jet. From the current observations it is not clear if more than one YSO is present.

A11 IRAS 06061+2151 - *Mol 16*
(*d = 0.1; 2.0 kpc, L = 0.0278; 4.0×10^3 L$_\odot$*)

The dense core associated with IRAS 06061+2151 has been mapped in NH_3 (Molinari et al. 1996; Jijina, Myers & Adams 1999) and in CS (J=2-1) (Bronfman et al. 1996; Carpenter, Snell & Schloerb 1995). The estimate of the distance towards this source (and thereby, the luminosity) has considerable uncertainty. Molinari et al. (1996) determined a kinematic distance of 0.1 kpc and derived a FIR luminosity of 27.8 $L_\odot$, whereas Carpenter et al. (1995) assigned a membership in the Gemini OB1 molecular cloud complex and derived a far-IR luminosity of 4000 $L_\odot$ at a distance of ∼2 kpc. Powerful H_2O maser emission has been detected from this region where multiple (up to 6) maser spots were mapped at different radial velocities (Brand et al. 1994; Palla et al. 1991). Schutte et al. (1993) did not detect any CH_3OH maser, whereas the detections by Galt (2004) (observed in 1994) and Szymczak et al. (2000) differ in intensity and radial velocity, showing the variable nature of the CH_3OH maser emission from this region over a period of a few years. Wouterloot & Brand (1989) detected ^{12}CO (J=1-0) with a red wing and derived a kinematic distance less than 0.1 kpc and a FIR luminosity of 27 $L_\odot$. Shepherd & Churchwell (1996a) also detected ^{12}CO (J=1-0) emission. Faint (0.6–3.4 mJy) 3.6-cm continuum emission was detected by Kurtz, Churchwell & Wood (1994) from three locations within 15 arcsec of the IRAS position. The source was also detected at 1.3 mm with a flux density of 4.2 Jy by Chini et al. (1986). Near-IR H_2 images of this object were recently published by Anandaro et al. (2004). They proposed that the cluster hosts multiple YSOs, the brightest being of early-B spectral type. They also deteced two knots of H_2 emission.

Fig. A11 shows our *K*-band and continuum-subtracted H_2 images. No extended Brγ emission was detected, so this image is not shown. Our *K*-band image unveils a rich cluster embedded in nebulosity. A major part of this nebulosity disappears in the continuum-subtracted H_2 image. Of the H_2 emission features, the prominent ones are the NW and the SE knots detected by Anandaro et al.

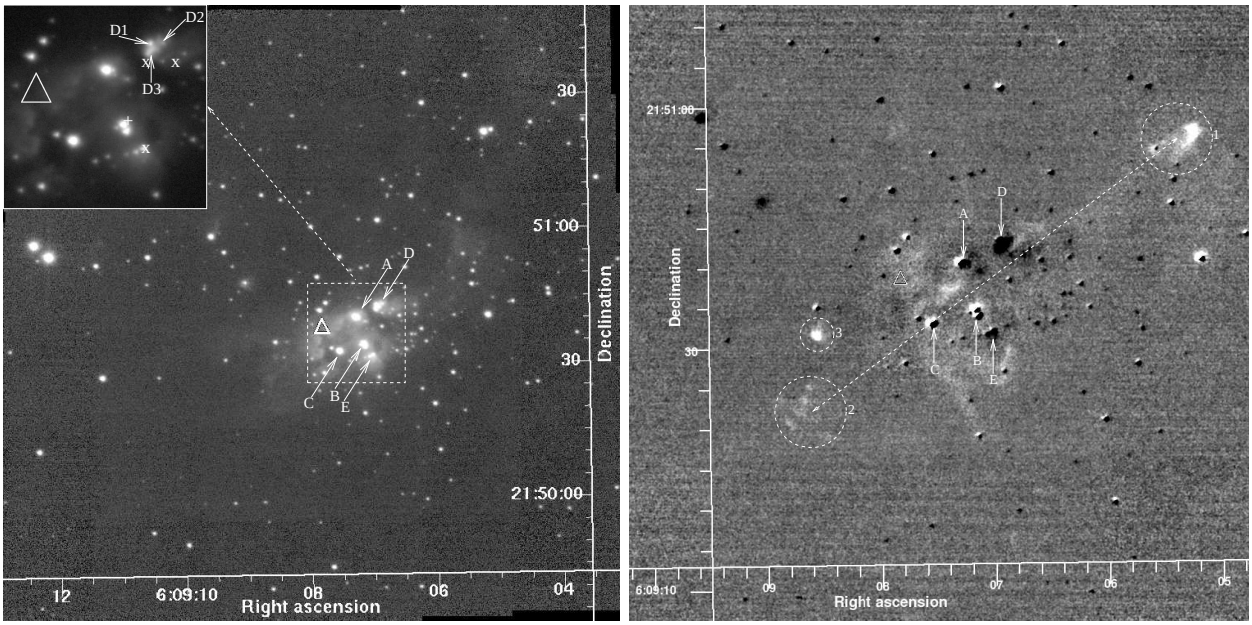

Figure A11. Left: *K*-band image of IRAS 06061+2151. The three radio positions listed in Kurtz et al. (1994) are shown by "x". Right: central region of the continuum-subtracted H_2 image.

(2004), the locations of which are "1" (α=6:9:5.22, δ=21:50:6) and "2" (α=6:9:8.69, δ=21:50:22.8) respectively. "2" is resolved into at least four components. There is another feature labelled "3" (α=6:9:8.55, δ=21:50:31.7) located in the SE direction, close to "2". The NW knot ("1") is a bow shock. The main jet, composed of at least "1" and "2", appears to be well collimated. These two features together give an outflow angle of 128° and a collimation factor of 4.3. The collimation factor would be higher if the multiple bow shocks seen in "2" are due to precession or multiple jets. The five prominent sources detected by Anandaro et al. (2004) are labelled on Fig. A11, with "A–E" representing the stars "1–5" discussed by them. At our high spatial resolution, all five sources are resolved into multiple components as seen in the inset. 2MASS colours of "A" (α=06:09:07.28, δ=21:50:40.4) and "B" (centroid: α=06:09:07.14, δ=21:50:34.2) do not exhibit any excess. However, it should be noted that "A" has faint companions and "B" is composed of more than one object. Both "A" and "B" are poorly detected by 2MASS in K_s. "D" (centroid: α=6:9:6.91, δ=21:50:42.8) appears to be the driving source of the main outflow (represented by "1" and "2") in this region. It is resolved into multiple components, three of which are labelled on the figure. "D3" appears to be an extended feature directed away from "D1/D2" in the SE direction, but this feature gives strong negative residuals upon continuum subtraction implying that it is probably dominated by emission from dust. The IRAS position is 13.5 arcsec SE of "D" and 10.2 arcsec NE of "B". The location of the MSX source is 8 arcsec SE of "D" and nearly coincides with "B". It is possible that more than one source is contributing to the IRAS and MSX fluxes. "D" shows large excess in its 2MASS colours (not detected in *J*). Near-IR spectroscopy of Hanson, Luhman & Rieke (2002) detected 2.122-μm H_2 line emission from "D" or its vicinity. 2MASS detection near "E" only in *K* and the coordinates centred off the source that we label here. So "E" is not shown in Fig. 1. Also obvious in Fig. A11 is the line emission in the H_2 from within the cluster, many of which appear filamentary and arc-like. Some of these could be due to jets from other sources within the cluster or fluorescence due to the emission from more evolved sources in the cluster. Deeper imaging in H_2 is required to properly map these. Overall, this cluster appears to host several YSOs.

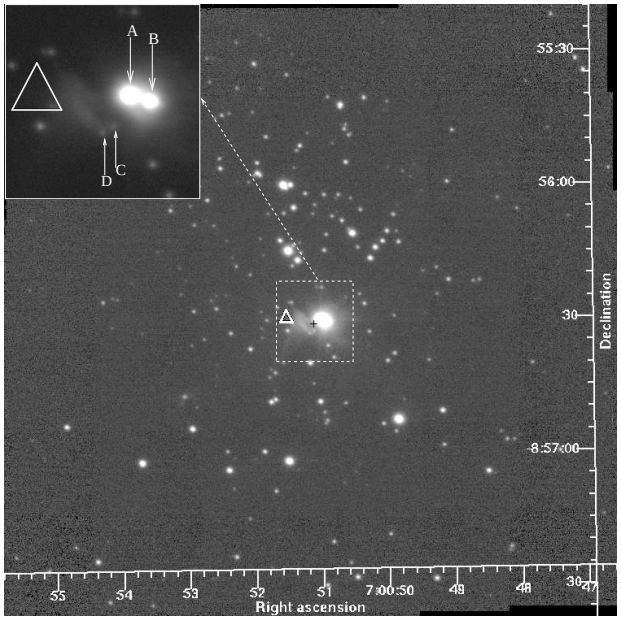

Figure A12. *K*-band image of IRAS 06584-0852. The inset shows an expanded view of the central region showing the nebulosity and the near-IR sources well resolved.

A12 IRAS 06584-0852 – *Mol 28*
(*d = 4.48 kpc, L = 5.67×10^3 L$_\odot$*)

Molinari et al. (1996) detected a dense core at this location in NH_3 emission. They determined a kinematic distance of 4.48 kpc and derived a far-IR luminosity of 9.08 ×10^3 L$_\odot$. Molinari et al. (2000)

obtained (sub)mm photometry and derived a bolometric luminosity of $5.6 \times 10^3 L_\odot$ for the core. Ishii et al. (2002) included IRAS 06584-0852 in their JHK' survey of clusters associated with luminous IRAS sources. They detected a reflection nebula in this cluster. The source was not detected by the VLA at 2 and 6 cm (Molinari et al. 1998). Wouterloot & Brand (1989) detected red-shifted CO emission and Zhang et al. (2005) mapped a molecular outflow in CO (J=1-0) line emission. Brand et al. (1994) and Palla et al. (1991) detected H_2O maser from this region.

Fig. A12 shows our K-band image of the region; an expanded view of the central region with higher contrast is shown in the inset. The near-IR image reveals a cluster of objects with two bright stars ("A" and "B") near the centre of the field separated by ∼1.73 arcsec, and located at (α=07:00:51.01, δ=-08:56:29.8) and (α=07:00:50.90, δ=-08:56:30.3) respectively. There are two stars located to the SE of this pair, that are much fainter than "A" and "B". These two objects located at (α=7:00:51.10, δ=-8:56:32.5) and (α=7:00:51.16, δ=-8:56:3) are labelled "C" and "D" respectively. "D" has a cometary nebula associated with it. The continuum-subtracted H_2 and Brγ images reveal no line emission. Hence these images are not shown here. The bright central pair is well detected by 2MASS, but the components are not resolved in the 2MASS image. The colours of the two objects combined, as derived from 2MASS photometry, exhibit large reddening and IR excess, placing them in the region of reddened YSOs on the colour-colour diagram (Fig. 1). The IRAS source is located ∼8.5 arcsec east of the centroid of "A" and "B" and the MSX source is 2.3 arcsec SE. These observations show that "A" and "B" are probably the near-IR counterparts of the YSO. The source has probably past its very early stage of formation.

A13 IRAS 18144-1723 – *Mol 45*

(d = 4.33 kpc, $L = 21.2 \times 10^3 L_\odot$)

IRAS 18144-1723 is associated with an ammonia core (Molinari et al. 1996) and water and methanol masers (Palla et al. 1991; Szymczak et al. 2000; Kurtz et al. 2004). Molinari et al. (1998) detected radio emission at 6 cm from a region located 93 arcsecs away from the location of the IRAS source and the masers. Hence, the radio emission does not appear to be associated with the IRAS source. CO observations of this region by Zhang et al. (2005) did not reveal any outflow.

Fig. A13 shows our K-band and continuum-subtracted H_2 images of IRAS 18144-1723. There is a point source, "A" (at α=18:17:24.38, δ=-17:22:14.7), located within 1.3 arcsec of the IRAS position. This object was not detected in the 2MASS J-band data, was only marginally detected in H, but is bright in K_s. Our K-band image shows nebulosity around "A", most of which disappears in the continuum-subtracted H_2 image. The H_2 image reveals a bow-shock like feature located at (α=18:17:23.13, δ=-17:22:13.5) with an extent of over 2 arcsec, mostly in the EW direction, which is circled in the figure. If the H_2 emission feature originates from "A", the outflow is at an angle of 274° with a collimation factor ∼10. Notably, "A" is located within 0.4 arcsec of the MSX position. It exhibits large infrared excess and is located in the region occupied by reddened YSOs in the JHK colour-colour diagram (Fig. 1). "A" is the most likely IR counterpart of the YSO producing the outflow in this region. The region was not observed in Brγ. The lack of strong radio emission from "A" at 6 cm (Molinari et al. 1998) indicates that "A" is probably in a pre-UCHII stage.

A14 IRAS 18151-1208 – *Mol 46*

(d = 3.0 kpc, $L = 19.95 \times 10^3 L_\odot$)

IRAS 18151-1208 is embedded in a high-density core detected in CS and NH_3 emissions in the surveys carried out by Bronfman et al. (1996) and Molinari et al. (1996) respectively. The IRAS source is bright and has FIR colours typical of UCHII regions (Wood & Churchwell 1989a). However, the source was not detected at 3.6 cm by Sridharan et al. (2002), which indicates the lack of a substantial HII region. Instead, the source may be in a pre-UCHII phase; its double-peaked SED is typical of low-mass Class I YSOs, where the cold dust component, peaking at ∼100 μm, dominates over the warmer dust component at ∼20 μm. The bolometric luminosity of the source, derived from IRAS HiRes photometry, is ∼20,000 $L_\odot$ (Sridharan et al. 2002). The kinematic distance to IRAS 18151-1208 is 3.0 kpc (Brand and Blitz 1993).

A moderately collimated (collimation factor=2.1) molecular outflow was mapped in the ^{12}CO (J=2-1) transition by Beuther et al. (2002c). Beuther et al. (2002d) observed methanol maser emission from this region, from a location very close to the luminous YSO that we identify here. They also detected faint H_2O maser emission. However, the location of the water maser detected by them is far away from the YSO and is outside the field of view of our H_2 image. Hence it is not related to the YSO detected here. The survey by Palla et al. (1991) also failed to detect any H_2O maser emission from IRAS 18151-1208.

Our infrared images reveal a cluster of objects embedded in nebulosity and two well-collimated outflows for the first time in this region. Fig. A14 shows our K-band and continuum-subtracted H_2 images. The central object labelled "A" (α=18:17:58.12, δ=-12:07:24.7) is deeply embedded. 2MASS gives only an upper limit in J; the $H - K$ colour shows large reddening and excess, typical of a deeply embedded luminous YSO (Fig. 1). The H_2 image shows two jets, the directions of which are shown by the two arrows on Fig. A14, labelled "1" and "2" respectively. The brighter of the two ("1") is in the NW-SE direction, at an angle 131° and has a collimation factor of ∼6.3. If we consider that the feature circled and labelled "3" is part of the same outflow, the collimation factor could be as high as 12.8. "A" is located at the centroid of the NW-SE jet and is most probably the driving source of the jet in the direction of "1". The methanol maser detected by Beuther et al. (2002d) appears to be associated with "A"; it is located only 0.75 arcsec SW of "A". This separation is within the positional accuracies quoted by Beuther et al. (Table C1). The 15.1 arcsec offset from the IRAS position could be due to the positional inaccuracy of the IRAS detection. The MSX mission indeed detected a mid-IR source at wavelengths above 8.28 μm within 0.5 arcsec of "A", and the 1.2-mm continuum peak observed by Beuther et al. (2002b) is only 2.21 arcsec SW of "A". The second outflow ("2") appears to be driven by another embedded source SW of "A" which is not detected in the near IR. This outflow is at an angle 35.5° and has a collimation factor of ∼5.7. A comparison of the directions of the two jets with that of the CO outflow reveals that these two well-collimated jets together drive the molecular outflow mapped by Beuther et al. (2002c). If the driving source of the outflow "2" is deeply embedded and is located at the centroid of "2", it is likely to be at ∼15 arcsec SW of "A". This source also may be contributing to the 1.2-mm continuum source detected by Beuther et al. (2002b). Millimetre observations at high angular resolution are therefore required to understand that.

Our discovery images prompted the detailed follow-up observations of Davis et al. (2004), who obtained near-IR echelle and

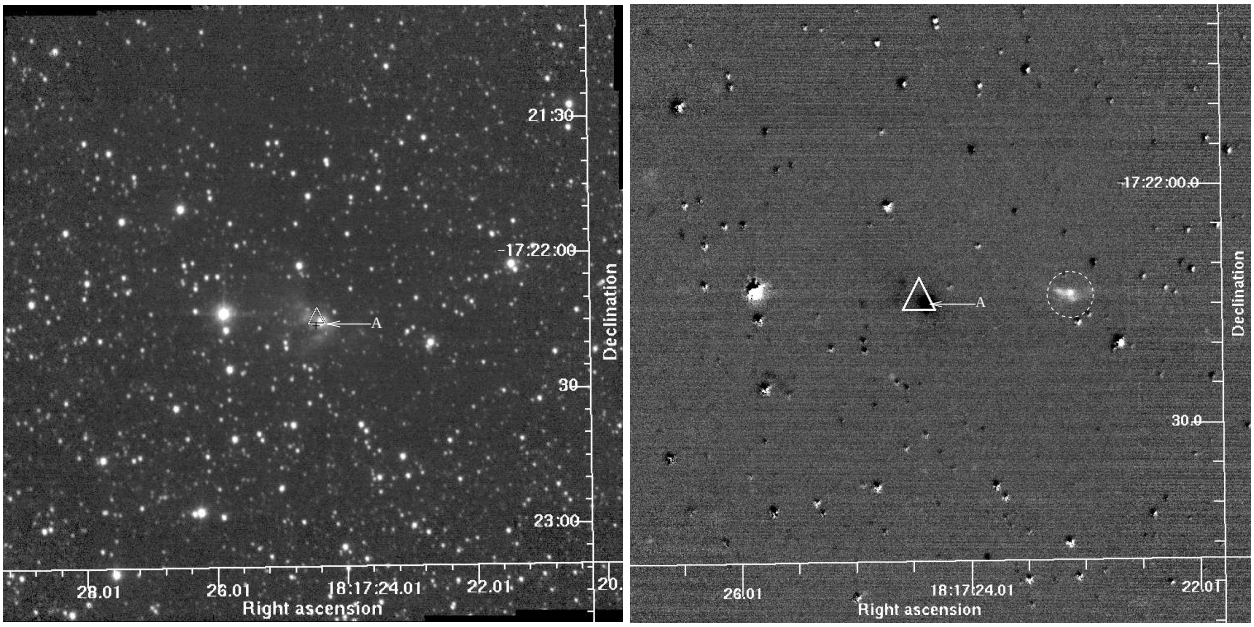

Figure A13. Left: *K*-band image of IRAS 18144-1723. Right: The central portion of the continuum-subtracted H_2 image.

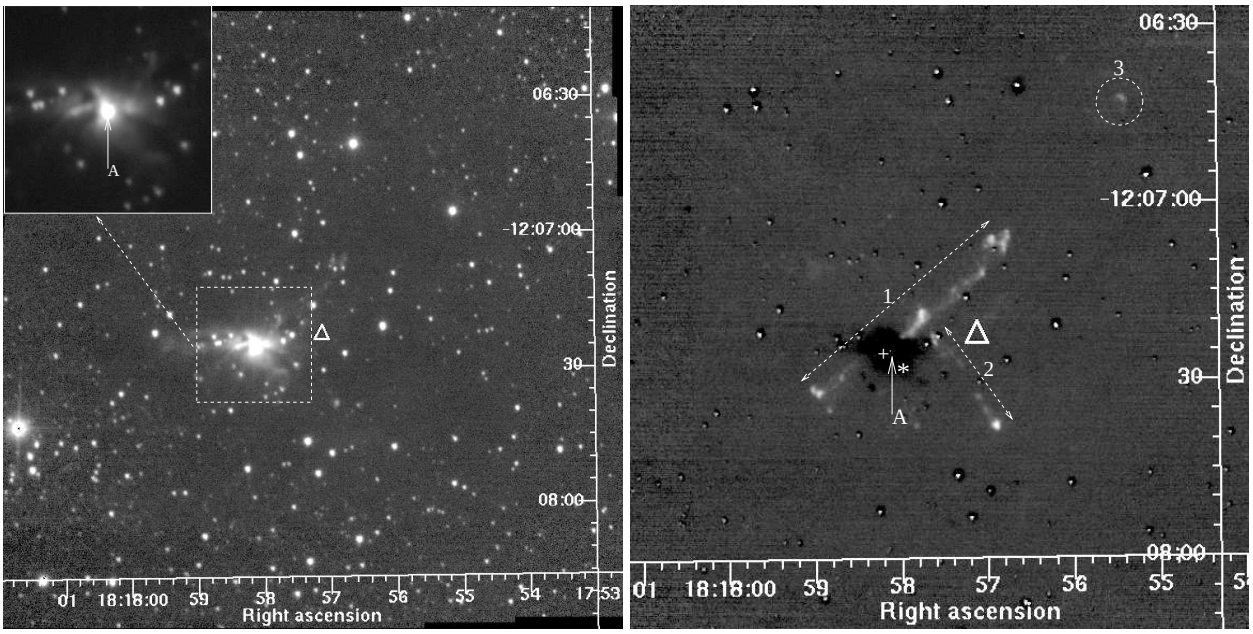

Figure A14. The left panel shows the *K*-band image of IRAS 18151-1208 and the right panel shows the central portion of the continuum-subtracted H_2 image. The 1.2-mm continuum peak observed by Beuther et al. (2002b) is shown by "*". The H_2 image has been smoothed with a Gaussian of FWHM=2 pixels.

Integral Field spectra. Their *HK* spectroscopy revealed a steeply rising SED for "A" with Brγ and CO overtone emission, which are typical of an accreting source with a disc. High-resolution spectroscopy at 2.122 μm shows that the H_2 emission from the jet is blue- and red-shifted on either sides of "A". The IFU data also reveal a collimated jet from "A". Davis et al. (2004) found that the general properties of the two outflows are similar to those of low-mass outflows, and that these jets are very much like scaled up versions of their low-mass counterparts.

A15 IRAS 18159-1648 - *Mol 49*

(*d = 2.5 kpc, L = 29.5×10^3 L$_\odot$*)

IRAS 18159-1648 (GAL 014.33-00.64) was detected in CS(2-1) by Bronfman et al. (1996). Molinari et al. (1996) detected the dense core in NH_3 emission. Harju et al. (1998) detected SiO (2-1) and (3-2), both at the same peak velocity. This is also consistent with the detection of two methanol maser spots at a velocity of 21 kms^{-1} by Walsh et al. (1997), though this detection was not confirmed by Szymczak et al. (2000) or Slysh et al. (1999), probably because their observations were less sensitive. Water maser emission was observed from this region by Palla et al. (1991).

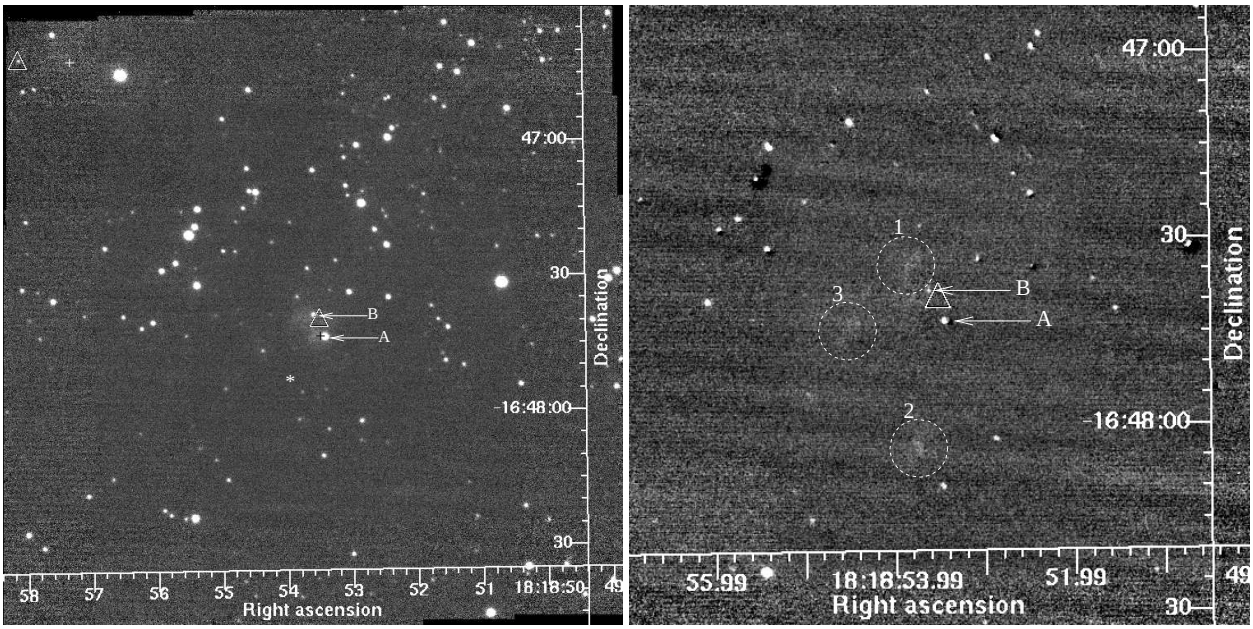

Figure A15. Left: *K*-band image of IRAS 18159-1648. "*" shows the 1.2-mm peak position of Faúndez et al. (2004). Right: Continuum-subtracted H_2 image of the central region.

Fig. A15 shows our *K* and H_2 images. Two objects are labelled in the figure - "A" (α=18:18:53.41, δ=-16:47:43.1) and "B" (α=18:18:53.58, δ=-16:47:38.2) - both are embedded in faint nebulosity. The 2MASS colours of "A" shows excess and reddening, whereas "B" is located in the reddening band (Fig. 1). However, it should be noted that "B" has only upper limits in the 2MASS *J* and *H* and has poor S/N in K_s, whereas "A" has only upper limits in *J* and has poor S/N in *H*. The 1.2-mm continuum source detected by Faúndez et al. (2004) is only 12.25 arcsec SE of "A". This separation is less than their beamsize of 24 arcsec. The IRAS source is located 4.55 arcsec NE of "A" and the MSX detection is at 1.25 arcsec east and 0.1 arcsec north of "A". From the near-IR excess and reddening and the close proximity of the MSX, IRAS and 1.2-mm sources, it appears that "A" is the luminous YSO in this field. It remains to be investigated from better photometry if "B" also is a YSO.

There is a tentative detection of H_2 line emission close to the centre of the field. The H_2 image (Fig. A15 - right panel) is smoothed with a 2-pixel FWHM Gaussian to enhance the very faint emission features. Three features detected are circled and labelled "1–3" on the H_2 image. A deeper integration in H_2 is required if we are to comment further on these possible outflow features.

A16 IRAS 18174-1612 - *G15.04-0.68, M17-UC1*
(*d = 2.1 kpc, L = 433×10^3 $L_\odot$*)

Commonly known as M17-UC1, IRAS 18174-1612 is a Hyper Compact HII (HCHII) region (Johnson, Depree & Goss, 1998; Sewilo et al. 2004) located near the centre of the southern bar of the M17 (NGC 6618) molecular cloud, identified by Felli, Johnston & Churchwell (1980). The object was resolved at radio wavelengths by Felli, Churchwell & Massi (1984) using the VLA at high angular resolution, who showed that the M17-UC1 is a tiny shell of gas (diameter ~0.4 arcsec or 1.4×10^{16} cm) ionized from within by a B0–0.5 YSO. Their observations revealed M17-UC1 as a powerful radio emitter with 147±7, 118±7, 28±3 and < 7 mJy at 1.2, 2, 6 and 21 cm respectively. They interpret this object as the result of shock-induced star formation in the H^+-H_2 interface. An "arc"-type emission nebulosity was discovered ~4 arcsec east of the UCHII at radio wavelengths. OH masers (Caswell 1997; Forster & Caswell 1999) and Class II methanol masers (Menten 1991; Walsh et al. 1998) have been detected within an arcsec of M17-UC1. Methanol masers have been detected by several other investigators too. Błaszkiewicz & Kus (2004) reported the variable nature of the 6.7 GHz methanol maser emission from this region. However, H_2O maser detections are away from it by ~30 arcsec or more; a group of them are located NW, ~6 arcsec north of the IRAS position and another group ~30 arcsec SW of M17-UC1 (Massi, Felli & Churchwell 1988, Forster & Caswell 1999). H_2O maser spots observed by Johnson et al. (1998) are also offset NW and SW of M17-UC1 (with some of them located closer than those detected by Massi et al. 1988). NH_3 maps of this region show the clumpy nature of the molecular cloud, with the NH_3 clumps, the HCHII M17-UC1 and the IR and radio continuum emission of the ionization front all well separated. They suggest that the clumps detected in NH_3 may be producing low-mass stars.

Through near- and mid-IR imaging and spectroscopy, Nielbock et al. (2007) proposed that M17-UC1 is surrounded by a disc of cool dust. The photometric distance towards this object (2.2 ± 0.2 kpc) derived by Chini, Elsäesser and Neckel (1980) is in agreement with the kinematic distance. A search by Shepherd & Churchwell (1996b) in CO found no evidence of a bipolar molecular outflow from this region.

The 2.3×2.3 arcmin^2 field observed by us is rather complex and rich in nebulosity. Fig. A16a shows the *K*-band and continuum-subtracted H_2 images observed by us and Fig. A16b shows our continuum-subtracted Brγ image. Three sources imaged previously at high angular resolution in the near-IR (Nielbock et al. 2007) are labelled in Fig. A16a: "A" (α=18:20:24.60, δ=-16:11:39.5), "B" (α=18:20:24.83, δ=-16:11:35.3) and "C" (α=18:20:25.08, δ=-16:11:34.1). "B" is the near-IR counterpart of M17-UC1. It is not detected in the 2MASS images. Nielbock et al. detected it in *H*

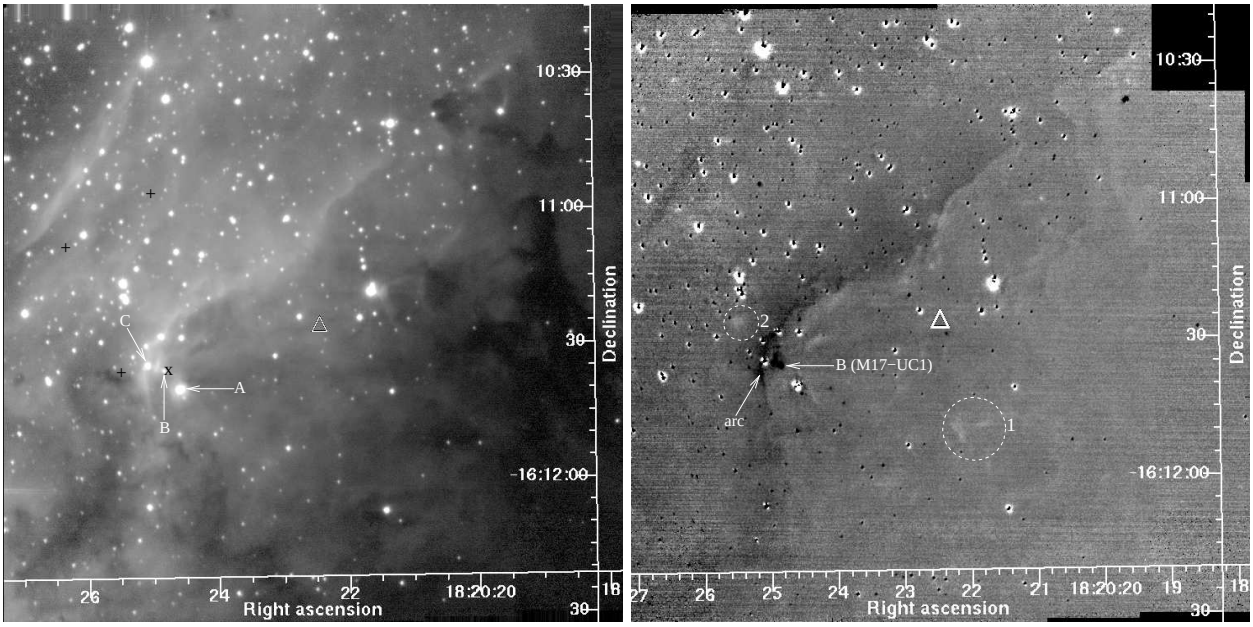

Figure A16a. The left panel shows the *K*-band image of IRAS 18174-1612 and the right panel shows the continuum-subtracted H_2 image smoothed with a Gaussian of 2-pixel FWHM. "x" shows the radio position of the UCHII given by Wood & Churchwell (1989b).

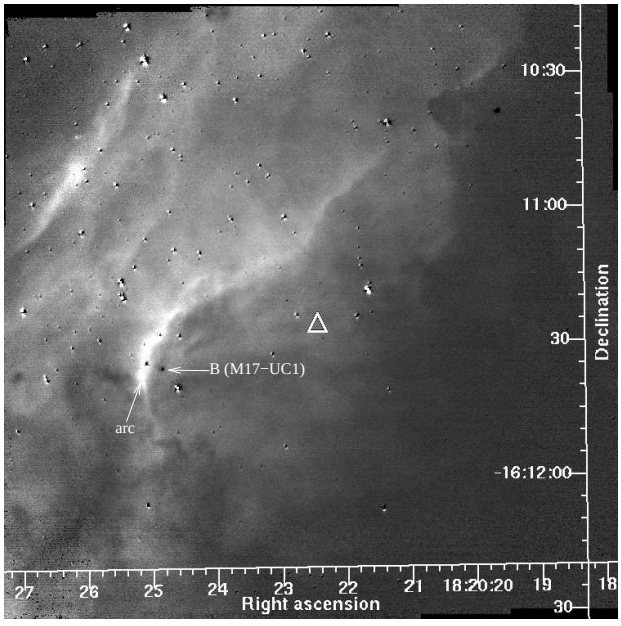

Figure A16b. Continuum-subtracted Brγ image of IRAS 18174-1612.

and K_s only. The location of M17-UC1 in Fig. 1 using the H and K_s magnitudes of Nielbock et al. and using their J-band detection limit shows that it has large reddening and IR excess. However, for an A_V=40 derived by Nielbock et al., the J magnitude of "B" will be much fainter than the detection limit, which will move it further up and place it in a region of larger reddening and lesser excess in Fig. 1. "A" and "C" are identified with IRS5 and B273 respectively of Nielbock et al. (2007). "A" has a faint companion located ~0.35 arcsec north and ~0.95 arcsec west of the brighter one. The physical association of these two stars is not certain at this stage. The 2MASS colours of "A" are dominated by the brighter component and do not exhibit any IR excess. "C" exhibits slight IR excess. Both "A" and "C" exhibit large reddening. Part of the southern bar of M17 is seen in emission in Brγ, diagonally across the image. M17-UC1 ("B") and the emission "arc" are labelled on the image. As can be expected for an ionization front, the "arc" is very bright in the continuum-subtracted Brγ image.

Our H_2 image does not reveal any major collimated outflow in this region. Two faint bow-shock-like H_2 line emission features are circled and are labelled "1" and "2" in Fig. A16a . There is also very faint H_2 emission seen from the inner edge of the Brγ "arc" and at the boundary of the bright Brγ emission ridge and the H_2 cloud, near the centre of the field. It is not clear if these are due to shocks or fluorescence. The massive protostellar disc proposed by Chini et al. (2004) is further SE of "B" and is not related to any of the sources considered here.

The IRAS source is located ~36 arcsec NW of M17-UC1 and is probably not related to the radio source. Three MSX sources are present in the field. One of the sources is in the vicinity of M17-UC1. There are no near-IR counterparts identified for the other two MSX sources. None of the MSX sources is in the vicinity of the IRAS source, which is probably very young and not very bright in the near- and mid-IR. The lack of any convincing signatures of powerful outflow in H_2 and CO and the presence of strong radio emission show that M17-UC1 has probably passed its main accretion and outflow stage and is actively moving towards a UCHII stage via its present HCHII phase.

A17 IRAS 18182-1433

(*d = 4.5, 11.8 kpc, L = (20, 125.9; 50.1)* $\times 10^3$ $L_\odot$)

This object was detected in CS emission by Bronfman et al. (1996) and Beuther et al. (2002b). Walsh et al. (1998) detected CH_3OH maser emission in this region, located NE of the IRAS position. Beuther et al. (2002d) resolved five H_2O maser spots, very close to the location of the CH_3OH maser and the single 1.2-mm peak of Beuther et al. (2002b). Observations of Sridharan et al. (2002) revealed the presence of H_2O and CH_3OH masers and emission

by SiO, CH_3CN and NH_3. They also reported the detection of CO emission line wings implying the presence of a molecular outflow. Beuther et al. (2002c) mapped the blue- and red-shifted lobes of the outflow and derived a collimation factor of 1.7. Beuther et al. (2006) performed high-angular-resolution observations of IRAS 18182-1433 in 1.3-mm continuum emission and in a number of molecular species including ^{12}CO (2-1). In the CO data obtained using the SMA and IRAM, they detect two outflows, inclined ∼90° with each other. Their SiO data (obtained using the VLA) is suggestive of the possibility of an additional third outflow, emanating towards the north. The southern lobe of this outflow is not detected in their SiO data. Most of the molecular species peak ∼1-2 arcsec SE of the 1.2-mm peak and appear to coincide with one of the nearby radio sources detected by Zapata et al. (2006). Williams, Fuller & Sridharan (2004) imaged a core at 450 and 850 μm. By modelling the 850-μm data, Williams et al. (2005) proposed a core with isothermal density profile producing an O9 star.

The VLA observations of Sridharan et al. (2002) did not find any radio emission at 3.6 cm from this region, suggestive of a pre-UCHII source. Later observations of Zapata et al. (2006) revealed two faint radio sources in this region at 1.3 and 3.6 cm. The first radio source ("b"), which is interpreted as due to a thermal jet, is located near, but offset by ∼1.9 arcsec SE from, a 7-mm continuum source ("a") detected by them. The 7-mm source is also detected at 1.2 mm by Beuther et al. (2002b) and later at 1.3 mm at high angular resolution using the SMA by Beuther et al. (2006). The cm emission is considered by Beuther et al. (2006) as due to an unresolved companion to the mm emitting source or due to a thermal jet. A second radio source detected by Zapata et al. (2006) ("c") is 9.7 arcsec SE of the first and is considered to be due to strong shocks. The labels "a–c" are given to be consistent with those of Zapata et al. (2006).

Fig. A17 shows our K-band image of IRAS 18182-1433. Since no extended emission was detected in H_2 or Brγ, those images are not shown here. Four objects are labelled on the K-band image. The object labelled "A" (α=18:21:9.10, δ=-14:31:49.1) is located within one arcsecond of the H_2O maser position of Beuther et al. (2002d). Its 2MASS colours place it in the region of evolved stars (Fig. 1). However, the 2MASS K_s magnitude of this object is only an upper limit. Using a rough estimate of the K-magnitude from our image (comparing with brighter nearby objects), the location of the object comes closer to the reddening band. The object "B" (α=18:21:9.70, δ=-14:31:35.5) appears with a large IR excess. Similarly, "C" (α=18:21:9.48, δ=-14:31:56.1) also displays large excess. However, "B" and "C" are detected only in K_s by 2MASS; they are not detected in J and H and have only upper limit magnitudes. Deeper JH imaging of the field is therefore required. "C" has a fainter companion located 1.4 arcsec NW and both are embedded in faint nebulosity in our K-band image. The coordinates given here are those of the brighter component. This source also exhibits IR excess. Finally, "D" (α=18:21:8.83, δ=-14:31:54.95) is a very faint object that is not detected by 2MASS. It is associated with an arc-like feature in K, which is located 1.7 arcsec NE of a faint point source and has an extent of ∼2.5 arcsec in the NE direction. There is no H_2 emission associated with this.

One of the two radio sources detected by Zapata et al. (2006) at 1.3 and 3.6 cm (their 18182-1433b), which is in the vicinity of the millimetre source, is located very close to "A". This source also is associated with the CH_3OH maser detected by Beuther et al. (2002b) and is interpreted by Zapata et al. (2006) as due to free-free emission from a thermal jet or a stellar wind. The brightest of their radio sources (18182-1433c), the origin of which is suspected

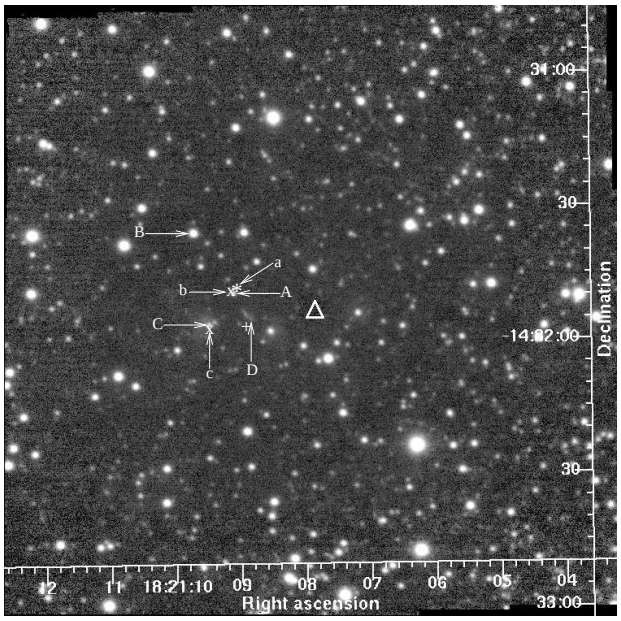

Figure A17. *K*-band image of IRAS 18182-1433. "* (a)" shows the location of the 7-mm peak of Zapata et al. (2006) and the 1.3-mm peak of Beuther et al. (2006). The 3.6-cm sources of Zapata et al. (2006) are shown by "x (b and c)".

by them as due to strong shocks, is located very close to the bright near-IR source in "C". They did not detect any 7-mm emission associated with this. The location of the MSX source is between "C" and "D", closer to "D" (2.3 arcsec SE of "D"). The mid-IR observations of De Buizer et al. (2005) resolved two sources in this region, the fainter one is located close to the location of the water masers and a brighter, more extended one is located further SE. The fainter one also agrees with a detection in the near-IR by Testi et al. (1994). We do not see any near-IR source at the location of either of these mid-IR sources. However, applying a translation of ∼2.4 arcsec towards the north to the mid-IR positions of De Buizer et al. (2005), the fainter mid-IR source agrees with "A" and the brighter and extended mid-IR source agrees with the binary "C", with the direction of extension of similar to that of the direction of orientation of the binary components. This gives justification in identifying "A" and "C" as two candidates for the near-IR sources of the YSOs in this region. The mutual association of the sources detected at different wavelengths in this region needs to be thoroughly investigated.

A18 IRAS 18264-1152

(*d = 3.5, 12.5 kpc, L = (10, 125.9)*$\times 10^3$ $L_\odot$)

Bronfman et al. (1996) and Beuther et al. (2002b) detected CS emission from this source. Sridharan et al. (2002) observed CO emission line wings implying the presence of bipolar outflows; observations by Beuther et al. (2002c) indeed mapped the red- and blue- shifted lobes of the CO outflow, which are located close to the 1.2-mm emission peak of Beuther et al. (2002b). Sridharan et al. (2002) and Beuther et al. (2002d) observed H_2O and CH_3OH maser emission from this region, from locations very close to the millimeter peak. The location of the 1.2-mm peak and the masers were found to be north and west of the MSX position by ∼8.5 and 1 arcsec respectively. However, this offset is within the spatial resolution of the MSX data. Sridharan et al. (2002) also discovered line emissions in NH_3, SiO, CH_3OH, and CH_3CN from this region in

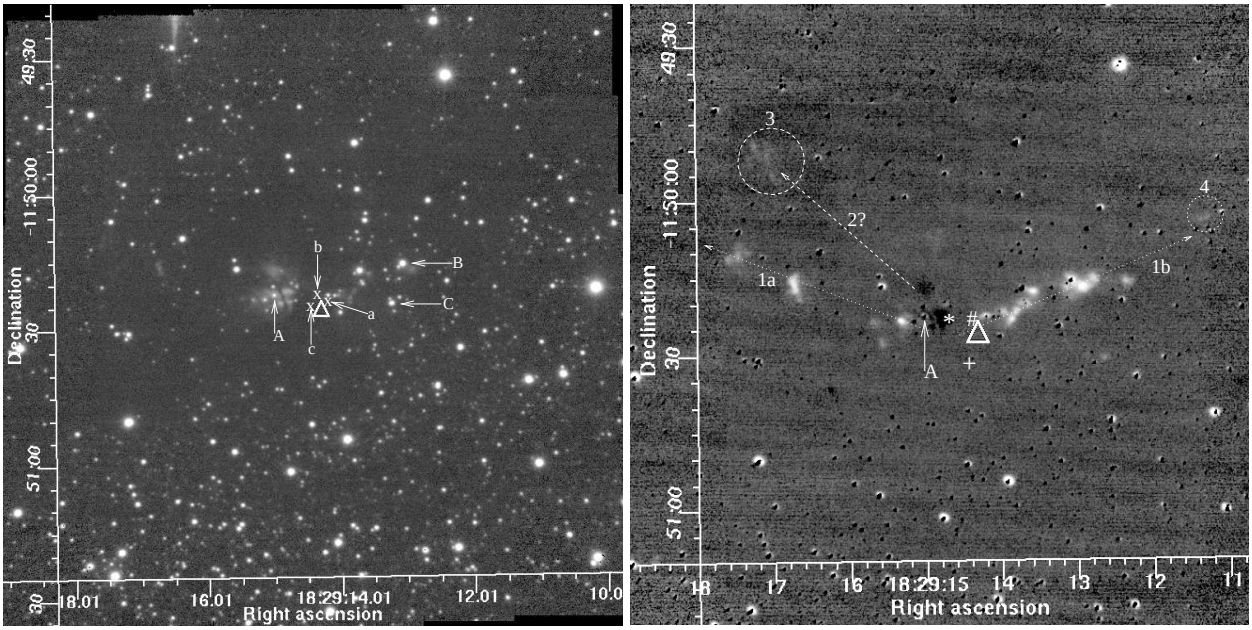

Figure A18. The left panel shows the *K*-band image of IRAS 18264-1152 and the right panel shows the continuum-subtracted H_2 image smoothed with a 2-pixel FWHM Gaussian. The arrows show the directions of the outflows. The "*" sign shows the location of the 1.2-mm centroid of Beuther et al. (2002b). The 1.3-cm positions of Zapata et al. (2006) are shown by "x" (labelled "a–c" to be consistent with their original naming); their 7-mm position is shown by "#".

addition to H_2O and CH_3OH masers. Their observation at 3.6 cm using the VLA resulted in a null detection (< 1mJy).

Our H_2 observations reveal a spectacular bipolar outflow from this source (Fig. A18). The continuum-subtracted H_2 image shows an outflow roughly in the EW direction, originating from a source somewhere near the millimetre position, the near-IR counterpart of which is not detected here. The direction of the outflow traced by the H_2 emission is in agreement with the direction inferred from the CO map of Beuther et al. (2002c). The 1.2-mm continuum peak of Beuther et al. (2002b) is located near the centre of the H_2 lobes. One or both of the lobes of this bipolar outflow, the directions of which are shown by the arrows labelled "1a" and "1b" at angles 63.5° and 291° respectively, appear bent northward. The outflow has a collimation factor of ∼7. At this stage, we also cannot rule out the possibility that "1a" and "1b" represent two different outflows rather than being a bent outflow as described above. Detailed radial velocity studies are required to ascertain this. There is another H_2 emission feature towards the west, circled and labelled "4", which is possibly part of the outflow lobe in the direction of "1b". There is also some faint H_2 emission feature shaped like a bow-shock, circled and labelled "3". This is very faint and we are not sure at this stage if this feature reveals the bow-shock of a separate outflow or fluorescent emission. If it is due to an outflow, it is possibly in the direction of the arrow labelled "2" at an angle of ∼48°. Observations by Zapata et al. (2006) at 7 mm and 1.3 cm resolved the YSO as a possible triple system, with components separated by ∼2 arcsec and the brightest peak at 7 mm coinciding with the brightest at 1.3 cm. Hence it is possible that "3" is the bow shock of another outflow. No emission was seen in our Brγ image; hence it is not displayed here.

Three objects located close to the IRAS position are labelled on the Fig. A18. "A" (α=18:29:15.01, δ=-11:50:22.5) is 11 arcsec NE of the IRAS position and is near the geometric centre of the two lobes. However, it is not clear if this is the driving source of the H_2 outflow. The objects labelled "B" and "C" also show excess, but they are far away from the apparent centre of the flow and are not the driving sources of the outflow/s traced by "1a" and "1b" (they are located along the western branch of the H_2 outflow). All three sources are shown in the 2MASS colour-colour diagram (Fig. 1) and do show reddening and excess. Many of the fainter objects detected in our *K*-band image are not detected by 2MASS. Hence we do not have any colour information on them. Overall, IRAS 18264-1152 appears to be young, in a phase of active accretion and outflow. Detailed near-IR studies of this object and its multiplicity are underway.

A19 IRAS 18316-0602 – *Mol 62*

(*d = 3.17 kpc, L = 44.1×10^3 L$_\odot$*)

IRAS 18316-0602 (also known as G25.65+1.05 or RAFGL 7009S) is associated with an irregular compact radio source, first identified at 3.6 cm by Kurtz et al. (1994) with an integrated flux density of 3.8 mJy. This is close in position to the radio source detected at 3.6 cm by Walsh et al. (1998) with a peak flux density of 1 mJy. The radio peak of Kurtz et al. (1994) is coincident with an unresolved infrared source, identified as a young B1V star with a large *K*-band excess (Zavagno et al. 2002). It is also closely associated with NH_3 emission (Molinari et al. 1996) and strong CH_3OH (Walsh et al. 1997; Slysh et al. 1999; Szymczak et al. 2000) and H_2O maser (Brand et al. 1994; Kurtz & Hofner 2005) emissions. Sub-mm continuum observations at 350 μm by Hunter et al. (2000) and at 450 μm and 850 μm by Walsh et al. (2003) are all peaked at the position of the radio continuum and maser sources. Observation of the CS (2-1) line by Bronfman et al. (1996) shows good agreement with the observed radial velocity from the masers (40.8-42.4 km s^{-1}, Walsh et al. 2003) and the line emission (41.4 km s^{-1}) indicating a strong link between the dense gas, the maser sources and the massive star. This also implies that the outflow is probably

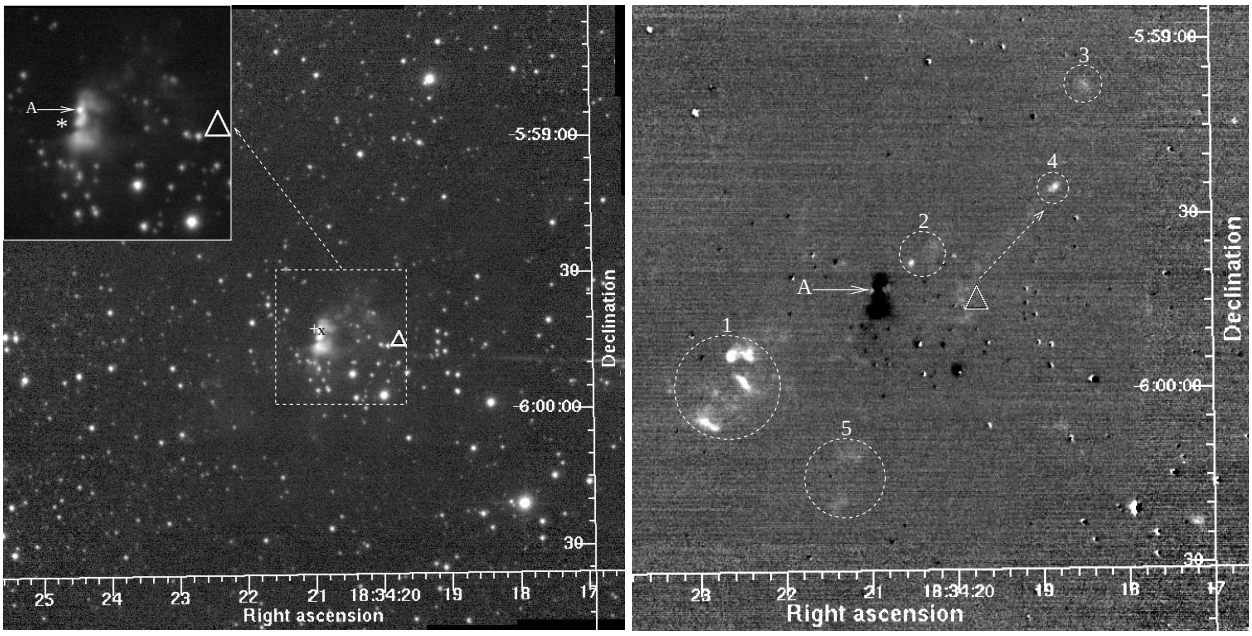

Figure A19. The left panel shows the *K*-band image of IRAS 18316-0602. The inset shows an expanded view of the central object. "x" marks the 3.6-cm radio continuum position of Kurtz et al. (1994); "*" marks the 450-μm position of Walsh et al. (2003). The right panel shows the continuum-subtracted H_2 image smoothed with a 2-pixel FWHM Gaussian.

inclined close to the sky plane. Shepherd & Churchwell (1996a) observed G26.65+1.05 in their survey of high-velocity CO; they detected an energetic bipolar outflow centred on the radio source. Todd & Ramsay Howat (2006) have recently presented high angular resolution images of this source in the *K* band and the v=1-0 S(1) line of H_2. The source has an extremely complex morphology and jet-like features abound. They conclude that these features arise from a single source centred on the IRAS position.

Fig. A19 shows our *K* and H_2 images. The *K*-band image reveals a cluster with a bright point source ("A"; α=18:34:20.92, δ=-05:59:42.3) located towards the centre of the field. "A" is embedded in a compact nebula extending roughly NS, most of which disappears in the continuum-subtracted H_2 image and leaves a large negative residual implying a cold environment, probably dominated by dust. The continuum-subtracted H_2 image reveals emission features NW and SE of "A", which are encircled and labelled "1–5" on the figure. The IRAS source is located 17.6 arcsec SW of "A", but the MSX source location is very close to "A" (1.2 arcsec east and 0.15 arcsec north). The 3.6-cm continuum source observed by Kurtz et al. (1994) nearly coincides with "A". This source was not detected by 2MASS in *J* and *H*. The colours derived from the upper limits place it in the region of high reddening and excess in the JHK_s colour-colour diagram (Fig. 1), typical of YSOs. The 2MASS colours would also be affected by the presence of nebulosity close to "A". We identify "A" as the HMYSO here, which drives the outflow traced by the H_2 emission features and is the most likely counterpart of the IRAS and the MSX sources. Zavagno et al. (2002) proposed the possibility of a disc associated with "A". If the features labelled "1–3" are produced by an outflow from "A", we get a position angle of 130° (125° in the SE and 315° in the NW) and a collimation factor of ~4.5. However, if the multiple bow shock like features in "1" are due to precession of the jet, the collimation factor would be higher.

The locations of the H_2 emission features indicate the probable presence of more than one outflow in this region. Considering the direction of "4" as seen by the line emission traced in the direction of the dotted arrow shown on the H_2 image, one would get an impression that "4" and "5" may well be due to an outflow from a second source in the vicinity of the IRAS position. This needs to be examined with observations at longer wavelengths at high spatial resolution. Nevertheless, the 450-μm image obtained by Thompson et al. (2006) (FWHM=8 arcsec) shows only a single peak at "A".

The 3.6-cm radio continuum map of Kurtz et al. (1994) is suggestive of a fainter radio companion at ~2 arcsec SW of the bright source. Their map does not extend to the expected position of the driving source of the second jet seen in our H_2 image. It remains to be investigated through multi-wavelength high angular resolution studies if "1–5" originate from a single (wide angle or precessing) outflow, or from two different outflows which is more likely.

A20 IRAS 18345-0641

(*d = 9.5 kpc, L = 39.8×10^3 L$_\odot$*)

IRAS 18345-0641 is one of the high mass YSOs surveyed by Sridharan et al. (2002) and Beuther et al. (2002b,c,d). Their ^{12}CO (2-1) map shows a single, moderately collimated (collimation factor~1.5) outflow, extending over 1.84 pc and centred close to the location of the peak mm-emission (Beuther et al. 2002c) which is also at the IRAS position. The estimated mass of the outflow is 143 M$_\odot$. They (Sridharan et al. 2002; Beuther et al. 2002d) also detected water and methanol masers from this source. Comparison of the methanol maser observations of van der Walt et al. (1995) with their own led Szymczak et al. (2000) to report that the maser emission from this source is highly variable and was dominated by two main components at the time of their observations.

Fig. A20 shows our *K*-band image of IRAS 18345-0641 on which the continuum-subtracted H_2 image of the central region is shown in the inset. Two sources are labelled "A" (α=18:37:7.00, δ=-06:38:24.5) and "B" (α=18:37:6.91, δ=-06:38:30.7) in the fig-

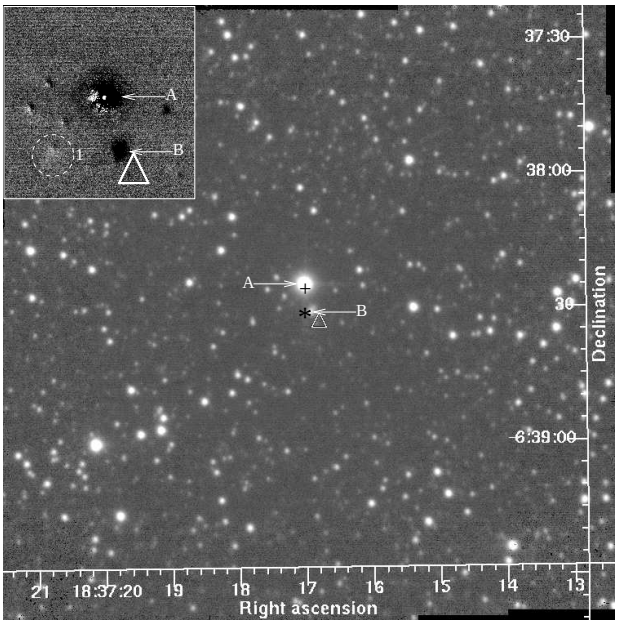

Figure A20. *K*-band image of IRAS 18345-0641. The continuum-subtracted H_2 image of the central region is shown in the inset. "*" shows the location of the 1.2-mm continuum peak of Beuther et al. (2002b).

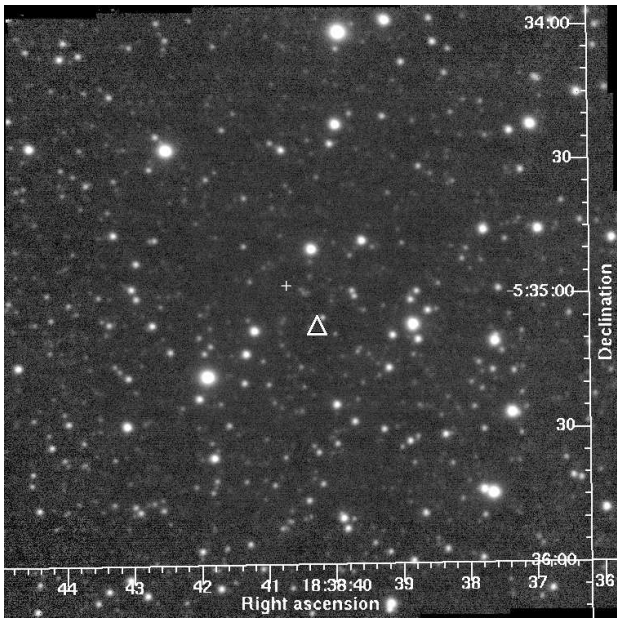

Figure A21. *K*-band image of IRAS 18360-0537

ure, with "B" 6.5 arcsec SW (nearly south) of "A". This region does not exhibit much H_2 emission except for a very faint feature circled and labelled "1" in the inset, which is located at (α=18:37:17.41, δ=-06:38:30.4). The direction of the blue-shifted lobe of the bipolar outflow mapped in CO by Beuther et al. (2002c) is roughly in the same direction as the H_2 emission feature "1" if it is produced by an outflow from "A". Deeper images in H_2 are clearly warranted to ascertain any association of the H_2 emission with the CO outflow. Both "A" and "B" are detected by 2MASS. "A" has only an upper limit magnitude in *J* and for "B", 2MASS gives only upper limits in both *J* and *H*. Their 2MASS near-IR colours exhibit large reddening and excess, with "A" much more reddened than "B" (Fig. 1). The IRAS source is 8.5 arc SW of "A" and 2.4 arc SW of "B". However, the location of the MSX source is within 0.5 arcsec of "A". The peak of the 1.2-mm continuum imaged by Beuther et al. (2002b) is only 1.65 arcsec SE of "B" and the two CH_3OH maser spots detected by Beuther et al. (2002d) are close to "B". However, both "A" and "B" are within the 11 arcsec beam of the 1.2 mm observations of Beuther et al. (2002b)(Table C1). Sridharan et al. (2002) reported a 3.6-cm radio continuum source in this region, with a flux density of 27 mJy. The position of the radio source is not available to look for an association with any of the near-IR sources. Possibly both "A" and "B" are YSOs with one of them in a more advanced (UCHII) stage than the other.

A21 IRAS 18360-0537 –*Mol 65*

(*d = 6.28 kpc, L = 116×10^3 L$_\odot$*)

Brand et al. (1994) and Palla et al. (1991) detected water masers associated with IRAS 18360-0537; Brand et al. found two spots with peak velocities 104.36 kms^{-1} and 105.01 kms^{-1} respectively. Searches for 6.7-GHz methanol maser emission by van der Walt et al. (1995) found no emission. A dense ammonia core associated with this source was reported by Molinari et al. (1996) and CS (2-1) was detected by Bronfman et al. (1996). The peak velocities of the molecular species were 102.3 km s^{-1} and 101.6 km s^{-1} respectively, confirming the observed link between emission from the dense molecular gas and masers.

Fig. A21 shows our observed *K*-band image. The continuum-subtracted H_2 image did not reveal any line emission. Hence, it is not shown here. Since the region did not exhibit any extended features, we did not observe it in Brγ. The location of the MSX object is ~10.8 arcsec NE of the IRAS position. From Fig. A21, we cannot identify any near-IR counterpart of the HMYSO. It is likely to be very young.

A22 IRAS 18385-0512

(*d = 2, 13.1 kpc, L = (5, 199.5)×10^3 L$_\odot$*)

Brand et al. (1994), Sridharan et al. (2002) and Beuther et al. (2002d) observed H_2O maser emission from this region. Searches for CH_3OH emission by Walsh et al. (1998), Sridharan et al. (2002) and Beuther et al. (2002d) did not yield a detection. Sridharan et al. detected CO emission line wings giving the indication of bipolar outflow. They also detected a 3.6-cm free-free continuum source, at a flux density of 29 mJy, near the millimetre source and the masers.

No near-IR observations of this object have been published. Our *K*-band image shows a crowded field with a very bright source (2MASS K_s=4.97 mag) located at (α=18:41:10.93, δ=-5:09:20.8), ~21.7 arcsec SW of the IRAS position. This object does not show any significant IR excess. It is likely to be a foreground object. Hence it is not included in Fig. 1. No Brγ observations were acquired since we did not detect convincing signs of outflow in the H_2 image. Hence, only the *K*-band image is displayed here (Fig. A22).

Williams et al. (2004) detected a sub-mm core at 450 μm and 850 μm; modelling of the radial density profile by Williams et al. (2005) shows a core with L~10^4 L$_\odot$, which could be the pre-cursor of a B1 star. It should be noted that the 1.2-mm continuum source, the location of the H_2O masers and the 3.6-cm emission shown by Beuther et al. (2002d) all appear to be offset NE of the IRAS position, with the centroid of the centimetre emission offset from that

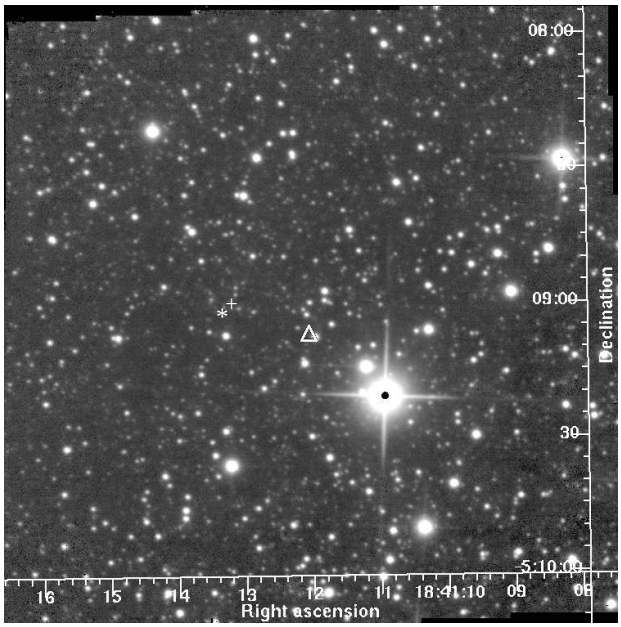

Figure A22. *K*-band image of IRAS 18385-0512. The location of the brightest 1.2-mm peak of Beuther et al. (2002b) is shown by "*".

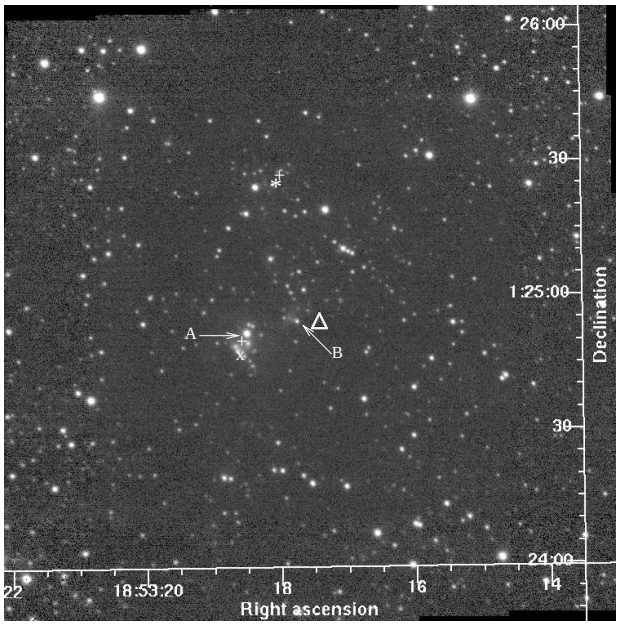

Figure A23. *K*-band image of IRAS 18507+0121. The location of the 3-mm continuum peak imaged by Shepherd et al. (2004b) is shown by "*". The 2- and 6-cm radio continuum peak of Miralles et al. (1994) is shown by "x". A second 6-cm source marginally detected by Shepherd et al. (2004b) coincides with their 3-mm source in the north.

of the millimetre emission by 3.4 arcsec (Sridharan et al. 2002). The H_2O masers are offset by only ∼1 arcsec (Beuther et al. 2002d) and the MSX position is only 2.8 arcsec away (Sridharan et al. 2002) from the 1.2-mm peak. These offsets are within the positional uncertainty of the 1.2-mm detection. The offsets of the IRAS and MSX positions from the mm and radio peaks are within their positional uncertainties. Both H_2O maser and 3.6-cm observations have good positional accuracy (∼1 arcsec; Table C1). A separation of ∼3.1 arcsec between them and the close proximity of the H_2O masers to the 1.2-mm source (Beuther et al. 2002d) suggests that there may be two YSOs here, one in a pre-UCHII stage detected at at 1.2 mm and responsible for the H_2O maser emission, and the other in a more evolved UCHII stage, detected in the radio. The offsets of the IRAS and MSX positions from the mm and radio peaks are within their positional uncertainties. 2MASS does not detect most of the faint objects in the *K* image, which makes identification of any near-IR counterpart difficult. Deep mid-infrared photometry of this region is therefore required.

A23 IRAS 18507+0121 -*Mol 74*

(*d = 3.87 kpc, L = 48.4×10³ L⊙*)

A detailed set of maps of this source has been made recently by Shepherd, Nürnberger & Bronfman (2004b) observing in the radio ($H^{13}CO^+$ and SiO), millimetre (3-mm continuum) and near-IR (*JHK′*). These are the highest angular resolution measurements, pre-dating those presented here. The $H^{13}CO^+$ maps show two distinct cores, separated by 40 arcsec. The more southerly peak is 3 arcsec NW of a UCHII region seen in 6-cm (12.24±0.1 mJy) radio continuum emission (Molinari et al. 1998). The southern radio source was detected by Shepherd et al. (2004b) at 6 cm with an integrated flux density of 9 mJy; a marginal detection (0.7 mJy) was made by them at the position of the northerly core. Miralles, Rodriguez & Scalise (1994) also detected an unresolved radio source at 2 and 6 cm (integrated flux densities of 9.9±0.2 and 9.1±0.1 mJy, respectively) located very close to the 6-cm peak of Molinari et al. (1998). The 3-mm continuum observations of Shepherd et al. (2004b) show a single source at the position of the northerly core seen in $H^{13}CO^+$. Previous studies in molecular lines have been made by Miralles et al. (1994), Harju et al. (1998), Bronfman et al. (1996) and Ramesh, Bronfman & Deguchi (1997). Although the ammonia maps of Miralles et al. are consistent with that from $H^{13}CO^+$, the SiO emission seen by Harju et al. was not detected by Shepherd et al., probably due to the smaller beam size of their interferometric observations. Shepherd et al. (2004b) detected 146 infrared sources in their images, the brightest of which is in a young cluster on the western edge of the southern HCO^+ peak. There is evidence for circumstellar material around 50% of the NIR sources. There is strong and variable methanol emission from this region, measured by Szymczak et al. (2000) and Schutte et al. (1993) at velocities of 55–64 km s^{-1}. Copious water maser emission is also seen at these velocities (Brand et al. 1994; Miralles et al. 1994). Shepherd et al. (2004b) derived spectral types of B2 and B0.5 for the northern and the southern cores, respectively.

Fig. A23 shows our *K*-band image. H_2 and Brγ images did not reveal any line emission, hence they are not displayed here. The source labelled "A" ("#54" of Shepherd et al. 2004b; α=18:53:18.49, δ=+01:24:51.8) is located ∼16.4 arcsec SW of the IRAS position. "A" is well detected by 2MASS in K_s only. The 2MASS magnitudes of this object are affected by the neighbouring sources. Hence, we used the magnitudes given by Shepherd et al. (2004b) in Fig. 1. The *JHK′* colours exhibit reddening, but no excess. "A", and some fainter stars in its vicinity which are not detected by 2MASS, appear to be embedded in a faint nebulosity. The fainter neighbours are detected by Shepherd et al. in *K′* only and not at shorter wavelengths. There are two MSX sources detected in this field, the brighter one is located within 2.5 arcsec of "A". It is possible that one of the neighbours of "A" is the near-IR counterpart of the YSO detected by MSX. Another object "B" ("#57" of Shepherd et al. 2004b; α=18:53:17.75, δ=+01:24:54.8) is located close

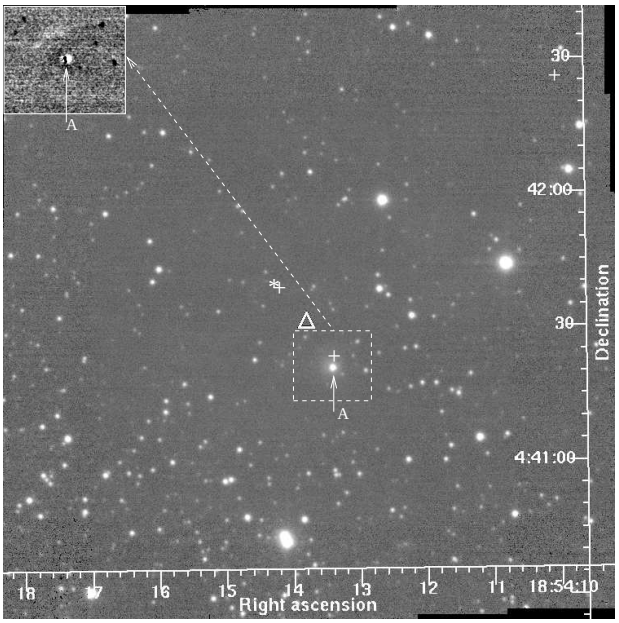

Figure A24. *K*-band image of IRAS 18517+0437. The inset shows the region of the continuum-subtracted H_2 image around source "A" (smoothed by a 2-pixel FWHM Gaussian) showing the faint H_2 emission in the vicinity. The location of the bright 1.2-mm continuum peak mapped by Beuther et al. (2002b) is shown by "*".

to the IRAS position; it is associated with a faint nebulosity in *K*. It was detected by 2MASS only in one band. Hence we have used its JHK' colours measured by Shepherd et al. (2004b) to plot it in Fig. 1. "B" exhibits reddening and mild excess. This could be another YSO in the field. The second MSX source, which appears to be much cooler than the first (it is detected only at 21.34 μm), is located ~33 arcsec NE of the IRAS position. The location of "A" and its sorrounding stars agree well with that of the UCHII identified at 6 cm (Miralles et al. 1994; Molinari et al. 1998; Shepherd et al. 2004b), the southern $H^{13}CO^+$ core with no millimetre continuum detected (Shepherd et al. 2004b) and the brighter MSX source in the field. The second YSO located northward was detected in mm continuum and $H^{13}CO^+$ emission (Shepherd et al. 2004b), while a fainter 6-cm emission peak located northward coincides well with the second MSX source (which appears only at longer wavelength). There are no IR sources identified with this source and in general, we agree with the conclusion of Shepherd et al. (2004b) that the mm source coinciding with the cooler MSX source is younger than the one associated with the UCHII; it is not certain from the current study whether any of the IR sources identified near the location of the UCHII is the IR counterpart of the massive YSO. More observations are underway.

A24 IRAS 18517+0437 – *Mol 76*
(*d = 2.9 kpc, L = 12.6×10^3 $L_\odot$*)

Towards this object, Molinari et al. (1996) discovered a dense core in NH_3 emission. Szymczak et al. (2000) detected strong CH_3OH maser emission. Brand et al. (1994), Codella, Felli & Natalle (1996) and Sridharan et al. (2002) observed H_2O maser emission. A search for 3.6-cm continuum free-free emission by Sridharan et al. (2002) did not yield any solid detection. They discovered CO line wings indicating the presence of bipolar outflows from this region. However, CO observations by Zhang et al. (2005) did not reveal an outflow.

No other near-IR observations of this region have been published. Fig. A24 shows our *K*-band image and the central region of the continuum-subtracted H_2 image. There is a source embedded in faint nebulosity, located ~11.5 arcsec SW of the IRAS position, labelled "A" (α=18:54:13.40, δ=+4:41:21.1). It is well detected by 2MASS in all three bands and the JHK colours place it within the reddening band. Thus, there is no significant amount of IR excess. No collimated emission is detected in H_2; the only H_2 line emission seen is a very faint arc-like feature ~5 arcsec NE of "A".

The MSX mission detected three objects in this field, with two of them located towards the central region, NE and SW of the IRAS position. The IRAS source is likely to represent combined emission from these two. The brighter of the three MSX sources is 5.4 arcsec west and 9.1 arcsec south of the IRAS position and is only 1.98 arcsec north of "A". The 1.2-mm continuum core mapped by Beuther et al. (2002b) is NE of the IRAS position, by ~8 arcsec in both RA and Dec. The redder of the three MSX sources is 8.8 arcsec NE of the IRAS position. It is indeed only 2.1 arcsec SW of the 1.2-mm peak and is likely to be the MSX counterpart of the millimetre source. It is not detected in the near-IR. Beuther et al. (2002b) also discovered CS line emission from this region.

All these observations imply that the HMYSO is a very young object, possibly in a pre-UCHII phase; the IR source "A" is unrelated and is likely to be a more evolved object.

A25 IRAS 19088+0902 – *Mol 97*
(*d = 4.71 kpc, L = 29.9×10^3 $L_\odot$*)

IRAS 19088+0902 is one of the UCHII candidates from Palla et al. (1991), that is associated with H_2O maser emission (see also Brand et al. 1994; MacLeod et al. 1998a for water maser detection from this source). Searches for CH_3OH maser emission from this region did not yield any detection (MacLeod et al. 1998a; Szymczak et al. 2000; van der Walt et al. 1995). The water maser emission peaks are associated with the CO emission observed by Osterloh, Henning & Launhardt (1997). An additional CO peak has no corresponding maser emission, but broad line wings are evident. Osterloh et al. (1997) also present K' images, but those of IRAS 19088+0902 are of low quality and do not reveal any extended, diffuse emission. The dense core was detected in ammonia emission (Molinari et al. 1996) and in CS (2-1) emission (Bronfman et al. 1996).

The VLA observations of Molinari et al. (1998) at 6 cm reveal an unresolved source with an integrated flux density of 10.78 mJy, located 17 arcsec away from the IRAS position. From the 20-cm radio flux (observations by Zoonematkermani et al. 1990), MacLeod et al. (1998a) derived a spectral type earlier than B0.8.

Fig. A25 shows our *K*-band image. No line emission was detected either in the H_2 or Brγ image. Hence these are not shown here. A near-IR source embedded in faint nebulosity in *K* is labelled on the figure ("A"; α=19:11:16.97, δ=09:07:28.6). The IRAS source is located 15.9 arcsec SW of "A". However, the MSX source is just 1.7 arcsec NW of "A". This object is well detected in K_s in 2MASS, but has only upper limits in *J* and *H*. The derived colours show excess (Fig. 1). The 6-cm radio source detected by Molinari et al. (1998) is within 0.9 arcsec of "A". These observations show that "A" is certainly a candidate for the HMYSO in this field. It is probably in its UCHII phase.

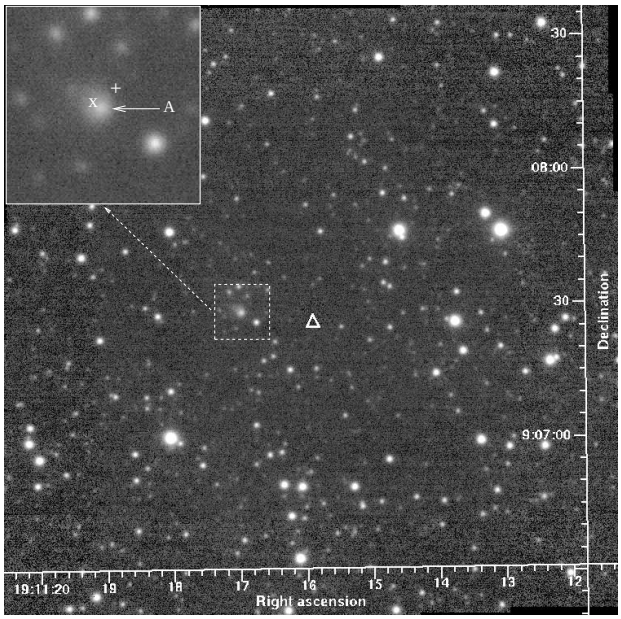

Figure A25. *K*-band image of IRAS 19088+0902. An expanded view of the vicinity of the proposed YSO is shown in the inset. "x" shows the location of the 6-cm radio source detected by Molinari et al. (1998).

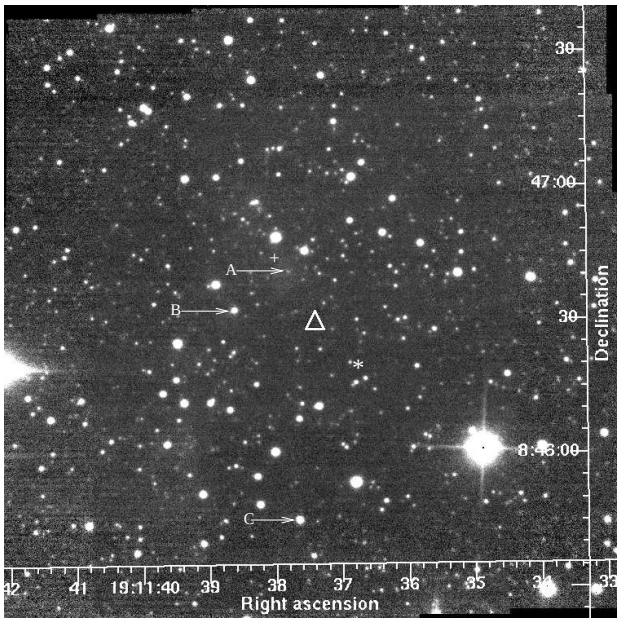

Figure A26. *K*-band image of IRAS 19092+0841. "*" shows the 1.1-mm position of Molinari et al. (2000).

A26 IRAS 19092+0841 – *Mol 98*

(*d = 4.48 kpc, L = 9.2×10*^{3} $L_\odot$)

IRAS 19092+0841 is considered to be a good candidate pre-UCHII object (Molinari et al. 1996). Water maser emission was detected by Brand et al. (1994) and Palla et al. (1991) and an ammonia core was found at the same velocity (~58 km s^{-1}; Molinari et al. 1996). Methanol and Hydroxyl masers were observed close to this velocity by MacLeod et al. (1998b), with the methanol maser confirmed by Szymczak et al. (2000). The source strength (~10 Jy) is consistent between the two methanol maser observations and so this methanol maser appears to be non-variable. Molinari et al. (1998) detected a source at 6 cm from this region, but offset from the IRAS position by 110 arcsec in the NE direction. Hence the radio detection by Molinari et al. (1998) is not from the IRAS source. A search by Zhang et al. (2005) failed to detect any CO outflow from this region.

Fig. A26 shows our *K*-band image. No outflows are detected in H_2 in the 2.25×2.25 arcmin^2 field. There is a faint object labelled "A" (α=19:11:37.79, δ=8:46:41.2) located ~12.3 arcsec NE of the IRAS position, which appears to be surrounded by very faint nebulosity in *K*. It is located 4.25 arcsec SW of the brightest of the three MSX sources detected within this field. (The other two MSX sources are far from the centre and are not detected at longer wavelengths). This object is not detected by 2MASS and is deeply embeded. At this stage, it is not clear if "A" is the near-IR counterpart of the HMYSO. The 1.1-mm peak reported by Molinari et al. (2000) is offset 10 arcsec south and west of the IRAS position, ie., offset from the IRAS position in a direction opposite to that of "A". Deep IR imaging would be required to obtain its colours. Two other objects closest to the IRAS position, detected by 2MASS with an appreciable amount of IR excess (Fig. 1) are labelled "B" (α=19:11:38.61, δ=+8:46:32.6) and "C" (α=19:11:37.65, δ=+8:45:45.5). All three objects are away from the mm position. The YSO in this field may be in a pre–UCHII stage. From the current observations, we cannot identify any of the near-IR objects in the field as an IR counterpart.

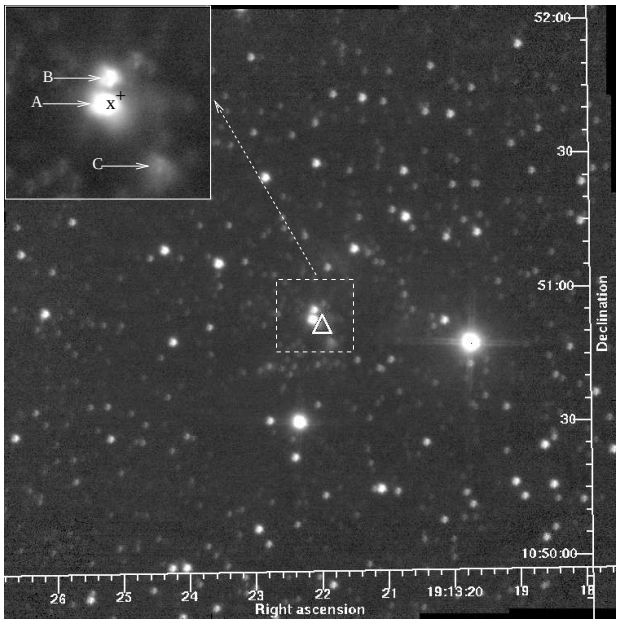

Figure A27. *K*-band image of IRAS 19110+1045. "x" shows the peak position of the radio source detected by Wood & Churchwell (1989b).

Deeper IR imaging and longer wavelength observations with better positional accuracy are required.

A27 IRAS 19110+1045 – (G45.07+0.13)

(*d =6; 8.3; 9.7 kpc, L = (330; 588.8)×10*^{3} $L_\odot$)

IRAS 19110+1045, also referred to as G45.07+0.13, is a known UCHII region (Wood & Churchwell 1989b). Hunter, Phillips & Menten (1997) were the first to detect outflows from this source. Their CO (J=6-5) map shows an unresolved bipolar outflow (beam size 10 arsec) whose origin is well centred on the radio position

of the UCHII region. The estimated mass of the outflow is 45 $M_\odot$ and the length is 0.3 pc. Based on the relatively small extent of the outflow, the existence of H_2O maser emission from this source (Hofner & Churchwell 1996), thought to trace the earliest stages of star formation, and on the compactness of the source (appeared to contain a single core), Hunter et al. (1997) argue that G45.07+0.13 is a younger source than the nearby G45.12+0.13. The single core has been resolved into three sources in the mid-infrared images of Kraemer et al. (2003) and previous near-infrared imaging and spectroscopy towards this source by Hanson et al. (2002) showed it to be highly reddened (A_K=8). They detected very faint Brγ and H_2 1-0 S(1) emission from this source. 6.7-GHz methanol maser was detected by Caswell et al. (1995), Menten (1991) and Szymczak et al. (2000) with varying intensities suggesting a variable nature of the maser emission.

Fig. A27 shows our *K*-band image. Our data did not reveal any significant emission in H_2 or Brγ, so those images are not shown here. The source labelled "A" (α=19:13:22.09, δ=10:50:53.4) and a neighbouring source located ~2.15 arcsec NW ("B": α=19:13:22.07, δ=10:50:55.5) exhibit large large negative residuals in the continuum-subtracted H_2 image. location of the IRAS source is 2.2 arcsec SW of "A"; the the MSX source is 1.4 arcsec NW of "A" and 2.05 arcsec SW of "B". These two sources are not resolved in the 2MASS images and the aggregate has only upper limit magnitudes in *J* and *H*. Their combined colours exhibit IR excess and place the pair in the region of reddened YSOs (Fig. 1). It appears that both "A" and "B" are YSOs. These two objects are, in fact, the near-IR counterparts of the two bright mid-IR sources "2" and "3" of De Buizer et al. (2005) which are associated with the H_2O and OH masers. The brighter component "A" ("2" of De Buizer et al.) is associated with the unresolved (at 2 cm and 6 cm) radio continuum source of Wood & Churchwell (1989b) with integrated flux densities of 594.2 and 141.9 mJy respectively. There is a fainter object in the vicinity, "C" (α=19:13:21.83, δ=+10:50:48.2), which also exhibits negative residuals on the continuum-subtracted images. This object is reddened and is detected by 2MASS only in K_s. This corresponds to the mid-IR object "1" of De Buizer et al. (2005), which is not associated with any maser emission. The MIR sources were also detected at 3 mm by Hunter et al. (1997). Vig et al. (2006) detected low-frequency radio emission from the vicinity of these sources using the Giant Metrewave Radio Telescope (GMRT). They estimate a total luminosity of 3.3×10^5 $L_\odot$ by integrating the observed SED (adopting a distance of 6 kpc from Araya et al. 2002).

With the brightness in the near-to-mid infrared and its association with the compact radio source, "A" appears to be the leading YSO in this region. It is probably in a UCHII stage. "B" and "C" are also probably YSOs. It remains to be investigated which one of these is the driving source of the CO outflow mapped by Hunter et al. (1997).

A28 IRAS 19213+1723 – *Mol 103*
(*d = 4.12 kpc, L = 28.2×10^3 $L_\odot$*)

IRAS 19213+1723 is one of the large sample of CO outflow sources assembled by Wu et al. (2004). The source is reported by them as having a bipolar outflow 1.1 pc in length with a collimation factor 1.44. From CO (2-1) observations, Zhang et al. (2001) derived the mass and momentum of the outflow as 3.9 $M_\odot$ and 24.8 $M_\odot$ kms^{-1} respectively. The centre of the CO emission peak, derived by Zhang et al. (2005), is close to the IRAS position.

IRAS 19213+1723 was included in the SiO survey of Harju et al. (1998), but no detection was made. Bronfman et al. (1996) do find CS (2-1) associated with this source at a velocity of 42.1 kms^{-1}, close to the velocity at which the NH_3 emission was detected by Molinari et al. (1996) (41.7 kms^{-1}). PAH emission from IRAS 19213+1723 has been studied by Zavagno, Cox & Baluteau (1992) in the mid-infrared at 7.7 μm and 11.3 μm and by Jourdain de Muizon, D'Hendecourt & Geballe (1990) at 3.4 μm. Methanol maser emission was sought by Szymczak et al. (2000), Slysh et al. (1999) and van der Walt et al. (1995), though none was detected. Palla et al. (1991) and Brand et al. (1994) detected strong H_2O maser emission from this region at v_{peak}~-27 km s^{-1}, blue-shifted considerably with respect to the core velocity (v_{LSR}~+42 km s^{-1}). The masers are probably excited in a face-on flow. The CO map of Zhang et al. (2005) shows the red- and blue-shifted wings overlapping.

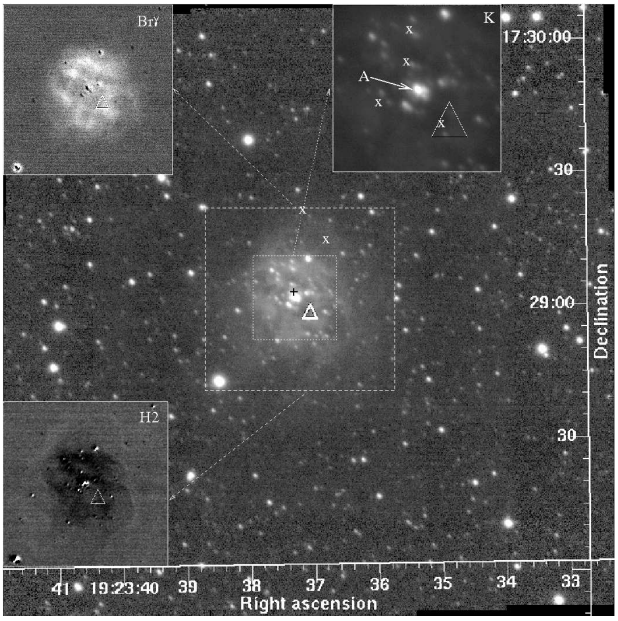

Figure A28. *K*-band image of IRAS 19213+1723. The continuum-subtracted Brγ and H_2 images of the central region are shown inset top-left and bottom-left respectively. An expanded view of the central region of the *K*-band image is shown inset top-right. The six radio peaks detected at 6 cm by Molinari et al. (1998) are shown by "x".

Fig. A28 shows our *K*-band image. The central regions of the *K* and the continuum-subtracted Brγ and H_2 images are shown in the insets. The bright source close to the IRAS position is labelled "A" (α=19:23:37.29, δ=17:29:02.5). The location of the IRAS source is ~4.8 arcsec SW of "A"; the MSX source is only 0.5 arcsec NE of "A". However, the 2MASS colours of "A" do not exhibit any significant amount of IR excess. It should be noticed that "A" has many fainter close companions (Fig. A28), which would not have been resolved by 2MASS. The *K*-band image shows copious amount of nebulosity around the central region. The Brγ image shows line emission in the nebulosity, distributed around the central source. The H_2 image does not reveal an outflow, but shows only faint filamentary emission surrounding the region exhibiting the Brγ emission. This emission is probably due to fluorescence; spectroscopy is required to confirm whether the H_2 emission originates in a PDR or in a wide angle wind. Six spatially-resolved 6-cm radio continuum emission cores within an extended halo of dimension 30×30 arcsec^2 were detected by Molinari et al. (1998), with an integrated flux density of 496.25 mJy. The dimensions of the halo

of radio emission roughly agrees with the diameter of the extended emission in Brγ (~26 arcsec) observed in our data. It is possible that this cluster hosts stars at different stages of youth, with some in a UCHII stage. From the current images, we cannot identify the YSO responsible for the outflow detected in CO. More multi-wavelength observations are warranted.

A29 IRAS 19217+1651

(*d = 10.5 kpc, L = 79.4×10^3 L$_\odot$*)

IRAS 19217+1651 has been studied in detail at radio and mm wavelengths (Sridharan et al. 2002; Beuther et al. 2002b,d; Beuther, Schilke & Gueth 2004a). Sridharan et al. (2002) & Beuther et al. (2002d) detected H_2O and CH_3OH masers, 3.6-cm radio continuum emission and line emission from CO, SiO and CH_3CN. This source is associated with both methanol and water masers. The dense core mapped in CS (Bronfman et al. 1996; Beuther et al. 2002b) is also coincident with the mm peak. High angular resolution CO (2-1) and SiO (2-1) maps of Beuther et al. (2004a) show an energetic, moderately collimated outflow (collimation factor = 3) which is interpreted as a single flow, originating at the millimetre dust continuum peak. At an angular resolution of 1.5 arcsec, their 1.3-mm continuum emission appears with a single peak ~5 arcsec north of the IRAS position, almost coincident with the 3-mm peak and the 32 mJy 3.6-cm free-free continuum source. The outflow mass in the red wing is 50.4 $M_\odot$ with 24.4 $M_\odot$ in the blue wing; the momentum is 2210 $M_\odot$ kms^{-1} and the total extent, 1.6 pc. Beuther et al. (2004a) conclude that their observations allow the driving mechanism to be the same as for low mass sources and that massive stars may form via accretion.

Fig. A29 presents our *K*-band image of IRAS 19217+1651 on which an expanded view of the central region is shown in the inset. The field does not exhibit any significant amount of emission in H_2 or Brγ, so these images are not shown here. Four sources are labelled "A–D" in the figure, which are located close to the IRAS position. MSX detected a single source 3.6 arcsec NE of the IRAS position (1.88 arcsec SE of "B" and 3.7 arcsec SE of "A"). In the field shown in the inset, the 2MASS detection is centred between "A" and "B" and thus represents the combined light from the two objects; it does not exhibit any IR excess (Fig. 1). However, our continuum-subtracted H_2 image shows large negative residuals for "B" (α=19:23:58.80, δ=16:57:40.9), which suggests that this could be a source with a steeply rising SED in the *K* band. "C" comprises two sources connected by an arc-like nebulosity. "D" (α=19:23:58.64, δ=16:57:39.2) is a faint nebulous patch. "C" and "D" are not detected by 2MASS. The centroids of the 1.3-mm, 3-mm and 3.6-cm emissions shown by Beuther et al. (2004a) appear to coincide with the location of "B" to better than an arcsecond. However, with the apparent offsets of the centroids from each other, it is difficult to ascertain the association of these with any of the near-IR sources discussed here. It is not clear if the millimeter and centimetre emissions are from the same YSO or represent objects at different ages.

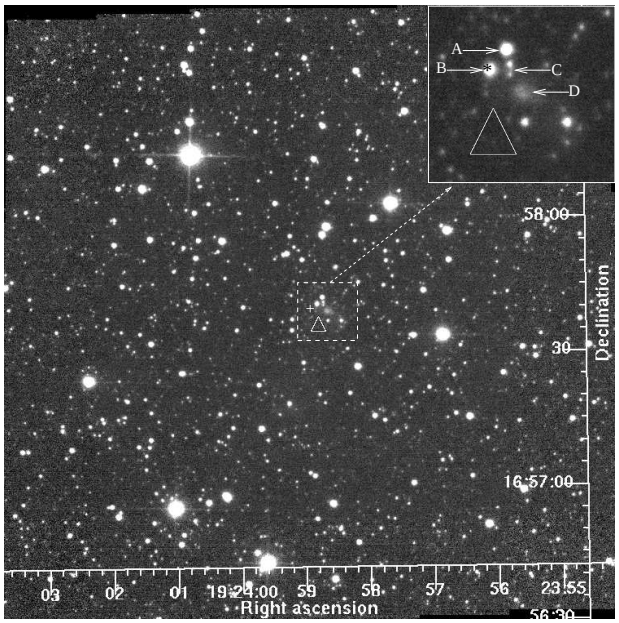

Figure A29. *K*-band image of IRAS 19217+1651; an expanded view of the central region is shown in the inset. "*" shows the 3-mm peak position of Beuther et al. (2004a); the locations of the 3.6-cm radio continuum source, the 22-GHz H_2O maser and the 6.7-GHz CH_3OH maser agree with that of the mm peak.

A30 IRAS 19374+2352 - *Mol 109*

(*d = 4.3 kpc, L = 26.7×10^3 L$_\odot$*)

IRAS 19374+2352 (G59.60+0.92) is associated with a dense core detected in NH_3 emission by Molinari et al. (1996) and in CS by Bronfman et al. (1996). An HII region was detected towards this source at 6 cm by Molinari et al. (1998). H_2O maser emission was observed by Palla et al. (1991) and Brand et al. (1994). Schutte et al. (1993) did not detect any 6.6-GHz CH_3OH maser emission from this region at a 3σ level of 3 Jy. Watson et al. (2003) estimated a kinematic distance of 4.3 kpc using H_2CO observations. Through CO (J=2-1) observations, Zhang et al. (2005) mapped a molecular outflow.

Fig. A30 shows our *K*-band image and the central portion of our H_2 image. The *K*-band image shows a ring of very faint nebulosity, outlined by the dotted circle on the image. The combined 2MASS colours of the three bright sources located (the centroid is labelled "B") at the centre of the ring do not exhibit any IR excess. The fainter of the two MSX sources in this field (26 arcsec NE of the IRAS position) is located within this ring. This ring of nebulosity disappears in the continuum-subtracted H_2 image and there is no line emission detected within the ring. However, we see some H_2 line emission features near the central region of the image, which are circled on the H_2 image in Fig. A30 and labelled "1–3". "1" is observed to be closely associated with a pair of stars at a separation of 1.5 arcsec, labelled "A" (α=19:39:35.04, δ=23:59:42.1) in the figure. The combined 2MASS colours of "A" do not exhibit any IR excess (Fig. 1). However, note that one of the components of "A" is much fainter than the other and the 2MASS magnitudes will be dominated by the brighter component. The brighter of the two MSX sources in the field, located 22 arcsec SE of the IRAS position, is 9.5 arcsec NE of "A". This MSX detection is only 3.2 arcsec NE of the 72.5-mJy 6-cm radio continumm source of Molinari et al. (1998). Our *K*-band image shows a faint patch of nebulosity very close to this radio source. This nebulosity disappears in the continuum-subtracted images and leaves a large negative residual, implying the possible presence of dust. "2" is split into two separate blobs of emission.

The H_2 features, along with the MSX sources, the radio source and the CO map of Zhang et al. (2005), suggest that there is more than one outflow source in this region. From the available photom-

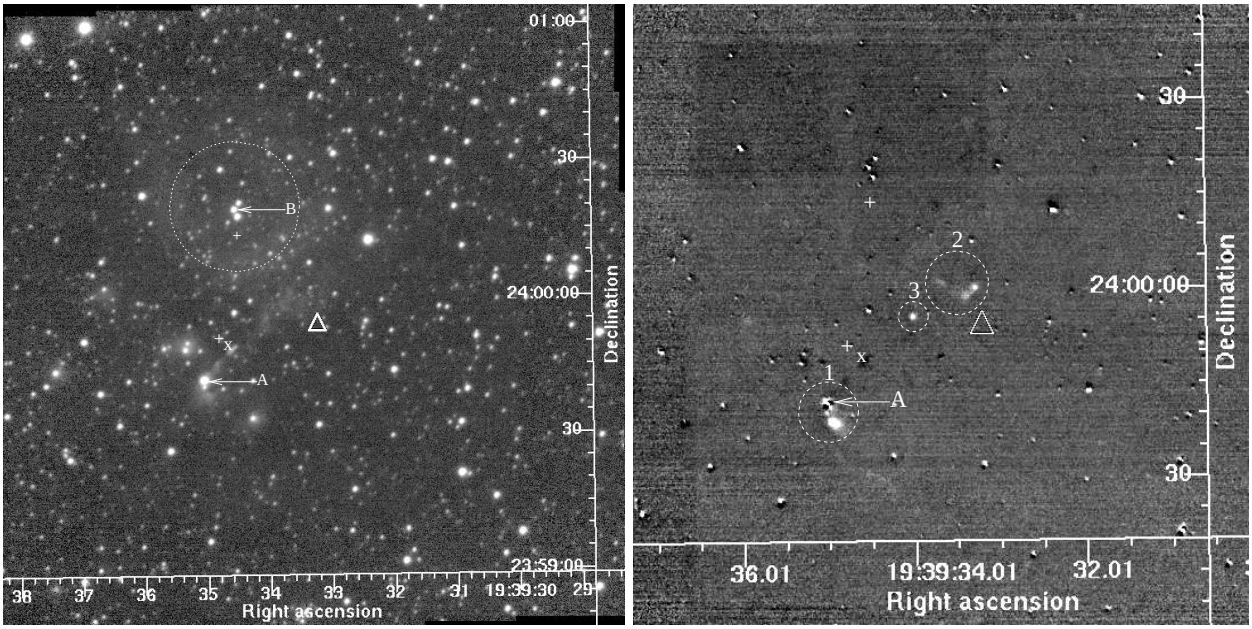

Figure A30. Left: *K*-band image of IRAS 19374+2352. Right: Continuum-subtracted H_2 image. The 6-cm position of Molinari et al. (1998) is shown by "x".

etry we are not able to associate the outflow drivers with any of the near-IR sources at this stage. Even so, a collimated outflow is inferred from our H_2 data. Spatially resolved colours of "A" and its companion need to be obtained to establish if either is the driving source of the outflow traced by the H_2 emission near "A".

A31 IRAS 19388+2357 – *Mol 110*

(*d = 4.27 kpc, L = 14.8×10^3 L$_\odot$*)

IRAS 19388+2357 is associated with H_2O maser emission (Palla et al. 1991; Brand et al. 1994), a radio source (Hughes & MacLeod 1994; Molinari et al. 1998) and dense molecular gas traced in NH_3 (Molinari et al. 1996) and CS (Bronfman et al. 1996). CH_3OH maser was also detected from this source (Schutte et al. 1993; Slysh et al. 1994). No near-IR observations were found in the literature. Zhang et al. (2005) mapped a CO outflow. The centroid of their CO emission is 29 arcsec south of the IRAS position.

Fig. A31 shows our *K*-band and continuum-subtracted H_2 images. We see a set of aligned features embedded in nebulosity in the *K*-band. Due to the presence of the nebulosity, 2MASS does not appear to detect the sources close to the centre; therefore the 2MASS data are not included in Fig. 1. Our H_2 image shows a set of three emission features; three arrows are drawn in the directions of these features and are labelled "1", "2" and "3". As seen from the continuum-subtracted H_2 image, the sources close to the centre appear very much reddened, since they show large negative residuals upon continuum-subtraction. It is possible that some of these are the near-IR counterparts of the YSOs responsible for the outflows from this region implied by the H_2 jets. The MSX mission detected three objects in our two arcminute field of view; the one closest to the IRAS position (7.85 arcsec NW) is the brightest and shows a rising SED, typical of YSOs, and is located well within the central cluster. The second MSX source is 24.7 arcsec SE of the IRAS position (24.3 arcsec south, 3.8 arcsec east), close to the centre of the CO emission peak of Zhang et al. (2005). However, this MSX source is weak and is not detected in the 21.34-μm band of MSX. Hence it remains to be investigated if the CO outflow is produced

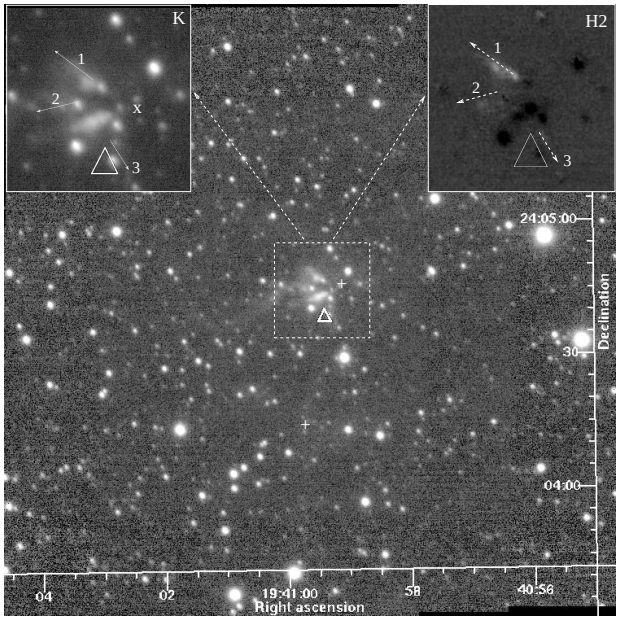

Figure A31. *K*-band image of IRAS 19388+2357. The inset on the top-left shows an expanded view of the central region of the *K*-band image, and that on the top-right shows the central region of the continuum-subtracted H_2 image. "x" shows the 6-cm position of Molinari et al. (1998).

by a different source located south of the IRAS position, as implied by the 29 arcsec offsets of the centroid of the outflow mapped by Zhang et al. (2005) (note that this offset is is only of the order of their beamsize [Table C1]) and the weak MSX detection, or by one or more of the sources in the central cluster itself as suggested by our H_2 image.

The 6-cm radio source reported by Molinari et al. (1998) is faint (2.96±0.06 mJy) and is separated by only 7 arcsec from the IRAS position. This region appears to host more than one YSO, some of which are in a pre-UCH$_{II}$ phase. More observations, espe-

cially in the mid-IR, are required to positively identify the sources driving the outflows.

A32 IRAS 19410+2336

(*d = 2.1, 6.4 kpc, L = (10, 100)*$\times 10^3$ $L_\odot$)

IRAS 19410+2336 is a good example for HMYSOs driving well-collimated outflows. Bronfman et al. (1996) detected a dense core towards IRAS 19410+2336 in the CS(2-1) transition and Sridharan et al. (2002) detected NH_3 emission. The observations of Sridharan et al. and Beuther et al. (2002d) revealed water maser emission. Strong 6.7-GHz methanol maser emission has been observed by many (Szymczak et al. 2000; Sridharan et al. 2002; Beuther et al. 2002d). Sridharan et al. also detected CO emission line wings implying outflows; the 3.6-cm radio continuum emission detected by them was very faint (1 mJy) implying a possible pre-UCHII stage for this source. Beuther, Schilke & Stanke (2003) observed this object in ^{12}CO (J=1-0) using Plateau de Bure Interferometer (PDBI), as well as in H_2 and K'. Their observations resolved seven (or possibly nine) bipolar outflows. They estimate an accretion rate of the order of 10^{-4} $M_\odot$ year^{-1} for these YSOs, which is more than the accretion rates of typical low-mass stars. CS observations at high angular resolution using PDBI (Beuther et al. 2004b) shows CS tracing some of the outflows mapped in CO.

Fig. A32 shows our K and H_2 images. Three sources are labelled on the figure, "A" (α=19:43:11.20, δ=23:44:03.9), "B" (α=19:43:10.81, δ=23:44:04.9) and "C" (α=19:43:11.19, δ=23:44:11.8). Both "A" and "B" are resolved and are found to have fainter companions located ∼0.9 arcsec SE of the brighter ones. The coordinates given here are those of the brighter components. "A" and "B" are separated by only 5.5 arcsec and would not be resolved by either IRAS or MSX. "A" is deeply embedded and is well detected by 2MASS, though only in K_s. The derived colours using the magnitude limits show that it has a large amount of reddening and IR excess (Fig. 1). "B" is detected by 2MASS in all three bands with large reddening and IR excess (although less than those of "A"). The brightest MSX source is located 1.8 arcsec NE of "A"; the IRAS position is 5 arcsec NE of "A". Twelve H_2 emission features are labelled on the H_2 image. The labels of the H_2 emission features "1–10" are chosen to be consistent with those used by Beuther et al. (2003) for ease of comparison. The location of "A" close to the centroid of the observed H_2 emission features "2" and "3", its high reddening and excess and the close association with the MSX source imply that this is the most likely candidate for the luminous YSO driving the jet, traced by "2" and "3". This jet, shown by the dotted arrow and named "II" on Fig. A32, is at an angle of 65° with a collimation factor of ∼4.1. Similarly, "B" and one of the components of "A" are other strong candidates for the YSO driving the outflow revealed by the H_2 features "1", "4–6" and "11–12". The lateral spread in the locations of these features shows that they represent more than one bipolar jet or a precessing jet. If "1" and "4–6" are due to an outflow from "B" in the direction of the dotted arrow labelled "I" on Fig. A32, the outflow direction is ∼99.5° with a collimation factor of ∼3.8. "C" is also a deeply embedded object with large reddening and excess. It is located 8.1 arcsec north of "A". This object is well detected only in K_s by 2MASS and exhibits deep reddening and a significant excess.

In addition to the line emission features mentioned above, there are several other features. Some of the brighter ones are labelled "7–10". These features could be driven by other YSOs in the field, like "C". We have not attempted to explain all the observed H_2 emission features in this complex region, which will instead be addressed in a forthcoming paper.

Single dish 1.2-mm continuum observations of Beuther et al. (2002b) revealed two massive cores, each associated with a bipolar molecular outflow as revealed in their maps in the CO(2-1) and in the CO maps at high angular resolution observed by Beuther et al. (2003). The blue- and red-shifted lobes of the CO emission around the southern core roughly trace the direction of the bright H_2 features "1" and "4–6" showing that the outflow mapped in CO is driven by the jet detected in H_2. The southern core appears centred close to the IRAS position and is resolved into four mm sources at 2.6 mm by Beuther et al. (2003). We have plotted the positions of these four 2.6-mm peaks near the sourthern core, "mm1–mm4", on Fig. A32. The position of "mm1" agrees well with that of "A", the object producing the outflow defined by the H_2 features "2" and "3" in the direction "II". Except for one methanol maser spot which is located 1.6 arcsec SW of "A", the locations of the remaining one methanol maser and the two water maser spots given by Beuther et al. (2002d) are within an arcsecond of "A" (their positional offsets are less than 1 arcsec; Table C1) implying that these are produced by "A" or its companion.

A33 IRAS 20050+2720 – *Mol 114*

(*d = 0.73 kpc, L = 0.388*$\times 10^3$ $L_\odot$)

IRAS 20050+2720 is associated with an extremely high velocity molecular jet, a dense core and a compact cluster. The outflow in this region appears to be the superposition of more than one, all of which radiate outward from the IRAS position (Bachiller, Fuente, & Tafalla 1995). Chen et al. (1997) obtained *JHKLM* photometry of the cluster, resolving a cluster population of over a hundred sources.

The dense core has been mapped in various gas and dust tracers (NH_3 - Molinari et al. 1996; CS - Bronfman et al. 1996; 450, 850 μm & 1.3 mm - Chini et al. 2001). Within a 5×5 arcmin^2 region, Ridge et al. (2003) resolved a number of cores enveloped by a diffuse cloud that extends roughly north-south. The brightest CO emission peak mapped by them coincides with the IRAS position. From the IRAS data, Ridge et al. derived a FIR luminosity of ∼230 $L_\odot$, adopting a distance of 700 pc. IRAS 20050+2720 is also associated with water maser emission (Palla et al. 1991). No strong compact radio emission is detected in this region. The radio observations at 6 cm by Molinari et al. (1998) reveal no sources within 120 arcsec of the IRAS position. Wilking et al. (1989) detected a faint 1.4 mJy extended source at 6 cm. The outflow from this region was mapped in CO by Zhang et al. (2005). It appears to be oriented roughly EW, although, from the morphology, more than one bipolar outflow appears to be contributing to their CO maps. The centroid of their outflow is offset 29 arcsec west and north from the IRAS position. Similarly, the high-velocity component of the outflow mapped in CO by Bachiller et al. (1995) is oriented roughly EW. Their map also is suggestive of the presence of multiple outflows in this region.

Fig. A33 displays our K-band image and the central region of our H_2 image. The continuum-subtracted H_2 image reveals at least one well collimated outflow, the direction of which is shown by the arrow on the image (labelled "1"). This outflow is roughly oriented EW with a position angle of 101°; it has a collimation factor of ∼4. The direction of the H_2 outflow is consistent with the flow direction inferred from the CO maps. Additionally, there are some faint features detected in the H_2 image, circled and labelled "2–5" in Fig. A33. "2" and "3" are possibly part of the same outflow

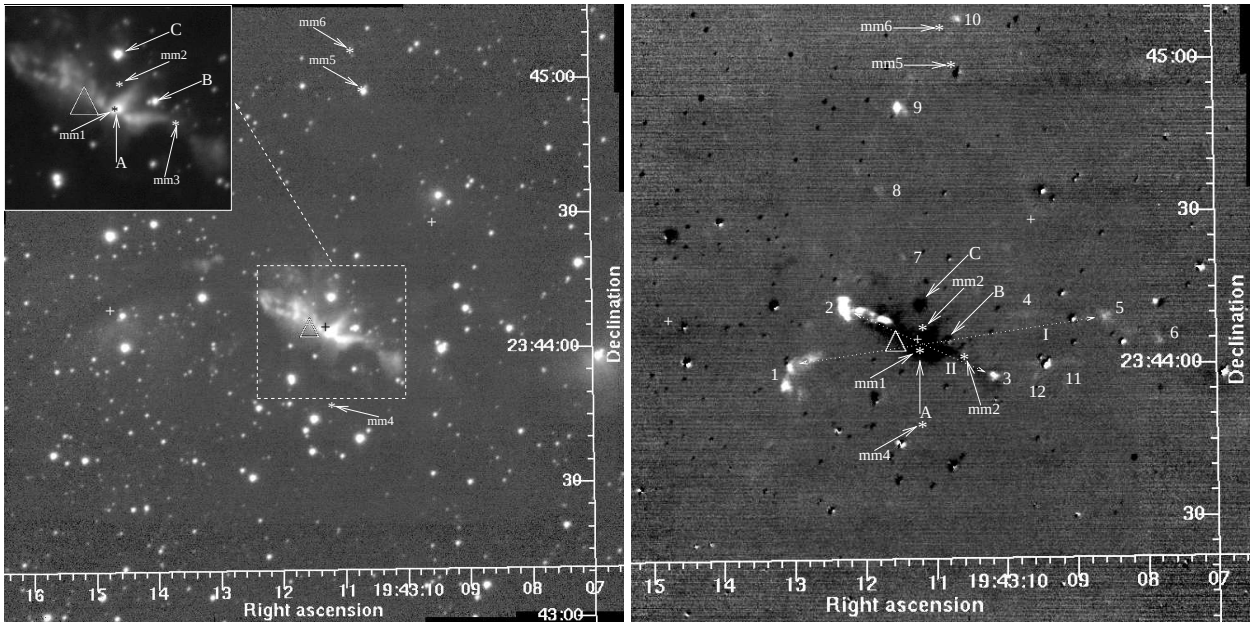

Figure A32. The left panel shows the *K*-band image of IRAS 19410+2336 and the right panel shows the continuum-subtracted H_2 image. The H_2 image is smoothed with a Gaussian of 2-pixel FWHM. The 2.6-mm positions ("mm1–mm6") of Beuther et al. (2003) are shown by "*".

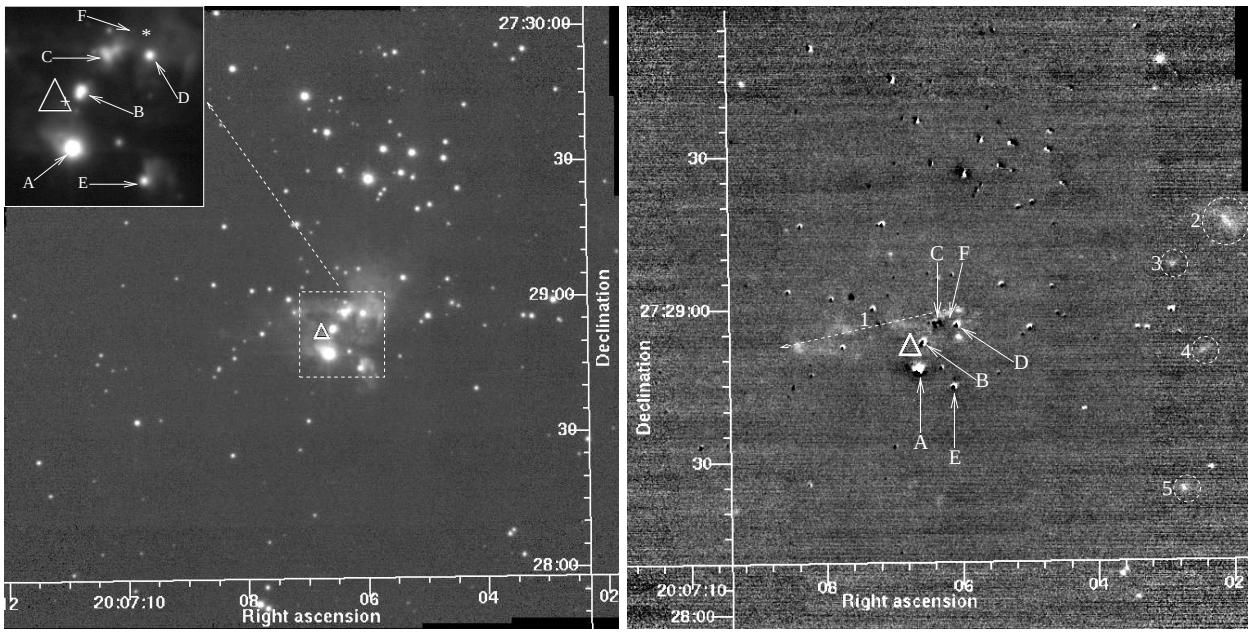

Figure A33. Left: *K*-band image of IRAS 20050+2720. "*" shows the mm and sub-mm continuum peak "MMS1" of Chini et al. (2001). Right: Continuum-subtracted H_2 image, smoothed with a 2-pixel FWHM Gaussian.

detected here, but we can't say for sure from the H_2 images alone. If these two features are part of the same outflow described above, the collimation factor would be much higher. The presence of the other features support the presence of multiple outflows in this field.

Six reddened sources, located near the centre of the field and embedded in nebulosity, are labelled "A–F" on Fig. A33. All these sources are not detected well in all three bands of 2MASS. So, we have used the *JHK* magnitudes of Chen et al. (1997) to plot them in the colour-colour diagram (Fig. 1). Source "F" is detected by Chen et al. only in *L* and *M*. Hence, that object is not shown in Fig. 1. Sources "A–E" show large and comparable reddening. The source "A" ("2" of Chen et al.; α=20:07:06.63, δ=27:28:47.7) exhibits mild IR excess. Both "B" and "E" ("5" and "1", respectively, of Chen et al.) do not exhibit IR excess. "B" is resolved into two components in our image. "D" ("7" of Chen et al.; α=20:07:06.05, δ=27:28:56.6) exhibits mild excess. "C" ("6" of Chen et al.; α=20:07:06.35, δ=27:28:56.9) has the highest IR excess among "A–E". "C" is resolved into at least four components in our image. Chen et al. detected an extremely red source (their "8") which was seen only in their *L* and *M*. We have a weak detection at its location; "F" (α=20:07:06.18, δ=27:28:59.1) is probably the *K* counterpart of "8". The IRAS position is 5.3 arcsec NE of

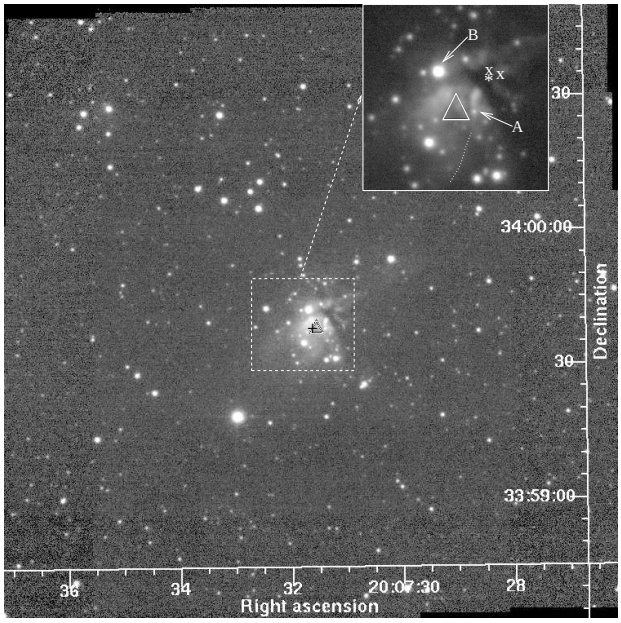

Figure A34. *K*-band image of IRAS 20056+3350. An expanded view of the central region of the *K*-band image is shown in the inset. 3.6-cm sources of Jenness et al. (1995) are shown by "x". The peak position of the 800-μm source detected by them is show by "*".

"A" and the MSX source is only 1.1 arcsec away from the IRAS position. From the location of the outflow detected in H_2 and the locations of the IRAS, MSX and *K*-band sources, "C", "D" or "F" could be the driving source of the outflow. The continuum source mapped by Chini et al. (2001) at sub-mm and mm wavelengths is only 4.15 arcsec NW of "C", 2.3 arcsec NE of "D" and nearly coincides with the position of "F". All three IR sources fall within their beam-size of 8.3–10.7 arcsec at these wavelengths. From our H_2 image, "F" and "C" are the most probable candidates for the driving source of the jet in the direction of "1".

A34 IRAS 20056+3350 - *Mol 115*
(*d = 1.67 kpc, L = 4.0 ×10^3 L$_\odot$*)

A number of groups detected H_2O maser emission from this source (Palla et al. 1991; Brand et al. 1994; Jenness et al. 1995). No CH_3OH maser emission has been reported. The dense core was detected in NH_3 emission (Molinari et al. 1996) and in CS(2-1) emission (Bronfman et al. 1996). VLA radio continuum observation by Molinari et al. (1998) did not detect any emission from this source, although Jenness et al. (1995) report very faint emission at 3.6 cm (from two locations separated by ∼1.35 arcsec with flux densities 0.93 mJy and 0.6 mJy, respectively). Jenness et al. (1995) detected the source at 450 μm and 800 μm as a single core with a faint extension in the SW direction, the peak position matching reasonably well with the location of the H_2O maser and their radio sources and located close to the IRAS position. They also detected the source in $C^{18}O$ (J=2-1) at the same v_{LSR} as the H_2O maser emission. IRAS 20056+3350 was also detected in ^{13}CO by Casoli et al. (1986) at a similar radial velocity. A bipolar outflow centred on the IRAS source has been mapped in this region by Zhang et al. (2005).

Fig. A34 shows our *K*-band image of the region. The image reveals an IR cluster towards the centre of the field and a significant amount of nebulosity. Most of the nebulosity disappears in the continuum-subtracted narrow-band images. The inset in Fig. A34 shows an expanded view of the central region with better contrast. The H_2 and Brγ images did not show any significant amount of line emission. Hence, these images are not shows here. There is a tentative detection of very faint H_2 emission along the dotted line in the inset of Fig. A34. This needs to be verified through deeper imaging in H_2. The object labelled "B" (α=20:07:31.68, δ=35:59:42.4) is well detected by 2MASS. It shows a small level of IR excess in our colour-colour diagram (Fig. 1). Most of the other bright stars embedded in the nebulosity detected by 2MASS have only upper limits of magnitudes listed in the catalogue. A major fraction of the fainter objects were not detected in the 2MASS survey. Especially noteworthy among those objects is the one labelled "A"(α=20:07:31.38, δ=35:59:38.2). This object is located ∼2 arcsec SW of the IRAS position and has a "coma-shaped" nebulosity associated with it. The centroid of this structure is ∼1.3 arcsec north of "A" and is ∼2 arcsec in extent. It appears that none of the bright objects are related to the IRAS source. The near IR counterpart of the IRAS source could be one of the fainter objects not detected by 2MASS, or an object which is deeply embedded and is not detected here. Note that the 3.6-cm sources detected using the VLA (Jenness et al. 1995) are located close to the dark lane in Fig. A34. This object appears to be an intermediate mass YSO. We do not detect any signs of collimated outflows in our H_2 image.

A35 IRAS 20062+3550 – *Mol 116*
(*d = 4.9 kpc, L = 3.2 ×10^3 L$_\odot$*)

A dense core was mapped in this region using the emission lines of NH_3 (Molinari et al. 1996) and CS (Bronfman et al. 1996). Palla et al. (1991) and Brand et al. (1994) detected H_2O maser emission. The source shows variable CH_3OH maser emission (Slysh et al. 1999; Szymczak et al. 2000; Galt 2004). Search for 6-cm radio emission by Molinari et al. (1998) did not yield any detection. The region hosts a well defined bipolar outflow, which was detected in CO by Zhang et al. (2005).

Fig. A35 shows our *K* and H_2 images. Our near-IR images unveil a spectacular outflow in the NE-SW direction from this source. The outflow appears to emanate from an infrared source "A" (α=20:08:10.13, δ=35:59:24.2), which is located ∼6 arcsec NE of the IRAS position. This offset is consistent with the NE offset of the centroid of the outflow given by Zhang et al. (2005). "A" is embedded in nebulosity and consists of two components at a separation of 1.1 arcsec and an angle of ∼106° from the fainter to the brighter component; the coordinates given here are of the brighter of the two. We also see very faint objects in the vicinity of the pair. Multiwavelength imaging with higher spatial resolution is required to understand if more than two components are present. "A" is detected only in K_s in the 2MASS observations. In our *K*-band image, the outflow is roughly hourglass-shaped. The NE lobe of the outflow, in the direction of the dashed arrow labelled "1a" in the continuum-subtracted H_2 image, is at an angle of 43° and extends up to 10 arcsec from "A". The southwest lobe of the outflow (in the direction of "1b") is inclined at 212° east of north, extends up to 16 arcsec in the H_2 image and shows a bow shock. The NE lobe also shows a bright blob in H_2 at its NE extreme, which could be the emission from the apex of the bow shock. The direction of the jet revealed here in H_2 agrees with the direction of the CO outflow mapped by Zhang et al. (2005).

Molinari et al. (2002) observed this object in HCO^+(1-0) and resolved four distinct cores with a complex velocity structure. They also detected two of these cores in $H^{13}CO^+$ and one in continuum emission at 3.4 mm. Upon continuum-subtraction, our H_2 image

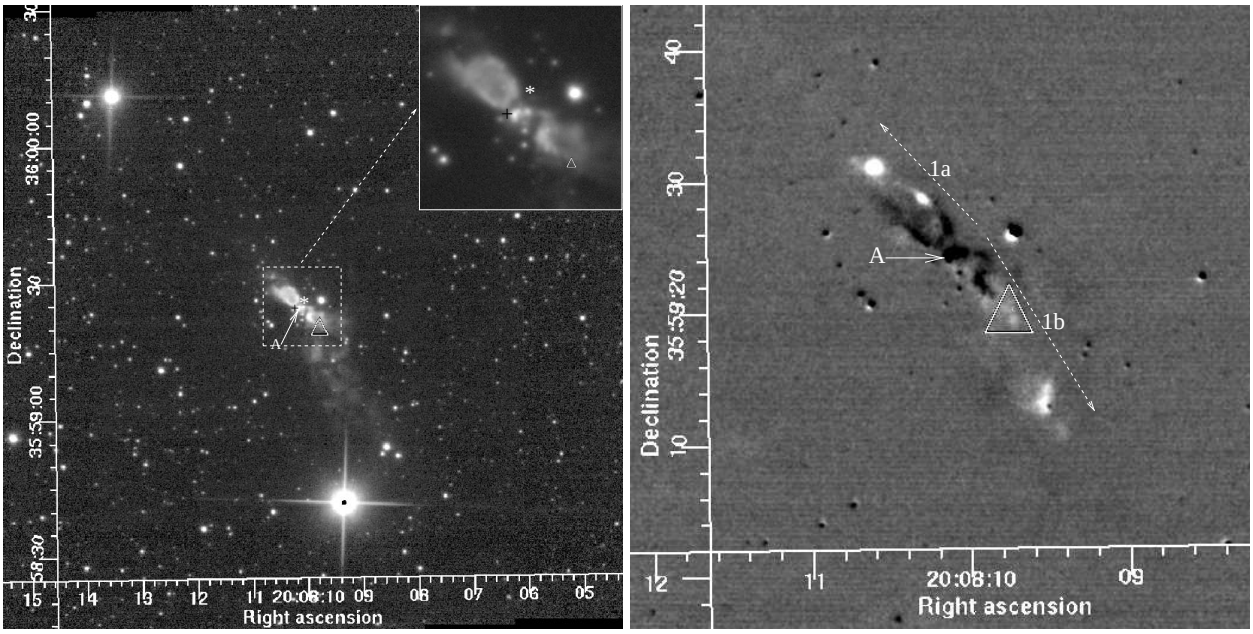

Figure A35. The left panel shows the *K*-band image of IRAS 20062+3550. "*" shows the 3.4-mm continuum position of Molinari et al. (2002). The right panel shows the continuum-subtracted H_2 image.

exhibits large negative residuals on "A", along the edges of the NE lobe of the hourglass, and in some regions of the SW lobe. This is likely due to emission from dust dominating in these regions, which results in a steeply rising SED within the pass band of the *K* filter.

No emission was detected from the outflow or from the central core in the Brγ image. Most of the nebular emission in *K* towards the South of the bipolar emission is subtracted out upon continuum subtraction. The MSX position is 0.82 arcsec SE of "A". These observations suggest that "A" is the near-IR counterpart of the YSO.

A36 IRAS 20126+4104 – *Mol 119*

(*d = 1.7 kpc, L = 10.0×10^3 L$_\odot$*)

IRAS 20126+4104 is a well studied luminous YSO. Still, the intricacies of this field are far from being unveiled. It is embedded in a massive core of 230 $M_\odot$, which was detected in NH_3 by Estalella et al. (1993) with a diameter of ∼0.4 pc (see also Molinari et al. 1996). The core was also detected in CS (Bronfman et al. 1996).

A NW-SE bipolar jet has been detected in H_2 *v*=1-0 S(1) (Ayala et al. 1998; Cesaroni et al. 1997; Caratti O Garatti et al. 2008) and SiO (2-1) (Cesaroni et al. 1999a) lines. A compact molecular outflow, the direction of which agrees very well with that of the jet traced in H_2 and SiO (∼120°), has been mapped in HCO^+ (Cesaroni et al. 1997). Zhang et al. (1999) discovered shock-excited NH_3 emission tracing the jet revealed in SiO and H_2. However, the large scale outflow mapped in CO is oriented roughly north-south (∼171°; Shepherd et al. 2000). Recently, high velocity bipolar outflows have been mapped in CO by Lebrón et al. (2006). The direction of the CO outflow is roughly traced by the large scale arrangement of all the H_2 knots detected throughout the region covered by the CO maps, with the innermost H_2 knots tracing the SiO jet (Shepherd et al. 2000). Detailed near-IR spectroscopic study of the jet by Caratti O Garatti et al. (2008) showed that the outflow is like a scaled-up version of the outflows from low-mass YSOs.

The continuum emission from the sources on which the outflow is centred has been detected from infrared to millimetre wavelengths (e.g. Sridharan et al. 2005; De Buizer 2007; Cesaroni et al. 1999a; Shepherd et al. 2000). A Keplerian circumstellar disc was detected in NH_3, CS and CH_3CN (Zhang et al. 1998; Cesaroni et al. 1997, 1999a, 2005) with the disc plane oriented roughly perpendicular to the direction of the jet/outflow detected in SiO, H_2, and HCO^+ by Cesaroni et al. (1999a) and Cesaroni et al. (1997).

The source exhibits methanol maser (e.g. Slysh et al. 1999; Szymczak et al. 2000, Minier, Conway & Booth 2001; Galt 2004; Kurtz et al. 2004) and water maser emission (e.g. Comoretto et al. 1990; Palla et al. 1991; Tofani et al. 1995; Moscadelli et al. 2000, 2005). The location of the water maser spots mapped by Tofani et al. (1995) have good positional agreement with the millimetre continuum source of Cesaroni et al. (1997), Cesaroni et al. (1999a) and Shepherd et al. (2000); they are located central to the jet and the millimetre source and are aligned in the direction of the jet of Cesaroni et al. (1997, 1999a). High-angular-resolution VLBA observations (Moscadelli et al. 2000, 2005) show that the water maser spots move along the surface of a conical jet. Edris et al. (2005) also detected OH, H_2O and 6.7-GHz methanol masers from this source with the OH and methanol masers tracing a Keplerian disc and the water maser the outflow. However, the 44-GHz methanol maser spots imaged by Kurtz et al. (2004) using the VLA trace the shocked H_2 and SiO emission from the jet (Cesaroni et al. 2005).

The outflow axis, as derived from the SiO jet, is inclined only slightly with respect to the sky plane (i ∼10°; Cesaroni et al. 1999a). However, the large scale CO outflow is found to have i ∼45° (Shepherd et al. 2000). The differences in the angle of inclination with respect to the sky plane and in the directions of the H_2/SiO jet and the CO outflow are interpreted as due to a precession of the jet by ∼45° (Shepherd et al. 2000; Cesaroni et al. 2005). The precession could be due to the presence of a binary in a non-coplanar orbit or to anisotropic accretion events (Shepherd et al. 2000).

A binary or a multiple system for the YSO has been proposed by several investigators. Hofner et al. (1999) carried out high angular resolution observations of IRAS 20126+4104 at 7 mm and

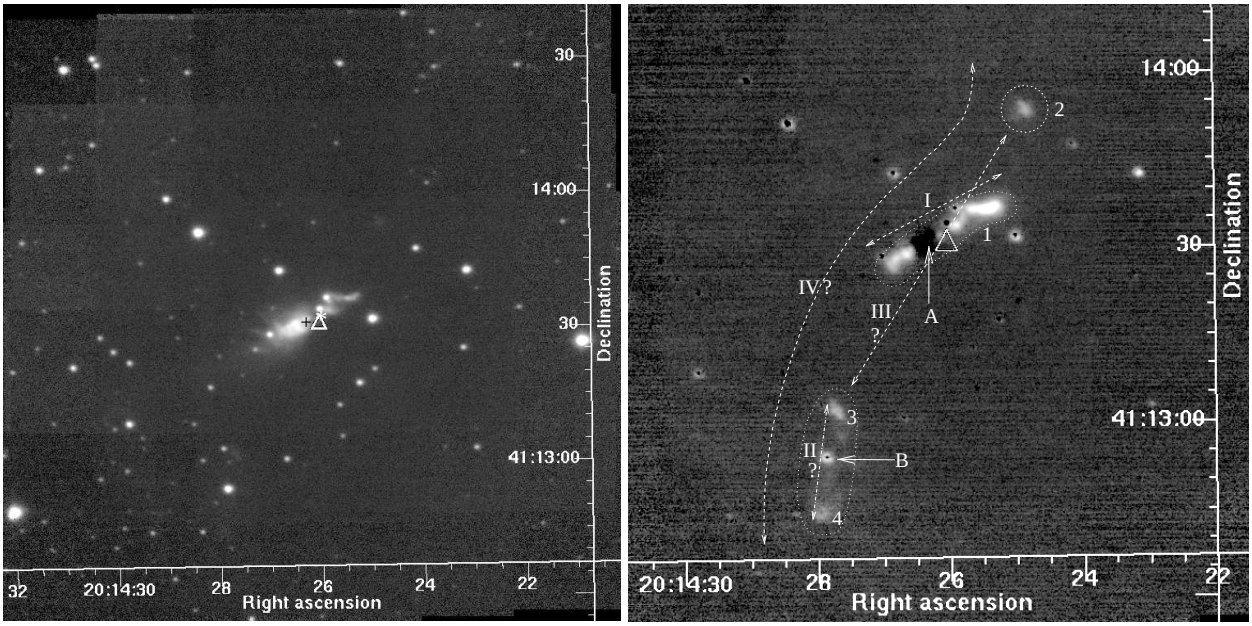

Figure A36. The left panel shows the *K*-band image of IRAS 20126+4104. The 7-mm continuum peak of Hofner et al. (1999) is shown by "*". The right panel shows the continuum-subtracted H_2 image of the central region smoothed with a 2-pixel FWHM Gaussian.

3.6 cm using the VLA. They detected a single unresolved peak at 7 mm, coincident with the 3-mm peak of Cesaroni et al. (1997). Their 3.6-cm continuum emission consisted of two distinct elongated sources (separated by nearly an arcsec in declination and with flux densities of ∼0.2 and 0.1 mJy for the northern and southern components respectively), with the major axes appearing to be aligned and oriented at an angle ∼117°, which is in the same direction as the moleculear outflow imaged in HCO^+(1-0) by Cesaroni et al. (1997) and the jet traced in SiO and H_2. The H_2O maser sources resolved by Tofani et al. (1995) are located along the northern 3.6-cm continuum source and are also aligned in the same direction as the northern jet. Hofner et al. (1999) interpreted the two 3.6-cm continuum sources as due to two ionized jets from two YSOs, both contributing to the outflow observed in this field. The 1-mm and 3-mm peaks of Shepherd et al. (2000) are coincident with the northern ionized jet of Hofner et al. (1999). The southern ionized jet was not detected at 1 mm by Shepherd et al. (2000). However, their 3-mm source exhibits an extension to the south, in agreement with the presence of the southern cm source. Cesaroni et al. (1997) proposed a pre-UCHII stage for IRAS 20126+4104.

Through imaging in the *K*, *L′* and *M′* bands, Sridharan et al. (2005) proposed that the central object is a binary/disc system, with the components of the binary system separated by ∼0.5 arcsec and located nearly in the disc plane. They estimated the thickness of the disc to be ∼850 AU for radii ≲1000 AU. However, mid-IR observations by De Buizer (2007) suggest that the near- and mid-IR emission could be produced by either multiple YSOs or by scattered and direct emission from dust in the cavity walls of an outflow from a luminous YSO.

Fig. A36 shows our *K*-band and H_2 images of IRAS 20126+4104. The main outflow traced by the H_2 emission feature "1" (shown in the direction of the arrow "I") is oriented in the NW–SE direction at an angle of ∼122° and has a collimation factor of ∼5. The source driving this outflow is not resolved in *K* and appears to be obscured by the disc. The point sources detected by IRAS and MSX are within 3 arcsec of each other and are located close to the centroid of the H_2 jet feature. The twisted nature of the H_2 emission in "1" gives strong indication of a precessing jet (see also Caratti O Garatti et al. 2008). This H_2 emission is in very good agreement with the SiO jet discovered by Cesaroni et al. (1999a) and traces the direction of the HCO^+ outflow imaged by Cesaroni et al. (1997) as was noted by previous investigators.

There are additional features unveiled in H_2, which were also observed by previous investigators. The prominent ones are labelled "2–4". Four different scenarios for the outflow are indicated on the figure, the directions of which are shown by lines labelled "I–IV". Of these, only "I" could be treated as conclusive, the rest require confirmation with additional observations. "2" and "3" in the direction of "III" are nearly equidistant from the centre of the flow "I" (at "A") and therefore could be interpreted as arising from a second object located near the driving source of "I". "3" and "4" are located on either sides and are nearly equidistant from a point source "B" (α=20:14:27.87, δ=+41:12:54.4). This source is well detected by 2MASS. As pointed out by Shepherd et al. (2000) (from the photometry given by Cesaroni et al. 1997) and confirmed by the 2MASS photometry, "B" does not exhibit any excess (Fig. 1) and it appears to be a foreground object. However, "3" and "4" do resemble bow shocks and are directed as if produced by an outflow (represented by "II") emanating from "B" or an embedded source located close to "B". There is also faint emission in H_2 between "B" and "3" and "4". It has been suggested that the features "1–4" are caused by a single precessing jet (Shepherd et al. 2000; Cesaroni et al. 2005), the direction of which is shown by "IV". However, their observations could not rule out multiple outflows produced by more than one YSOs. It remains to be investigated through further observations which of these scenarios is a true representation of this interesting object.

A37 IRAS 20188+3928 – *Mol 121*
(*d = 0.31; 3.91 kpc, L = (0.343; 52.8)×10^3 L$_\odot$*)

Little et al. (1988) mapped IRAS 20188+3928 in HCO^+ and CO emission lines and discovered a dense bipolar molecular outflow associated with this source in the N-SW direction. Bronfman et al. (1996) detected the source in CS(2-1) line emission. Several observers detected NH_3 emission (Molinari et al. 1996; Jijina, Myers & Adams 1999; Anglada, Sepulveda & Gomez 1997) implying that the source is deeply embedded. NH_3 observations by Anglada et al. (1997) showed a velocity gradient indicating entrainment by high velocity gas. They also detected a variable H_2O maser ∼1 arcmin NW of the IRAS position. H_2O maser emission was detected by several other investigators (Palla et al. 1991; Brand et al. 1994; Jenness et al. 1995), some from more than one location in the field. McCutcheon et al. (1995) detected continuum emission at 450, 800 and 1100 μm. Jenness et al. (1995) imaged two sources at 450 and 800 μm with the brighter and the fainter ones located NW of the IRAS position by 4.2 arcsec and 28.4 arcsec respectively. They detected three-component emission at 3.6 cm, with the brightest one (24.1 mJy) and the faintest (2.2 mJy) closer to the IRAS position than another faint source (3.4 mJy) 20.7 arcsec north and 1.95 arcsec east of the IRAS position. The brightest 3.6-cm source was also detected by them at 1.95 cm. $C^{18}O$ emission was also observed to be peaking in its vicinity. Molinari et al. (1998) detected two-component 6-cm emission using the VLA, with the stronger component (29.95 mJy) within one arcsec of the IRAS position and agreeing with the position of the brightest radio source of Jenness et al. (1995) and the weaker one (3.82 mJy) located ∼21 arcsec NE, and agreeing in position with the northern radio source of Jenness et al. The distance estimated to this source varies from 0.31 to 4 kpc (Molinari et al. 1996; Palla et al. 1991; Little et al. 1988; etc). Accordingly the luminosity also is highly uncertain.

Our near IR images (Fig. A37) show a cluster of deeply embedded objects towards the centre of the field, very close to the IRAS position. The MSX mission detected mid-IR emission from this region at 8.28 μm and above, within 1.4 arcsec of the IRAS position. The good agreement of these positions indicates that the outflow source is located within this cluster. Most of the nebulosity disappears in the continuum-subtracted H_2 image, leaving faint line emission features that are labelled "1–5" in Fig. A37. Features "1–3" appear aligned, as do "3–5", though in a different direction. The faint radio peak ∼20 arcsec north of the IRAS position detected by Jenness et al. (1995) and Molinari et al. (1998) is located between "2" and "3". This radio emission is likely to be from a highly embedded source, although it is not clear if it is the source which drives an outflow seen in H_2 emission. There is a pair of faint stars ("A") located close to the centre of the feature labelled "3". With the radio positions of Jenness et al. (1995) and Molinari et al. (1998) agreeing very well and separated from "A", it is unlikely that any of these two stars is the IR counterpart of the YSO seen in radio emission. The 2MASS measurement of this source is contaminated by the surrounding nebulosity and therefore we can't say if the source shows any excess. Likewise, the IR magnitudes of the stars "B", "C", "D" etc. near the IRAS position are also contaminated by the presence of nebulosity. However, the presence of the radio sources and the outflows implies that there are multiple YSOs in the region, which are likely to be at different stages of evolution.

Zhang et al. (2005) observed a bipolar outflow in CO centred on the IRAS source and roughly in the NS direction. This direction is consistent with the H_2 emission features "3–5". They note that the outflow in CO is better centred on the illuminating source ∼6 arcsec north of the IRAS position, in agreement with the location of the deeply embedded source northward of the IRAS position proposed by Yao et al. (2000) from near-IR polarization studies. However, the presence of the H_2 emission features "1–2" is suggestive of an additional outflow in the field. High angular resolution CO observations of the field is required to understand that.

A38 IRAS 20198+3716
(*d = 0.9, 5.5 kpc, L = (20, 605)×10^3 L$_\odot$*)

IRAS 20198+3716 (ECX6-7b) coincides with the extensive ON2 star forming region, which extends over roughly 15 pc at a distance of 5.5 kpc. ON2-N (the northern region in our image, referred to as ON2-N by Shepherd, Churchwell & Wilner 1997 and as ON2(C) by Matthews, Anderson & MacDonald 1986) contains the UCHII region G75.78+0.34 while the southern cloud contains the HII region G75.77+0.34. The location of the latter is close to the IRAS position. The location of the ON2(S) given by Matthews et al. (1986) is further SE of the IRAS position by ∼30 arcsec, which is close to their spatial resolution.

ON2 has been studied in considerable detail by Shepherd et al. (1997) in 3-mm continuum emission, CO, SiO, $H^{13}CO^+$ and SO_2 at high spatial resolution. They find evidence for at least four outflows. Matthews et al. (1986) present CO observations of the region and Dent, MacDonald & Anderson (1988) present NH_3 and HCO^+ observations. Water and Methanol masers are observed at various locations throughout the region (Hofner & Churchwell 1996; Szymczak et al. 2000). Forster et al. (1978) found water maser emission closely associated with the northern source. Dent et al. (1988) derive a late O spectral type for the southern HII region HIIS (G75.77+0.34) (ON2(S) of Matthews et al.) and an early B spectral type for HIIC (G75.78+0.34; ON2(C) of Matthews et al.; ON2-N of Shepherd et al. 1997).

Comerón & Torra (2001) present low-resolution *JHK* images of the region, together with colour-colour diagrams. They point out that because the near-IR cluster is offset SW of the high-density regions mapped by Shepherd et al. (1997), the cluster may be a blister HII region where newly formed stars are disrupting the dense molecular cloud that still composes the core of ON2.

Fig. A38a and A38b show our *K*, H_2 and Brγ images. Our observations centred on the IRAS position reveal a rich cluster of IR sources embedded in nebulosity. 2MASS detects only a few of the bright objects in the field and many of the detections have poor quality flags, probably due to the clustering and the nebulosity. Hence, we cannot draw solid conclusions about the colours of many of the candidate YSOs. A few objects and regions of interest are labelled on the figure. The bright source near the IRAS position does not exhibit any excess in the 2MASS colours. However, it is not well detected in their *J* band. The MSX mission detected two objects in this field. The brighter of the two is ∼4 arcsec SE of the IRAS position, located in between the IRAS position and source "A". Source "B" shows IR excess (Fig. 1). There is a fainter MSX source, ∼56 arcsec NE of the IRAS position and located between the two sources in the NE detected by Comerón & Torra (2001). We label these sources "C" (α=20:21:43.34, δ=37:26:35.5) and "D" (α=20:21:44.68, δ=37:26:41.9).

Shepherd et al. (1997) resolved four millimeter continuum sources in this region. The positions of these are indicated by "*" on Fig. A38a and labelled "mm1–mm4", consistent with "1–4" of Shepherd et al. The brightest of these ("mm2") is located within a few acrseconds of "A" and "B", but it does not coincide with either of these or with the MSX source near "A". "mm1", "mm3" and

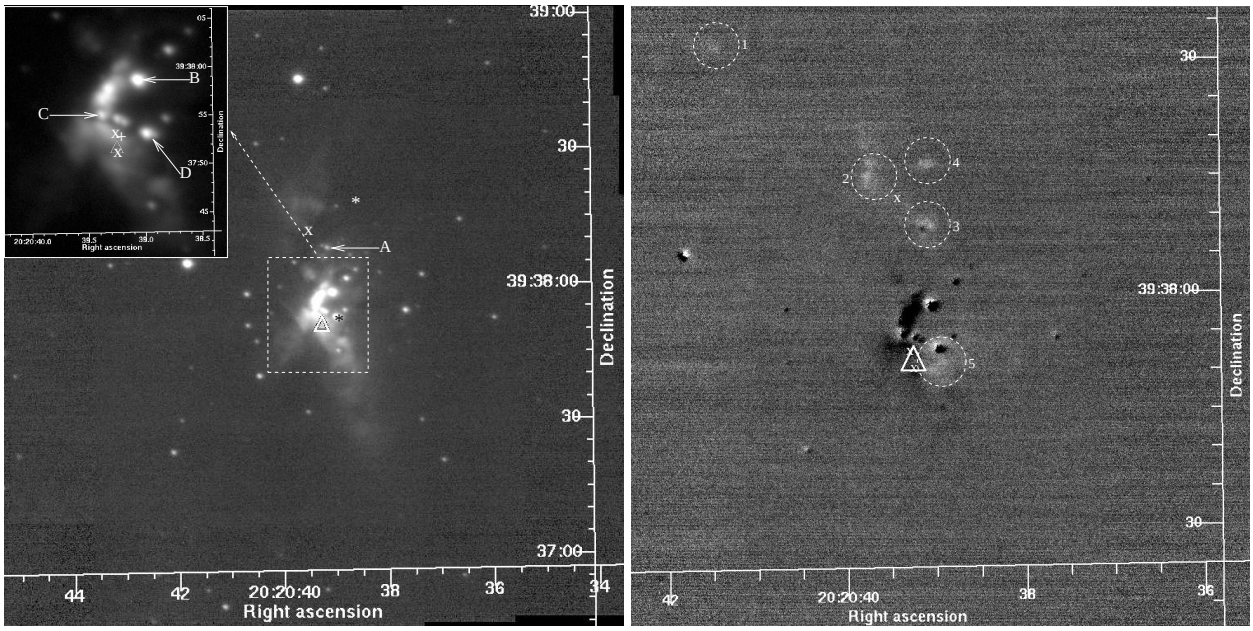

Figure A37. Left: our *K* band image of IRAS 20188+3928. The inset shows an expanded view of the central region with higher contrast. Right: the continuum-subtracted H_2 image of the central region. "*" shows the 850-μm positions and "x" shows the 3.6-cm peaks of Jenness et al. (1995).

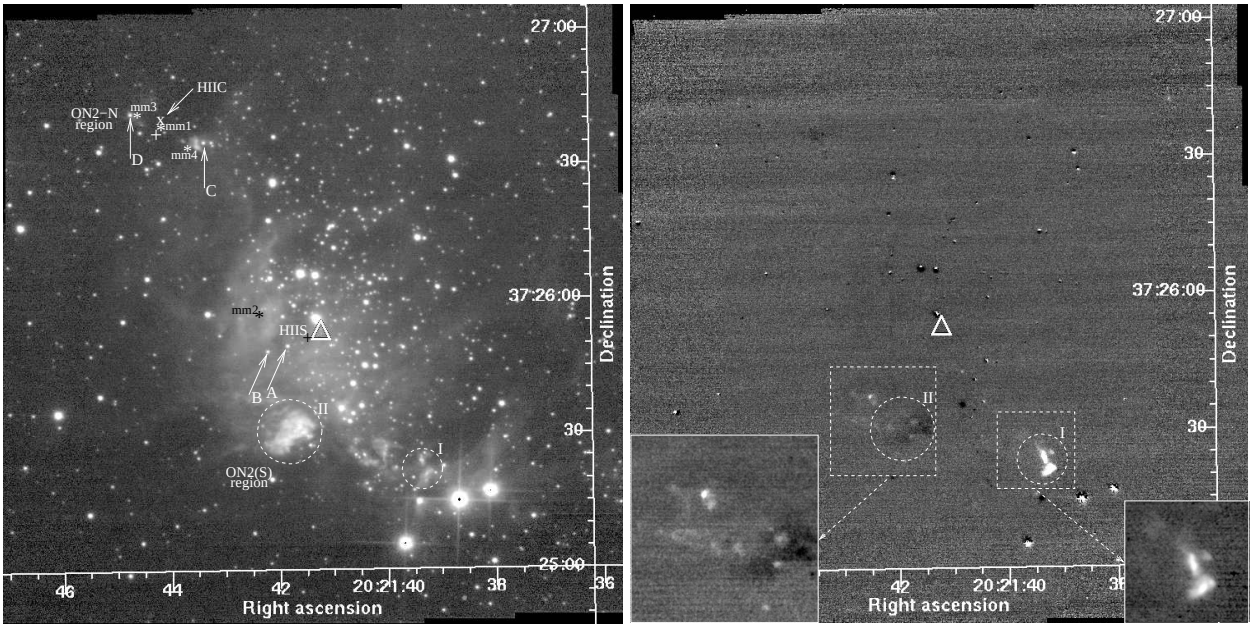

Figure A38a. The left panel shows the *K* band image of IRAS 20198+3716. The location of the millimeter continuum peaks of Shepherd et al. (1997) are shown by "*" and labelled "mm1–mm4". "x" shows the location of the 6-cm peak emission of Wood & Churchwell (1989b). The right panel shows the continuum-subtracted H_2 image on which expanded views of the regions shown in the boxes are overlaid as inset. The regions in the insets are Gaussian smoothed with an FWHM=2 pixels to improve the contrast against the background noise.

"mm4" are located between "C" and "D", with "C" and "D" located close to "mm4" and "mm3", respectively. The second brightest mm source ("mm1") is within 2 arcsec of the MSX source (towards the NW corner in Fig. A38a) and could be the mm counterpart of the MSX source. However, with an ~18 arcsec spatial resolution of the MSX, more than one mm source could be contributing to the MSX detection. H_2O (Forster et al. 1978; Hofner & Churchwell 1996) and OH (Hardebeck & Wilson 1971) masers detected in this region are located close to "mm1".

Wood & Churchwell (1989b) detected a cometary UCHII region located between "C" and "D" and very close to "mm1", at an integrated flux density of 40.4 mJy at 6 cm. 7-mm continuum observations at high angular resolution (Carral et al. 1997) resolve "mm1" into two sources; one source coincides with the UCHII region and the second one is located ~2 arcsec SW, agreeing well with the location of the H_2O masers. Kurtz (2005) discusses the possibility of the 7-mm source coinciding with the H_2O masers being in an HCHII phase.

The "Central" and "Western" outflows mapped by Shepherd et al. appear to be centred near "mm3" and "mm1" respectively; observations of outflows at higher spatial resolution are required to confirm any association. They have not mapped any CO emission around the IRAS source and "mm2". Both "C" and "D" have nebulosity around them in the *K* band and there is a clumpy emission feature located ∼1.6 arcsec west of "C", which disappears in the continuum-subtracted narrow-band images. Our H_2 imaging did not detect any line emission from the northern cluster close to "C"and "D" where they detected the outflow. However, from the southern region, we detect some well-collimated outflows.

Two regions of interest in the southern region are circled in Fig. A38a. Region "II" shows faint IR sources hidden in strong nebulosity; most of the nebulosity disappear in the continuum-subtracted images. The H_2 image shows several bow shocks, which appear to be emanating from region "II", implying the presence of one or more YSOs within "II". The H_2 features from region "II" reveal at least two outflows. Region "I" shows some very bright H_2 emission features which appear to be a bow-shock of the jet from a YSO in the IR cluster or could be the bow-shock/s of counter jet/s from the sources producing the outflows seen in region "II". Both H_2 and Brγ images show negative residuals in this region upon continuumm subtraction, which implies that there could be thermal emission from dust here, making the SED steep. As is seen from Fig. A38b, there is no Brγ emission emanating from the regions "I" and "II". However, the Brγ image (Fig. A38b) shows a copious amount of line emission from the nebulosity in which the IR cluster is embedded. The location of the HII region G75.77+0.35 is within this cluster. With the positional uncertainties of the IRAS and the MSX detections, it is difficult to say if region "II" hosts the IRAS source and the MSX object near it, or if it is separate. Note that the IRAS and MSX positions are closer to "mm2" than to "II".

Together, these observations imply that this is a region very active in star formation. The YSOs present here drive the outflow that we observe in H_2, while more evolved, luminous objects ionize the circumstellar medium. Since it is not clear which are the driving sources of the outflows traced by these H_2 emission features, we do not list the outflow angles and the collimation factors. It should be noted that the ON2(S) outflow observed by Matthews et al. (1986) is centred close to "II". It is not clear if "I" is produced by counter jet/s originating from the sources producing the outflows in "II", or if it is from a source responsible for the millimeter continuum source "mm2" and the MSX and IRAS sources. What is important is that Dent et al. (1988) derived a late O-type for the driving source of the outflow in the ON2(S), from which, presumably, we see the strongly emitting bow-shock in the H_2 image.

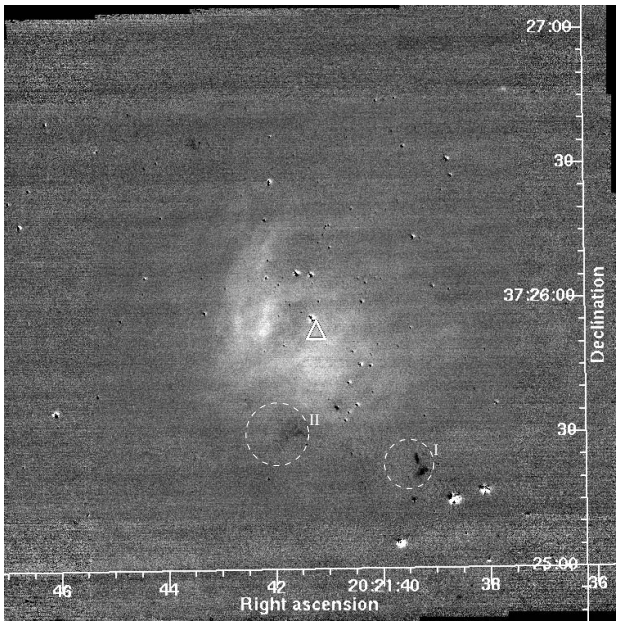

Figure A38b. The continuum-subtracted Brγ image of IRAS 20198+3716.

A39 IRAS 20227+4154 – *Mol 124*
(*d = 0.1; 3.39 kpc, L = (0.00914; 9.59)* $\times 10^3$ $L_\odot$)

There is large uncertainty in the distance and, thereby, in the luminosity of this object. Palla et al. (1991), using their estimate of 3.39 kpc for the kinematic distance, calculated a FIR luminosity of $9.59\times10^3 L_\odot$, whereas Molinari et al. (1996), through observations of NH_3 emission, estimated a kinematic distance of 0.1 kpc and a luminosity of 9.14 $L_\odot$. The v_{LSR} of the H_2O maser emission detected by Palla et al. (1991) and Brand et al. (1994) are comparable (v_{peak} at -2.06 and -1.99 km s^{-1} respectively), whereas these values differ significantly from the v_{LSR} of the NH_3 emission lines (+5.8/9 km s^{-1}; Molinari et al. 1996), CS emission (+5.8 km s^{-1}; Bronfman et al. 1996) and 1665 and 1667 MHz OH absorption line (+5.6 km s^{-1}; Slysh et al. 1994). At 1667 MHz, Slysh et al. also detected an OH emission component at -10.4 km s^{-1}. A search for 6.7-GHz methanol maser emission by Schutte et al. (1993) did not yield any detection at a 3σ level of 3 Jy. Wilking et al. (1989) detected ^{12}CO and ^{13}CO line emission from this region at v_{LSR}=+5.5 kms^{-1}. Their observations set upper limits of 48 mJy, 0.8 mJy and 0.6 mJy for flux densities at 2.7 mm, 2 cm and 6 cm, respectively.

Fig. A39 shows our *K*-band and H_2 images. The near-IR point source close to the IRAS position is labelled "A" (α=20:24:30.49, δ=42:04:9.3) in the figure. This is an extremely red object with IR excess (Fig. 1). It has a K_s magnitude of 10.39 and is not detected in the *J*-band by 2MASS. The H_2 image shows at least one well defined bow shock, which is circled and labelled "1" on the figure. It appears to be directed away from "A". This bow shock appears bright and we do not see any emission from the counter jet. Hence, this outflow could be highly inclined with respect to the line of sight. The bow-shock is likely to be from the blue lobe of the jet. From the very red IR colours, "A" appears to be a YSO. However, "A" is located ∼12.3 arcsec SW of the IRAS position. The MSX detected a source, separated by only 1.9 arcsec from the IRAS position, at wavelengths 8.28 μm and above. With the MSX and IRAS positions agreeing reasonably well and located away from our near-IR source, "A" is unlikely to be the near-IR counterpart of the object detected by IRAS and MSX. The mid-IR source could be a more deeply embedded one. Our *K*-band image does not reveal any near-IR source close to the IRAS position.

The H_2 image reveals two emission features circled and labelled "2" and "3" in Fig. A39. The centroid of these two features falls close to the IRAS position. These two could be produced by shocked emission from a bipolar outflow from the far-IR source. There are two other emission features, which are labelled "4" and "5" on the diagram. Together, these observations reveal at least two different outflows in this region. The recent CO observations by Kim & Kurtz (2006) confirm this result - the two outflows detected by them in CO are roughly in the directions of the two outflows that we label "I" and "II" on the H_2 image. From the two different ranges of distance estimates discussed above, it is possible that the two different YSOs in the field are at different distances from us,

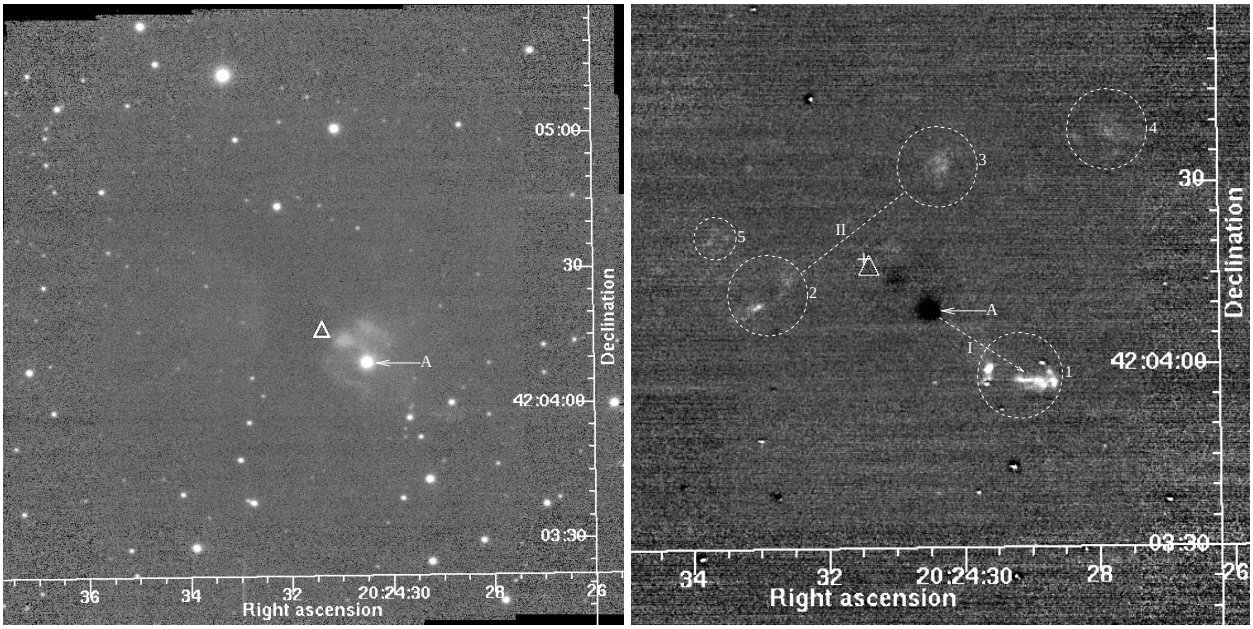

Figure A39. Left: *K*-band image of IRAS 20227+4154. Right: continuum-subtracted H_2 image of the central region.

with IRAS and MSX detecting a more luminous object farther from us, which is not detected in the near-IR. However, it should be noted that we have to be careful with ascribing the differences in the v_{LSR} of different species to different distances - CS and NH_3 emission probe the core (Bronfman et al. 1996; Molinari et al. 1996) whereas H_2O maser emission traces the jet (Moscadelli et al. 2005). More observations are required to understand if the two outflows are from objects at different distances. Assuming that the H_2 emission feature "1" is produced by "A" and "2" and "3" are produced by the IRAS/MSX source not detected in the near IR, we measure a collimation factor and outflow angle 4.5 and 239.3°, respectively, for outflow "I", and 8.3 and 128°, respectively, for outflow "II". A poor collimation is inferred for outflow "II" if "4" and "5" are part of it. If the outflow "I" also originate from a source near the IRAS position instead of from "A", its collimation factor would be as high as 6.9.

A40 IRAS 20286+4105 – *Mol 126*
($d = 3.72$ *kpc*, $L = 39 \times 10^3\ L_\odot$)

IRAS 20286+4105 is associated with a dense core detected in NH_3 (Molinari et al. 1996) and in CS (Bronfman et al. 1996). Palla et al. (1991) and Brand et al. (1994) detected H_2O maser from this region. The IRAS source has the colours of a UCHII region and, in optical images, lies at the centre of a ring-shaped nebula (Odenwald & Schwartz 1989). However, Molinari et al. (1998) did not detect any radio emission at 6 cm. Comerón & Torra (2001) present low-resolution *JHK* images of this source, together with near-IR colour-colour diagrams. They also estimate a distance of 1 kpc to this star forming region, which differs considerably from the kinematic distance of 3.72 kpc estimated by Molinari et al. (1996) from NH_3 observations. Molinari et al. (1996) determined a luminosity of $3.9 \times 10^4\ L_\odot$. Zhang et al. (2005) detected a CO outflow in the CO (J=2-1) line.

Four objects surrounded by nebulosity are labelled in the figures - "A" (α=20:30:27.41, δ=41:15:59.7), "B" (α=20:30:27.45, δ=41:16:5.6), "C" (α=20:30:29.41, δ=41:15:57.5), and "D" (α=20:30:27.32, δ=41:15:27.3). "A" is associated with an extended cometary nebulosity in *K* and is detected by the 2MASS only in *H* and K_s. There appears to be a faint source deeply embedded in this nebulosity and located ∼2.2 arcsec NW of "A". Another faint source located 2.7 arcsec SW of "A" is also associated with a cometary nebula. The continuum-subtracted H_2 image shows aligned emission feature, the direction of which is denoted by the dashed arrow (labelled "1") on the figure. From the direction of "1", it appears to be produced by the outflow from a deeply embedded source located towards the north of "A", which is not detected in our image. There is a brighter H_2 emission feature, which is circled and labelled "2" in Fig. 1. It is located at the apex of the cometary nebulosity seen to be associated with "B" in *K* and is probably the bow-shock of an outflow from "B" in the direction of the dashed arrow shown from "B". "C" also is embedded in strong nebulosity. "B" and "C" are detected by 2MASS only in K_s. The 2MASS colours of all three objects exhibit reddening and excess (Fig. 1), though their colours could have large uncertainty. All three objects appear to be YSOs.

MSX detected three objects in this field, the positions of which are denoted by "+" on the *K*-band image. The brightest MSX object is within an arcsec of "A"; the second brightest is within an arcsec of "D". The faintest object towards the east is poorly detected by MSX and does not show any obvious near-IR counterpart. The 2MASS colours of "D" exhibit reddening, but do not exhibit any IR excess. The continuum-subtracted H_2 image exhibits a very faint shell of H_2 emission around "D", which is marginally detected here. "D" is probably a more evolved object. However, "D" has very faint neighbours which are not detected by 2MASS.

The direction of the outflow as implied from the direction of "1" is roughly in the EW direction. It is also noteworthy that the location of the centre of the outflow imaged in CO by Zhang et al. (2005) is offset northward from the IRAS position, which is consistent with the location of the H_2 features and the reddened objects with excess in our image northward of the IRAS position. The offsets of the CO and H_2 features from the IRAS position are different by ∼10 arcsec, but agree within the positional accuracy of Zhang et al. 2005. Overall, the region appears to be active in star formation,

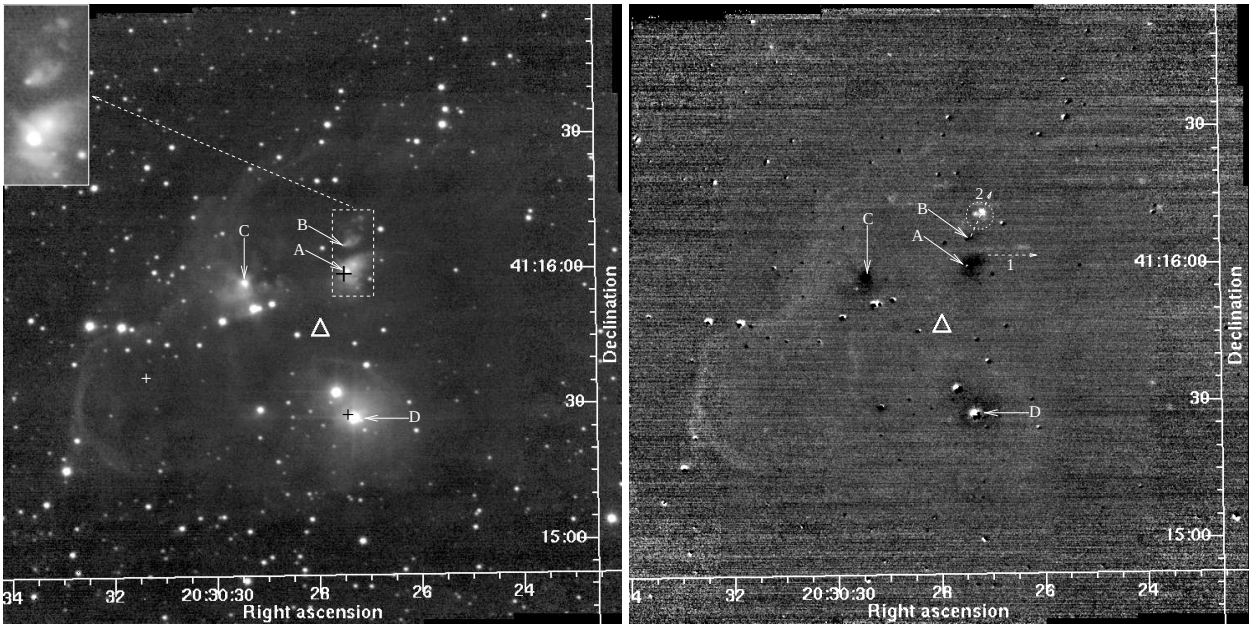

Figure A40. Left: *K*-band image of IRAS 20286+4105. An expanded view of the region around "A" and "B" is shown in the inset. Right: Continuum-subtracted H_2 image.

with more than one YSO present. We positively identify "B" as the YSO responsible for the outflow in the direction of "2". A deeply embedded YSO located north of "A" is likely to be responsible for the outflow in the direction of "1"; high angular resolution imaging at longer wavelengths is required to understand that.

There are also other fainter H_2 emission features detected, the prominent ones being the extended filementary structures seen towards the east and NE in the H_2 image. This is probably fluorescent emission either from the periphery of materials pushed away by more than one bright stars near the centre of the field or from externally illuminated cloud boundaries.

A41 IRAS 20293+3952

(*d = 1.3, 2 kpc, L = (2.5, 6.3)*$\times 10^3\ L_\odot$)

Beuther et al. (2002b) detected a dense core in CS and 1.2 mm dust continuum emission ~23 arcsec to the east and 3.4 arcsec north of the IRAS position. They also detected a much fainter peak located NW of the IRAS position. The bright mm continuum peak was resolved into three at 1.3 mm and 3 mm using high angular resolution interferometric observations using PDBI (Beuther et al. 2004a,b). High resolution CO and SiO maps of Beuther et al. (2004a) resolve four outflows in this region. A water maser is detected towards the dust core and outflow source, while a resolved 3.6-cm radio continuum source with an integrated flux density of 7.6 mJy is detected toward the IRAS position suggesting the presence of an HII region (Sridharan et al. 2002; Beuther et al. 2002d, 2004a). Sridharan et al. also detected the hot-core tracers CH_3OH and CH_3CN towards the IRAS source. Sridharan et al. (2002) did not find any evidence for the presence of 6.7-GHz methanol maser. They detected strong H_2O maser, located close to the dust continuum peak.

Kumar et al. (2002) present near-IR images of IRAS 20293+3952; they detect H_2 emission coincident with the blue-shifted CO lobe (Beuther et al. 2002c), as well as compact features to the NE and SE. They also observed a ring of H_2 emission surrounding one of the two bright near-IR sources in the cluster near the IRAS position.

Three sources are labelled on our IR images (Fig. A41) - "A"(α=20:31:11.26, δ=+40:03:07.4), "B"(α=20:31:10.30, δ=+40:03:16.5) and "C"(α=20:31:12.47, δ=+40:03:19.9). "A" is resolved into multiple components. The 2MASS colours of "A" show it to be a reddened object without any IR excess (Fig. 1). However, it should be noted that the 2MASS survey detected only one object here and it is probably dominated by the luminosity of the brightest source, which we label "A". There are several fainter sources detected in the proximity of "A". The 2MASS colours of "B" exhibit large reddening and IR excess and place it in the region occupied by YSOs in the colour-colour diagram. The MSX source is located 6.2 arcsec SE of "B" and 3.7 arcsec NE of the IRAS position, between "A" and "B". The 3.6-cm radio continuum source of Sridharan et al. (2002), Beuther et al. (2002d) and Beuther et al. (2004a) (7.6 mJy) is located closer to "A" than "B" (Fig. A41) and is likely to be from one of the sources within the cluster associted with "A". "C" exhibits reddening and excess (Fig. 1). "C" is detected by 2MASS in H and K_s only.

Our continuum-subtracted H_2 image exhibits several interesting features; the brighter ones are labelled on Fig. A41. The most prominent is the ring of H_2 emission encircling the cluster containing "A" (also reported by Kumar et al. 2002 and Beuther et al. 2004a). The ring appears elliptical and has a major axis of ~20 arcsec inclined at ~125° and a minor axis of ~15.5 arcsec. Embedded in this ring is the feature circled and labelled "1". All of the features "1–6" appear to be split into multiple components. "2", "4" and "5" appear to be bow shocks. There are also other fainter features seen in our image which are not labelled here. Obviously, this is a region where multiple star formation is taking place. Some of the possible drivers of the outflows are "B", "C" and some of the fainter objects near "A" and "C". The brightest of the 1.3-mm sources mapped in this region by Beuther et al. (2004a) peaks near "C". It should be noted that, in addition to "A–C", several other objects in the field exhibit large reddening and excess, which warrants

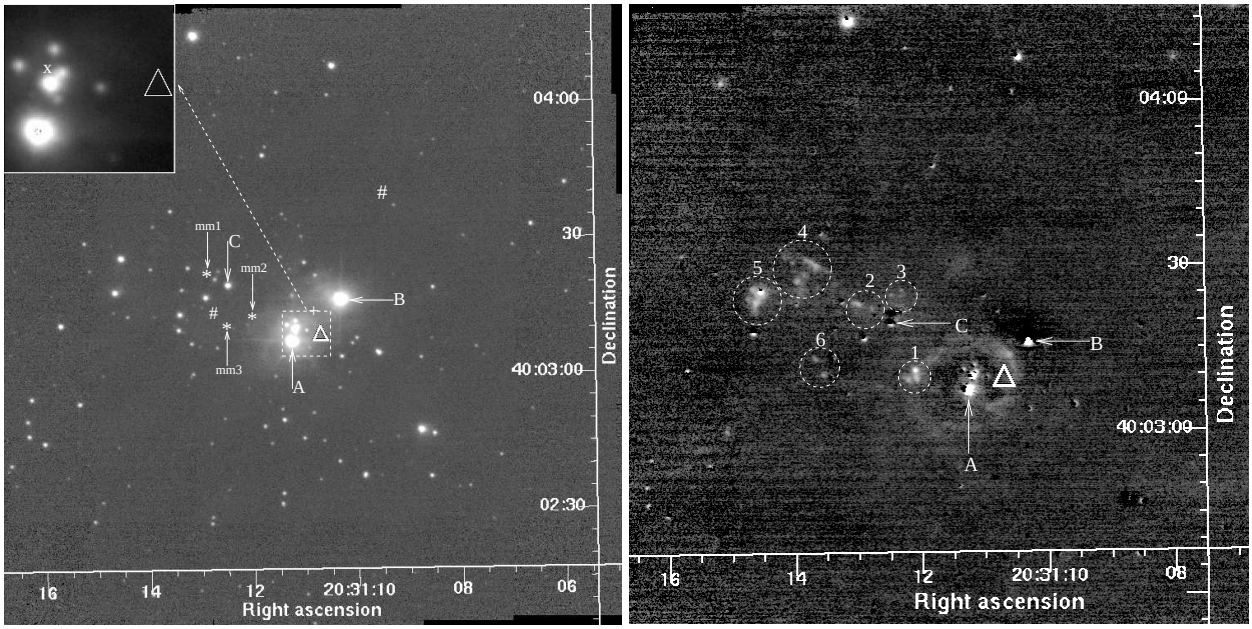

Figure A41. The left panel shows the *K*-band image of IRAS 20293+3952. The 1.2-mm continuum peaks (from IRAM 30-m telescope) of Beuther et al. (2002b) are shown by "#". "*" represents the peaks ("mm1–mm3") of the higher resolution 1.3-mm maps shown by Beuther et al. (2004a) observed using PDBI. "x" shows the location of the radio source (Sridharan et al. 2002; Beuther et al. 2004a). The right panel shows the continuum-subtracted H_2 image of the central region.

a detailed investigation of the field. Deep infrared photometry and spectroscopy are needed to study the cluster, to identify the outflow driving sources and to understand the nature of the H_2 ring/shell. The radio detection is not from the mm source or "B". With the 1 arcec positional accuracy of the radio observations of Beuther et al. (2002d), it is most probably from one of the fainter objects located towards the north of "A" within the cluster (shown in the inset on Fig. A41). The radio source is resolved (Beuther et al. 2004a, Figs. 3 and 7); it is much smaller than the H_2 ring.

A42 IRAS 20444+4629 – *Mol 131*
(*d = 2.42 kpc, L = 3.34×10^3 L$_\odot$*)

The dense cloud core towards this region is detected in CS (Bronfman et al. 1996) and in NH_3 emission (Molinari et al. 1996). Molinari et al. (1998) observed an unresolved radio source towards the NH_3 core, only one arcsec offset from the IRAS position. Wouterloot & Brand (1989) detected asymmetric CO lines. Dobashi et al. (1995) mapped the region in ^{12}CO and ^{13}CO lines. The intensity of the ^{13}CO emission detected by them peaks near the IRAS source indicating a possible association. They also detected a bipolar outflow in ^{12}CO (though this outflow was not evident in the CO observations of Zhang et al. 2005). Assuming a distance of 1.7 kpc, they estimate the total mass of the cloud core to be 450 $M_\odot$ and the YSO to be ~8.5 $M_\odot$. A search for 22.2-GHz water maser emission towards this source by Palla et al. (1991) and Wouterloot et al. (1993) did not find any emission. Nor was 6.7-GHz methanol maser emission detected (MacLeod et al. 1998b).

Fig. A42 shows our *K*-band image on which the central region of the continuum-subtracted H_2 image is shown in the inset. The *K*-band image reveals a cluster of objects with a bright source "A" (α=20:46:8.35, δ=46:40:39.7) located close to the IRAS position with some fainter stars embedded in nebulosity. The 2MASS colours of "A" do not appear to be highly reddened; it is at the

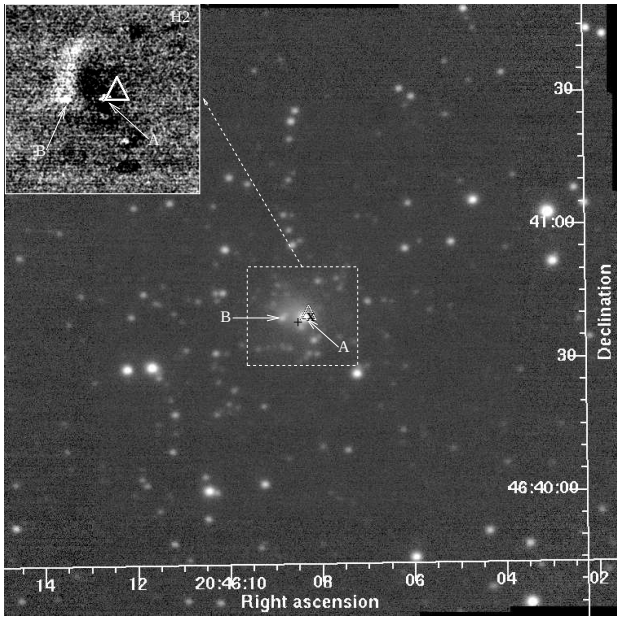

Figure A42. The *K*-band image of IRAS 20444+4629. A continuum-subtracted H_2 image of the central region is shown in the inset. "x" shows the 6-cm position of Molinari et al. (1998).

boundary of the reddening band (Fig. 1). However, it should be noted that the source is poorly detected by 2MASS in K_s. "B" is an object nearby, which shows a comet-like nebulosity embedded in the nebula. The cometary nebulosity associated with "B" disappears in the continuum-subtracted H_2 image. No bipolar emission is seen in this field in H_2 emission. The H_2 image, however, shows a faint arc-like line emission, originating from the position of "B" and extending ~7.5 north and slightly NW (see the inset in Fig.

Fig. A42). It is not clear if this is due to shock or fluorescence. The IRAS position is 1.45 arcsec NW of "A"; the MSX source detected is offset 3.7 arcsec from the IRAS position and 2.25 arcsec SE of "A". The unresolved 6-cm radio continuum source (flux density = 2.88 mJy) detected by Molinari et al. (1998) is within 1.8 arcsec of "A". Given the agreement of the radio, IRAS, MSX and near-IR positions, "A" is likely to be the near-IR counterpart of the YSO; it has possibly evolved out of the very early phases of formation and may be in a UCHII phase. The status of "B" needs to be investigated more through multi-wavelength infrared observations with good angular resolution.

A43 IRAS 21078+5211 - *Mol 133*
(*d = 1.49 kpc, L = 13.4×10^3 L$_\odot$*)

IRAS 21078+5211 is associated with a bright millimetre and sub-millimetre source GH2O 092.67+03.07, located 30 arcsec south of a compact HII region (Bernard, Dobashi & Momose 1999). Wouterloot & Brand (1989) observed a red-asymmetry in the CO line implying a possible outflow. Through interferometric imaging in CS and line observations of CS and CO, Bernard et al. (1999) observed a circumstellar disc (12 M$_\odot$) and a very young outflow (0.6 M$_\odot$; t$_{dyn}$ $\simeq$ 3500 yr) associated with GH2O 092.67+03.07. The disc shows evidence for infall consistent with a high mass central object and so GH2O 092.67+03.07 is believed to be protostellar. They derived a mass loss rate $\simeq 2\times10^{-4}$ M$_\odot$ yr^{-1} and a mass of the central star to be $\sim$6 M$_\odot$.

IRAS 21078+5211 was selected as a candidate HMYSO by Molinari and co-workers, who report the presence of a dense NH_3 core (Molinari et al. 1996) and a radio detection at 6 cm (Molinari et al. 1998). Bronfman et al. (1996) detected CS (2-1) with a velocity of -6.4 kms^{-1}. Neither Szymczak et al. (2000) nor Slysh et al. (1999) found any evidence for CH_3OH maser emission. The source was included in the OH maser survey of Baudry et al. (1997), but again no detection was made. H_2O maser emission was detected by several investigators (Palla et al. 1991; Brand et al. 1994; Miralles et al. 1994; Codella et al. 1996; Jenness et al. 1995).

Our *K*-band image is presented in Fig. A43. The continuum-subtracted H_2 and Brγ images do not show any extended emission. We do not see any significant IR sources, with excess emission in 2MASS, near the IRAS or radio positions. The three MSX sources detected in the field are towards the east of the IRAS position and none of these appear to be associated with the IRAS or the radio position of Molinari et al. (1998).

There is a cometary UCHII region in this field detected by Miralles et al. (1994) at 2 and 6 cm with flux densities of 31±1 mJy and 40±1 mJy, respectively. This radio source is located towards the SW of the IRAS position in our field (its location is shown in Fig. A43). The 6-cm position of Molinari et al. (1998) is offset from the position given by Miralles et al. (1994), but agrees within the angular extent of the core of the radio source at 6 cm (11.46 arcsec×16.16 arcsec - Molinari et al., 19 arcsec - Miralles et al). The observations of Molinari et al. (1998) also revealed an extended halo at 6 cm (60×45 arcsec) and an integrated flux density of 263.73 mJy. In Fig. A43, we have labelled a bright 2MASS source "A" (α=21:09:21.77 δ=52:23:10.8) detected near the radio sources and surrounded by faint nebulosity. "A" has multiple faint neighbours resolved in our images; the coordinates given here are those of the brightest object. The 2MASS colours, which will be dominated by that of the brightest component "A" do not exhibit any IR excess (Fig. 1). It is close to one of the MSX sources in this field, but the radio detections of both Miralles et al. (1994) and Molinari et al. (1998) are offset from it in a similar fashion suggesting that "A" is not the object responsible for the radio emission.

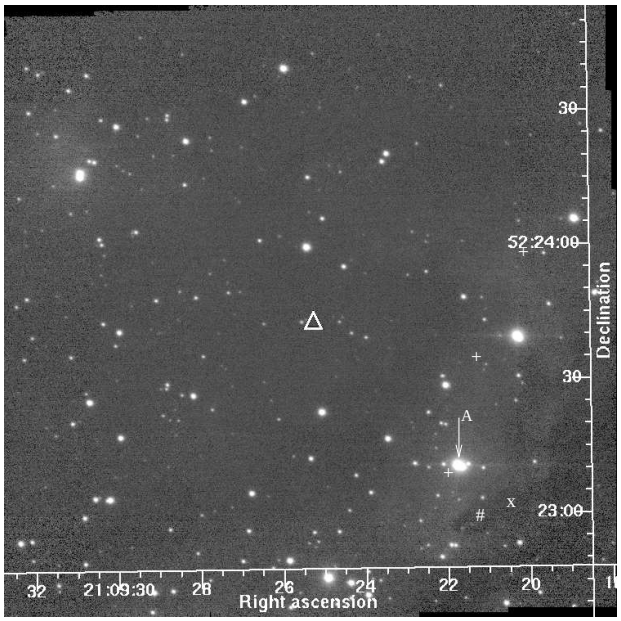

Figure A43. *K*-band image of IRAS 21078+5211. The 6-cm position of Molinari et al. (1998) is shown by "x" and that of Miralles et al. (1994) is shown by "#"

The locations of the water maser (detected using the VLA) and 850-μm continuum peak (observed using the JCMT) given by Jenness et al. (1995) agree well; they fall outside the radio contours and are further SE from the radio positions, outside the field of view of our images. The CS emission from the disc detected by Bernard et al. (1999) also appears to be close to the location of the H_2O maser observed by Jenness et al. (1995). Hence, it is possible that the youngest source in this region is located outside our field, towards the SW. It is noteworthy that the outflow is associated with the sub-mm source (located outside our field) and not from the UCHII detected in the radio. None of these fall within the error ellipse of the IRAS position (20 arcsec×7 arcsec). It remains to be investigated whether the object implied by the IRAS detection is a deeply embedded and very young source different from those seen at longer wavelengths or if it is the combined emission from several objects.

A44 IRAS 21307+5049 - *Mol 136*
(*d = 3.6 kpc, L = 4.0×10^3 L$_\odot$*)

A dense core was detected towards this source in NH_3 by Molinari et al. (1996). Molinari et al. (2002) present high-spatial-resolution observations of IRAS 21307+5049 in HCO^+ and 3.6-cm continuum emission. They find a compact molecular core with no free-free emission, suggesting the presence of a very young, pre-UCHII object. The extended 3.6-cm emission detected by them is offset NE of their mm continuum and HCO^+ emission peaks and the IRAS and MSX positions. It is believed to be part of a supernova remnant and not connected with the YSO. IRAS 21307+5049 is also associated with water maser (Palla et al. 1991).

Our near-IR images of this region reveal a cluster with a bright object "A" (α=21:32:30.60, δ=+51:02:16.0) located 10.3 arcsec SW of the IRAS position . "A" is associated with a cometary nebula (which opens towards the NW) in the *K*-band image, and a few

much fainter companions. Fig. A44 shows our *K*-band image on which source "A" is labelled. Our continuum-subtracted Brγ image does not show any extended emission. The H_2 image reveals a faint emission feature ~3.7 arcsec SE of "A", which is circled and labelled "1" on the figure. The region of the H_2 image close to "A" is shown in the inset in Fig. A44. The continuum-subtracted image exhibits a large negative residual on the source "A", which implies a steep SED, probably arising from the presence of heated dust. This is consistent with the detection of a single continuum emitting core at 3.4 mm by Molinari et al. (2002). The MSX position is 10.2 arcsec NE of "A" and is just 2.7 arcsec SE of the IRAS position, which casts doubt on "A" being the IR counterpart of the YSO. However, the location of the 3.4-mm core imaged by Molinari et al. (2002) is only 0.5 arcsec NE of "A" which gives confidence in identifying "A" as the near-IR counterpart of the HMYSO. Moreover, the 2MASS JHK_s colours of "A" exhibit large reddening and IR excess (Fig. 1), and place it in the region occupied by YSOs in the colour-colour diagram (although the source is poorly detected in *J* and *H* by 2MASS). The faint 44-GHz CH_3OH maser is in fact detected just 2.2 arcsec SE of "A" (Kurtz et al. 2004). The location of "A" is offset by only ~1 arcsec from the peak of the centroid of the 3-mm OVRO source of Fontani et al. (2004). The peak position of their 850-μm SCUBA source is also close to "A". Fontani et al. (2004) also imaged IRAS 21307+5049 in the near-IR JHK_s bands and in H_2 and FeII; they did not detect line emission in H_2 and FeII.

Zhang et al. (2005) detected a bipolar outflow in CO, the blue- and red-shifted wings of which are oriented roughly in the NW-SE direction. This is in agreement with the location of the H_2 emission feature "1" SE of "A". The centroid of the CO emission detected by them is 14 arcsec west and north of the IRAS position, which is within their spatial resolution (Table C1). More recent ^{12}CO maps (Fontani et al. 2004), made with better resolution and positional accuracy, also show a bipolar outflow, oriented NW-SE and centred on the 3-mm core, the location of which is close to that of "A" (suggesting that "A" is the driving source of the outflow). From its morphology, they suspect that the outflow is made up of two components.

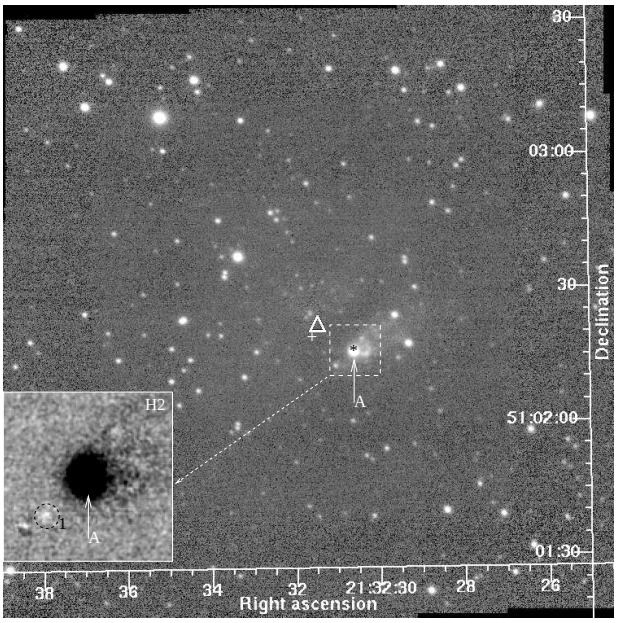

Figure A44. Observed *K*-band image of IRAS 21307+5049. Continuum-subtracted H_2 image of the region around the IR source is shown in the inset. "*" shows the 3.4-mm continuum peak of Molinari et al. (2002).

A45 IRAS 21391+5802 –*Mol 138*
(*d = 0.75 kpc, L = (0.0939; 0.15)*$\times 10^3$ $L_\odot$)

IRAS 21391+5802 is embedded in the bright-rimmed globule IC1396(N) in the HII region IC1396 in Cepheus. It was identified as an intermediate-mass protostar by Wilking et al. (1993) and was detected in NH_3 emission by Molinari et al. (1996). Methanol masers from this region have been observed by Kurtz et al. (2004) and water maser emission has been detected by Felli, Palagi & Tofani (1992), Tofani et al. (1995) and Patel et al. (2000). The multi-epoch observations of Patel et al. (2000) allowed the proper motions to be measured for ten water masers. These were consistent with the masers tracing the dominant bipolar outflow in this source, even within ~1AU of the source.

A number of outflows have been discovered in this region. A bipolar outflow on arcminute scales was discovered by Sugitani et al. (1989) in CO (J=1-0); it was subsequently mapped by Wilking et al. (1990) (CO, J=2-1) and Codella et al. (2001). Shock-excited emission from [OI] was seen in the outflow in the ISO LWS spectra of Saraceno et al. (1996); their spectra also revealed CO, OH and H_2O emission toward IRAS 21391+5802 showing the presence of warm, dense molecular gas. They also obtained continuum observations from 350 μm to 1.3 mm and derived a bolometric luminosity of 235 $L_\odot$.

More recent studies of the region at millimetre wavelengths have since revealed three embedded sources, the strongest of which (BIMA 2) is associated with the IRAS source (Beltrán et al. 2002, 2004). At higher angular resolution (~4 arcsec), CO maps by Beltrán et al. (2002) show a collimated outflow oriented approximately EW centred on "BIMA 2", and a second, lower velocity outflow running NS from "BIMA 1". The east-west flow is easily identified as bipolar at high velocities (the 15.5-20.5kms^{-1} channel in Beltrán et al. 2002) whereas at low velocity, the kinematics are complex and the outflow loses its identity. It is speculated that other outflows may be confusing the picture. The CS (2-1) emission echoes the characteristics of the "BIMA 2" flow, being clearly bipolar at high velocity, though less distinct at lower velocities. Observations in CH_3OH and CS (5-4) reveal clumps of emission along the outflow axis. The total mass of the EW outflow is estimated to be $13.6\times10^{-2}M_\odot$; the NS outflow mass is estimated to be $1.2\times10^{-2}M_\odot$ (Beltrán et al. 2002). Beltrán et al. also estimated a luminosity of ~150 $L_\odot$ for "BIMA 2" and suggest that "BIMA 1" and "BIMA 3" are more evolved lower-mass objects. No radio emission has been detected towards this region at 6 cm by Molinari et al. (1998). However, VLA observations of Beltrán et al. (2002) at 3.6 cm revealed three faint continuum sources "VLA 1" (0.21 mJy), "VLA 2" (0.27 mJy) and "VLA 3" (0.43 mJy), spatially coinciding with "BIMA 1", "BIMA 2" and "BIMA 3" respectively.

Previous infrared observations by Nisini et al. (2001) show H_2 v =1-0 S(1) emission extending along the "BIMA 2" outflow. They also identify two additional outflows oriented EW, by associating the H_2 emission with previous CO (J=2-1) maps from Codella et al. (2001). On larger scales, Reipurth et al. (2003) discovered a new Herbig-Haro flow from IC1396N, with the working surface located 0.6 pc from the putative source newly identified in their JHK imaging and located on the HH 777 flow axis. They label this source as HH 777 IRS. Reipurth et al. (2003) found no H_2 emission clearly associated with the HH 777 flow, but do confirm most of the small scale flows observed by Nisini et al. (2001).

Fig. A45 shows our *K*-band and continuum-subtracted H_2 im-

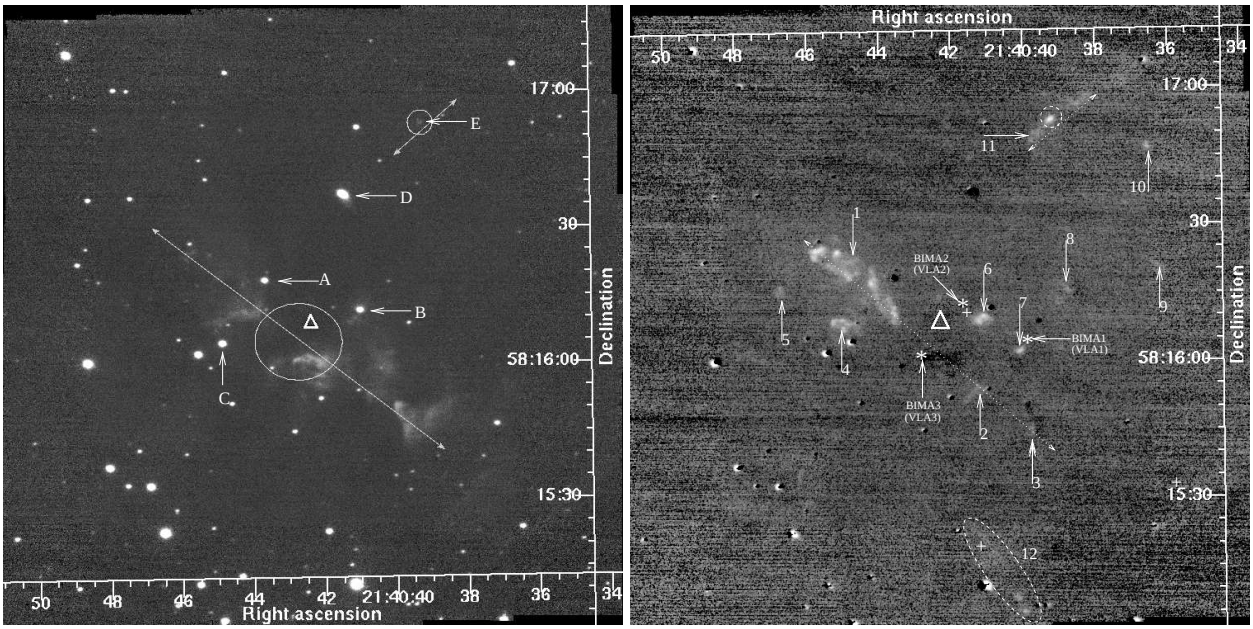

Figure A45. The left panel shows the *K*-band image of IRAS 21391+5802. The right panel shows the continuum-subtracted H_2 image. The H_2 has been smoothed with a Gaussian of FWHM=2 pixels to enhance the faint emission features. The three mm and radio continuum sources detected by Beltrán et al. (2002) are indicated by "*" and are labelled "BIMA1–3" and "VLA1–3". The locations of the brighter of the three ("BIMA2–3") agree with those of the two mm continuum positions of Codella et al. (2001)

ages. No Brγ emission is observed from this region. Our observations cover a field much smaller than that obtained by Nissini et al (2001), but have better spatial resolution. There is a spectacular outflow in the NE-SW direction, along the dotted arrow and traced by the H_2 emission features labelled "1–3". There is a second bipolar outflow emanating from the centre; the features labelled "4" and "5" appear to be tracing one of the the lobes of this bipolar outflow. It is not clear if "6" and "7" trace the other lobe of this flow or represent another outflow. The centre of the field around the IRAS position is devoid of near-IR sources. The region appears to be suffering from large extinction and the driving sources of the jets revealed in H_2 are not detected in *K*. Four near-IR point sources closest to the IRAS position are labelled "A–D". All four sources exhibit reddening and excess (Fig. 1). However, from their locations, these stars do not appear to be driving the two outflows mentioned above. "D"(α=21:40:41.46, δ=58:16:37.7) is identified as HH 777 IRS detected by Reipurth et al. (2003) and our *K*-band image shows a cometrary nebula associated with it. "D" is the only source detected in the 11.6 μm image obtained by Reipurth et al.

The YSOs driving the two outflows mentioned above are likely to be located within the circle shown near the centre of the field, which includes the IRAS, MSX and mm continuum positions. Other H_2 emission features detected in this field are labelled "8–12". It remains to be investigated if "8–9" are associated with the outflow from "D", detected by Reipurth et al. (2003). The feature labelled "11" appears to be another bipolar outflow, probably produced by the object labelled "E" (α=21:40:39.26, δ=58:16:53.2), which is not detected by 2MASS. Multiple stars of intermediate and low mass are probably being formed in the central region. This is confirmed by the multiple outflows suggested by the H_2 knots and the three millimetre sources detected by Beltrán et al. (2002). The outflow defined by the direction of "1" is oriented at a position angle of 50° and has a collimation factor of 6.5. The blue-shifted lobe of the outflow from "BIMA 2" mapped in CO by Beltrán et al. (2002) roughly traces the jets "1" and/or "2". Wilking et al. (1990) derived a position angle of 75 degrees for the CO outflow detected by them. The locations of the three faint MSX sources in this field (detected only at 8.28 μm) are shown on Fig. A45. The first one is 5.9 arcsec NW of the IRAS position, close to "B" and "BIMA2". The second source is near the knotty H_2 emission feature "12".

A46 IRAS 21519+5613 - *Mol 139*

(*d = 7.3 kpc, L = 19.1×10^3 L$_\odot$*)

Early observations by Cesaroni et al. (1988) found H_2O maser emission from this source at 35 Jy, though some of the later attempts by Comoretto et al. (1990), Gyulbudaghian, Rodriguez & Curiel (1990), Palagi et al. (1993) and Palla et al. (1991) did not result in a solid detection, yielding only upper limits. However, Wouterloot et al. (1993) detected three-component H_2O maser emission, ~8.6 arcsec NW of the IRAS position. No CH_3OH maser emission was found (MacLeod et al. 1998b). A search by Wouterloot et al. (1993) for OH masers also resulted in a null detection. There was no 6-cm free-free continuum emission detected from this region (Molinari et al. 1998). Molinari et al. (1996) and Bronfman et al. (1996) detected a core in NH_3 and CS(2-1) respectively. CO lines were observed by several investigators (Wouterloot & Brand 1989; Wouterloot et al. 1993; Su, Zhang and Lim 2004). All of the detected line emissions were at a v_{LSR} close to -63 km s^{-1}.

No H_2 imaging of this region appears to have been done before. Our *K*-band image reveals a cluster of IR sources close to the IRAS position. Most of the associated nebulosity disappears in our continuum-subtracted H_2 image (right half of Fig. A46). However, the H_2 image reveals two faint well defined bipolar outflows, the directions of which are shown by two arrows labelled "1" and "2". "1" is oriented in the NE-SW direction at an angle ~48°; it

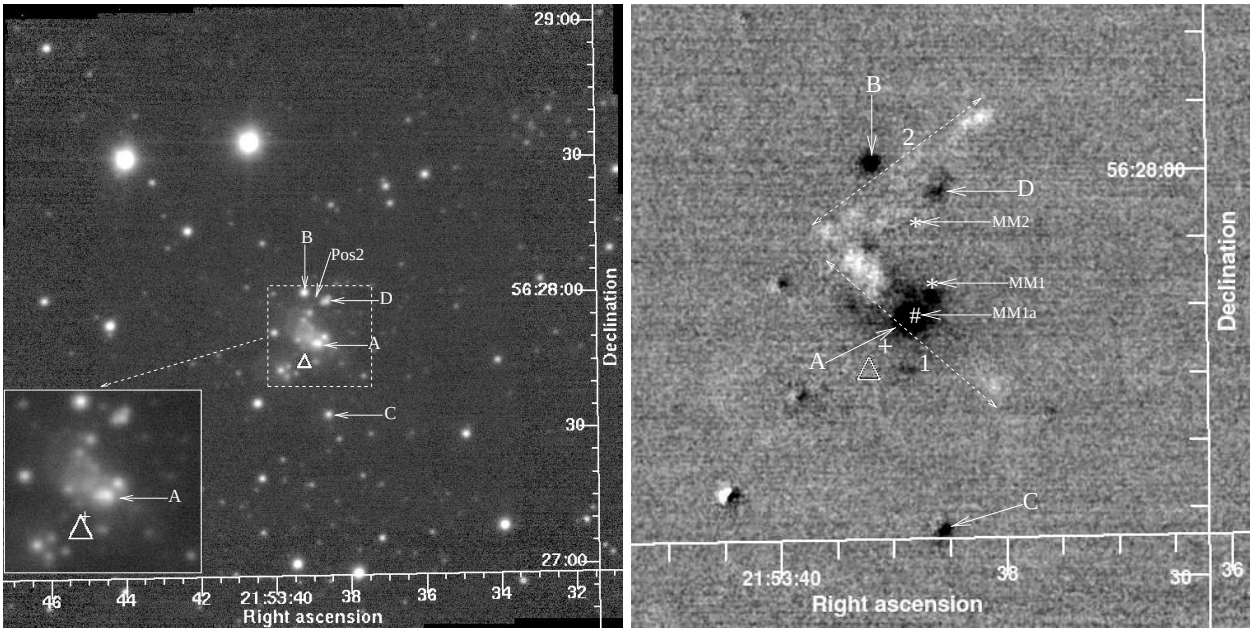

Figure A46. Left: *K*-band image of IRAS 21519+5613. An enlarged view of the central region is shown in the inset. Right: continuum-subtracted H_2 image of the central region. "#" shows the 1.3-mm continuum peak and "*" shows the two 3.4-mm continuum peaks detected by Molinari et al. (2002) .

appears to be bipolar in nature about an IR source labelled "A" (α=21:53:38.82, δ=56:27:49.3). This source appears slightly extended EW and may be a binary. There appears to be a companion ~0.8 arcsec east of "A"; the seeing was ~1 arcsec when we observed this field, so they are not very well resolved. There is another point source NW of "A" at a separation of ~2.1 arcsec. The 2MASS magnitude of "A", which is a composite of all three sources, some other fainter components and the faint nebulosity associated with the central region, shows IR excess (Fig. 1). The outflow "2" is located north of "1" and is directed in the NW-SE direction with an angle of ~126.5°. The point source labelled "B" (α=21:53:39.19 and δ=56:28:0.7) is slightly offset from the axis and centre of "2". This source exhibits IR excess in the 2MASS data. "D" (α=21:53:38.59, δ=56:27:58.6) is located near, but slightly offset from, the centre of "2". "D" is extended in NW-SE, implying the possible presence of companions and the aggregate 2MASS colours do not exhibit any IR excess. The coordinates given here are that of the brightest point source in "D". There is a source labelled "C" (α=21:53:38.58 and δ=56:27:33.6), which is detected in *H* and *K* only by 2MASS. The colours derived using the 2MASS *H* and *K* magnitudes and the upper limit magnitude in *J* place it in the region of a reddened sources with IR excess in Fig. 1; deeper near-IR photometry is required to undertand its nature. No H_2 line emission is observed in its near vicinity. Brγ was not detected from either jet "1" or jet "2".

Our observations are consistent with the longer wavelength observations of Molinari et al. (2002). They discovered a very well defined core, extended in the NS direction in HCO^+ emission. They also detected two continuum emitting cores at 3.4 mm - one source named MM1 coinciding with the brightest region of the HCO^+ core and the other, MM2, located north of MM1. A bright 1.3 mm continuum source (MM1a) detected by them is nearly coincident with MM1 and is offset by only ~2.2 arcsec SE from MM1. The mm continuum sources are close to the two jets discovered in our H_2 image and possibly harbour their driving sources. The millimetre positions are labelled on Fig. A46. The location of MM1a coincides with that of "A", confirming that "A" is the near-IR counterpart of the YSO driving the outflow "1". The location of MM2 is between "A" and the "BD" axis. MM2 is located close to the centre of "2", but is slightly offset towards MM1. The MSX mission also detected an IR source at wavelengths from and above 8.28 μm (in C, D & E bands). The position of the detected MSX source is 3.4 arcsec SE of "A", close to the IRAS source which is 5 arcsec SE of "A".

Su et al. (2004) observed this region in 3-mm continuum and in ^{12}CO, ^{13}CO and $C^{18}O$ lines. The 3-mm observations showed a peak, a few arcsec NW of the IRAS position. The location of the 3-mm continuum peak agrees well with the location of "A" to within 0.6 arcsec. Their $C^{18}O$ centroid also is very close to the 3-mm peak. The origin of the outflow mapped in ^{12}CO and ^{13}CO appear to be closely coincident with the centroid of the molecular gas and dust continuum. Their velocity integrated ^{12}CO line map shows blue- and red-shifted lobes extending NE and SW respectively from the 3-mm peak, with a position angle of ~75°. This is consistent with the fact that, in our H_2 image, the NE lobe of the jet labelled "1" is brighter than the SW lobe. It should be noted that the integrated ^{12}CO map, especially the blue-shifted lobe, also shows an elongation in the NW-SE direction, which is consistent with the presence of the second outflow ("2") in our H_2 image. Su et al. derived a collimation factor of 1.6 for the observed outflow and 2.4 after deconvolution. From our H_2 images, we estimate collimation factors of 3.3 and 5.5, respectively, for the two outflows. Zhang et al. (2005) detected a bipolar outflow in CO, the centroid of which is offset north and west of the IRAS location by 14 arcsec each, the direction of which is consistent with the NW offset of "A" from the IRAS position, even though the offset is within their angular resolution.

Overall, this region appears to host two collimated outflows. "A", and possibly "B" or its neighbours, appear to be the near-IR counterpart/s of the IRAS and MSX object and are the most likely candidate HMYSOs in this region.

A47 IRAS 22172+5549 - *Mol 143*
($d = 2.4\,kpc$, $L = 1.8{\times}10^3\,L_\odot$)

This is a known HII region. However, Molinari et al. (1998) did not find any radio emission from this source at 2 cm or 6 cm. The dense core towards this region was detected in NH_3 emission by Molinari et al. (1996). The H_2O maser emission from this source is extremely faint. Palla et al. (1991, 1993) did not detect H_2O maser emission. Nor did Comoretto et al. (1990) or Palagi et al. (1993) who give only upper flux limits. Cesaroni et al. (1988) and Wouterloot et al. (1993) detected faint H_2O maser emission. A search by Wouterloot et al. (1993) for the 1665 MHz OH maser did not yield any detection.

Fich, Dahl & Treffers (1990) detected H_α emission from this source using Fabry-Perot observations. Molinari et al. (2002) present high-spatial-resolution HCO^+, 3.4-mm and 3.6-cm observations of IRAS 22172+5549. They find a compact molecular core with no free-free emission, suggesting the presence of a very young pre-UCHII protostar. Wouterloot & Brand (1989) detected red-shifted CO (1-0) emission. Zhang et al. (2005) have also mapped a compact CO outflow toward this source. Recently, Fontani et al. (2004) have observed IRAS 22172+5549 in a number of molecular tracers, and have obtained near-IR images in H_2 and [FeII]. They observed line emission features associated with a compact north-south CO outflow.

Our K and H_2 images of this region show a cluster of objects centred north of the IRAS position (Fig. A47), with some members of the cluster distributed in a ring-like pattern where most of the activity appears to be happening. The continuum-subtracted H_2 image reveals two or more well collimated jets. Molinari et al. (2002) detected HCO^+ from the cluster, which appears to be a single condensation in their integrated maps, but is resolved into three separate condensations in their velocity resolved maps. Two of these cores show 3.4-mm continuum-emitting counterparts. Their 3.4-mm position appears to be located within the cluster, NE of the IRAS position. The location of the centroid of HCO^+ emission is also very close to the 3.4-mm peak. The brighter of the two mm sources (MM2) is only 2.7 arcsec NW of the source labelled "A" (α=22:19:9.48, δ=56:5:0.3) in Fig. A47; the fainter mm peak (MM1) is 6.6 arcsec NW of "A". The 3-mm peak position of Fontani et al. (2004) also agrees with the mm position of Molinari et al. (2002). The MSX mission detected a mid-IR source at wavelengths 8.28 μm and above. The location of the MSX source is ~17.3 arcsec NE of the IRAS position and is only 2.8 arcsec NW of "A", nearly coincident with MM2. "A" itself is double with the components separated by ~1 arcsec at an angle of 102°. It is detected by 2MASS in H and K_s with an $H - K_s$ colour of 1.97. It is not well detected by 2MASS in J, however, and the pair is not resolved.

There are several other fainter objects in the vicinity of "A", most of which were not detected by 2MASS. Our K-band image shows that "A" is associated with a broken ring-like nebulosity, with a diameter of ~2.8 arcsec, with "A" offset from the centre and embedded in the ring. The nebulosity disappears upon continuum-subtraction. Our continuum-subtracted H_2 image shows H_2 line emission on the NE and SW sides of "A", which are labelled "1" and "2". Also obvious in the figure are the H_2 emission features circled and labelled "3–5". "5" appears to contain the bow-shock of a jet; there is some faint H_2 emission seen along the dotted arrow drawn near "5". The NS oriented bipolar outflow mapped in CO by Fontani et al. (2004) has the centroid of the two lobes close to "A" and is in the direction of "5". The near-IR images of Fontani et al. (2004) also show most of the H_2 emission features labelled on Fig. A47. Their H_2 and [FeII] images show the NE-SW oriented features in the direction of "1–2", with "5" located towards the outer region of the red-shifted lobe of their CO map. Hence it is possible that the CO outflow mapped by them is composed of more than one. Overall, this region appears to be active in star formation, hosting at least two outflows. With the positional accuracy quoted by Molinari et al. (2002) and the proximity of the mm sources and the centroid of the CO outflow to "A", this source and/or some of its very near neighbours are YSOs, which are responsible for the outflows discussed here. Deeper IR imaging at sub-arcsec resolution is certainly warranted.

A48 IRAS 22305+5803 - *Mol 148*
($d = 5.4\,kpc$, $L = 14.1{\times}10^3\,L_\odot$)

A dense core was detected towards IRAS 22305+5803 in CS (Bronfman et al. 1996) and NH_3 (Molinari et al. 1996). The source is associated with H_2O maser emission (Palla et al. 1991). Molinari et al. (2002) mapped the region at high spatial resolution in HCO^+(1-0) and resolved a remarkable, clumpy ring of line emission with the IRAS position located in the SW part of the ring. However, their 3.4-mm maps did not reveal any continuum emitting compact source within the ring. 3.6-cm radio continuum observations obtained by them using the VLA detected a faint radio source (0.12±0.03 mJy) within the western part of the HCO^+ ring. Their IRAM observations at 1.3 mm revealed a compact core associated with the source detected at 3.6 cm. From the radio flux, they derive a B2 ZAMS star. Wouterloot & Brand (1989) detected CO (1-0) emission (with a blue shoulder). Zhang et al. (2005) mapped a bipolar outflow in CO line, close to the IRAS source.

Fig. A48 shows our K-band and continuum-subtracted H_2 images. The K-band image reveals a compact cluster of IR sources embedded in nebulosity at the centre of the field. Most of the objects in the cluster are located along a ridge extending roughly NS. The continuum-subtracted H_2 image shows large negative residuals associated with the nebulosity towards the centre of the field. Most of the diffuse emission towards the northern part of the cluster disappears except for three clumpy line emission features labelled "1" on the H_2 image. No point sources are seen at the location of these H_2 emission features; i.e, they are true H_2 emission features rather than residuals from continuum subtraction. These features could be produced by one or more jets.

Three sources are labelled on Fig. A48 - "A" (α=22:32:23.77, δ=58:18:59.7), "B" (α=22:32:23.77, δ=58:19:07.7) and "C" (α=22:32:24.09, δ=58:19:11.4). These bright sources are associated with the HII region and the SW and western sides of the HCO^+ ring. "A" is not detected by 2MASS; the 2MASS detection is instead centred on the nebulosity. "B" exhibits slight excess in 2MASS data and "'C" does not exhibit any excess (Fig. 1). The location of the IRAS object is 4.5 arcsec SE of "A"; the MSX source is 1.65 arcsec NE of "A". The peak of the 3.6-cm emission detected by Molinari et al. (2002) is only 0.98 arcsec NW of "A".

The centre of the blue-shifted lobe of the CO outflow detected by Zhang et al. (2005) appears close to the region of line emission seen in our H_2 image. The H_2 emission features that we see are therefore probably from the blue-shifted lobe of a highly inclined jet. We do not know if more than one outflow is involved here. However, the close proximity of the IRAS, MSX and 3.6-cm positions suggests that "A", rather than "B" or "C", is the likely outflow source. The nature of "A" and its neighbours needs to be probed through near- and mid-IR obsevations.

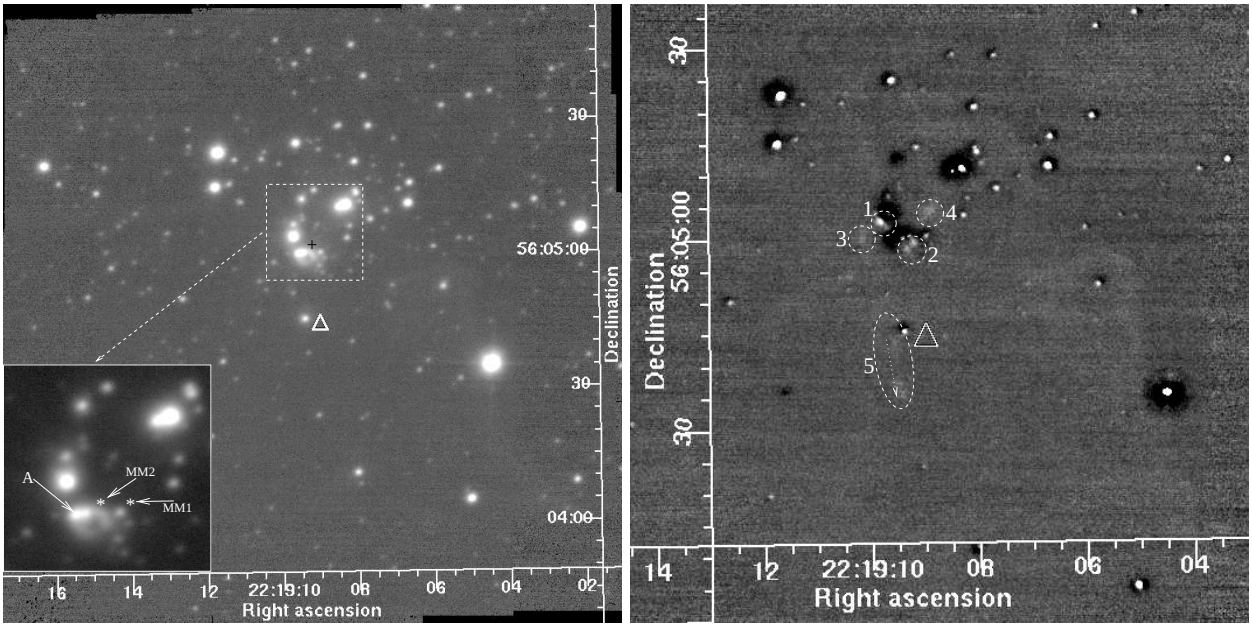

Figure A47. Left: *K*-band image of IRAS 22172+5549. An enlarged view of the central region is shown in the inset. The two 3.4-mm continuum sources of Molinari et al. (2002) are shown by "*" in the inset. Right: continuum-subtracted H_2 image of the central region smoothed with a Gaussian of 2-pixel FWHM.

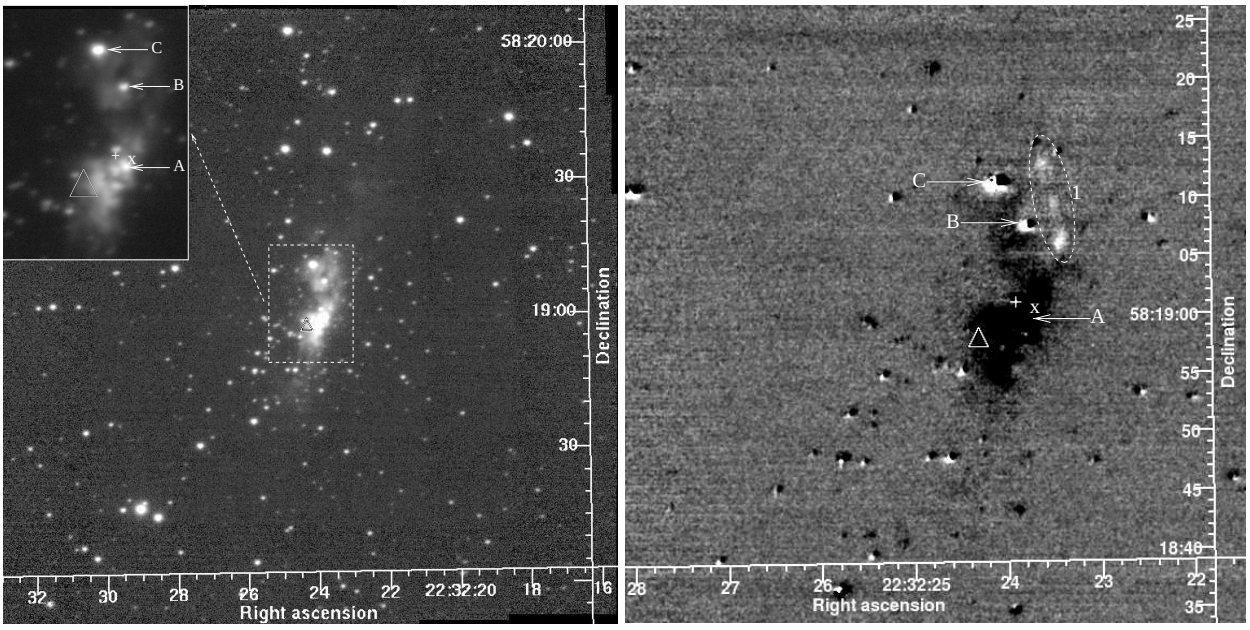

Figure A48. The left panel shows the *K*-band image of IRAS 22305+5803. An enlarged view of the central region is shown in the inset. The 3.6-cm radio continuum position of Molinari et al. (2002) is shown by "x". The right panel shows the continuum-subtracted H_2 image of the central region smoothed with a Gaussian of 2-pixel FWHM to enhance the faint emission features.

A49 IRAS 22570+5912 - *Mol 153*
(*d = 2.92; 5.1 kpc, L = 20.1; 50.1×10^3 L$_\odot$*)

High velocity CO was identified from IRAS 22570+5912 by Shepherd & Churchwell (1996a). In their follow-up observations, Beuther et al. (2002c) mapped the outflow in CO (2–1) and found a complex morphology with the flow centred off the peak 1.2-mm position. This fact, coupled with the broad extent of the flow at low angular resolution, leads them to posit that there may be several outflows in the region. The emission extends over 1.5 pc; the mass of the outflow is estimated at 73 M$_\odot$. No emission from either H_2O (Palla et al. 1991; Sridharan et al. 2002) or CH_3OH (MacLeod et al. 1998b; Slysh et al. 1999; Sridharan et al. 2002) masers has been found, nor emission from SiO or CH_3CN (Sridharan et al. 2002). The dense core towards this region was detected in CS emission (Bronfman et al. 1996; Beuther et al. 2002b). No ammonia emission was detected by Molinari et al. (1996). Observations of the dust continuum by Beuther et al. (2002b) at 1.2 mm reveal four clumps, with the brightest one located close to the centre of our field, near the IRAS position. The second brightest source is also

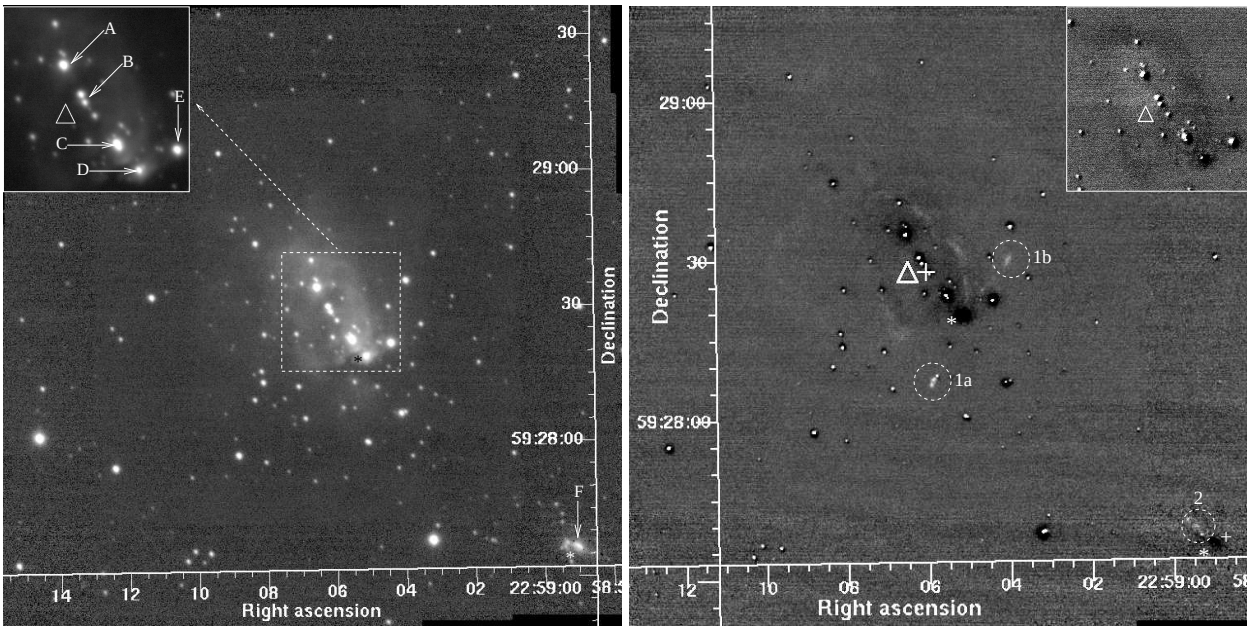

Figure A49. The left panel shows the *K*-band image of IRAS 22570+5912. The right panel shows the continuum-subtracted H_2 image of the central region on which the continuum-subtracted Brγ image of the central cluster is shown in the inset. The H_2 image has been smoothed with a Gaussian of 2-pixel FWHM. The peak positions of the two 1.2-mm sources of Beuther et al. (2002b) are shown by "*".

within our field, located towards the bottom right corner. This structure is partly repeated in their observations of dense gas tracers (CS, $C^{34}S$), where three of the four 1.2-mm sources have counterparts.

Fig. A49 shows our *K*, H_2 and Brγ images. The *K*-band image reveals a cluster, roughly centred on the IRAS position. A set of IR-bright objects is seen roughly aligned in the NE-SW direction and embedded in nebulosity. The nebula is roughly elliptical in morphology, the major axis of which is closely aligned with the string of bright stars. A few of the sources are labelled on Fig. A49 - "A" (α=22:59:06.52, δ=+59:28:34.7), "B" (α=22:59:06.18, δ=+59:28:30.1), "C" (α=22:59:05.54, δ=+59:28:23.2), "D" (α=22:59:05.12, δ=+59:28:19.3), "E" (α=22:59:04.40, δ=+59:28:22.2) and "F" (α=22:58:59.05, δ=+59:27:36.4). Most of these are resolved into multiple components in our image and all exhibit reddening (Fig. 1). "A" shows slight excess; it is resolved into a bright source with a few fainter ones in the neighbourhood. "B" is the object closest to the IRAS position; it is composed of a binary with components of comparable brightness separated by 1.3 arcsec. The coordinates of "B" given here are of the centroid of the pair. There is a third source ~3 arcsec SW of the pair and a much fainter 4th object is located in between the pair and the third source. 2MASS does not resolve these and the 2MASS magnitudes, which are composites of these four stars and dominated by the pair, do not exhibit any IR excess. "C" is again resolved into multiple components; the coordinates given here are that of the brightest. Its 2MASS colours do not exhibit excess. "D" is deeply embedded. It is not detected by 2MASS in *J* and *H*, where the magnitudes given are only upper limits; its 2MASS K_s magnitude is of poor quality. The 2MASS 'magnitude limits' locate "D" in the region of the giants (Fig. 1). This is likely to be due to the large uncertainties in its colours. This object exhibits large reddening and is most likely to be a YSO. "E" also exhibits large reddening and excess.

The MSX mission detected two objects in this field. The brighter one is only 2.9 arcsec from the IRAS position and is located close to "B". However it should be noted that within the positional uncertainties and spatial resolutions of IRAS and MSX, some or all of the objects labelled "A–E" may be contributing to the IRAS and MSX fluxes.

Several interesting H_2 emission features are seen in this region. The most prominent of these are circled and labelled "1a" and "1b" on the continuum-subtracted image. These appear to be the two lobes of a bipolar jet. Either "D" or "E" could be the driving source of this outflow; considering the large reddening and the location close to the centroid of these two H_2 lobes, "D" is the most likely candidate. The brightest 1.2-mm peak of Beuther et al. (2002b) is closest to "D" and is located merely 2.1 arcsec from it implying that "D" is the YSO driving the outflow traced by "1a" and "1b". However, the 3.6-cm radio continuum source (flux density = 29 mJy) of Sridharan et al. (2002) is located 7.3 arcsec from the 1.2-mm peak, implying that the radio emission is produced by a more evolved source in the cluster. Our H_2 image also shows collimated emission features SW of the cluster, in the bottom right corner of the figure, which are circled and labelled "2". "2" appears to emanate from the object labelled "F" on the *K*-band image. "F" is detected by 2MASS in K_s only. This source is nebulous, slightly elongated and is probably composed of one or more objects embedded in nebulosity; the point sources within "F" are not resolved here. The second MSX object is notably within 1.2 arcsec of "F". The second brightest 1.2-mm peak of Beuther et al. (2002b) is located only 2.7 arcsec SE of "F". We conclude that "F" hosts a YSO which produces the jet "2" detected in H_2. In addition to these, there is also some faint H_2 emission enveloping "A–D" on the NW and SE sides of these diagonally aligned sources. There is also some faint emission extending east. These are probably caused by fluorescent emission due to the combined radiation from the more evolved stars within this central cluster.

The CO map of Beuther et al. (2002c) could probably be the result of at least two outflows from two different YSOs, one detected as the near-IR source "D" and the second an embedded

source within "F". From our H_2 image, we derive collimation factors of 11.5 and 4.5 for the two outflows, "1" and "2", respectively.

There is very faint Brγ emission detected towards the central region of the cluster. This may be due to emission from the more evolved bright stars in the central region of the cluster. The central portion of the Brγ image is shown in the inset on the H_2 image. This region appears to host multiple YSOs in different stages of evolution. The presence of outflow/s, multiple YSOs and the alignment of the bright objects nearly at the centre makes this region interesting, warranting detailed study.

A50 IRAS 23139+5939

(*d = 4.8 kpc, L = 25×10^3 L$_\odot$*)

Observations by Beuther et al. (2002b) reveal IRAS 23139+5939 to be single peaked in both dust continuum emission and dense gas tracers. The CO (J=2-1) emission from this source exhibits both red- and blue-shifted components that are largely overlapping and centred on the millimetre continuum peak (Beuther et al. 2002c). The outflow is possibly nearly along the line of sight. They estimate the mass of the gas in the outflow to be 57 M$_\odot$. The multi-wavelength study of Sridharan et al. (2002) and Beuther et al. (2002d) reveal a mid-infrared MSX source (positional accuracy of 5 arcsec), nearly coincident with a 1.2-mm continuum source, H_2O masers and a faint 3.6-cm continum source detected at two different epochs using the VLA (Tofani et al. 1995, 0.92±0.15 mJy; Sridharan et al. 2002, 1.4 mJy). The centres of all these detections are offset to the north and east of the IRAS position by 8.7 arcsec and 5.5 arcsec respectively.

Beuther et al. (2002d) found three water masers associated with IRAS 23139+5939, spatially coincident (within 1 arcsec) with the radio, millimetre and mid-infrared positions. Methanol maser emission is reported by Szymczak et al. (2000). A multi-epoch observational study of the H_2O maser emission has been carried out by Goddi et al. (2005) at very high spatial resolution using the VLBA. They resolved several components and derived proper motions of the individual components of the maser. Their observations support a conical outflow from the YSO and show that the observed masers are preferentially arranged along the inner regions of the blue-shifted lobe of the outflow, which is oriented nearly along the line of sight. A model for Keplerian motion in a disc does not fit the maser data well. They propose that the masers are preferentially associated with collimated flows of gas found at the base of large-scale molecular outflows. The proper motions indicate a general expansion of the masers at 10's of km s^{-1}, as would be expected when the outflow along the line-of-light is projected on to the sky plane.

IRAS 23139+5939 was included in the *K*-band imaging survey of Hodapp (1994), but no outflow drivers were detected. Observations by Carnkner, Kozak & Feigelson (1998) did not detect any X-ray emission from this source.

Fig. A50 shows our *K*-band image of the field. The bright object "A"(α=23:16:10.39, δ=59:55:28.3), located close to the IRAS position, is associated with a cometary nebula. This object is just resolved as a binary in our images. The components of the binary are at a separation of ∼0.4″ in the NW-SE direction, the object in the SE being brighter than the one in the NW. The inset in Fig. A50 shows the source "A" resolved. The continuum-subtracted H_2 image (not shown here) revealed a faint H_2 emission features located at the position enclosed by a circle and labelled "1" (α=23:16:13.22, δ=+59:55:38.1) on Fig. A50; it is not clear whether "1" is produced by the outflow from "A".

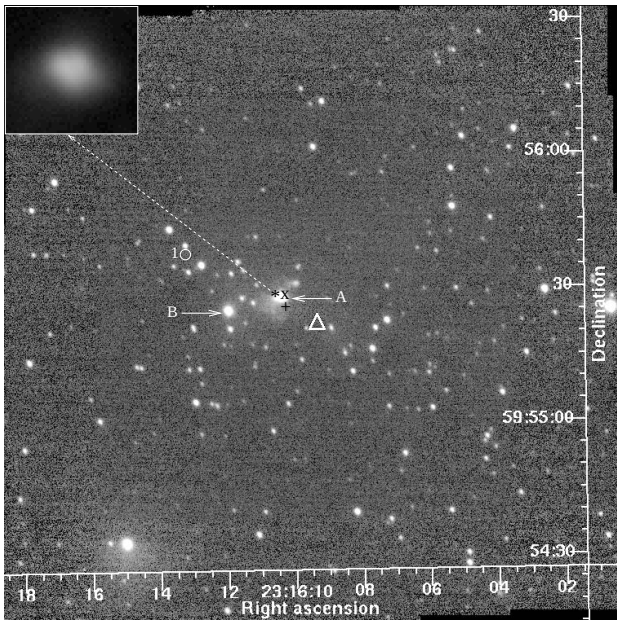

Figure A50. *K*-band image of IRAS 23139+5939. The inset shows an enlarged view of the central object with the binary resolved . "*" shows the peak of the 1.2-mm continuum emission of Beuther et al. (2002c) and "x" shows the 3.6-cm peak position of Tofani et al. (1995).

There is a cluster associated with this star forming region towards the centre of the observed field, with most of the cluster members located south of "A". This object and a fainter object, "B" (α=23:16:11.95, δ=59:55:25.4), both exhibit IR excess in their 2MASS colours and occupy the region of YSOs on the *JHK* colour-colour diagram (Fig. 1). "A" is located 9.8 arcsec NE of the IRAS position (8.2 arcsec east and 5.3 arcsec north). The MSX position is only 2.7 arcsec SW of "A" (1.5 arcsec west, 2.24 arcsec South). It is important to note that the peak of the 1.2-mm continuum located by Beuther et al. (2002b) is in very good agreement (to within 0.5 arcsec) with the location of "A", as well as the centimetre source, the centroid of the CO outflow and the location of water maser spots. We therefore identify "A" as the YSO driving the main outflow in this field. The faint radio emission from "A" suggests that it is likely to be in a pre-UCHII stage.

APPENDIX B: MHO NUMBERS

Only a few lines of Table B1 are printed here. The complete form of the table is available on-line only.

APPENDIX C: SOURCE RESOLUTIONS

This paper has been typeset from a TEX/ LATEX file prepared by the author.

Table B1. MHO numbers of the H_2 line emission features identified in this paper (from http://www.jach.hawaii.edu/UKIRT/MHCat/).

No.	Object Name (IRAS)	H_2 features in this paper[1]	MHO number
1	00420+5530	1 - 1–4	2900–2903
2	04579+4703	2 - 1,2; 3,4	1000; 1001
3	05137+3919	3 - 1a,1b; 2	1002,1003; 1004
5	05274+3345	5 - 1	1005
	05274+3345	5 - 2–7	1006 – 1011
6	05345+3157	6 - 1; 2–4	1016; 1018
	05345+3157	6 - 5; 6	1019; 1017
	05345+3157	6 - 7–11	1012–1015
7	05358+3543	7 - 1; 2; 3	1044; 1042; 1043
	05358+3543	7 - 4; 5; 6	1023; 1024; 1046
	05358+3543	7 - 7; 8; 9	1045; 1048; 1028
8	05373+2349	8	734
9	05490+2658	9 - 1	721
10	05553+1631	10 - 1–3	1200
11	06061+2151	11 - 1–3	1201–1203
13	18144-1723	13 - 1	2302
14	18151-1208	14 - 1; 3	2201; 2212
	18151-1208	14 - 2	2202
18	18264-1152	18 - 1a; 1b,4	2203; 2204
	18264-1152	18 - 3	2205
19	18316-0602	19 - 1–3	2206–2208
	18316-0602	19 - 4,5	2209,2210
20	18345-0641	20 - 1	2211
30	19374+2352	30 - 1–3	2600–2602
31	19388+2357	31 - 1–3	2613–2615
32	19410+2336	32 - 1; 32 - 2–3	2603; 2604
	19410+2336	32 - 4–6, 11,12	2606
	19410+2336	32 - 7,8	2607
	19410+2336	32 - 9,10	2620
33	20050+2720	33 - 1–3	2608–2610
	20050+2720	33 - 4; 5	2611; 2612
35	20062+3550	35 - 1a; 1b	858; 859
36	20126+4104	36 - 1; 2	860; 861
	20126+4104	36 - 3,4	862
37	20188+3928	37 - 1–5	863–867
38	20198+3716	38 - I; II	868; 869
39	20227+4154	39 - 1	870
	20227+4154	39 - 2–5	871–874
40	20286+4105	40	875
41	20293+3952	41 - 1–6	876–881
44	21307+5049		882
45	21391+5802	45 - 1; 2,3	2753; 2754
	21391+5802	45 - 4,5	2755
	21391+5802	45 - 6–10	2756–2760
	21391+5802	45 - 11; 12	2761; 2762
46	21519+5613	46 - 1; 2	2764; 2763
47	22172+5549	47 - 1–4	2765
	22172+5549	47 - 5	2766
48	22305+5803	48 - 1	2700
49	22570+5912	49 - 1a,1b	2701
	22570+5912	49 - 2	2702

[1]Object numbers - H_2 line emission features (labelled on Figs. A1–A50)

Table C1. Details of existing observations

Reference	Species	frequency/ wavelength	Telescope used	HPBW/FWHM (arcsec)	Pointing accuracy[1] (arcsec)
Anglada et al. (1997)	H_2O maser; NH_3	22.2; 23.7 GHz	Haystack 37-m, MA, USA	84	15
Bachiller et al. (1995)	CS(3-2); CO(2-1)	147; 230.5 GHz	IRAM 30-m, Spain	16; 11	3
Bernard et al. (1999)	CS(2-1)	98 GHz	NMA Interferometer, Japan	3.4×3	
	CS; CO	98–115 GHz	NRO 45-m, Japan	~17	~10
Baudry et al. (1997)	OH maser	6.031; 6.035 GHz	Effelsberg 100-m, Germany	130	
Beltrán et al. (2002)	Continuum	3.6 cm	VLA, New Mexico	⩽17.9×8.8	
	Cont.;CS;CO;CH_3OH	96.25–244.936 GHz	BIMA interferometer, CA	8.0×6.7–1.1×0.9	
Beltrán et al. (2004)	see Beltrán et al. (2002)				
Beuther et al. (2002a)	CO(1-0)	115.27; 110.20 GHz	IRAM 30-m	22	
	CO(1-0)	115.27 GHz	IRAM PdBI, Spain	4.1×3.3	
	SiO(2-1);$H^{13}CO^+$	86.85; 86.75 GHz	IRAM 30-m	29	
	SiO(2-1);$H^{13}CO^+$	86.85; 86.75 GHz	IRAM PdBI	5.8×5.36	
	CO(2-1);CH_3OH	230.54; 241.79 GHz	IRAM 30-m	11	
	CO(6-5)	691.47 GHz	CSO 10.4-m, Hawaii	11	
	Continuum	2.6 mm	IRAM PdBI	4×3	
Beuther et al. (2002b)	Continuum	1.2 mm	IRAM 30-m	11	
	CS(2-1)	97.98 GHz	IRAM 30-m	27	
	CS(3-2)	146.97 GHz	IRAM 30-m	17	
	CS(5-4)	244.936 GHz	IRAM 30-m	11	
Beuther et al. (2002c)	^{12}CO(2-1)	230.5 GHz	IRAM 30-m	11	
Beuther et al. (2002d)	H_2O Maser	22.235 GHz	Effelsberg 100-m; see Sridharan et al. (2002)		
	CH_3OH Maser	6.7 GHz	Effelsberg 100-m; see Sridharan et al. (2002)		
	H_2O Maser	22.235 GHz	VLA	~0.4	<1 (abs), ~0.1 (rel.)
	CH_3OH Maser	6.7 GHz	ATCA, Australia	~1.9	~1 (abs), ~0.1 (rel.)
	Continuum	1.2 mm	IRAM 30-m; see Sridharan et al. (2002)		~5
	Continuum	2.6 mm	IRAM PdBI + BIMA; see Beuther et al. (2002a)		~1
	Continuum	3.6 cm	VLA; see Sridharan et al. (2002)		1
Beuther et al. (2003)	CO(1-0)	115.27 GHz	IRAM 30-m	3.9×3.6	
Beuther et al. (2004a)	Continuum	1.3; 3 mm	IRAM PdBI	⩽1.91×1.75;⩽5.1×4.31	
	CO; SiO(2-1)	1.3; 3 mm	IRAM PdBI + 30-m	⩽1.96×1.79;⩽5.1×4.36	
Beuther et al. (2004b)	CN; CS	113.385; 97.981 GHz	IRAM PdBI	~1.46×1.21–5.31×3.42	
	CN; CS	226.656; 244.936 GHz	IRAM PdBI	~0.76×0.61–1.52×1.03	
Beuther et al. (2006)	CO(2-1); Cont.	1.3 mm	SMA, Hawaii	3.6×2.5–3.9×2.5	
	CO(2-1)	1.3 mm	IRAM 30-m+SMA data	4.2×2.8	
Brand et al. (1994)	H_2O Maser	22.235 GHz	Medicina 32-m, Italy	114	<20
Brand et al. (2001)	Different molecules	89.19–220.75 GHz	IRAM 30-m	27–17	3
	HCO^+(4–3)	356.73 GHz	KOSMA 3-m, Switzerland	70×78	
Bronfman et al. (1996)	CS(2-1)	97.981 GHz	15-m SEST, La Silla, Chile	50	~3
	CS(2-1)	97.981 GHz	OSO 20-m, Sweeden	39	~3
Carral et al. (1997)	Continuum	7 mm	VLA	2.5×0.5	~0.2
Carpenter et al. (1995)	CS(2-1)	97.981 GHz	FCRAO 14-m, Massachusetts	50×100	
Casoli et al. (1986)	$^{12;13}$CO(1-0)	115; 110.2 GHz	Bordeaux 2.5-m	264	
	^{12}CO(1-0)	115 GHz	IRAM 30-m	22	5-10
	^{12}CO(2-1)	230 GHz	McDonald 4.9-m, Texas	78	
Cesaroni et al. (1988)	H_2O Maser	22.235 GHz	Medicina 32-m	114	20
Cesaroni et al. (1997)	Different molecules		IRAM 30-m	27–11	4
	CH_3OH; HCO^+; CH_3CN, Cont.	88.93–92.25 GHz	IRAM PdBI	3.7–2.7	
Cesaroni et al. (1999)	Different molecules	88.6–241.7 GHz	IRAM 30-m	27–10	4
Cesaroni et al. (2005)	CS; CH_3OH	96.356–241.144 GHz	IRAM PdBI	~2.4–0.85	
Chini et al. (1986)	Continuum	1.3 mm	3-m NASA IRTF, Hawaii	90	
Chini et al. (2001)	Continuum	450; 850 μm	15-m JCMT, Hawaii	8.3; 15	
	Continuum	1.3 mm	IRAM 30-m	10.7	
Codella et al. (1996)	H_2O Maser				
Codella et al. (2001)	SiO; CO; DCO^+;CS	86.8–230.5 GHz	IRAM 30-m	29–10	~3
	Continuum	88; 92; 110 GHz	OVRO interferometer, BP	6.2×3.4–5.2×3	
	HCO^+(1-0)	89.2 GHz	OVRO interferometer, BP	6.2×3.4	
Comoretto et al. (1990)	H_2O Maser	22.235 GHz	Medicina 32-m	114	20
De Buizer et al. (2005)	Continuum	11.7; 20.81 μm	3-m NASA IRTF	1.3; 1.7	<1
De Buizer et al. (2007)	Continuum	12.5; 18.3 μm	Gemini N. 8.1-m, Hawaii	0.33; 0.48	<0.1

[1] a "<" implies that the pointing accuracy is better than the given value

Table C1 – *continued*

Dent et al. (1988)	NH_3	23.7 GHz	SERC 25-m, England	132	
	NH_3	23.7 GHz	Effelsberg 100-m	40	
	HCO^+(1-0)	89.188 GHz	OSO 20-m	45	
	HCO^+(3-2)	267.557 GHz	3.8-m UKIRT, Hawaii	75	
Dobashi et al. (1995)	$^{12;13}CO$	115 GHz	NRO 45-m	16	<10
Edris et al. (2005)	OH Maser	1.665;1.667 GHz	MERLIN, England	0.174×0.137	0.025 (abs.), 0.010 (rel.)
	CH_3OH Maser	6.7 GHz	MERLIN interferometer	0.026×0.026	0.015 (abs.)
	H_2O Maser	22.2 GHz	MERLIN interferometer	0.04×0.008	0.012 (abs.)
Estalella et al. (1993)	NH_3	23.7 GHz	Effelsberg 100-m	40	<8
	$C^{18}O$(2-1);CS(3-2)	219.56;146.97 GHz	IRAM 30-m	~13;17	~4
Felli et al. (1992)	H_2O Maser	22.235 GHz	Medicina 32-m	114	15
Faúndez et al., 2004	Continuum	1.2 mm	15-m SEST	24	
Fontani et al. (2004)	Continuum	850 μm	15-m JCMT	14	
	^{12}CO(1-0)	115.271 GHz	OVRO interferometer	6.95×6.12	
	^{12}CO(2-1)	230.538 GHz	NRAO 12-m, Kit Peak	29	
	^{12}CO; $C^{18}O$(2-1)	230.54; 219.56 GHz	IRAM 30-m	11; 12	2
	$H^{13}CO^+$; SiO	217.11–86.75 GHz	IRAM 30-m	12–29	2
	CH_3C_2H	222.17–102.55 GHz	IRAM 30-m	11–29	
Forster et al. (1978)	Continuum	1.3 cm	Hat Creek Interferometer	6×10.5	
Galt (2004)	CH_3OH Maser	6.7 GHz	DRAO 25.6-m, Canada	420	
Goddi et al. (2004)	H_2O Maser	22.235 GHz	European VLBI Network	$(2.1\times1.1)\times10^{-3}$	$(50–100)\times10^{-6}$
Goddi et al. (2005)	H_2O Maser	22.235 GHz	European VLBI Network	$(1.1\times1–2.9\times1.4)\times10^{-3}$	
Gyulbudaghian et al. (1990)	H_2O Maser	22.235 GHz	Haystack 37-m	90	~20
Hardebeck & Wilson (1971)	OH Maser	1.665;1.667 GHz	OVRO Interferometer		5–15
Harju et al. (1998)	SiO(2-1)	86.847 GHz	15-m SEST	57	3
	SiO(3-2)	130.2687 GHz	15-m SEST	40	3
	SiO(2-1)	86.847 GHz	OSO 20-m	43	4
Hofner & Churchwell (1996)	H_2O Maser	22.235 GHz	VLA	0.46×0.4–0.75×0.4	0.1 (rel.)
Hofner et al. (1999)	Continuum	7 mm; 3.6 cm	VLA	1.7×1; 0.5×0.5	
Hughes & MacLeod (1994)	Continuum	6 cm	VLA	~3	
Hunter et al. (1995)	CO(2-1)	230 GHz	CSO 10.4-m	31	4
	CO(3-2);CS(7-6)	~345 GHz	CSO 10.4-m	20	4
	^{13}CO(6-5)	661.068 GHz	CSO 10.4-m	11	4
	H_2O Maser; Cont.	22.235; 8.4 GHz	VLA	0.12×0.11;0.28×0.27	
Hunter et al. (1997)	Continuum	800 μm	CSO 10.4-m		5
	Continuum	350; 450 μm	CSO 10.4-m	12	5
	$^{12;13}CO$;$C^{18}O$(2-1)	~230 GHz	CSO 10.4-m	31	5
	CO(3-2); CS(7-6)	~345 GHz	CSO 10.4-m	20	5
	CO(4-3); (6-5)	291; 436 GHz	CSO 10.4-m	15;11	5
	^{13}CO; $C^{18}O$(1-0); CS(2-1); Cont.	110–115 GHz	OVRO Interferometer	2.71×2.11	
Hunter et al. (1999)	H_2O Maser	22.235 GHz	VLA	0.0786×0.0704	
	Continuum	8.4 GHz	VLA	1.4×0.87	
	HCO^+; $H^{13}CO^+$; SiO; Continuum	~88 GHz	OVRO Interferometer	2.7×2.5	
	CH_3CN	~257 GHz	CSO 10.4-m	30	
Hunter et al. (2000)	Continuum	350 μm	CSO 10.4-m	11	5
Jenness et al. (1995)	Continuum	800/850 μm	15-m JCMT	17/18	~4
	Continuum	450 mm	15-m JCMT	7/18	~4
	Continuum	2 cm	RT (Ryle) Interferometer	30×30 cosecδ	
	CO(2-1); CS(5-4)	230.5–244.9 GHz	15-m JCMT	21	
	Continuum	3.6 cm	VLA	0.9	
	H_2O Maser	22.235 GHz	VLA	0.4	
Kraemer et al. (2003)	Continuum	12.5; 20.6 μm	3-m NASA IRTF	1.1; 1.7	
Kurtz et al. (1994)	Continuum	2; 3.6 cm	VLA	~0.5; 0.9	
Kurtz et al. (2004)	CH_3OH Maser	44.069; 23.2 GHz	VLA	0.44×0.38–4.18×1.89	0.5–0.6
Kurtz & Hofner (2005)	H_2O Maser	22.235 GHz	Effelsberg 100-m	40	5
	H_2O Maser	22.235 GHz	VLA	0.52×0.26–4.5×2.3	
Lebrón et al. (2006)	CO(2-1)	230.5 GHz	IRAM 30-m	11	
Little et al. (1988)	HCO^+(1-0)	89.19 GHz	Metsähovi 14-m, Finland	50	
	HCO^+(3-2)	267.56 GHz	3.8-m UKIRT	66	
	$^{12;13}CO$(1-0)	115.27; 110.2 GHz	OSO 20-m	33; 35	
McCutcheon et al. (1995)	Continuum	450; 800; 1100 μm	15-m JCMT	8; 14; 18	
MacLeod et al. (1998a)	OH; HCHO,CH_3OH	1.6–12.2 GHz	HRAO 26-m, S. Africa	1800–210	
	OH; CH_3OH Maser	1.6; 6.7 GHz	DRAO 26-m	1800; 420	
	H_2O Maser	22.235 GHz	IRO 14-m, Brazil	222	

Table C1 – *continued*

MacLeod et al. (1998b)	CH_3OH Maser	6.7; 12.2 GHz	HRAO 26-m	420; 210	
	CH_3OH Maser	6.7 GHz	DRAO 26-m	420	
Matthews et al. (1986)	$^{12;13}$CO(1-0)	115.27; 110.2 GHz	OSO 20-m	33; 35	
	$^{12;13}$CO(1-0)	115.27; 110.2 GHz	3.8-m UKIRT	75	
Menten (1991)	CH_3OH Maser	6.7 GHz	NRAO 43-m, Green Bank, WV	300	
Migenes et al. (1999)	H_2O Maser	22.235 GHz	VLBA	$(0.21–0.31)\times10^{-3}$	
Minier et al. (2001)	CH_3OH Maser	6.7 GHz	EVN		~0.03
	CH_3OH Maser	12.2 GHz	VLBA		~0.03
	CH_3OH Maser	6.7; 12.2 GHz	ATCA		~0.3
Minier et al. (2005)	sub-mm Cont.	450; 850 μm	15-m JCMT	8; 15	
	mm Cont.	1.2 mm	15-m SEST	24	
Miralles et al. (1994)	radio Cont.	2; 6 cm	VLA	~5	
	H_2O Maser,NH_3	22-23 GHz	Haystack 36.6-m	~90	~8
Molinari et al. (1996)	NH3	23.7	Effelsberg 100-m	40	
Molinari et al. (1998)	Continuum	2 cm	VLA	0.6×0.47–1.3×0.6	
	Continuum	2 cm	VLA	1.3×0.57–2.2×0.57	
	Continuum	2 cm	VLA	3.7×1.7–9.3×1.7	
	Continuum	6 cm	VLA	1.8×1.4–4×1.8	
	Continuum	6 cm	VLA	4×1.7–6.5×1.7	
Molinari et al. (2000)	Continuum	0.35–1.1 mm	15-m JCMT	18.5	
	Continuum	1.3; 2.0 mm	15-m JCMT	19.5; 27	
Molinari et al. (2002)	HCO^+,HCN,SiO	~88 GHz	OVRO interferometer	4×5	
	Continuum	3.4; 1.3 mm	OVRO interferometer	4×5	
	Continuum	3.6 cm	VLA	9×4	
Moscadelli et al. (2000)	H_2O Maser	22.235 GHz	NRAO VLBA	$(1.2\times1.1)\times10^{-3}$	$<0.2\times10^{-3}$
Moscadelli et al. (2005)	H_2O Maser	22.235 GHz	EVN+VLBA	$(0.6–0.8)\times10^{-3}$	$<10^{-3}$(abs.), $(0.1–100)\times10^{-6}$(rel.)
Palagi et al. (1993)	H_2O Maser	22.235 GHz	Medicina 32-m	114	25
Palla et al. (1991)	H_2O Maser	22.235 GHz	Medicina 32-m	114	
Palla et al. (1993)	H_2O Maser	22.235 GHz	Medicina 32-m	114	
Patel et al. (2000)	H_2O Maser	22.235 GHz	VLBA	$\sim0.8\times10^{-3}$	$\sim10^{-5}$(rel.)
Ramesh et al. (1997)	HCO^+;CS	86–99 GHz	NRO 45-m	~16	<5
Reipurth et al. (2003)	Continuum	11.6 μm	3.8-m UKIRT		<2
Ridge & Moore (2001)	^{12}CO(2-1);(1-0)	230 GHz;115 GHz	NRAO 12-m	27; 55	
	^{12}CO(2-1)	230 GHz	15-m JCMT	21	5
Ridge et al. (2003)	^{13}CO;C^{18}O(1-0)	110.2; 109.78 GHz	FCRAO 14-m		5
	C^{18}O(2-1)	219.56 GHz	10-m HHT, Arizona	35	2
Saraceno et al. (1996)	Continuum	350–1300 μm	15-m JCMT	16–19	
Schutte et al. (1993)	CH_3OH Maser	6.7 GHz	HRAO 26-m	420	
Shepherd et al. (1997)	CO(1-0)	115.271 GHz	BIMA interferometer	4.6×5.7	
	SiO;$H^{13}CO^+$; SO_2;Continuum	86.847–86.639 GHz	BIMA interferometer	6.8×5.3;6.8×5.4; 7.2×5.4	
Shepherd et al. (1998)	CO(1-0)	115.271 GHz	OVRO interferometer	5.55×4.47	0.2
	Continuum	112.3 GHz(2.7 mm)	OVRO interferometer	2.71×2.15	0.2
Shepherd & Churchsell (1996a)	^{12}CO(1-0)	115.271 GHz	NRAO 12-m	~60	
Shepherd & Churchsell (1996b)	$^{12;13}$CO(1-0)	115.27; 110.2 GHz	NRAO 12-m	~60 (at 115 GHz)	
Shepherd & Kurtz (1999)	Continuum	2.6 mm	OVRO interferometer	1.59×1.48	0.2
	C^{18}O;^{13}CO (1-0)	~110 GHz	OVRO interferometer	5.24×4.59; 5.76×5.24	0.2
	Continuum	7 mm; 3.6 cm	VLA	0.56×0.45; 0.28×0.25	<<FWHM
	Continuum	3.6 cm	VLA	0.28×0.25	<<FWHM
	H_2O maser	22.235 GHz	VLA	1.01×0.91–3.15×2.84	<<FWHM
Shepherd et al. (2000)	CO(1-0); Cont.	2.7; 1.3 mm	OVRO	<7.5–3.5;<2.9–1.2	
	Continuum	12.5; 17.9 μm	10-m Keck, Hawaii	~0.4;0.5	<1
Shepherd et al. (2001)	Continuum	3 mm	OVRO interferometer	2.05×1.43, 2.96×2.44	
	Continuum	1 mm	OVRO interferometer	0.89×0.79, 1.34×0.97	
Shepherd et al. (2004a)	NH_3(1,1)	23.695 GHz	VLA	2.93×2.55	0.1
	Continuum	1.3 mm	VLA	2.93×2.55	0.1
	H_2O Maser	22.235 GHz	VLA	0.68×0.27	0.1
	H_2O Maser	22.235 GHz	VLBA	$(0.86–1.1\times0.36)\times10^{-3}$	
	Continuum	850 μm	JCMT	15	
Shepherd et al. (2004b)	Continuum	3.3 mm	OVRO	4.9×4.2	
	$H^{13}CO^+$; SiO	86.75; 86.85 GHz	OVRO	5.3×4.5	
	Continuum	6 cm	VLA (archival data)	5.65×2.98	
Slysh et al. (1994)	OH maser	1.665; 1.667 GHz	Nancay Radio Tel., France	210×1140	
Slysh et al. (1999)	CH_3OH Maser	6.7 GHz	Medicina 32-m	336	

Table C1 – *continued*

Snell et al. (1988; 1990)	^{12}CO(1-0)	115.271 GHz	FCRAO 14-m	45	
Sridharan et al. (2002)	^{12}CO(2-1)	230.5 GHz	IRAM 30-m	11	
	SiO(2-1),H^{13}CO$^+$(1-0)	86.9 GHz	IRAM 30-m	29	
	^{13}CO(1-0);CH$_3$CN(6-5)	110.2; 110.4 GHz	IRAM 30-m	22	
	CH$_3$OH	241.8 GHz	IRAM 30-m	11	
	^{12}CO(2-1)	230.5 GHz	CSO 10.4-m	27	
	NH3; H$_2$O Maser	~22.7; 22.2 GHz	Effelsberg 100-m	40	
	CH$_3$OH Maser	6.7 GHz	Effelsberg 100-m	130	
	Continuum	3.6 cm	VLA	0.7	
	Continuum	1.2 mm	IRAM 30-m	11	
Sridharan et al. (2005)	Continuum	2.2-4.7μm	3.8-m UKIRT	<0.3	0.15
Su et al. (2004)	CO(1-0); Cont.	~3 mm	BIMA; NRAO 12-m	~6–10	
Sugitani et al. (1989)	$^{12;13}$CO(1-0)	115; 110 GHz	NRO 4.5-m	17	
Szymczak et al. (2000)	CH$_3$OH Maser	6.7 GHz	32-m Toruń Radio Tel.	330	<25
Thompson et al. (2006)	Continuum	450; 850 μm	15-m JCMT	8; 14	<5
Tofani et al. (1995)	Continuum	3.6 cm	VLA	0.3	
	H$_2$O Maser	22.235 GHz	VLA	0.1	<0.1(abs),<0.003(rel.)
	H$_2$O Maser	22.235 GHz	Medicina 32-m	114	25
Torrelles et al. (1992b)	H$_2$O Maser	22.235 GHz	VLA	~1.1×0.9	10% of beamsize
	Rad. Continuum	3.6 cm	VLA	~4×3.5	10% of beamsize
van der Walt et al. (1995)	CH$_3$OH Maser	6.7 GHz	HRAO 26-m	420	
Verdes-Montenegro et al. (1989)	NH3	~23.7 GHz	Haystack 37-m	84	~15
	H$_2$O Maser	22.235 GHz	Haystack 37-m	84	~15
Vig. et al. (2006)	Continuum	1.28 GHz	GMRT interferometer	7.5×3.8	
	Continuum	610; 325 MHz	GMRT, India	8.4×6.6; 14.4×11.5	
	Continuum	450; 850 μm	15-m JCMT	~7×11; ~13×17	
	Continuum	130; 200 μm	TIFR Balloon Facility 1-m	~60	~48
Walsh et al. (1997)	CH$_3$OH Maser	6.669 GHz	Parkes 64-m	198	
Walsh et al. (1998)	CH$_3$OH Maser; Cont.	6.669; 8.64 GHz	ATCA, Australia	<2	1 (abs.), 0.05(rel.)
Walsh et al. (2003)	Continuum	450; 850 μm	15-m JCMT	8; 15	
Watson et al. (2003)	H$_2$CO;H110$_\alpha$	4.83; 4.87 GHz	Arecibo 305-m, Puerto Rico	57	
Wilking et al. (1989)	CO(2-1)		MWO 4.9-m, Texas, USA	72	
	Continuum	2.7 mm	OVRO interferometer	35	
	Continuum	2; 6 cm	VLA	5.5; 16	
	Continuum	2; 6 cm	VLA (for IRAS 20227)	3.3×1.2; 6.3×3.8	
Wilking et al. (1990)	$^{12;13}$CO(2-1)	230.5; 220.4 GHz	NRAO 12-m	28	5
Wilking et al. (1993)	Continuum	2.7 mm	OVRO interferometer	7.3×7.5&1.2	
	Continuum	1.25 mm	CSO 10.4-m	30	5
	CS(2-1)	97.97; 96.41 GHz	NRAO 12-m	66	8
Williams et al. (2004)	Continuum	450; 850 μm	15-m JCMT	8; 14.4	
Wu et al. (2001)	^{13}CO (1-0)	110.201 GHz	13.7-mm QST	55	
Wood & Churchwell (1989b)	Rad. Cont.	6 cm	VLA	0.38×0.38–1.6×1.4	
	Rad. Cont.	2 cm	VLA	0.41×0.41	
Wouterloot et al. (1993)	H$_2$O Maser	22.235 GHz	Effelsberg 100-m	40	7–8
	H$_2$O Maser	22.235 GHz	Medicina 32-m	114	15
	OH Maser	1.665 GHz	Effelsberg 100-m	468	
	CH$_3$OH Maser	12.179 GHz	Medicina 32-m	150	
	^{12}CO(2-1); (3-2)	230; 345 GHz	KOSMA 3-m	132; 66	
Wouterloot &	^{12}CO(1-0)	115 GHz	15-m SEST	43	10
Brand (1989)	^{12}CO(1-0)	115 GHz	IRAM 30-m	21	5
Zapata et al. (2006)	Continuum	0.7; 1.3 cm	VLA	~1.8×1.6; ~2.4×1.6	
	Continuum	3.6 cm	VLA	4.7×2.7	
Zhang et al. (1998)	NH$_3$	~22.7 GHz	VLA	4.2×2.8	
Zhang et al. (1999)	NH$_3$	23.87; 24.14 GHz	VLA	1;0.31×0.37;3.9×3.1	
Zhang et al. (2001)	^{12}CO(2-1)	230.5 GHz	NRAO 12-m;15-m JCMT	see Zhang et al. (2005)	
Zhang et al. (2002)	NH3	~22.7; 24 GHz	VLA	3–5	
Zhang et al. (2005)	^{12}CO(2-1)	230.5 GHz	NRAO 12-m	~29	
	^{12}CO(2-1); (3-2)	230.5; 345 GHz	CSO 10.4-m	~30	
Zinchenko et al. (2000)	HNCO	330–461 GHz	10-m HHT	25–18	5
	HNCO; C^{18}O(2-1)	110–220 GHz	SEST 15-m	47–24	5
	HNCO; C^{18}O(1-0)	88–110 GHz	OSO 20-m	40–35	5
	HNCO	21.981 GHz	Effelsberg 100-m	40	10
Zoonematkermani et al. (1990)	Continuum	20 cm	VLA	>5.07	~3